UNIVERSITY OF
BIRMINGHAM

Understanding the Mechanical Strength of Microcapsules and Their Adhesion on Fabric Surfaces

by

Min Liu

A thesis submitted to
The University of Birmingham
for the degree of
DOCTOR OF PHILOSOPHY

School of Chemical Engineering
The University of Birmingham
April 2010

Abstract

There is a growing interest to incorporate melamine formaldehyde (MF) microcapsules containing perfume oil in detergents, which can be delivered to consumers at end-use applications. The microcapsules should have desirable properties including optimum mechanical strength and capability to adhere on fabric surfaces after laundry. They should be strong enough to withstand a serious of engineering processes including pumping, mixing, drying etc, but be weak enough to be ruptured by consumers in post-laundry handling. For this purpose, the mechanical strength of MF microcapsules made by different processing conditions, with additional coating, after being dried using different methods and being exposed to various suspending liquids were characterised in this work. Moreover, the adhesion of single MF microcapsules or single MF microspheres on flat fabric films in air or in liquids with different concentrations of detergent, surfactants, pH etc was investigated.

The mechanical strength of MF microcapsules produced using an in-situ polymerisation technique were characterised by a micromanipulation technique. Conventionally, the mechanical strength parameters include microcapsule diameter, rupture force, deformation at rupture and nominal rupture stress (the ratio of the rupture force to the initial cross-sectional area of individual microcapsule). It was found that larger microcapsules in a sample on average had greater rupture force but small ones had higher nominal rupture stress. Since the rupture force or nominal rupture stress depends on the size of microcapsules, which is not easy to use particularly for comparison of the mechanical strength of microcapsules in different samples, a new strength parameter nominal wall tension at rupture has been proposed in this work, which is defined as the ratio of the rupture force to the circumference of individual microcapsule. The results from micromanipulation measurements showed that the increase of core/capsule ratio in weight percentage reduced the nominal wall tension of microcapsules. The use of silicate coating on surface of MF microcapsules increased the nominal wall tension of microcapsules and made microcapsules more brittle. The nominal wall tension of microcapsules did not differ significantly when the pH of their suspending liquid ranged from 2 to 11 for a duration of 25 hours. It has also been shown that the prolonged polymerisation time alone or combined with the elevated polymerisation temperature increased the nominal wall tension of MF microcapsules. Furthermore, there was no significant change in the nominal wall tension of microcapsules after being oven dried, fluidised bed dried or freeze dried. However, there was a significant increase in the nominal rupture tension of microcapsules after being spray dried, which resulted from destroying weak (in general large) microcapsules in the drying process.

Modelling of the force versus displacement data from micromanipulation has been attempted in order to determine intrinsic mechanical property parameters, such as Young's modulus, yield stress and stress at rupture that requires to know the contact area between a compressed microcapsule and force probe at rupture. The mean Young's modulus of MF microcapsules E_c predicted from the Hertz model was found to be 32±4 MPa which represents the modulus of single whole microcapsule. In addition, the Young's modulus of MF microcapsule wall material E_w was found to be 8±1 GPa by applying finite element analysis with a linear elastic model. A correlation describing the relationship between E_c and E_w has been developed based on the modelled results, wall thickness and diameter of microcapsules. The Hertz model and

Johnson's plastic model were further applied to determine the rupture stress of single MF microcapsules, which take their rupture deformation into consideration. The models help to determine the mechanical strength of microcapsules precisely.

Real fabric surface can be very rough, and quantification of the adhesion of single microcapsules on such rough surface can be difficult so that flat fabric surface was fabricated. Cotton films were successfully generated by dissolving cotton powder and their properties were also characterised including their surface roughness, thickness, contact angle and purity. The adhesive forces between MF microcapsules/MF microparticles and cotton films under ambient condition at air RH above 40% were measured using an AFM technique, which was considered to be dominated by capillary forces. It was also found that there was little adhesion between MF microparticle and cotton films in detergent or surfactant solution. Instead, repulsion between them was observed and reduced with the increase of detergent/surfactant concentration and the decrease in solution pH. It was suggested that the repulsion was contributed from two mechanisms of steric interaction and electrostatic repulsion.

It is believed that this work can be used to guide formulation and processing of MF microcapsules with desirable mechanical strength. The studies on the adhesion between MF microcapsules/microparticles and cotton films under ambient condition or in the detergent solutions should be beneficial to the future work to enhance adhesion of microcapsules on fabric surface via modification of the surface compositions and morphology of microcapsules.

Dedicated to my beloved grandfather

who recently passed away, but will always be remembered.

Acknowledgements

I would like to express my deepest gratitude towards my supervisors Prof. Zhibing Zhang, Prof. Jon Preece and Prof. David York for their excellent supervision, constant guidance, valuable advice as well as their encouragement and patience throughout the course of this research.

Thanks also go to Dr. James Bowen for the training of AFM equipment and the helpful discussions and Dr. Bac Nguyen for his support on the modelling work. I am very thankful to Dr. Jiten Dihora, John Burdis, Nick Guillard and Malcolm Curtis from Procter & Gamble for their support on this project.

I would also like to acknowledge the financial support provided by The School of Chemical Engineering at The University of Birmingham and Procter & Gamble, Newcastle to this research. Thanks are extended to the excellent staff in The School of Chemical Engineering in particular Hazel Jennings, Elaine Mitchell, Liz Hares, Lynn Draper, and Jason Mahoney for their technical assistance and administration support. I am also very grateful for the friendship, encouragement and hands-on help given by the members of Micromanipulation Research Group.

I would like to express my deepest appreciation towards my parents and brother for their love, support, encouragement and understanding throughout my studies.

Last but not least, I would like to thank my dear husband Dr. Kenneth Chung for his love and motivation. I couldn't have done it without you, too.

Table of Contents

List of Figures

List of Tables

Nomenclature

a_h	Contact radius determined by Hertz model, m
A_{inner}	Inner cross-sectional area of microcapsule, m^2
A_{outer}	Outer cross-sectional area of microcapsule, m^2
C_1	Material constant
C_{COM}	Compliance of force transducer, mN^{-1}
d_{10}	Number mean diameter, m
d_{43}	Volume weighted mean diameter, m
D	Tip-sample distance, m
D_m	Diameter of a single microcapsule before compression, m
E	Young's Modulus, Pa
E_c	Young's modulus of whole microcapsule, Pa
E_w	Young's modulus of microcapsule wall material, Pa
F	Force, N
F_C	Capillary force, N
F_J	Contact force estimated using JKR theory, N
F_R	Rupture force of a single microcapsule, N
h	Wall thickness of microcapsule/biological cell, m
H_0	Null hypothesis
H_1	Alternative hypothesis
H_i	Wall thickness of microcapsule ultra thin section, m
k	Spring constant of cantilever, Nm^{-1}
k_B	Boltzmann's constant, 1.38×10^{-23}

k_{ref}	Spring constant of the reference cantilever, Nm^{-1}
k_t	Spring constant of cantilever calibrated using thermal noise method, Nm^{-1}
k_{test}	Spring constant of the cantilever under test, Nm^{-1}
K_S	Force transducer sensitivity, mNV^{-1}
l	Effective segment length, m
$\overline{m}$	Mean gradient, V
m_{test}	Slope of the force versus distance curve when cantilever under test is in contact with the free end of the reference cantilever, Nm^{-1}
m_{tot}	Slope of the force versus distance curve when the cantilever under test is in contact with a hard surface, Nm^{-1}
M	Molecular weight of the polymer
M_0	Segment molecular weight
n	Size of a random sample
n_s	Number of segments
P	Area of the power spectrum of the thermal fluctuations of the cantilever, m^2
P_{50}	Pressure to achieve 50% capsule breakage, Pa
r_0	Initial radius of a microcapsule/biological cell, m
r_i	Inflated radius of a biological cell, m
R	Radius, m
R_g	Radius of gyration, m
R_i	Inner radius of microcapsule ultra thin section, m
R_o	Outer radius of microcapsule ultra thin section, m
S	Standard deviation of a random sample

S^2	Variance of a random sample
t	Probe travelling time, s
t_0^*	Calculated test statistic
t_a	Time between two consecutive sampling points, s
t_S	Time taken for the probe to travel a pre-set distance, s
$t_{\alpha/2,n-1}$	t statistic value with n-1 degrees of freedom
T	Absolute temperature, K
T_g	Glass transition temperature, ºC
T_R	The nominal wall tension of a single microcapsule, Nm^{-1}
v	Compression speed, ms^{-1}
v_c	Calibrated compression speed, ms^{-1}
V	Voltage, V
x	Fractional deformation
x_c	Deflection of cantilever, m
x_L	Fractional deformation in Lardner & Pujara (1980)
X	Half of the displacement when a microcapsule/cell is compressed, m
$\overline{X}$	Mean of a random sample
X_1	Independent population 1 with a normal distribution
X_2	Independent population 2 with a normal distribution
y	Dimensionless force
y_L	Dimensionless force in Lardner & Pujara (1980)
Z	Distance between the sample and the cantilever rest position (piezo), m

Greek Symbol

α	Significance level
δ	Half of total compressive displacement, m
δ_c	Deflection of cantilever, m
δ_C	Compressive displacement, m
δ_s	Deformation distance of sample substrate, m
δ_S	A pre-set distance to calibrate the compression speed, m
ε	Strain
γ_L	Surface tension of liquid, Nm^{-1}
γ_{SV}	Solid-vapour interfacial energy, Nm^{-1}
$\overline{\eta}$	Distance between probe and the equator of microparticle, m
λs	Initial stretch ratio
μ	Mean of an independent population with a normal distribution
ν	Degree of freedom
ν_P	Poisson's ratio
θ	Contact angle where a liquid/vapour interface contacts the solid surface, °
θ_c	Contact angle of water on the two surfaces of sphere and substrate, °
θ_t	Angle between the cantilever under test and the reference cantilever, °
σ	Standard deviation of an independent population with a normal distribution
σ_h	Contact stress of a single microcapsule determined from Hertz model, Pa
σ_s	Stress, Pa
σ^2	Variance of an independent population with a normal distribution

$\hat{\tau}$	Ratio of initial wall thickness to radius of microcapsule/cell

Abbreviations

AFM	Atomic Force Microscopy
BKB	β-keto Butyramide
CSTR	Continuous Stirred Tank Reactor
DLVO	Derjaguin–Landau–Verweij–Overbeek Theory
DMSO	Dimethyl Sulfoxide
DMT	Derjaguin-Muller-Toporov Theory
DSC	Differential Scanning Calorimetry
ESCA	Electron Spectroscopy for Chemical Analysis
ESEM	Environmental Scanning Electron Microscopy
FEA	Finite Element Analysis
HPLC	High Performance Liquid Chromatography
JKR	Johnson-Kendall-Roberts Theory
MBS	Methyl and Benzisothiazolinone
MF	Melamine Formaldehyde
NMMO	N-methylmorpholine-N-oxide
PEI	Poly(ethyleneimine)
RH	Relative Humidity
RMS	Root Mean Square
SAM	Self-Assembled Monolayer
SDBS	Sodium Dodecylbenzenesulfonate

SEM	Scanning Electron Microscopy
SFA	Surface Forces Apparatus
SNOBS	Sodium Nonanoyloxybenzenesulfonate
SPM	Scanning Probe Microscopy
STM	Scanning Tunnelling Microscope
TAED	Tetraacetylethylenediamine
TEM	Transmission Electron Microscopy
TIRM	Total Internal Reflection Microscopy
XPS	X-ray Photoelectron Microscopy

1. INTRODUCTION

Microcapsules with a core-wall structure confer the unique characteristics of masking the core material to reduce unnecessary reaction with outside agents. Hence, microcapsules have been widely applied in a large number of industrial sectors including pharmaceutical (Youan *et al.*, 2001), food (Greenblatt *et al.*, 1993), agriculture (Chamberlain & Symes, 1993), cosmetics (Turner & Levey, 1993) and construction (Janssen *et al.*, 1993).

In the use of household/personal care products such as detergents, some perfume constituents tend to react with air during storage on the shelf (Jellinek, 1975) or be eliminated in the successive rinses of laundry process, if such perfume constituents are directly incorporated into the detergents. Microcapsules containing perfume constituents were therefore introduced into the softeners and detergent powder to overcome the problems (Ho, 2000). Of particular interest in this work are melamine formaldehyde (MF) microcapsules containing perfume oil which are included in the detergents for the end-use applications. MF microcapsules are produced by an in-situ polymerisation technique, since the technique is relatively simple and the MF wall is highly crosslinked to be able to mask the core contents (Usami *et al.*, 1999).

There is a growing need in the industries to deliver the perfume oil from the core of the MF microcapsules to the surface of fabrics, both woven and non-woven. As a result, MF microcapsules in the detergents should ideally be able to remain intact during a series of processes such as preparation, transportation, washing and drying; moreover, MF microcapsules are required to adhere to the fabrics during the process of washing, before the encapsulated perfume oil is released under a given mechanical load after the drying process.

As such, understanding the mechanical strength of MF microcapsules becomes extremely critical, since microcapsules need to be strong enough to stand the series of processes and be able to rupture when required.

The relationship between rupture force, one of the mechanical strength parameters, and size of microcapsules has been reported by Sun & Zhang (2001). However, little is known on how the mechanical strength of MF microcapsules is influenced by the variation of formulations such as providing an additional layer of coating around microcapsules or modification of preparation conditions including change in polymerisation reaction time/temperature. The applicability and limitations of some mechanical strength parameters such as nominal rupture stress has not been addressed in the literature. Moreover, limited works have been performed on the application of modelling to the compression data of MF microcapsules to determine their intrinsic mechanical properties, such as Young's modulus and the rupture stress by taking their deformation at rupture into consideration.

Furthermore, in order to allow the MF microcapsules to deposit on the surface of fabric in the laundry process, first of all, it is important to understand the interaction between MF microcapsules and the fabrics in the detergent or surfactant solutions. To the best of the author's knowledge, there is no published research on directly measuring the adhesion between MF microcapsule/microparticles and fabrics. In addition, it is difficult to conduct experiments on real fibre samples due to structural inconsistency of the fibres (Notley *et al.*, 2006).

The above areas where researches are limited are studied in this work. Therefore, this work aims to study the mechanical strength of MF microcapsules using micromanipulation and measuring their adhesion using Atomic force microscopy (AFM). All the MF microcapsules characterised in this work were supplied by Procter & Gamble (Cincinnati, USA and Newcastle, UK), which were produced with variation of formulations or under different preparation and processing conditions. Certain information relevant to formulation and processing conditions is proprietary and is therefore not specified in this work due to the company's policy.

The outline of this thesis is summarized as follows:

Chapter 2 The applications of microcapsules in a wide range of industrial sectors are introduced; different types of mechanical characterisation techniques which can be used to study the mechanical strength of microcapsules are also reviewed. A general survey is conducted on the modelling methods to determine the intrinsic mechanical properties of microparticles, such as Young's modulus. An adhesion measurement technique (AFM) is introduced together with its working principle and operating modes. Possible mechanisms of adhesion under ambient condition or in the liquid are also reviewed in detail.

Chapter 3 The materials and equipment, which were employed for characterisation of MF microcapsules as well as the adhesion measurement, are presented. The experimental conditions and procedures are also described in detail.

Chapter 4 The measurement results of morphology, size distribution, wall thickness, visco-elastic property, elastic limit and the mechanical strength of MF microcapsules are presented. In particular, the applicability and limitation of the mechanical strength parameters were discussed. MF microcapsules prepared using different formulations were characterised using micromanipulation to study how their mechanical strength was influenced.

Chapter 5 Microcapsules prepared under various conditions such as different polymerisation time and temperature, and production scale were characterised to study how such conditions influence the mechanical strength of MF microcapsules. Furthermore, the effects of processing conditions on the mechanical strength of microcapsules were also examined including the effect of different types of drying.

Chapter 6 The loading data of compressing single MF microcapsules were fitted by models to determine their Young's modulus. Moreover, models were also applied to the compression data of MF microcapsules by micromanipulation to determine the contact area of single MF microcapsules during compression to obtain their real rupture stress.

Chapter 7 The characterisation results of cotton films are presented, which include their surface images, roughness, thickness, contact angle and purity. This chapter also provides an insight into the adhesion between single MF microcapsule/microparticle and cotton films under ambient conditions as well as in the liquid environment of detergents and surfactant solutions, and the possible mechanisms involved are also suggested.

Chapter 8 The overall conclusions of this work are presented and the recommendations for future work are also given.

2. LITERATURE REVIEW

In this chapter, the application of microcapsules in a variety of industries is presented. Understanding the mechanical strength of melamine formaldehyde (MF) microcapsules is of special interest to this project. Hence, past literatures concerning the mechanical behaviours of MF microcapsules are studied. In addition, various techniques which are capable of investigating the mechanical strength of microcapsules are reviewed and their advantages and disadvantages are shown in detail. A technique which can be best applied to characterise single MF microcapsules is identified. A number of modelling methods are also evaluated so that an appropriate method can be selected to determine the intrinsic mechanical properties of MF microcapsules. A cellulose preparation method described in the literature is reviewed to study its feasibility to be adapted to dissolve cotton fibres/powder for the current project. Furthermore, a technique which is most suitable to measure the adhesion between microcapsules and the fibre/cellulose surface was chosen by comparing with other techniques. The working principle and operating modes of this technique as well as the calibration methods of the cantilevers were outlined in this chapter. Finally, all kinds of adhesion mechanisms under ambient condition or in the liquid media featured in the literatures are also reviewed in detail.

2.1 Detergents for Laundry Processes

Two forms of detergents are commercially available: powder and liquids. Conventional powdered detergents represent more than 60% of the world's detergent production. Washing powder contains a high level of secondary ingredients, which either aids manufacturing

process or acts as fillers, and yet has little effect on the product performance, e.g. Na_2SO_4 (Ho, 2000). Liquid detergents are convenient products and dissolved more rapidly compared with powdered detergents, particularly in cold water. Furthermore, liquid detergents generate no dust and are easy to dose (Cahn, 1997).

2.1.1 Compositions of Detergents

Table 2.1 lists the composition of traditional washing powder used in Europe, The United States (U.S.) and Japan (Ho, 2000). Surfactants are the most essential ingredient in a laundering product. A surfactant molecule consists of two parts, a hydrophobic part (insoluble in water) and a hydrophilic part (soluble in water). Their purpose is first to remove soil and more importantly to keep it suspended in the wash solution and prevent its redeposition on clothes. The surfactants available are predominantly anionic; anionic surfactants have a polar group that is linked in a covalent manner with a hydrophobic part and carry negative charges (i.e. $–COO^-$). Nonionics are sometimes added in a complementary role but at a lower concentration, i.e. 1/5 or ¼ of those anionics. Nonionic surfactants have a polar group that cannot be ionized in an aqueous solution.

Builders are sometimes referred to water softeners, of which the primary functions are to decrease the concentration of the calcium and magnesium ions in the washing water by forming either soluble or insoluble complexes with the ions; this in turn increases the effectiveness of detergents by preventing these ions reacting with the ingredients in the detergents (Sachdev & Krishnan, 1997). Washing powder also includes bleaching agents, such as perborate, TAED (tetraacetylethylenediamine) and SNOBS (sodium

nonanoyloxybenzenesulfonate). TAED becomes effective at relatively high temperature, i.e. > 40 ºC, whereas, SNOBS is more effective at lower temperature. Hence, it is more suitable for the United States and Japan, where the detergent concentrations used and wash temperatures are often lower than that in Europe. The main differences in these formulations used in different geographical locations are the higher levels of anionics and the choice of bleaching agents (SNOBS) in the United States and Japan.

Table 2.1 Composition of traditional washing powder used in Europe, US and Japan .

Components	Europe (%)	U.S. (%)	Japan (%)
Surfactants			
Anionic	5-15	8-22	15-25
Nonionic	3-7	0-6	0-4
Builders and others	30-45	30-50	25-40
Perborate	15-25	-	-
TAED	2-5	-	-
SNOBS (U.S., Japan)	-	0-4	0-4
Secondary agents	15-25	15-30	25-40

2.1.2 Problems of Direct Inclusion of Perfume Constituents in the Detergent Products

Perfume is sometimes included in the washing powder to attract consumers and to enhance product image, leading to a subjective reinforcement in product performance, although perfume on its own has no influence on the performance of detergent. Perfume is sometimes considered to be a determining factor in the purchase and repurchase process. Consumer tests have shown that products with almost any reasonably selected perfume are preferred to one which is unperfumed (Wollatt, 1985). However, problems may arise during packaging, storage and laundry processes, if perfume constituents are to be directly incorporated into detergent products. These issues are discussed in this section.

2.1.2.1 Packaging & Storage

Most perfume materials are made of alcohols, esters, aldehydes, ketones, phenols or unsaturated hydrocarbons. In the packaging process when perfume constituents are mixed with other components, some of these perfume constituents may react with product components that are proteins or polypeptides, such as, protein shampoos and enzyme detergents. Moreover, a significant part of the perfume in detergent powder is lost through evaporation even before the products go on sale. This loss is between a few percent and 50% depending on storage conditions, e.g. temperature and humidity (Ho, 2000). In addition, some perfume constituents, notably aldehydes and unsaturated hydrocarbons, may undergo slow chemical changes by reacting with air in the package during storage (Jellinek, 1975).

2.1.2.2 Laundry Process

Perfume deposition efficiency during the laundry process may also decrease due to the interaction of perfume with surfactant. The role of surfactants is to eliminate oily soils and hold them in suspension; however, the physico-chemical characteristics of perfume are very similar to those of oily soils and hence prevent their deposition.

Ho (2000) studied the deposition of perfume constituents on the fabrics in a washing machine. Fragrant materials are listed in order of volatility and the perfume is grouped under respective evaporation coefficients (perfume notes). The efficiency of perfume constituents' deposition is determined by quantifying the retention of top note, middle note and base note on the clothes.

It was shown that the top notes, the most volatile odorants among the three, tend to be eliminated during successive rinses and the middle notes deposit more strongly on the wash; the least volatile base notes, unsurprisingly, are relatively unaffected by successive rinses.

2.2 Microcapsules

Due to the problems discussed above, efforts need to be made to ensure perfume is preserved during a range of processes, and can be delivered effectively to the targeted site. One approach is to encapsulate perfume in microcapsules; as such, perfume is protected by a barrier made of polymer. Furthermore, microcapsules can contain up to 95wt.% perfume constituents, and such microcapsules have been made for softeners and detergent powder (Ho, 2000). It is of great importance to understand their mechanical strength; as such, they can remain intact during washing and perfume can be released under a given mechanical load after drying process.

2.2.1 Introduction to Microcapsules

A capsule typically consists of a core material surrounded by a single or multi-layered shell. The core material is also refereed to as the core, internal phase or fill, whereas the wall is sometimes called a shell, coating or membrane. The shell may be a single layer or a combination of several shell layers, and each shell layer consists of either a single wall material, or a blend of different constituents (Greenblatt *et al.*, 1993).

The relative contents of core and wall materials in microcapsules can be expressed as "Core content", "Core/capsule ratio" or sometimes "Core/wall ratio" in literature, which is linked to wall thickness. Optimal core/wall ratio has a profound commercial significance in terms of storage stability and release behaviour. For example, high core/wall ratio would cause undesirable rapid release. In contrast, low core/wall ratio would lead to the addition of wall material cost to the production costs (Arshady, 1999). Therefore, in order to produce microcapsules with desirable mechanical strength and optical release of core materials for end-use applications, it is important to study and understand the relationship between their mechanical strength and the core/wall ratio or core/capsule ratio of microcapsules.

Microcapsules are capsules ranging from 1 μm to 1000 μm in diameter. They have gained wide interests in a number of industrial sectors due to their unique characteristics, such as their ability (i) to reduce the reactivity between the sensitive core material and the outside environment, (ii) to slow down the rate of evaporation and release of the core material before reaching its targeted sites, and (iii) to mask its odour and taste. Therefore, microcapsules have been widely used in a multitude of industrial fields, ranging from pharmaceuticals, biomedical, agriculture, food and personal care products to photography and printing.

2.2.2 Applications of Microcapsules

Microcapsules have been extensively used in pharmaceutical industry for controlled delivery of protein and DNA vaccines to enhance the immunogenicity of some weak subunit vaccine candidates (Youan *et al.*, 2001). In food industry, flavours were encapsulated to achieve a gradual and controlled release when exposed to microwave during cooking (Greenblatt *et al.*,

1993). In agriculture, the application of microcapsules also increases the efficiency and effectiveness of a pesticide by improved targeting and controlled release; this could in turn reduce the amount of active ingredient required, with a consequential reduction in potential hazards to the environment (Chamberlain & Symes, 1993).

Microcapsules also play a vital role in cosmetics industry. For example, microcapsules with diameters of approximately 180 μm are used in Estee Lauder Exfoliating Cleansers to create an abrasive effect as well as releasing moisturiser during rubbing. Avon Cosmetics also incorporated microcapsules with a size of 32 μm into several products including lipsticks and eye powder (Turner & Levey, 1993). In the field of paints and construction, the main interest is to focus on the polymer encapsulation of inorganic particles like pigments and fillers; this optimises the mechanical properties by improving the interaction between the hydrophilic inorganic particles (TiO_2) and the hydrophobic polymeric matrix (Janssen *et al.*, 1993). The microcapsules have also been used in pressure sensitive copying paper where the produced microcapsules contained colourless chromogenic material. The microcapsules and a coreactant material were deposited on the surface of two sheets of paper respectively, which face each other. When pressure is exerted on the paper during writing or typing, the microcapsules are ruptured, leading to release the chromogenic material, which in turn reacts with the coreactant material to produce a colour.

2.2.3 Encapsulation Methods

Microencapsulation is an encapsulation method that can encapsulate or coat small particles or droplets to produce capsules in the micrometer to millimetre range, i.e. the microcapsules.

Microencapsulation methods can be classified according to the nature of suspending media: liquid suspending medium and vapour suspending medium. If the suspending medium is liquid, microencapsulation is achieved by emulsification or dispersion of two or more immiscible phases. If the suspending medium is vapour, the microcapsules are produced by atomization of liquid phase. The detailed classification of microencapsulation methods (Finch & Bodmeier, 2002) is summarized in Table 2.2.

Table 2.2 Microencapsulation methods classified according to nature of suspending medium.

Liquid suspending medium	Vapour suspending medium
• Complex coacervation • Polymer – polymer incompatibility • Interfacial polymerization • In-situ polymerization • Desolvation • Solvent evaporation from emulsion • Gelation • Pressure extrusion • Supercritical fluid technology	• Spray drying and congealing • Fluidized-bed process (including Wurster process) • Gelation • Electrostatic deposition

Of the microencapsulation methods in Table 2.2, in-situ polymerisation technique has been adopted to produce the melamine formaldehyde (MF) microcapsules. It is based on the polymerisation reaction of MF resin condensates with acrylamide-acrylic acid copolymers (Finch, 1993). Using such technique, the MF microcapsules containing chromogenic material used in pressure sensitive copying paper was prepared (US Patent 4552811) for an improved drop size distribution and impermeability. The MF microcapsules produced (Hong & Park, 1999) had a narrow size distribution, smooth surface, and were capable of preserving fragrant Migrin oil for a longer shelf life. MF microcapsules encapsulating solvent based acrylate

adhesives (Pernot *et al.*, 1999) were also produced; the obtained non-tacky microcapsules on paper possess long storage stability and adhesiveness upon applying pressure (i.e. by the thumb). The detailed procedures of the in-situ polymerisation technique were outlined in detail by Sun & Zhang (2001) and are also presented in Figure 3.1 of Chapter 3.

2.2.4 Melamine Formaldehyde (MF) Microcapsules

2.2.4.1 Introduction

Melamine formaldehyde (MF) is a type of synthetic polymers. The main advantages of synthetic polymer microcapsules are as follows (Usami *et al.*, 1999):

- The walls of microcapsules are tightly crosslinked to enhance core stability.
- The process of encapsulation is relatively simple.
- Higher microcapsule concentration in the dispersion can be produced.
- Control of capsule size and wall thickness is easy.

Melamine formaldehyde microcapsule is one type of amino resin microcapsules, which are less expensive compared with the other type of microcapsules, such as gelatin or polyurea microcapsules; they are also moisture and surfactant resistant, and in turn impose fewer solvent restrictions. Their major disadvantage is attributed to the manufacturing process, as the wall polymer is deposited in a uniform thickness on all surfaces within a batch of production (Blythe *et al.*, 1999). Therefore, when larger microcapsules are produced, they have thin walls relative to their diameter and are weaker. In contrast, smaller microcapsules have proportionally thicker wall and are more difficult to rupture than larger ones. In the industry

with respect to detergent application, the produced MF microcapsules are not only required to remain intact during a range of processing stages, such as mixing, drying, transporting, but also be able to rupture under a given mechanical load for the product application. In order to produce MF microcapsules with optimum mechanical strength, it is of great importance to understand the effect of formulation and processing conditions on the mechanical strength of microcapsules by applying appropriate characterisation techniques.

2.2.4.2 Mechanical Behaviours & Properties

The mechanical behaviours of MF microcapsules with diameters between 1-12 μm were studied by Sun & Zhang (2001) using a micromanipulation technique. The MF microcapsules studied contained 68 wt.% core material which was a 10:1(w/w) mixture of partially hydrogenated terphenyls and kerosene. It was found that MF microcapsules exhibited visco-elastic behaviours up to a deformation of 19±1%; this is the pseudo yield point which distinguishes the elastic and plastic regions. Plastic behaviours were observed when microcapsules underwent further compression beyond the pseudo yield point and up to the point of rupture at 70±1% deformation. Various modelling work has been applied to determine the intrinsic mechanical property parameters (e.g. Young's modulus) of microparticles with core-wall structure: cells (Wang *et al.*, 2004; Stenson *et al.*, 2009), desiccated ragweed pollen grains (Liu & Zhang, 2004) and microcapsules (Liu *et al.*, 1996; Keller & Sottos, 2006), however, no studies on MF microcapsules are published.

Young's modulus is defined through Hooke's law. When strains are small, the strain is very nearly proportional to the stress; that is, they are linear elastic. The stress, σ_s, is proportional to

the strain, ε. For simple compression, the relationship can be expressed in Equation 2.1 (Ashby & Jones, 2005):

$$\sigma_s = E\varepsilon \tag{2.1}$$

where E is called Young's modulus or elastic modulus.

2.3 Techniques to Characterise Microcapsules

This section reviews the techniques to characterise the mechanical strength of microcapsules as well as the techniques to measure wall thickness of microcapsules. Understanding the mechanical strength of microcapsules helps to prevent the damage of microcapsules in their processing equipment (e.g. stirred vessels), maintain their long term mechanical stability, and to realize the triggered release of active ingredients by mechanical forces. Various techniques have been developed in the past to characterize the mechanical strength of microcapsules, and the following sections give a brief review. They are summarized in Table 2.3 and can be categorized into two groups: characterisation of microcapsule population and characterisation of single microcapsules.

Table 2.3 Techniques to characterise the mechanical properties of microcapsules

Characterisation of microcapsule population	Characterisation of single microcapsules
• Compression between plates • Shear breakage of microcapsules in a turbine reactor • Osmotic pressure test	• Atomic force microscopy (AFM) • Micropipette aspiration • Texture analyser • Micromanipulation • Nanomanipulation

2.3.1 Mechanical Strength of Microcapsule Population

This section highlights the techniques to characterise the mechanical strength of a population of microcapsules at once.

2.3.1.1 Compression between Two Plates

Compression between two plates (Ohtsubo *et al.*, 1991) is one of the available breaking tests to characterise the mechanical strength of polyurethane microcapsules encapsulating fenitrothion, which is a widely used insecticide. A prescribed amount of microcapsules ranging from 18.7 μm to 48.1 μm in diameter were dried on a glass plate (2.6cm×7.6cm) before being covered by another glass plate. The glass plates were subsequently sandwiched between two rubber sheets to ensure uniform weight distribution. A known amount of weight was then gently applied on the top rubber sheet for around 1 minute to rupture the microcapsules and then removed. As a result, the percentage of microcapsules broken was determined from the ratio of active ingredient from the burst microcapsules to the total amount of active ingredient. Hence, the mechanical strength of microcapsules was represented by the pressure exerted on a single microcapsule, P_{50}, when bursting of 50% microcapsules was achieved. However, there is a limitation on this technique, as it only can be applied to those microcapsules of which breaking forces are much greater than the gravity force exerted on them by the glass and rubber; microcapsules with a weak mechanical strength may rupture as soon as glass is applied on top of microcapsules.

2.3.1.2 Shear Breakage of Microcapsules in a Turbine Reactor

It was reported that cellulose nitrate membrane microcapsules with a typical diameter of 80 μm could maintain a uniform suspension in a continuous stirred tank reactor (CSTR), but rupture would occur at agitation speeds higher than 220 rpm (Ortmanis *et al.*, 1984). In order to further understand effect of shear on microcapsules, Poncelet & Neufeld (1989) then studied the mechanical strength of nylon membrane microcapsules encapsulating dextran by applying shear forces to break such microcapsules in a turbine reactor. A standard flat-bottom cylindrical plexiglass tank with four baffles and a six-blade Rushton turbine was used to pre-mix the microcapsule suspension. The breakage of microcapsules was accomplished by agitation with 1 mm glass beads using a magnetic stir bar only. However, the use of glass beads was not quantified. After a period of half an hour, complete disruption of microcapsules was achieved. Breaking of microcapsules resulted in release of encapsulated content – dextran. Hence, by measuring the concentrations of dextran before and after shear breakage, the volumetric fraction of unbroken microcapsules was determined, leading to the determination of breakage kinetics. In addition to the above study, Leblond *et al.* (1996) also employed agitation with glass beads (3 mm size) to evaluate the strength of biomicrocapsules with diameters of around 302μm. However, the data generated from this indirect method showed that the mechanical damage is a complex function of capsule properties such as the size and average shear rates, whilst the hydrodynamics of the processing equipment was not well defined (Schuldt & Hunkeler, 2000).

2.3.1.3 Osmotic Pressure Test

An osmotic pressure test was employed as a rapid method to assess the mechanical strength of semi-permeable microcapsules (Thu *et al.*, 1996; Gaserod *et al.*, 1999). Van Raamsdonk & Chang (2001) used this test to quantify the strength of alginate microcapsules by exposing them to a series of hypotonic solutions with different osmolarity, and subsequently quantifying the percentage of broken microcapsules. This test is a simple and quantitative method for rapidly determining the strength of a large number of microcapsules. However, it is limited to microcapsules with semi-permeable walls and only suitable for monitoring the mechanical stability of semi-permeable microcapsules with relative low mechanical strength.

2.3.2 Mechanical Strength of Single Microcapsules

The major drawback of all the characterisation techniques for microcapsule population described above is their inability to provide information on individual microcapsules. Furthermore, the results obtained neglect the effect of microcapsule size on their mechanical strength, where variation of particle size exists in a sample. Therefore, it is essential to source for techniques which are capable of studying the mechanical properties of single microcapsules. The following sections present some techniques that are capable of characterising the mechanical properties of single microcapsules.

2.3.2.1 Atomic Force Microscopy (AFM)

A colloidal probe was initially developed for AFM to measure the adhesive force between a planar surface and an individual colloid particle (Ducker *et al.*, 1991). It was then adapted to

compress single particles between a colloidal particle of large radius of curvature and a flat surface for studying their deformation behaviour (Fery & Weinkamer, 2007).

Lulevich *et al.* (2003; 2004a; 2004b) applied AFM to measure the deformation of polyelectrolyte microcapsules under applied load. A rigid glass sphere with an approximate diameter of 40 μm was glued to a tipless cantilever with a pre-calibrated spring constant; it was used to compress a single microcapsule deposited on a glass substrate fixed over a confocal microscope. The use of confocal microscope allowed the change in microcapsule shape to be recorded throughout the force measurement experiment. The loading or unloading force was measured from the deflection of cantilever, which in turn was detected by a position sensitive photodiode through the reflection of a laser beam on the cantilever. More details on the working principle of AFM can be found in Chapter 2.5.3.1.

AFM was also employed to study the deformation of other microcapsules (Dubreuil *et al.*, 2003; Dubreuil *et al.*, 2004; Fery & Weinkamer, 2007). It is generally applicable to measure forces ranging from several tens of pN to several μN, depending on the sensitivity of cantilever used (Dubreuil *et al.*, 2003). However, the size of microcapsules being studied was limited by the size of glass sphere used, as the microcapsule is required to be smaller than the glass sphere in order for the deformation of the whole microcapsule to take place. AFM technique has also been used to derive the intrinsic mechanical properties of yeast cell wall (Young's modulus) by nano-indentation. Such technique is to detect the localized Young's modulus of cell wall, which can be an order of magnitude higher than the surrounding cell

wall area (Zhang *et al.*, 2009). The AFM technique can also be used to measure adhesive force between a microparticle and a surface of interest; the review is presented in Chapter 2.5.3.

2.3.2.2 Micropipette Aspiration

Micropipette aspiration was employed by Jay & Edwards (1968) to measure the deformability of single nylon microcapsules containing erythrocyte hemolysate when their deformation was small. This technique is based on sucking a part of a microcapsule into a micropipette and measuring the pressure difference between inside and outside of the pipette. Micropipette aspiration could also be applied to study the mechanical properties of neutrophils cells (Hochmuth, 2000), and microgel capsules (Fiddes *et al*, 2009). The main disadvantages of the micropipette aspiration technique are the stress concentration at the pipette edge and the friction existing between the micropipette surface and the cell membrane, which may complicate the force calibration process and interfere with the mechanical response of the cell during aspiration (Lim *et al.*, 2006). Nonetheless, it is difficult to apply this technique to measure the rupture strength of microcapsules, which often occurs at relatively large deformations.

2.3.2.3 Texture Analyser

A texture analyser consists of a penetrometer with a stress gauge. A 10 mm diameter ebonite piston was employed to compress single alginate beads with diameters between 2-3 mm (Ewards-Levy & Levy, 1999). The texture analyser was also used to measure the effect of probe moving speed on bursting strength of multicomponent microcapsules with diameters

from 400-1000 μm (Rehor *et al.*, 2001); only the bursting forces greater than 74 mN were measured. It was suggested that for smaller microcapsules more sensitive apparatuses should be employed. The texture analyser is applicable to particles ranging from a few hundred micrometers to a few millimetres in diameter (Rosinski *et al.*, 2002), but it is difficult to use for particles with size of a few micrometers as studied in this work.

2.3.2.4 Micromanipulation

A technique that can overcome the limitation of the above described methods, such as, size limitation, is a novel micromanipulation technique. This technique was developed by Zhang *et al.* (1999) to compress single MF microcapsules containing a chromogenic material vertically between the two parallel surfaces (A glass probe with flat end and a flat glass slide). It was concluded that micromanipulation is suitable for characterising microcapsules as small as 0.7 μm in diameter. The results obtained allow a direct comparison of the mechanical strength of microcapsules in different samples. Since the micromanipulation technique was proven to be a powerful technique, it was employed to study elastic or plastic behaviours of microcapsules (Sun & Zhang, 2001) and characterise and compare the mechanical strength of microcapsules made of different wall materials, including melamine formaldehyde resin, urea-formaldehyde resin and gelatine-gum arabic coacervate (Sun & Zhang, 2002). In addition to the above studies, micromanipulation was frequently employed to characterise the mechanical properties of other particles: pollen grains (Liu & Zhang, 2004), alginate microspheres and alginate-chitosan microcapsules (Zhao & Zhang, 2004), dex-HEMA hydrogels (Chung *et al.*, 2005) and Eudragit particles (Yap *et al.*, 2008). The limitation of micromanipulation technique is that the testing process is slow. Furthermore, the smallest force which can be measured using

micromanipulation is around 1 μN, and such technique is not able to measure particles with size in sub-micron range.

In all the above studies, the mechanical strength parameters including rupture force and nominal rupture stress have been applied to compare the mechanical strength of microparticles. However, the limitations on application of such parameters had not been discussed. In addition, one key mechanical strength parameter, rupture stress, which takes the deformation of microcapsules at rupture into consideration, had also not been applied. Contact area of microcapsules at rupture is required to determine rupture stress, which can be obtained by either measuring in an environmental scanning electron microscope (Stenson *et al.*, 2008) or applying appropriate modelling methods such as Hertz model (Adams *et al.*, 2004). Furthermore, the investigation regarding the influence of formulation and processing conditions on the mechanical strength of microcapsules remains limited in the literature.

2.3.2.5 Nanomanipulation

The smallest size of microcapsules that the micromanipulation technique could measure is around 1 μm (Zhang *et al.*, 1999b). A novel nanomanipulation technique (Liu *et al.*, 2005), on the other hand, was developed to measure the force required to cause a given deformation of single polymethylmethacrylate nanoparticles (530-950 nm) in an environmental scanning electron microscope under dry mode (high vacuum). The experimental data obtained was validated by the more established micromanipulation technique using Eudragit E100 particles (1-3 μm); no significant difference was found in the results obtained from the two techniques. The nanomanipulation technique has provided researchers an accurate means to characterise

the mechanical strength of nanoparticles. However, it is well known that the radiation in the chamber of an electron microscope may damage the specimens being studied and undermine their mechanical properties. Ren *et al.* (2007) has investigated the radiation damage to MF microcapsules (11.83-22.60 μm) in an environmental scanning electron microscope in both dry and wet mode (low vacuum) and identified a time window within which microcapsules are not damaged under radiation, which serves as a good guidance for conducting similar types of experiments.

2.3.3 Wall Thickness of Microcapsules

Since many researchers applied numerical simulation to theoretically model the membrane/wall of spheres (e.g. microcapsules) as reviewed later in Chapter 2.4.3, it is a prerequisite to determine the wall thickness of microcapsules before the modelling work starts. Researchers in the past have attempted to use a few different techniques to determine the wall thickness of microcapsules. The details are presented in the following sections.

2.3.3.1 Optical Microscopy

Yuan *et al.* (2006) studied the wall thickness of poly(urea-formaldehyde) microcapsules using optical microscopy. The experiments were undertaken by embedding a microcapsule specimen in an epoxy matrix before curing at room temperature. The harden specimen was then sectioned with a razor blade, and the sections were observed under an optical microscope. It was found that the wall thickness of microcapsules with sizes ranging from 50-380 μm was between 5 and 82 μm. Noises (shadows surrounding microcapsules) sometimes might be

present in the captured optical microscopy images, which leads to inaccuracy in the measured results. In addition, optical microscopy is not capable of measuring the wall thickness of microcapsules that are less than 1 μm. Most importantly, the measured wall thickness without corrections for random slicing cannot truly reflect the wall thickness of microcapsules, as microcapsules were sectioned randomly with the razor blade instead of being cut right at the centre of microcapsules.

2.3.3.2 Scanning Electron Microscopy (SEM)

Liu *et al.* (1996) briefly stated that the wall thickness of the investigated microcapsules with diameters around 65 μm was measured by scanning electron microscopy (SEM) following freeze fracture. Loxley & Vincent (1998) later described this technique in detail using an example of poly(methylmethacrylate) microcapsules with the mean size of 7.67 μm. A drop of microcapsule dispersion was air dried before they were ruptured using a clean, round-tipped glass rod under liquid nitrogen. The specimens were then observed by SEM to determine the wall thickness of the microcapsules. The advantage of the cryogenic breaking is the simplicity of the process, whilst the disadvantages are the requirement of the cryostat and its dependence on the specific density of the sample to achieve a satisfactory cut (Torras *et al.*, 2007). Keller & Sottos (2006) also employed a SEM technique to obtain a wall thickness of around 175 nm for poly(urea-formaldehyde) microcapsules with the average size ranging between 65 μm and 213 μm; however, the authors offered no information on either the detailed SEM procedures to determine wall thickness, or whether the wall thickness has been corrected for random slicing. The SEM technique was proved to be useful; there is also some other technique available to determine the wall thickness.

2.3.3.3 Transmission Electron Microscopy (TEM)

Smith *et al.* (2000a) embedded samples in resin, followed by trimming, sectioning and staining, and then applied a transmission electron microscopy (TEM) technique coupled with image analysis to study the wall thickness of baker's yeast cells. The TEM technique is capable of measuring wall thickness of microcapsules at the nanometer scale. The detailed procedures of sample preparation, TEM and image analysis are described in Chapter 3.1.5. The advantage of the resin inclusion method is the reliability; since once the resin block is produced, the cross-section can be seen in almost all the cases. The disadvantages are the long time (approximately 1 week) taken to form the resin block, the number of steps involved and chemicals needed to prepare the block (Torras *et al.*, 2007). A novel mathematical model was developed by Smith *et al.* (2000a) to correct for the effect of random slicing during TEM sample preparation; the corrected average wall thickness is 92 nm for the yeast cells with the mean diameter of 5.08 μm.

2.4 Modelling to Determine the Young's Moduli of Microparticles

Micromanipulation techniques are very useful to study the mechanical properties of particles of interest; however, the acquired force-displacement experimental data does not represent the intrinsic mechanical properties of microparticles (e.g. Young's modulus). The part of compression data that represents elastic deformation was therefore mathematically modelled by a large number of researchers for microcapsules and other particles; the application of various models is reviewed in detail in the following sections.

2.4.1 Hertz Model

Hertz model is very often applied to study the elastic behaviours of particles. The assumptions made in the Hertz model are as follows (Johnson, 1985):

- The surfaces are continuous and non-conforming.
- The strains are small.
- Each solid can be considered as an elastic half-space.
- The surfaces are frictionless.

Young's modulus can be calculated using Hertz model from Equation 2.2:

$$F = \frac{4E\sqrt{R}}{3(1-\nu_P{}^2)}\delta^{\frac{3}{2}} \tag{2.2}$$

where F is the applied force, E is the Young's modulus of the particle, R is the original particle radius, and ν_P is the Poisson's ratio of the particle, and δ is half of the total compressive displacement.

There has already been a significant amount of research dedicated to the application of Hertz model to determine the Young's modulus of single microspheres at a small elastic deformation. Microspheres have no well-defined wall or envelope compared with microcapsules. Liu *et al.* (1998) fitted the Hertz model to the compressive force-displacement data of single poly(urethane) microspheres (270 μm in diameter) with a deformation up to 10%. Results indicated that Hertz model was in good agreement with experimental results, and the predicted Young's modulus for the particular microsphere is 2.25 MPa. It was reported by Ding *et al.* (2008) that the data of elastic deformation (up to of 10%) of gelatine-rich

microparticles (20-120 μm) fitted well to Hertz model; the Young's moduli of microparticles studied ranged from 68 kPa to 115 kPa, depending on the percentage of the gelatine the microparticles contained. It was demonstrated that Hertz model is valid up to 10% strain of microparticles, which is equivalent to 30% deformation of microparticles (Wang *et al.*, 2005; Yan *et al.*, 2009). Hertz model was also successfully applied to other microspheres such as chromatographic particles (Muller *et al.*, 2005) and Eudragit particles (Yap *et al.*, 2008). Hertz model was also used by Ju *et al.* (2005) to model single microcapsules as a whole identity even though they had core/shell structure. It was found that a urea-formaldehyde biomimetic microcapsule with a diameter of 65 μm had a Young's modulus of 0.987 MPa.

2.4.2 Tatara Model

Since Hertz model is limited to the case of small linear elastic deformation, Tatara (1991) has developed a model for a large elastic deformation of a rubber sphere. Tatara's model is an extension of the Hertz model and can be applied to non-linear elastic material. Tatara model was verified (Tatara *et al.*, 1991) using experimental results from compressing a soft rubber sphere to a large deformation. A significant advantage of Tatara model is that it allows the good fitting of force-displacement data obtained from compression of a sphere to large strain (>15%); the primary drawback is the need for a numerical solution to the governing equations (Liu *et al.*, 1998). Muller *et al.* (2005) also reported a good fitting between compression data of chromatographic particles (30–300 μm) and Tatara model at a higher level of deformation of 50%.

2.4.3 Feng & Yang and Lardner & Pujara Models

In order to extract the information of mechanical property parameters of spherical capsules with filled gas/liquid from the experimental compression data, previous researchers have developed theoretical models to describe their deformation behaviour. Feng & Yang (1973) studied the deformation of a spherical object with a core/shell structure compressed between two frictionless rigid plates. The core gas and shell are nonlinear elastic. It was assumed that the material behaviour of the shell can be appropriately described by Mooney-Rivlin's constitutive equation. The choice of this constitutive equation is important, as it has a significant influence on the model prediction for the given wall material properties (Stenson *et al.*, 2009). The sets of modelling equations proposed by Feng & Yang (1973) are referred to as the membrane theory model in this thesis.

Lardner & Pujara (1980) further developed the membrane theory model, which is called the improved membrane theory model below. Such model was applied to spheres filled with incompressible liquid (e.g. sea-urchin eggs), and the enclosed volume was assumed constant during compression. A dimensionless curve, graph of "Dimensionless force" versus "Fractional deformation", was generated based on the Mooney-Rivlin's constitutive equation (Rubber like material). Dimensionless force, y_L, applied in dimensionless analysis is defined in Equation 2.3 as (Lardner & Pujara, 1980):

$$y_L = \frac{F}{C_1 h r_0 \lambda_s^{\,2}} \tag{2.3}$$

where F is compressive force, C_1 is a material constant related to elastic modules E by the relationship of $C_1 = E/6$, h is shell thickness, r_0 is initial radius of a spherical object, λ_s is initial stretch ratio, defined as $\lambda_s = r_i / r_0$ (Wang *et al.*, 2004). λ_s is considered in the dimensionless

analysis because in some cases when a biological cell is considered, the cell may be inflated by internal pressure; the outer radius of an inflated cell is r_i, which is larger than r_0. Fractional deformation, x_L, applied in dimensionless analysis is defined in Equation 2.4 as (Lardner & Pujara, 1980):

$$x_L = 1 - \frac{\bar{\eta}}{r_0 \lambda_s} \tag{2.4}$$

where $\bar{\eta}$ is the distance between the rigid plate and the equator of the deformed object after contact (Liu *et al.*, 1996). Using the least-squared method to fit the theoretical dimensionless curves to the experimental compression data, i.e. force & compressive displacement of single microcapsules, the extensional rigidity of the shell, *Eh*, was calculated (Liu *et al.*, 1996). With a known value of the shell thickness *h*, elastic modulus *E* could be determined. Moreover, they also calculated the internal pressure, the tension distribution on the shell and the geometric features of the deformation for the microcapsules. λ_s was assumed to equal to 1, as the liquid in the microcapsule suspension was isotonic with the liquid contained in the microcapsules. In summary, Feng & Yang (1973), Lardner & Pujara (1980) and Liu *et al.* (1996) applied a membrane model based on non-linear elastic Mooney-Rivlin material to study mechanical properties of spherical particles with a core/shell structure. In the numerical simulations, the membrane materials were assumed to be incompressible, equivalent to a Poisson's ratio, ν_P, of 0.5.

The above model was also extensively applied to different biological and non-biological samples. Wang *et al.* (2004) determined the Young's modulus of the wall of single

suspension-cultured tomato cells by modelling force-displacement data, using the Larder and Pujara's model, but used a constitutive equation based on linear elastic material, following Cheng's work (1987). The cell wall material was considered to be compressible, with a range of Poisson's ratio 0.3 to 0.5. The governing equations were solved by the Runge-Kutta method, using Matlab (MathWorks Inc.) ode45 solver. It was discovered that the linear elastic model was suitable to estimate the Young's modulus of the wall of single tomatoes cells. The mean Young's modulus for 2-week-old cells was found to be around 2.3 GPa at a pH of 5. The Young's modulus obtained based on the data from micromanipulation technique represents mean modulus of wall material, rather than localized modulus derived from the data of nano-indentation. From the dimensionless curves generated by Wang *et al.* (2004), the fractional deformation, x, is defined in Equation 2.5 as:

$$x = \frac{X}{r_0 \lambda_s} \tag{2.5}$$

where, X is half of the displacement when a cell is compressed. The dimensionless force, y, is defined in Equation 2.6 as:

$$y = \frac{F}{Ehr_0 \lambda_s^{\,2}} \tag{2.6}$$

where E is used instead of C_1 in Equation 2.3.

Liu & Zhang (2004) also adopted the improved membrane theory model to determine the Young's modulus of desiccated ragweed pollen grains by employing the constitutive equation based on linear elastic material, which was previously used by Cheng (1987). The pollen wall was assumed to be incompressible (ν_P=0.5). A good agreement was found between the

theoretical analysis and the experimental data, which gave the mean *Eh* value of 1653 Nm^{-1} for the wall of desiccated pollen grains, but the wall thickness was not determined.

In order to determine the Young's modulus of the wall of poly(urea-formaldehyde) microcapsules, Keller & Sottos (2006) followed the analysis of Wang *et al.* (2004) by choosing the same linear elastic strain energy function (Cheng, 1987) in conjunction with the improved membrane theory model. It was reported that the linear elastic model fits very well with the compression data of poly(urea-formaldehyde) microcapsules; as such, the average Young's modulus of microcapsules wall was estimated to be around 3.7 GPa. Based on the improved membrane theory model, a Hencky strain model with constant elastic modulus has been developed by Stenson *et al.* (2009), which is capable of extracting intrinsic material properties from compression experiments performed on single suspended yeast cells.

The above reviews have demonstrated that, analytical analysis based on the improved membrane theory and the selected linear/non-linear elastic strain-energy functions can be successfully applied to the compression data of various gas/liquid filled spheres to extract the intrinsic material properties, although the analytical method is complicated.

2.4.4 Finite Element Analysis (FEA)

Besides the analytical approach mentioned above, many researchers also used finite element analysis (FEA) coupled with a given material strain energy function to determine the Young's moduli of particles. Moreover, finite element approach offered the advantage of taking into consideration irregularities such as non-spherical cells, local and geometric material

differences (Zhang *et al.*, 2009). FEA is relatively easy for researchers who are familiar with the application of FEA software. Abaqus software was often used for FEA (Burnett, 1987). Smith *et al.* (1998, 2000b) applied FEA and the linear elastic strain energy function (Cheng, 1987) to determine the Young's moduli of yeast cells with permeable cell walls. Rachik *et al.* (2006) employed FEA and each of the material strain-energy functions of Mooney–Rivlin, Yeoh (Yeoh, 1993), STZC (Skalak *et al.*, 1973), and Evans–Skalak (Evans & Skalak, 1980) to the compression data of incompressible capsules (around 1.5 mm in radius) with serum albumin–alginate membrane and saline solution core to determine the Young's modulus of capsule membrane. Nguyen *et al.* (2009a) also successfully applied FEA and visco-elastic material model to determine the Young's moduli of calcium alginate microspheres with diameters between 80-130 μm.

2.5 Measurement of Adhesion

Within the industrial sectors, there is an ever growing need to deliver the perfume constituents from the core of the microcapsules to the surface of fabrics (both woven and non-woven). For such applications, the microcapsules should be able to adhere to fabrics during the washing stage of laundry process. As a result, it is of great importance to study and understand the adhesion between microcapsules and the substrates of interest under ambient condition or in various liquid media.

2.5.1 Generation of Cotton Films

It is difficult to conduct experiments on real fibre samples due to their structural inconsistency (Notley *et al.*, 2006). It is even more difficult to study the adhesion of particle on a single fibre under ambient condition or in the liquid environment. This leads to an increasing interest in developing a well-defined model substrate in order for the relevant research to be performed.

The difficulty of creating model surfaces from cellulose is its reluctance to dissolve in conventional organic and inorganic solvents (Kontturi *et al.*, 2003). Gunnars *et al.* (2002) presents a new method for the preparation of thin cellulose films; NMMO (N-methylmorpholine-N-oxide) was used to dissolve cellulose (wood pulps) and DMSO (dimethyl sulfoxide) was subsequently added to control the viscosity of cellulose solution. The cellulose solution was then placed onto a silicon wafer with approximately 2 nm native silicon oxide layer pre-coated with an anchoring polyvinylamine polymer, which was fixed on a spinning disc so that a thin layer of the cellulose solution was formed on the surface. The cellulose was then precipitated in deionised water. NMMO has the ability to disrupt the intermolecular hydrogen-bond network of cellulose and to form solvent complexes by establishing new hydrogen bonds between the macromolecules and solvent, thereby allowing cellulose dissolution (Rosenau *et al.*, 2001). Further investigations by Falt *et al.* (2004) revealed that the cellulose solution at a higher concentration produces a thicker cellulose film; reducing the temperature of cellulose solution had no effect on the final film thickness but was able to lower the roughness of the generated cellulose film. It was reported that the root mean square (RMS) roughness of a cellulose film over an area of 100 μm^2 was decreased from 9 nm to 7 nm whilst temperature of 0.47wt.% cellulose solution was reduced from 100 ºC to 50 ºC.

Model cellulose surface enables consistent results to be obtained between experiments. For example, Notley *et al.* (2006) performed a systematic study on the surface forces between a cellulose sphere and cellulose thin films as a function of ionic strength and pH. Aulin *et al.* (2008) adopted this method to successfully study the wetting behaviours of oil mixtures on cellulose films. Rosenau *et al.* (2001) reported that different materials, such as cotton, paper grade pulp, unbleached chemical pulp, rayon fibres and waste paper, can be dissolved in NMMO solution to produce fibres. This suggests that the method proposed by Gunnars *et al.* (2002) is feasible to be applied to cotton powder/fibres.

2.5.2 Characterisation of Cotton Films

Ellipsometry measurement of film thickness, contact angle measurement, X-ray photoelectron spectroscopy (XPS) and AFM are widely employed to characterise the properties of surfaces of interest. The applications of these techniques are reviewed in this section, except that AFM technique is further reviewed in Chapter 2.5.3 when its use in adhesion measurement is described.

2.5.2.1 Ellipsometry

Ellipsometry is capable of determining the thickness of single layers or complex multilayer stacks ranging from one angstrom to tens of micrometers. Ellipsometry is an optical non-destructive measurement technique that measures the change in polarized light upon reflection on a sample or light transmission by a sample (Fujiwara 2007). A schematic diagram is

presented in Figure 2.1 to illustrate the ellipsometry system. Light emitted by a light source is linearly polarized using a polarizer, before falling onto the sample. Upon reflection the light passes through an analyzer and is subsequently picked up by the detector, where the change in polarization is determined. The nature of the polarization change is determined by the samples' properties, such as thickness.

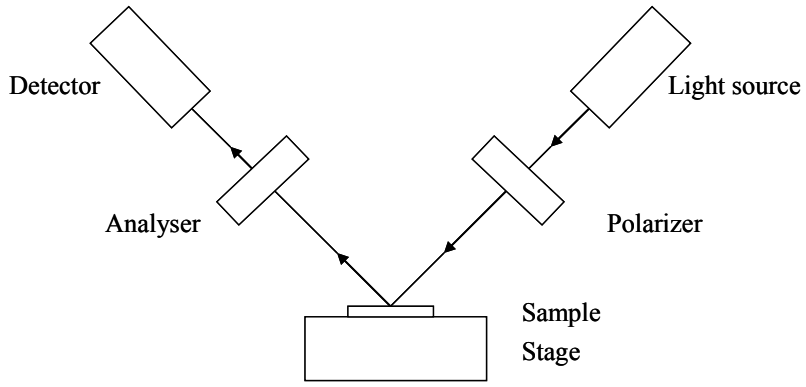

Figure 2.1 Schematic diagram to illustrate the ellipsometry technique.

Not only this technique was able to measure the thickness of silicon oxide layer, anchoring polymer layer and cellulose films (Gunnars *et al.*, 2002; Aulin *et al.*, 2008), but it is also to accurately measure the thickness of self-assembled monolayers (SAMs) at a few nanometers (Bowen *et al.*, 2008; Iqbal *et al.*, 2008; Marten *et al.*, 2008). Moreover, ellipsometry was used to study enzymatic adsorption and degradation of cellulose films; this was achieved by calculating the film mass using a two-component formula involving the mean refractive index and average thickness (Eriksson *et al.*, 2005).

2.5.2.2 Contact Angle Measurement

The contact angle, θ, is the angle between a liquid drop and solid surface where the former is resting on. Taking the wetting of a water droplet on a flat surface as an example, if the contact

angle is less than 90º (Figure 2.2 (a)), the surface exhibits hydrophilic properties; if the contact angle is more than 90º (Figure 2.2 (b)), the surface exhibits hydrophobic properties. Contact angle measurements are usually carried out using photographic techniques coupled with subsequent image analysis. Various liquids can be employed to study their wetting behaviours on the surfaces of interest, e.g. wetting of brine and crude oil on mica surfaces (Yang *et al.*, 1999), and more recently wetting of aqueous solutions of isopropanol (IPA) on polystyrene solid particles (Cheong *et al.*, 2009). Contact angles between water and cellulose surfaces were also measured in order to verify the purity of obtained cellulose films (Gunnars *et al.*, 2002). Contact angle knowledge is very useful in detergent cleaning process, mineral separation process using froth flotation, the design of non-stick cooking utensils and waterproofed fibre production (Israelachvili, 1985).

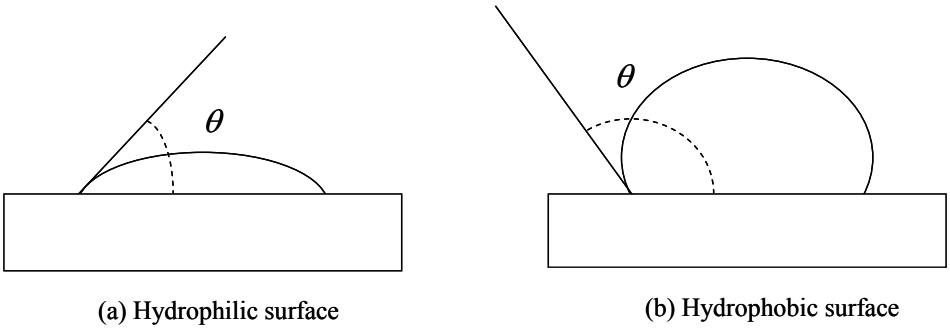

Figure 2.2 Illustration of a drop of water placed on (a) Hydrophilic surface (b) Hydrophobic surface. θ is contact angle.

2.5.2.3 X-ray Photoelectron Spectroscopy (XPS)

X-ray photoelectron spectroscopy (XPS), also called electron spectroscopy for chemical analysis (ESCA), was applied to study the chemical compositions of a large amount of surfaces, e.g. poly(etheretherketone) (Weidenhammer & Jacobasch, 1996), iron oxide on the surface of iron (Bhargava *et al.*, 2007), and SAMs (Bowen *et al.*, 2008). XPS analysis is

applicable to all the elements except hydrogen and helium. An X-ray photoelectron spectrometer consists of three parts: a primary radiation source, a sample stage and an electron energy analyser. They are all contained within a vacuum chamber, preferably operating in the ultra-high vacuum regime. The schematic diagram of an XPS system is illustrated in Figure 2.3.

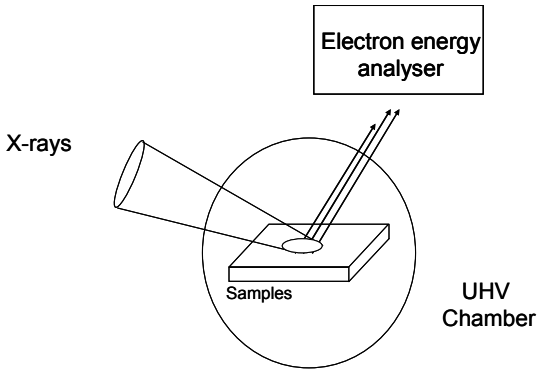

Figure 2.3 Schematic diagram of an X-ray photoelectron spectroscopy system.

The XPS is concerned with a special form of photoemission – the ejection of an electron from the core level by an X-ray photon of energy (Watts & Wolstenholme, 2003). The energy of the emitted photoelectrons is analysed by the electron energy analyser and the data presented as an X-ray induced photoelectron spectrum which is usually expressed as frequency (counts/s) versus binding energy. The binding energy is a parameter that indentifies the specific electron, in terms of both of its parent element and atomic energy level. In order to verify the purity of cellulose films produced, XPS was employed to analyse whether traces of nitrogen originating from the solvent NMMO are retained after production (Gunnars *et al.*, 2002; Aulin *et al.* 2008).

2.5.3 Force Measurement–Atomic Force Microscopy (AFM)

Atomic force microscopy (AFM) is one type of scanning probe microscopy (SPM), which consists of a family of microscopy forms where a sharp probe with a diameter approximately 20 nm is used to scan across a surface, and the probe-sample interactions are monitored. The first microscope in SPM family, scanning tunnelling microscope (STM), was built by Binnig *et al.* (1982); the most important feature of STM is the real-space visualization of surfaces on an atomic scale. While STM is limited to imaging the surfaces of conducting and semiconducting materials, an atomic force microscope was invented by Binnig *et al.* (1986) to enable the detection of atomic scale features of both conducting and insulating surfaces. The AFM technique is considered to be non-destructive and the lateral resolution can be of the order of angstroms (Meyer *et al.*, 1989). STM and AFM are by far the most advanced scanning probe methods and the only ones providing atomic-resolution images. AFM has much broader applications than STM and is currently the dominant scanning probe technique (Magonov & Whangbo, 1996). AFM studies are divided into topographical applications (imaging mode) and force spectroscopy, i.e. measuring force as a function of distance (Leite & Herrmann, 2005).

Many other techniques, such as surface forces apparatus (SFA), osmotic stress method and total internal reflection microscopy (TIRM), have allowed accurate measurement of surface and intermolecular forces. However, only a limited number of systems could be investigated because of the restrictions on material properties and the complexity of the equipment (Butt *et al.*, 2005). In contrast, AFM is relatively easy to use and can be applied to small samples due to its high lateral resolution. AFM has two distinct advantages over SFA. Firstly, AFM is able

to measure forces as small as 10^{-11} N but more commonly in the range of 10^{-9} N or larger, e.g. interparticle interaction forces in liquids (Hodges *et al.*, 2002). Secondly, AFM can be applied on the surfaces of opaque materials (Lea *et al.*, 1994).

2.5.3.1 Working Principles

Two types of atomic force microscopes, Dimension 3100 (D3100) AFM & MultiMode AFM (Digital Instruments, Santa Barbara, CA), are commonly employed by researchers, and they share the same working principles. The difference is that D3100 AFM consists of a stationary sample stage and a movable cantilever holder, whilst in MultiMode AFM, the sample stage moves with respect to a stationary cantilever holder. Both D3100 AFM and MultiMode AFM are capable of scanning images and measuring adhesive forces. The benefit of using MultiMode AFM, however, is that it is equipped with a fluid cell and relatively thermally stable, and adhesive force in liquid could be measured. D3100 AFM is generally used to measure adhesive force under ambient condition. Taking D3100 as an example, the working principle of AFM is described below.

The schematic diagram of an AFM system is shown in Figure 2.4. A piezoelectric scanner (piezo) holding the cantilever substrate, moves away or towards a sample placed on the stationary stage of an atomic force microscope periodically at a specified rate. The maximum distance the piezo travels is defined as Z scan range. Due to the presence of adhesive or repulsive force between the cantilever tip and sample, the cantilever will bend downwards or upwards prior to contact. The top surface of cantilever reflects the laser beam emitted from a

laser diode, and spatial change in the reflected laser beam due to deflection of cantilever is collected by a position sensitive photodiode (Veeco, 2000; Luckham, 2004).

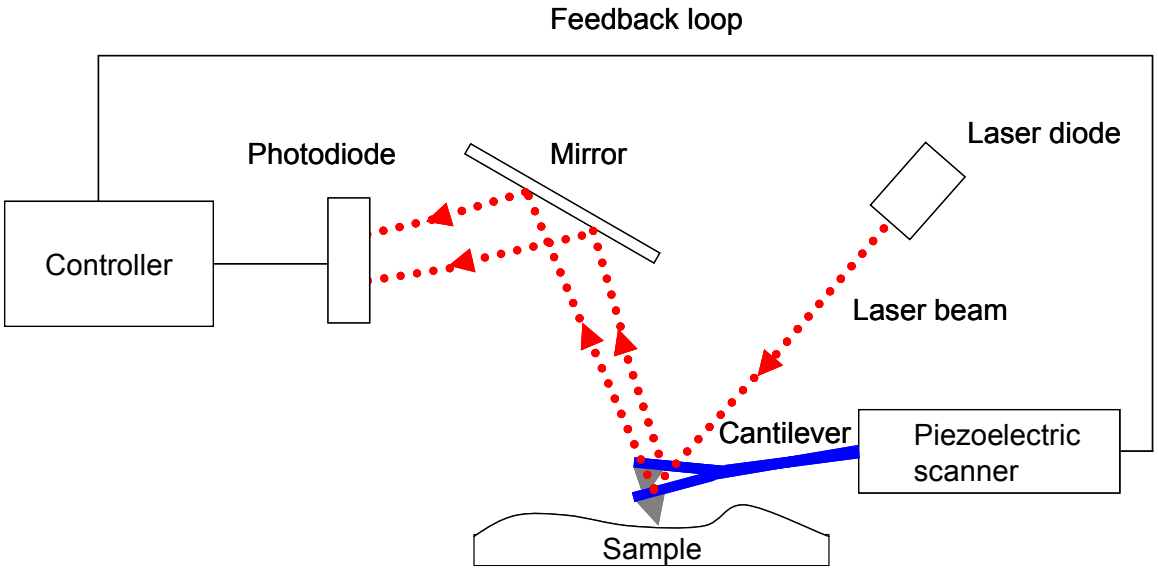

Figure 2.4 Schematic diagram of an AFM system.

2.5.3.2 Operating Modes

There are three types of operating modes in AFM: contact, tapping and non-contact modes. In contact mode, AFM operates by scanning across the sample surface with a tip attached to the end of a cantilever, whilst monitoring the change in cantilever deflection with a split photodiode detector. Here the cantilever tip is always in contact with the sample surface (Veeco, 2000). It is most suitable for rough and very rough surfaces, which commonly feature in real samples (Kaupp, 2006).

In tapping mode, AFM operates by scanning across the sample surface using a tip attached to the end of an oscillating cantilever. As such, the probing tip is periodically in contact with the sample surface, and surface structure is determined from the change of the oscillation

amplitude or phase of the oscillating cantilever (Sugawara, 2007). Since the tip is not in constant contact with the surface, both tip and sample degradations are minimized (Zhong *et al.*, 1993). Tapping mode is particular useful for delicate samples which may be damaged by imaging in the contact mode (Attard & Barnes, 1998).

In non-contact mode, the cantilever tip is not in contact with the sample surface; the sample structure is obtained from the change of vibration amplitude or resonant frequency of the oscillating cantilever. Although non-contact mode is ideal to study delicate samples, the cantilever tip tends to be affected by van der Waals attraction and then trapped in the liquid layer on the sample surface, due to small oscillation amplitude of cantilever (Zhong *et al.*, 1993).

2.5.3.3 Surfaces Imaging

Surface imaging using AFM confers significant advantages over other techniques; a resolution down to the atomic level can be achieved in a variety of environments, without the need for ultrahigh vacuum or other constraining environments as required by other techniques (Gewirth & LaGraff, 1995). Furthermore, AFM works equally well on insulating and conductive samples; this is not the case with either STM or the various scanning electron microscopes, e.g. SEM. AFM offers the possibility to measure the surface roughness at a resolution of ±0.1 nm. Although the imaging capability of AFM is superior, it is restricted to surface imaging and analysis only (Reimer & Kohl, 2008). The great capability of AFM to image non-conducting materials makes it ideal to characterize polymer surfaces at high resolutions. Two and three dimensional topographical views of cellulose films can be obtained. It is able to

determine a mean surface roughness of 5.0 nm to 6.2 nm of the analysed films, based on a scanned area of 1 μm^2 (Gunnars *et al.*, 2002; Aulin *et al.*, 2008).

2.5.3.4 Cantilevers & the Colloidal Probe Technique

A cantilever tip, if available, is often located at the apex of cantilever or a few micrometers away from the apex. Two types of AFM cantilevers are commercially available: rectangular-shaped and "V"-shaped, which are made of Si and Si_3N_4, respectively. It should be noted that Si cantilevers are usually stiffer than Si_3N_4 cantilevers. The back face of Si_3N_4 cantilever is usually plated with a layer of thin metal (often gold) to enhance reflectivity, especially in liquid where the reflectivity of Si_3N_4 is much reduced (Cappella & Dietler, 1999).

Tipless cantilevers are also available for attaching particles of interest to the cantilevers to measure their adhesion properties. This is sometimes called colloidal probe technique. The benefits of a colloidal probe technique were summarized by Butt *et al.* (2005): (1) The adhesive force can be analyzed more quantitatively with smooth spherical particles of defined radius; (2) it enables a variety of probing surfaces by attaching particles of different chemical composition to the cantilevers; and (3) it permits the measurement of hydrodynamic force.

Colloidal probe technique was first utilized by Ducker *et al.* (1991) who attached a silica sphere with a radius of 3.5 μm onto the apex of a tipless cantilever. It allowed the measurement of adhesive force between silica particle and silicon oxide surface in NaCl solution. Colloidal probe technique has also been used by other researchers to study the interaction force between specific particles and surfaces of interest with or without the

background electrolyte solutions, such as zirconia agglomerate and flat zirconia surface in the presence of polyvinyl pyrrolidone polymer (Biggs, 1996), yeast cells (Saccharomyces cerevisiae) and polymeric ultrafiltration membranes (Bowen et *al*., 1999), yeast cells and mica surfaces rendered with various properties including hydrophilic, hydrophobic or coated with protein (Bowen *et al*., 2001a), polystyrene spheres and stainless steel surfaces (Bowen *et al*., 2001b), glass beads and bacterial surfaces (Li & Logan, 2004), cellulose spheres and cellulose surfaces (Notley *et al.*, 2006).

To the best of the authors' knowledge, there is no published research on attaching single microcapsules to the tipless cantilever to be used as the colloidal probes, not to mention the direct measurement of adhesion between MF microcapsules and cotton films. Although Leporatti *et al*. (2006) utilized the colloidal probe technique to attach single rigid MF microparticles to tipless cantilevers, only the adhesion between MF microparticles (10 μm in diameter) coated with human serum proteins and macrophage was investigated. As a result, little information is known on the adhesion between MF microparticle and cotton films under ambient condition or in the liquid.

2.5.3.5 Cantilever Calibration

It is of great importance to accurately determine the stiffness of cantilever (Matei *et al.*, 2006). Clifford & Seah (2005) gave a comprehensive review of three principal methods to calibrate spring constants of cantilevers: (1) Dimensional, (2) Static experimental and (3) Dynamic experimental. In dimensional method, the spring constant of cantilever is determined from the elastic modulus of cantilever material and the geometrical properties, i.e. length, width and

thickness (Butt et *al.*, 1993); the drawback is that elastic modulus of the cantilever material is required and the thickness of cantilever is often difficult to measure (Neumeister & Ducker, 1994). Static experimental method uses a pre-calibrated reference cantilever to push on the cantilever under test (Tortonese and Kirk, 1997). In this case, the limitation is that matching spring constants are required for the two cantilevers used. Dynamic experimental method usually involves finding the cantilever's resonant frequency in air (Cleveland *et al.*, 1993) which is only applicable to rectangular cantilevers. Alternatively, thermal noise analysis (Hutter, 1993) can also be used, but it is generally suitable for soft cantilevers that possess low spring constant. Consequently, the calibration method of cantilevers to be employed depends on parameters such as, geometry, softness or stiffness of the cantilevers.

2.5.3.6 Force Curve Analysis

A typical output of AFM measurement is a force curve (see Figure 2.5), which shows the deflection of the cantilever as it contacts and separates from the sample during the extension and retraction of the piezo (Veeco, 2000). *y*-axis denotes the deflection of cantilever, while x-axis indicates the distance the piezo approaches or retracts in respect to the sample. Figure 2.5 also illustrates the schematic labelling which corresponds tip-sample interaction points to the respective regions in force curve. In Figure 2.5, solid line denotes extending curve, while dotted line denotes retracting curve. Curve A shows that piezo is approaching the sample. At curve B, the cantilever jumps to contact with sample surface due to attractive force, which is calculated from the deflection of cantilever incurred due to the "Jump to contact" action. The curve represented by curve C shows that cantilever remains in contact with sample while the piezo continues to travel down. When piezo moves to the lowest position, it will move

upwards while cantilever is still in contact with the sample, which is shown by curve D. When cantilever is finally pulled off from the surface, another deflection is incurred at curve E. The deflection of cantilever during the "Pull-off" phase is due to the adhesive force between cantilever tip and the sample. Hence, the adhesive force, F, can be calculated by Hooke's law, as shown in Equation 2.7:

$$F = -kx_c \tag{2.7}$$

where k denotes the spring constant of cantilever, and x_c refers to the deflection of cantilever.

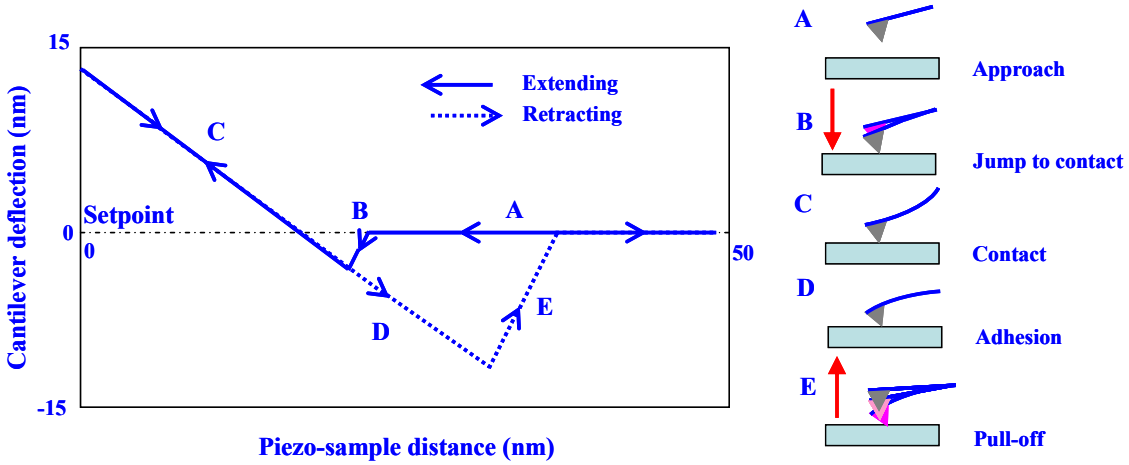

Figure 2.5 Typical force curves with schematic labelling corresponding tip-sample interaction points.

However, the distance between the piezo and the sample in Figure 2.5 does not reflect the real distance between the cantilever tip and the sample due to the deflection of cantilever; a schematic diagram is used to illustrate the former and latter distances as shown in Figure 2.6. The relationship between them was reported by Cappella & Dietler (1999) and expressed in Equation 2.8:

$$D = Z - (\delta_c + \delta_s) \tag{2.8}$$

where the tip-sample separation, D, is the actual tip-sample distance and Z is the distance between the sample and the cantilever rest position (piezo); δ_c denotes the deflection of cantilever and δ_s is the deformation distance of sample. δ_s in Equation 2.8 will reduce to zero if the deformation of sample is negligible as shown by Butt *et al.* (1995).

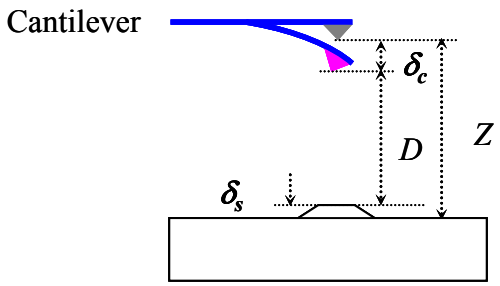

Figure 2.6 Illustration of tip-sample distance.

It is sometimes important to convert the "Force vs. Piezo-sample distance" graphs to the "Force vs. Tip-sample separation" graphs for determination of the exact distance between the tip of cantilever and the sample. The conversion of graphs was illustrated in detail by Hillier *et al.* (1996). By applying the procedures, Figure 2.5 can be converted to Figure 2.7.

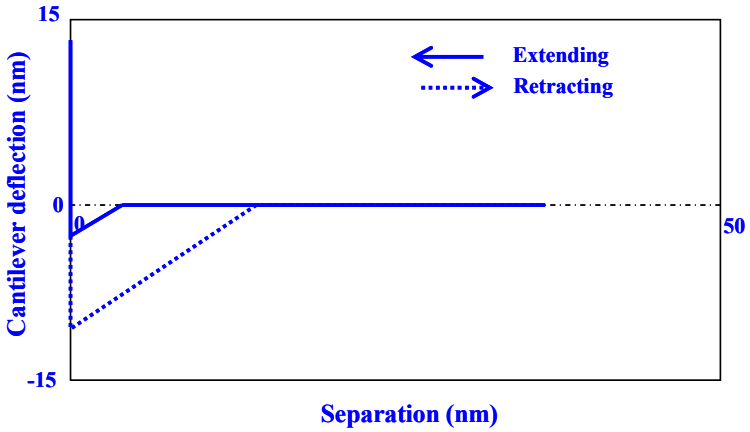

Figure 2.7 Force curves illustrating tip-sample separation distance.

2.5.3.7 Force Measurement under Ambient Condition

The particle-surface adhesive forces under ambient condition (in air) were recognized as van der Waals forces, capillary forces, contact forces and electrostatic forces (Jones *et al.*, 2002). van der Waals forces are omni-present and significant for smooth contact in all conditions, but relatively small in comparison to other forces with relatively rough surface under ambient condition.

Water moisture in air can condense around the contacting surface during capillary condensation; it has a profound effect on the strength of adhesion joints (Israelachvili, 1985). The humidity of air is a major contribution to the adhesion of particles to a substrate under ambient condition via capillary condensation (Visser, 1995), as shown in Figure 2.8.

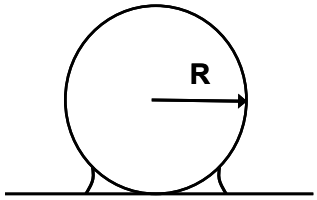

Figure 2.8 Illustration of water between a sphere of radius *R* and a flat plate in humid air due to capillary condensation.

Capillary force between particles and surfaces becomes the dominant adhesion forces above ~40% relative humidity (RH). The equation for capillary force, F_C, describing "sphere-on-flat" geometry can be expressed in Equation 2.9 as (Jones *et al.*, 2002):

$$F_C = 4\pi R\gamma_L \cos\theta_c \qquad (2.9)$$

where θ_c is the contact angle of water on the two surfaces of sphere and substrate (assuming identical θ_c). R denotes radius of sphere; γ_L is surface tension of liquid. This equation neglects

(i) any contribution to adhesion from the solid-solid interaction across the liquid bridge; (ii) any existing condensed liquid film before the surfaces is brought into contact. Equation 2.9 is normally applied to approximate the adhesion between a smooth sphere and a flat smooth substrate at zero separation distance (Rabinovich *et al.*, 2002). The capillary force between two spheres was also studied by Rabinovich *et al.* (2005) to control and modify the flow behaviour of powder systems. This work in turn aids to avoid segregation in key industrial processes, such as powder mixing. Capillary adhesion force was also noticeably lower in the presence of nanoscale roughness (Rabinovich *et al.*, 2002).

Young *et al.* (2003) studied the adhesion between salbutamol sulphate drugs using AFM. It was reported that capillary forces become the dominant force with an increase in humidity (15%-75% RH). Research carried out by many workers also revealed that the increase in RH leads to the increase in capillary forces (Fuji et *al.*, 1999; Quon *et al.*, 2000). Garoff and Zauscher (2002) reported that the degree of capillary condensation can be effectively suppressed by increasing the hydrophobicity of the contacting surfaces, which resulted in a decrease in adhesion.

For contact between hydrophobic surfaces, the adhesion is relatively small and constant over the full spectrum of RH compared to that between hydrophilic surfaces, where the contact force, F_J, can be explained by JKR (Johnson-Kendall-Roberts) theory as shown in Equation 2.10 (Jones *et al.*, 2002):

$$F_J = -3\pi R\gamma_{SV} \qquad (2.10)$$

where R is the sphere radius and γ_{SV} is the solid-vapour interfacial energy. The JKR theory can be applied in the case of larger and softer particles with a large adhesive force. For the case of smaller and harder particles with a small adhesive force, the DMT (Derjaguin-Muller-Toporov) theory is used to approximate the contact forces (Butt *et al.*, 2005).

Surface roughness can have a significant influence on the adhesion (Rabinovich *et al.*, 2000a; Rabinovich *et al.*, 2000b). Root mean square (RMS) roughness is often used to describe the roughness of surface, which represents the standard deviation of spatial height within a given area of sample surface. Electrostatic forces contribute to the adhesion of dry particles and are often noticeable in transport of powder through a pipe or in a fluidized bed; the electrostatic effects can be nullified by charge leakage, i.e. through moisture (Visser, 1995). The electrostatic forces are never seen at RH values greater than about 40% where rapid discharge is possible, and are not present either on good conductors, e.g. silicon, which could dissipate charges (Jones *et al.*, 2002).

2.5.3.8 Force Measurement in Liquid

Another great benefit of AFM is that the sample and probe can be fully immersed in liquid, so that the adhesion can be measured in a wide range of environments. The immediate conclusion from such measurements is that the adhesion is much reduced (Kendall, 2001). Weisenhorn *et al.* (1989) reported that typical adhesive force measured between a standard silicon nitride AFM tip and a mica surface in ambient air was about 100 nN; however, this reduced by a factor of 100 to about 1nN, by simply immersing the sample in water. The reason is that the capillary forces disappear when the entire cantilever and sample are completely submerged in

liquid (Prater *et al.*, 1995). Luckham (2004) summarized that there are three main types of colloidal forces:

- van der Waals interactions
- Electrical double layer repulsion
- Steric interactions

In addition, hydrophobic and solvation forces may also be important.

van der Waals forces are always present, such as intermolecular forces (Israelachvili, 1985). Electrical double layer interaction is that, if a charged interface exists in a polar solvent, then ions of opposite charge are attracted to that surface. Entropy ensures that the ions do not all adsorb onto the surface, leaving the ions to exist as a diffuse layer close to the charged surface (Luckham, 2004). DLVO (Derjaguin–Landau–Verweij–Overbeek) theory is usually used to describe the contribution of the van der Waals attraction and the electrical double-layer repulsion to the interaction between two particles in salt solution (Butt *et al.*, 2005). At low salt concentration, the double-layer repulsion keeps the colloidal particles apart. With the increase of salt concentration, the electrostatic repulsion is more and more screened due to the dissipation of charges. As a result, the van der Waals attraction overcomes the repulsive electrostatic barrier at a certain concentration and adhesion is therefore observed. The interaction forces agree very well with the DLVO theory in various systems, such as, between silica surfaces (Ducker *et al.*, 1992), gold–gold surfaces or silica–gold surfaces (Giesbers *et al.*, 2002) or cellulose surfaces (Notley *et al.*, 2006) as a function of NaCl concentration and pH.

When a polymer is adsorbed to the surface, some parts of the polymer adsorb to the surface and other parts extend to the medium from the surface. When two polymer-covered surfaces approach each other, they experience a force once the outer segments are brought closely, which usually leads to a repulsive force. In the case of polymers, this repulsion is usually referred to as the steric interaction (Israelachvili, 1985). This repulsion is caused by an increasing concentration of polymer in the gap, giving rise to a surge in osmotic pressure (Luckham, 2004). The repulsion of steric interaction was also observed by Lea *et al.* (1994) when they studied the interaction between silicon nitride surface coated with monomethoxypolyethylene glycol polymer and a silicon nitride cantilever tip in 0.1 M KNO_3 solution. The repulsive force gradually decreased with the addition of $MgSO_4$ until it finally vanished, revealing the attractive force that was being masked. It was interpreted that the addition of $MgSO_4$ generated a poor solvent condition for the polymer chains, and therefore eliminated the steric repulsive force through a collapse of the tethered chains.

Camesano & Logan (2000) found that the steric repulsion between a silicon nitride cantilever tip and the polymer present on bacteria surface increased with rising pH in background solutions. The observation was attributed to the fact that the polymer units have high charges at high pH, leading to a strong intra-molecular repulsion between individual units of the polymer and therefore causing such units to extend into solution. While the polymer was removed from bacterial surface, the repulsion behaviour was significantly reduced, which is a proof of the mechanism of steric interaction. Steric repulsion was also observed elsewhere, such as the interaction between a silicon nitride cantilever tip and a biopolymer surface in electrolyte solution (Abu-Lail & Camesano, 2003), or between glass beads and polymers on

bacterial surfaces (Li & Logan, 2004). The steric interaction explains not only the interaction of polymer related surface, but also the repulsion between a silicon nitride cantilever tip deposited with carbon microtips and protein neurofilament that resembled the grafted polymers in NaCl solutions (Brown & Hoh, 1997). The repulsion is caused by the sidearms of neurofilament forming an entropic brush, thereby providing a mechanism for maintaining spacing between surfaces.

Solvation forces, also referred to hydration, structural or hydrophilic forces, are short-range (<5 nm) repulsive forces compared to the long range forces of electrical double layer forces and van der Waals forces (Butt *et al.*, 2005). Solvation forces arise whenever water molecules bind to surfaces containing hydrophilic groups (i.e. H-bonding groups). Solvation forces were observed between the interaction of silicon nitride cantilever tip and glass surface in water (Hoh *et al.*, 1992). Hydrophobic interaction describes the unusually strong attraction between hydrophobic (i.e. hydrocarbon) surfaces in the water, which is often stronger than their van der Waals interaction in free space (Israelachvili, 1985).

2.6 Conclusions and Objectives of This Work

This chapter introduces the compositions of commercial available detergents as well as the problems encountered due to the direct inclusion of perfume constituents into them. It was reported in the literatures that the problems can be overcome by encapsulating perfume constituents into microcapsules. The extensive applications of microcapsules in a variety of industrial sectors as well as the different types of encapsulation methods are also summarized. A range of measurement techniques used to characterise a population of microcapsules or

single microcapsules were introduced. Their principles, advantages, drawbacks and previous applications were reviewed in detail. It has been demonstrated that the micromanipulation technique based on compression of single particles between two parallel surfaces is a very powerful tool and is able to characterise the mechanical properties of a large variety of single particles including microcapsules. Mechanical strength parameters such as rupture force, nominal rupture stress were used in the literature to compare the mechanical strength of microparticles, but their limitations were seldom addressed. Therefore, one of the objectives of this work is to study the applicability and limitations of various mechanical strength parameters. This work is also to determine another key mechanical strength parameter such as rupture stress, which accounts for the deformation of microcapsule at rupture and was not often reported in the literatures. In order to achieve this, the appropriate modelling methods need to be applied to determine the contact area of microcapsules during compression.

MF microcapsules produced by in-situ polymerisation are widely used in industries for various applications. However, understanding of the effect of formulation and processing conditions on the mechanical strength of MF microcapsules is so far rather limited. Therefore, another objective of this work was set to study the mechanical properties of MF microcapsules and indentify the factors which influence the mechanical strength of MF microcapsules by performing rupture tests, and also to examine how the mechanical strength of MF microcapsules is affected by change of formulations and processing conditions. Various models which were employed to determine the intrinsic mechanical properties of microparticles (e.g. Young's modulus) were reviewed. In particular, the analytical membrane theory developed by Feng & Yang (1973) and Lardner & Pujara (1980) in conjunction with

the linear elastic model (Keller & Sottos, 2006) was demonstrated to give good fitting to the compression data obtained from the micromanipulation technique, and hence Young's modulus of the poly(urea-formaldehyde) microcapsule wall was determined, although the analytical method is complicated. Literatures also suggested finite element analysis (FEA) coupled with the material model is a very powerful method to model the compression behaviour of microparticles. Since the Young's modulus of MF microcapsule wall was seldom reported in the literatures, another objective of this work is to determine the Young's moduli of MF microcapsules by applying appropriate modelling.

A novel technique described in the literature was able to generate cellulose films from wood pulps. Hence, another objective of this work is to develop such technique further to generate cotton films by dissolving cotton powder/fabrics. As such, the problems regarding inconsistency in cotton fabric surface could be eliminated for the adhesion measurements. The principles and applications of various techniques that are applicable to characterise cellulose films were also reviewed. An AFM technique was demonstrated to possess many advantages over others for measurement of adhesion between microparticles and surfaces of interest. The working principle and operating modes of AFM were described in detail. Furthermore, the literature regarding adhesion and their mechanisms between particles and surfaces under ambient condition or in the various liquid media are also reviewed in this chapter. It was found that there is no published work on the adhesion between MF microcapsules/microparticles and cotton surfaces, hence, the final objective of this work is to employ the AFM technique to investigate the adhesion between MF microcapsules and cotton films under ambient condition

as well as in the liquid of detergent and surfactant solutions with a variation of concentrations and pH.

3. MATERIALS AND METHODS

This chapter introduces the materials, techniques and all the experimental procedures applied in this work. It is divided into two sections. The first section concerns on techniques to measure the mechanical properties of single microcapsules. The second section describes the techniques and procedures used to generate and characterise cotton films, as well as the AFM technique employed to measure the adhesion of single microcapsules/microparticles on them.

3.1 Characterisation of Melamine Formaldehyde (MF) Microcapsules

3.1.1 Materials

All the melamine formaldehyde (MF) microcapsule samples used in this work, which had mean diameters ranging from 5 μm to 50 μm, were supplied by Procter & Gamble (Cincinnati, USA and Newcastle, UK). The microcapsules were produced by an in-situ polymerization technique described in a US Patent 4552811 (Brown & Bowman, 1985) with a variation of parameters such as polymerisation time, production scale and drying techniques; more details of these are specified in Chapter 4 & 5. The detailed procedures of in-situ polymerisation technique can be found in Sun & Zhang (2001) and the major steps of such technique to prepare MF microcapsules are illustrated in Figure 3.1, in which some parameters were varied for samples of interest including core/capsule ratios or polymerisation time. The wall of microcapsules was made of melamine-formaldehyde polymer and acrylamide/acrylic acid copolymer, and the core content was a perfume oil based industrial precursor. MF microcapsule samples with core contents ranging from 80 wt.% to 95 wt.% were characterised.

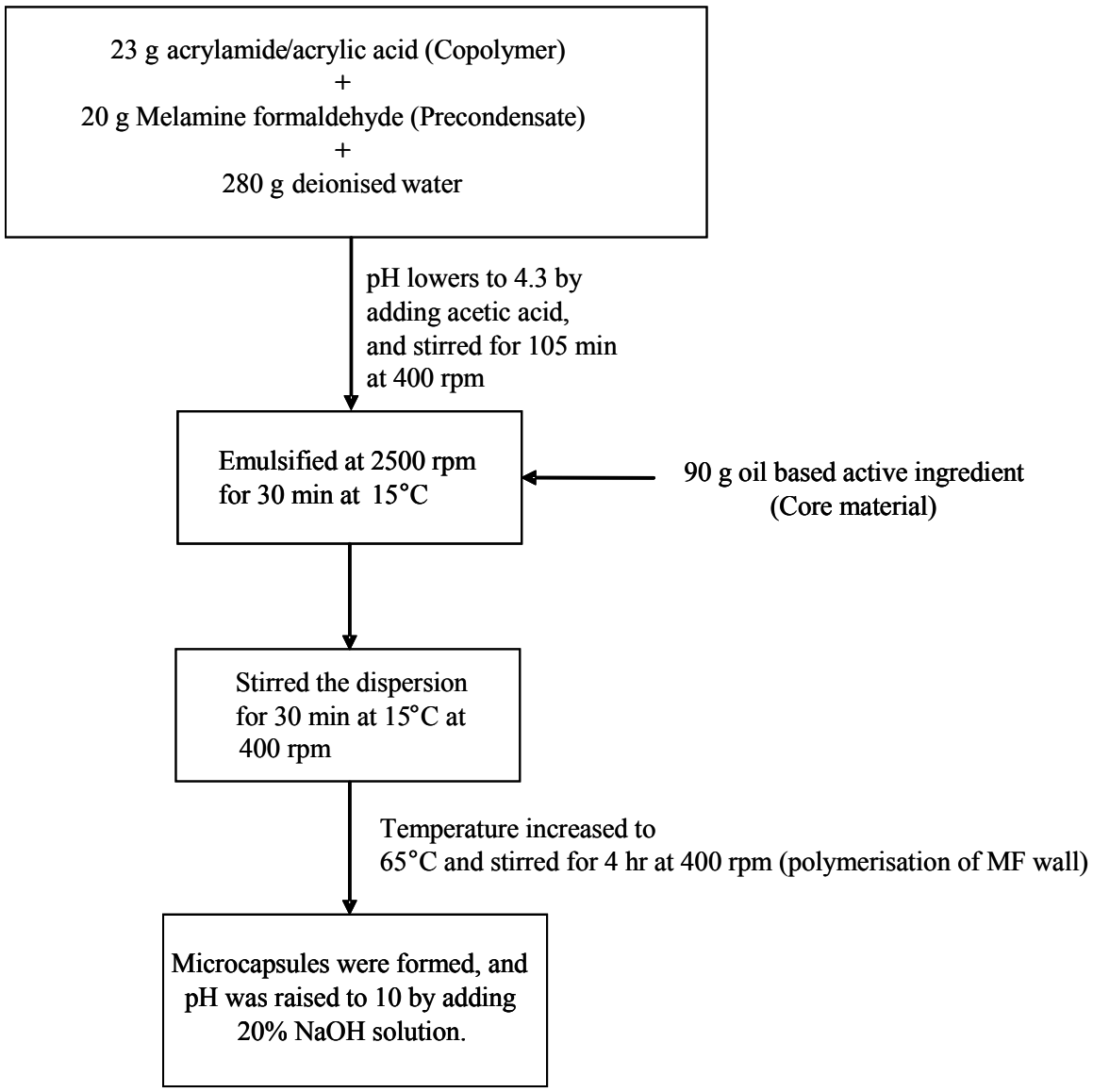

Figure 3.1 Schematic diagram to illustrate the in-situ polymerisation technique to produce melamine formaldehyde microcapsules.

3.1.2 Light Scattering Technique

A Malvern Mastersizer (APA2000, Malvern Instruments Ltd., UK) was employed to measure the volume weighted mean diameter and size distribution of microcapsules in aqueous suspension; and it is capable of measuring particles from 0.02 to 2000 microns in diameter (Malvern, 2007). The technique is based on Mie theory which is developed to predict the way light is scattered by spherical particles and deal with the way light is adsorbed by the particles. Some specific information about the particle needs to be known, such as its refractive index. The microcapsules in suspension were first gradually added into the sample dispersion unit, until the Mastersizer indicated that the ideal concentration had been achieved. The detector array, made up of many individual detectors, collects the light scattering patterns of particles that pass through the analyser beam. The refractive index used for the measurement and data analysis is 1.65, based on the value suggested by Brydson (1999) for the melamine formaldehyde polymer. The results presented in this work are the mean of 3 measurements per sample.

3.1.3 Optical Microscopy

Certain microcapsule slurries contained special chemicals that had created microcapsule aggregates. Hence, it was impossible to separate single microcapsules from the aggregates using only the stirrer in sample dispersion unit of the Malvern Mastersizer; this resulted in acquisition of inaccurate size distribution results. An optical microscope (Leica DM RBE, Leica Microsystems GmbH, Germany) was therefore employed to observe the appearance of microcapsules that were dispersed in water. The images of microcapsules were captured by an optical microscope equipped with Leica QWin Pro V2.8 software (Leica Microsystems

Imaging Solutions Ltd., UK). The images acquired were used to identify any aggregation of microcapsules in order to verify the data obtained from the Malvern Mastersizer described in Chapter 3.1.2. Around 5 to 10 images were obtained for every microcapsule sample being studied.

3.1.4 Environmental Scanning Electron Microscopy (ESEM)

An environmental scanning electron microscope (Philips XL30, The Netherlands) was used to investigate the morphology of microcapsules. Unlike other techniques, such as transmission electron microscopy (TEM), special specimen-preparation methods are rarely required in ESEM (Reimer & Kohl, 2008). ESEM is able to operate at two modes: dry mode (high vacuum) or wet mode (low vacuum). The examination of the microcapsules was conducted in dry mode at an accelerating voltage of 15 kV. When using dry mode in ESEM, it acts as a normal scanning electron microscope.

Microcapsules were first coated with a layer of gold with thickness of 5-6 nm in a sputter coater (Polaron S07640, Quorum Technologies Ltd, UK) to render microcapsule surface conductive before being examined in ESEM. This prevents charges from building up on sample surface that affects the quality of ESEM imaging. It was reported that within a range of accelerating voltages between 5 kV and 20 kV, MF microcapsules were undamaged by radiation within 1 minute of exposure time in dry mode (Ren *et al.*, 2007). Hence, it was always ensured that the exposure time of microcapsules in ESEM was well below 1 minute during the investigation of MF microcapsules. On average, five to ten ESEM images were acquired for every microcapsule sample.

3.1.5 Transmission Electron Microscopy (TEM)

Transmission electron microscopy (TEM) was employed to image the cross-sections of microcapsules and subsequently measure their wall thicknesses. The microcapsule samples were prepared prior to TEM examinations at Centre of Electron Microscopy of The University of Birmingham. The microcapsule preparation procedures were adapted from procedures that were used to prepare yeast cells (Smith *et al.*, 2000a). The following paragraphs highlight major steps to prepare microcapsule samples.

2 mL of microcapsule suspension was placed in an Eppendof tube and centrifuged at 2000 rpm for 1 min in a centrifuge (Biofuge B, Heraeus-Christ; Radius = 58 mm). The supernatant was removed before adding 1.5 mL of 2.5% glutaraldehyde in phosphate buffer solution. The purpose was to increase the mechanical strength of microcapsule wall and to ensure the wall of microcapsule was intact during preparation processes. After being shaken briefly, it was allowed to stand for 1 hour in a fridge at 4 ºC. The mixture in the Eppendof tube was once again centrifuged at 2000 rpm for 1 minute, and the excessive glutaraldehyde solution was then removed. Multiple dehydration steps were subsequently performed to remove water that is immiscible with the resin used in the later stage. The dehydrations were carried out by adding 50% graded ethanol/water solution and the mixture was let to settle for 30 minutes before it was centrifuged at 2000 rpm for 1 minute; and then the supernatant was removed. Similar dehydration procedures were performed with addition of 70%, 90% and 100% ethanol, respectively.

After dehydration, the resulting microcapsules were added to a mixture of Ethanol/LR white acrylic resin (50:50 weight ratio) (London Resin Company Ltd., UK) mixture, which was rotated in a rotator (Agar Scientific, UK) at the speed of 4 rpm for 12 hours before being embedded in 100% resin. The purpose of using resin was to support the sample matrix for trimming and sectioning. After the supernatant was removed, the microcapsules were then embedded in fresh 100% pure resin, and then continued to be rotated in the rotator for 2 days at 4 rpm to ensure thorough infiltration of the resin into microcapsules.

After the supernatant was again removed, one drop of microcapsule/resin mixture was then put into a commercially available gelatin capsule (0.37 ml in volume, 6 mm in diameter, Agar Scientific, UK) containing pure LR white resin. The gelatin capsule provides a convenient and economical means of producing resin blocks for sectioning. It is made of pure gelatin and easy to be removed from the resin block prior to sectioning. The gelatine capsule filled with resin and microcapsules was subsequently sealed with its cap to exclude air. The gelatin capsule was then placed in an oven at 60 ºC for 12 hours where polymerization took place. An ultramicrotome (Ultracut E, Reichert-Jung, Austria) was then employed to trim and section the polymerized resin block to ultrathin sections with thickness of approximately 80 nm. The commonly adopted "Staining" step introduced in the preparation of yeast cell procedures for wall thickness measurement (Smith *et al.*, 2000a) was not required here, as the ultrathin microcapsule sections could be clearly viewed under TEM without staining.

The ultra thin sections were imaged with a transmission emission microscope (Joel 1200EX, Joel UK Ltd, UK). The images showing cross-sections of microcapsules were captured at an

acceleration voltage of 80 kV. The acquired images were then analysed using ImageJ software (National Institute of Health, USA). Assuming microcapsules have perfect spherical shape, the measured wall thickness H_i can be determined using Equation 3.1 (Smith *et al.*, 2000a):

$$H_i = R_o - R_i = \sqrt{\frac{A_{outer}}{\pi}} - \sqrt{\frac{A_{inner}}{\pi}} \qquad (3.1)$$

where R_o is measured outer radius and R_i is measured inner radius; A_{outer} and A_{inner} are the outer and inner cross-sectional areas, respectively.

As TEM sections were cut at random distance from the microcapsule centre, the apparent radii and wall thicknesses of microcapsule as seen from the cross-sectional image are the functions of this random distance. In order to determine the real wall thickness of the microcapsule, a novel mathematical model (Smith *et al.*, 2000a) was employed to correlate the measured wall thickness to the real wall thickness. A thickness correction factor of 0.6 suggested by Smith *et al.* (2000a) was adopted in this work to determine the mean wall thickness and radius of the microcapsules from TEM images.

3.1.6 Micromanipulation Technique

3.1.6.1 Micromanipulation Rig

A well established micromanipulation technique (Zhang *et al*., 1999; Sun and Zhang, 2001; Sun and Zhang, 2002) was applied to determine the mechanical properties of single MF microcapsules. The detailed schematic diagram of the micromanipulation rig is shown in Figure 3.2. One drop of diluted MF microcapsules in suspension was placed on a piece of glass slide and air dried naturally. The glass slide was fixed on a stage and the microcapsules

were visualised using a side-view and a bottom-view camera (Cohu 4900 Series, Cohu Inc., USA); they were used primarily to align microcapsules with the compressing probe. The captured images from the side-view camera were further processed to determine particle size, as well as visualising the deformation of microcapsules during compression.

A force transducer (Models 400A, or 405A, 403A depending on samples, Aurora Scientific Inc., Canada) mounted on the micromanipulator was programmed to travel towards a microcapsule in focus to compress the microcapsule. It was reported by Sun and Zhang (2001) that a range of compression speed from 0.5 μms^{-1} to 6 μms^{-1} does not affect the deformation at rupture as well as rupture force of MF microcapsules. This implied that viscous effect of microcapsules on such parameters is not significant. Hence, a compression speed of 2 μms^{-1}, which is generally employed for this rig (Yap *et al.*, 2008; Xue and Zhang, 2009), was applied for all the experiments. A 3-D illustration of the force transducer with an attached glass probe is shown in Figure 3.3. The force transducer was connected to a data acquisition unit, which records the voltage output signals generated by the transducer during the compression of the microcapsule. The output voltage was subsequently converted to force using transducer sensitivity. With the selection of an appropriate probe size and transducer force scale, the micromanipulation rig is capable of characterising particles with size range from 1 μm to 100 μm in diameter through the following tests:

- Rupture test
- Loading and unloading test
- Compression and holding test

The detailed procedures are described in the following sections.

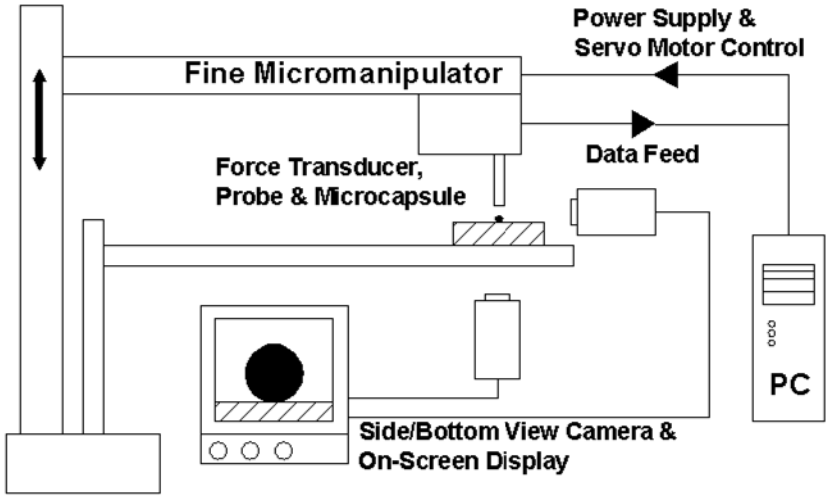

Figure 3.2 Schematic diagram of a micromanipulation rig.

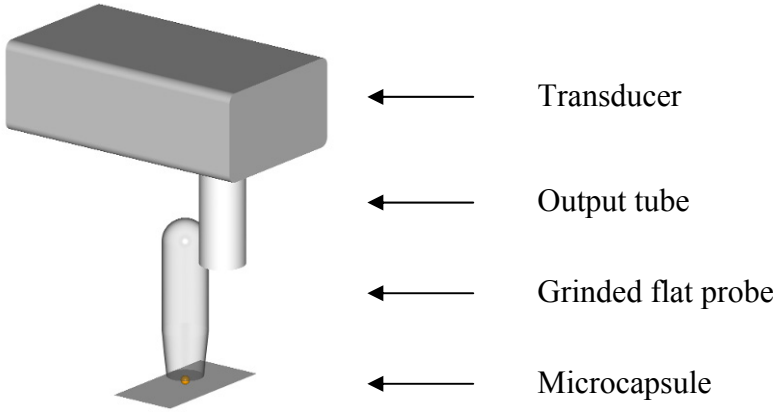

Figure 3.3 Illustration of a force transducer attached with a grinded flat probe and a microcapsule.

3.1.6.2 Experimental Procedures

A force transducer with desirable sensitivity was selected and calibrated. A flat end glass probe with appropriate size was chosen before being attached to the force transducer using superglue (Cyanoacrylate, RS components, UK). The force transducer was then mounted to the micromanipulation rig and connected to the power box and computer before experiments commenced. After starting up procedures were completed, one drop of diluted MF

microcapsules in suspension was placed and dried on a piece of glass slide mounted on the micromanipulation rig stage. The side and bottom view images of the microcapsules and transducer probe were focused by adjusting the positions of the sample stage and cameras. Experiments were conducted at room temperature of 25±1 ºC.

Rupture tests provide results of rupture force and displacement at rupture of single microcapsules by compressing them to rupture. For this test, the maximum measurable voltage of the transducer should be set at a value that is greater than the voltage equivalent to the rupture force of the microcapsule. Also the setting of the maximum probe travelling distance is required to be long enough to allow the microcapsule to rupture. By executing "Squash (D1)" command on the control panel, the probe was allowed to travel downwards to compress the microcapsule beyond the point of rupture.

The objective of loading and unloading experiments was to study the elastic or plastic property of the microcapsules by compressing them to different deformations and releasing, and hence the elastic limit (pseudo yield point) of the microcapsules could be determined. A single microcapsule was compressed and released repetitively with a gradual increase in applied force for each cycle, until the plastic behaviour was observed and compression was then stopped. Plastic behaviour was indicated by the fact that force had already reduced to zero, even if the probe was still far away from its original position. For this experiment, the set maximum force was the controlling factor. By executing "Squash (D1)" command on the control panel, the single microcapsule was compressed until the set maximum force was reached; it would then be released by immediately executing "Squash (D3)" command on the

control panel. At least 30 microcapsules were examined within a sample in order to determine the elastic limit of the microcapsules.

In compression and holding experiments, the probe travelled downwards to compress a single microcapsule until a pre-set displacement was reached. Then, the microcapsule was held at this compression deformation for 10 to 20 seconds, while the computer continued to record the experimental data showing force imposed on the microcapsule being held. The results obtained from this experiment were used to study visco-elastic properties of single microcapsules at a certain deformation (if any).

3.1.6.3 Number of Microcapsules Tested per Sample

Under the request of company, 30–60 microcapsules were usually compressed within a given microcapsule sample. For the same sample, test results based on 30 and 60 tested microcapsules are tabulated in Table 3.1. It is apparent that the standard errors decrease with the increase of total number of tested microcapsules. A statistic *t* test was applied to every mechanical property parameter listed in the table. The detailed procedures of *t* test are described in Appendix B. It was found that there is no significant difference between the results obtained from 30 or 60 tested microcapsules in the same sample, based on 95% confidence interval. It is therefore suggested that for the further analysis testing of 30 microcapsules per sample is enough to achieve statistically representative results.

Table 3.1 Comparison of mean mechanical property parameters of microcapsules in a given sample based on testing of 30 and 60 capsules from the same sample.

Number of capsule tested	Diameter (μm)	Rupture Force (mN)	Deformation at rupture (%)	Nominal rupture stress (MPa)	Nominal wall tension (N/m)
30	38.5±2.4	0.42±0.13	22±5	0.44±0.23	3.8±1.5
60	37.2±2.2	0.37±0.08	20±3	0.42±0.15	3.4±1.0

3.1.6.4 Calibration of Force Transducer Sensitivity

Within a force transducer, an output tube was fixed onto a cantilever beam by the manufacturer. When a given weight is applied to the output tube, the cantilever beam will deflect and result in an alteration of voltage output. The heavier the load applied onto the output tube, the more cantilever beam will bend, and the higher output voltage will be generated. The relationship between the applied weight and the corresponding voltage is represented by the sensitivity of force transducer, which needs to be calibrated before the experiments are carried out. For a normal transducer, applied weight is linearly proportional to transducer voltage output. Taking 1g transducer (Model 405A, Aurora Scientific Inc., Canada) as an example, the maximum force this transducer can measure is 1 gram force. Hence, papers were cut to square shape at the dimension of 1cm by 1cm, and Blue Tac was added to the papers in order to vary their weight. The paper with blue tac was then weighed using an analytical electronic scale (AC210S, Sartorius Ltd, UK) which was accurate to ± 0.0001 g.

The transducer was inversely placed on a desk and securely fixed with Blue-Tac as shown in Figure 3.4. Before any paper was added to the output tube, the output voltage of the force transducer was recorded which represented the baseline reading. Then, 13 pieces of papers with Blue-Tac of weight ranging from 0.0070 g to 0.7300 g were carefully put onto the output

tube of transducer, respectively. For each piece of paper added, a corresponding voltage was generated by the transducer and subsequently recorded. The forces in the downward direction were obtained by multiplying paper weight with gravity (9.81 ms^{-2}). The gradient of force-voltage graph (Figure 3.5) gives the sensitivity of the transducer, which was 1.05 mNV^{-1}; this agreed well with manufacturer's recommended value of 1.00 mNV^{-1}. Transducers with different sensitivities were chosen depending on the maximum rupture forces of the microcapsules in the sample, and calibration was carried out for each transducer being used.

Table 3.2 summarizes a list of transducers employed in the experiments as well as their calibrated sensitivities. With the calibrated value of sensitivity, K_S, the force imposed on the microcapsule, F, can be calculated using Equation 3.2:

$$F = VK_S \tag{3.2}$$

where V is the voltage generated by the transducer.

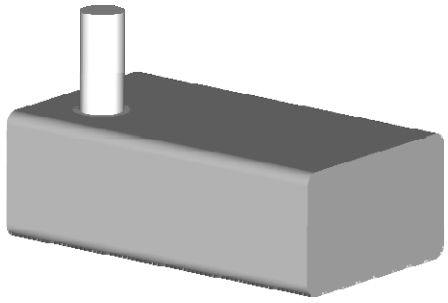

Figure 3.4 Diagram showing force transducer was inversely placed on the desk before its sensitivity was calibrated.

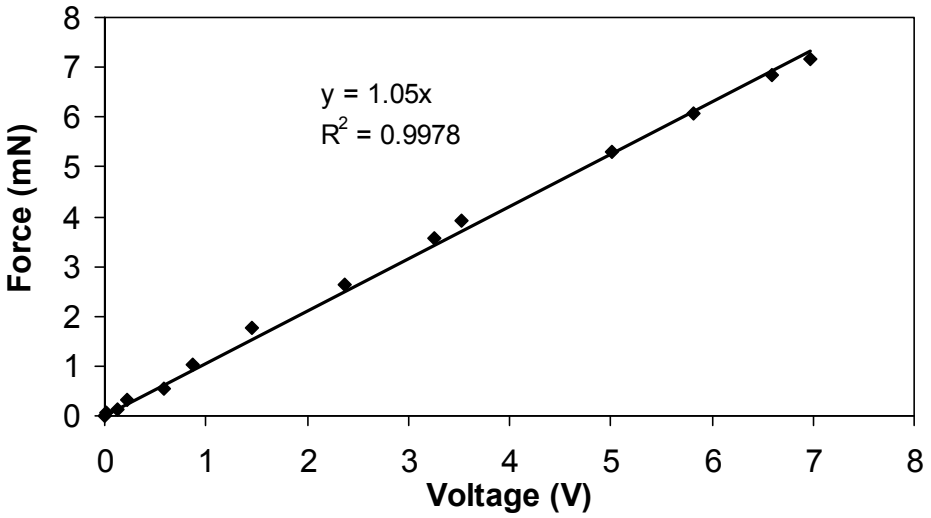

Figure 3.5 Force-voltage profile for sensitivity calibration of a force transducer (Model 405A). The calibrated sensitivity is 1.05 mNV^{-1}.

Table 3.2 Summary of calibrated sensitivities of force transducers

Models	Full scale force (mN)	Sensitivity by manufacturer (mNV^{-1})	Calibrated sensitivity (mNV^{-1})
400A	50	5.00	5.00
405A	10	1.00	1.05
403A	5	0.50	0.47

3.1.6.5 Calibration of Force Transducer Compliance

When single microcapsules are compressed, the cantilever beam will always bend towards the opposite direction of compression. Hence, in order to truly reflect the travelling distance of the probe, it is always necessary to take into account of the deflection of the cantilever beam. The compressive displacement (displacement of probe), δ_C, is calculated using Equation 3.3:

$$\delta_C = vt - FC_{COM} \tag{3.3}$$

where v is compression speed (probe travelling speed); t is probe travelling time; F, is force imposed on the microcapsule. Compliance, C_{COM}, was measured by using a flat probe attached to the transducer to compress a hard surface, i.e. a piece of empty glass slide, for 10 times. For every compression, a voltage–sampling point profile (Figure 3.6) was generated. As a result, the gradient of a linear line AB in Figure 3.6 could be calculated. The mean value of 10 gradients, $\overline{m}$, was then fit into Equation 3.4 to determine the compliance, C_{COM}.

$$C_{COM} = \frac{vt_a}{\overline{m}K_S} \tag{3.4}$$

where t_a is acquisition time, which represents the time between two consecutive sampling points; K_S is sensitivity of force transducer.

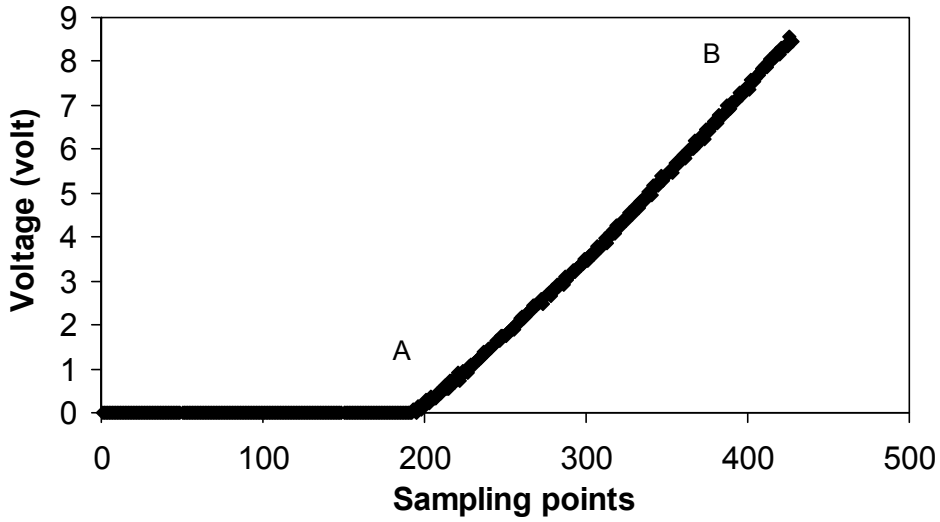

Figure 3.6 Voltage-sampling points profile to calculate the compliance.

3.1.6.6 Calibration of Compression Speed

A measurement graticule of 100 μm in length with 1 μm intervals was vertically placed on the stage and its image was captured by the side view camera; the scale on the graticule was shown on a TV monitor. A marker was used to accurately indicate a distance, δ_S, of 100 μm on the monitor screen. The force probe was then allowed to travel a distance of 100 μm distance, and a stop watch was employed to simultaneously record the amount of time taken, t_S. The calibrated compression speed, v_c, was calculated using Equation 3.5:

$$v_c = \frac{\delta_S}{t_S} \tag{3.5}$$

The above calibration procedures of compression speed were repeated 10 times, and the average speed obtained from the calibration data was 2.0 μms^{-1}, exactly as the setting speed of 2 μms^{-1}.

3.1.6.7 Preparation of Compression Probes

A borosilicate glass capillary tube with 1.0 mm o.d. (Outer Diameter) and 0.58 mm i.d. (Inner Diameter) (GC100-15, Harvard Apparatus Ltd, UK) was heated and pulled using a glass puller (MicroForge, MF-900, Narishige, Japan) to produce a glass probe with a flat end. The diameter of the glass probe should be at least 3 times of the initial diameter of single microcapsules to ensure the microcapsule is trapped between two parallel surfaces during compression, since modeling work in the micromanipulation research group shows microcapsules during compression are smaller than 3 times of their initial diameter. The finished glass probes from the glass puller, however, were often not flat enough; hence, they

must undergo a grinding process using a grinding apparatus (EG-40, Narishige, Japan). After grinding, the probes were further examined under a microscope; a probe with a flat end was then selected and ready to be attached to the output tube of the force transducer. The diagram of the force transducer with an attached glass probe is shown in Figure 3.3.

3.2 Measurement of Adhesion

3.2.1 Materials

Cotton films were prepared using the following ingredients: cotton linter cellulose powder, also called cotton powder (Sigma-Aldrich, UK), a piece of cotton cloth, 50 wt.% N-methylmorpholine-N-oxide (NMMO) solution (Sigma-Aldrich, UK), dimethyl sulfoxide (DMSO) (ACS spectrophotometric grade, ≥99.9%, Sigma-Aldrich, UK) and 50% (w/v) poly(ethyleneimine) (PEI) in water solution (Sigma-Aldrich, UK), general purpose grade sodium hydroxide powder (Sigma-Aldrich, UK) and water for gradient analysis of High Performance Liquid Chromatography (HPLC) (Fisher Scientific, UK). Silicon wafers with thickness of 381±25 μm (Type N <100> Phos, IDB Technologies Ltd, UK) were employed as substrates for cotton films to be deposited.

The particle samples studied included melamine formaldehyde (MF) microcapsules with a perfume oil-based industrial precursor as core material and a mean diameter of 37.2 μm (Procter & Gamble, Cincinnati, US), MF monodisperse microparticles with a mean diameter of 9.2 μm (MF-R-1097, Microparticles GmbH, Germany) and MF monodisperse

microparticles with a mean diameter of 12.5 μm (MF-R-5060, Microparticles GmbH, Germany).

Monodisperse MF microparticles were developed and patented by Microparticles GmbH, Germany. They were produced by hydrothermal acid-catalyzed polycondensation of methylol melamines in the temperature range 70-100 ºC without any surfactants. By varying the concentration of methylol melamine, pH-value, or temperature, monodisperse MF microparticles with diameters from 0.5 μm to 12.5 μm could be produced in a one step process (Fiedler, 2008).

In order to study the adhesion between MF microcapsules/microparticles and cotton films in the detergent solution, a typical household liquid detergent Biological Ariel (Procter & Gamble, UK) was diluted by HPLC water to the concentrations ranging between 0.0001 wt.% and 10 wt.% to act as liquid media. Anionic surfactant solutions were also used in the experiments in order to study the adhesion between microcapsules/microparticles and cotton films in the sole effect of surfactant solution. Anionic surfactant sodium dodecylbenzenesulfonate (SDBS) powder (Sigma-Aldrich, UK), which contributes to 5 wt.% of Ariel detergent, was diluted in deionised water to also act as liquid media for the adhesion measurement experiments. The amount of SDBS in its made up solution with concentration ranging from 0.1 mM to 14.4 mM was equivalent to that in Ariel detergent with concentration ranging from 0.09 wt.% to 10 wt.%. The pH of detergent or SDBS solutions was varied from 2 to 11 in order to study the effect of pH on the adhesion.

3.2.2 Generation of Cotton Films

A novel method was reported by Gunnars *et al*. (2002) to generate a thin and uniform cellulose film by dissolving wood pulps. This method was successfully adapted and applied in this work to prepare a thin cotton film by dissolving cotton powder/fibres. The following sub-sections present the detailed procedures to generate cotton films.

3.2.2.1 Preparation of Silica Substrates and Coating Anchoring Polymer Layers

Silicon wafer surface normally has a native layer of silicon oxide, of which the thickness is approximately between 1-2 nm (Taft, 1988). A silicon wafer was dipped into 10 wt.% NaOH solution for 30 seconds (Notley *et al.* 2006), and then rinsed with copious amount of HPLC water before being dried with a constant flow of nitrogen gas. The NaOH solution (pH=13.8) is able to make the hydroxyl group (OH-) on silicon surface to deprotonate to become O-, or a Si-O-Si bond to Si-O- plus Si-O-. As a result, silica is able to allow polymers to adsorb on it later. The silicon wafer was subsequently immersed in 1 gl^{-1} PEI solution for 10 min (Aulin *et al.* 2008), and then rinsed with copious amount of water and again dried with a constant flow of nitrogen gas.

3.2.2.2 Generation of Cotton Films

0.5 g of cotton powder or 0.2 g of cotton fibres from cotton cloth, were added to 25 g light yellowish 50 wt.% NMMO solution and heated to 115 ºC for about 2 hours using a magnetic stirrer hotplate (RCT basic, IKA, Germany). An image of the experimental apparatus is shown in Figure 3.7. As the quality of mixture could be affected at temperature above 130 ºC, a 200

mL beaker (D = 73 mm, H = 90 mm) containing the mixture was placed in a glass oil bath (D = 112 mm, H = 63 mm) containing paraffin liquid oil (Fisher Scientific, UK), and the level of paraffin oil in the oil bath was always kept higher than the mixture depth in the beaker to ensure a full submersion of such mixture. A contact thermometer with a Proportional-Integral-Derivative (PID) controller (ETS-D5, IKA, Germany) connected to the hotplate was employed to control the temperature of paraffin oil at 115.0±0.2 ºC; this was achieved by immersing a stainless steel sensor of the contact thermometer in the oil bath. As a result, the temperature of cotton powder/fibres and NMMO solution mixture was always maintained at 115.0 ºC.

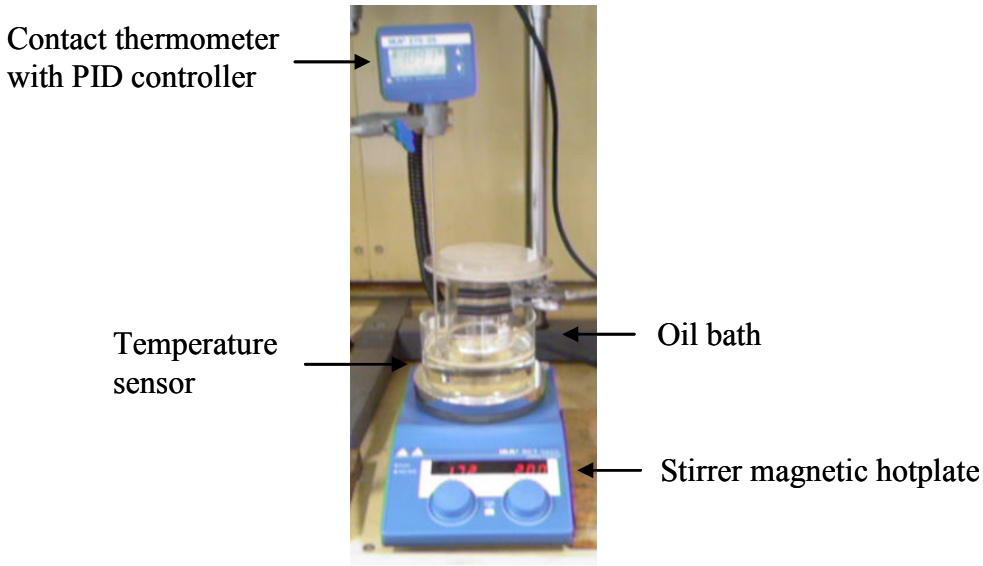

Figure 3.7 An image of the experimental apparatus used to dissolve cotton powder/fibres.

Once cotton powder/fibres were completely dissolved, the appearance of the mixture turned dark yellowish. 75 g of DMSO solvent was then gradually added to control the viscosity of the cotton mixture. This produced 0.5% w/w (0.2% w/w using cotton fibres) cotton solution that was ready for spin-coating. The cotton solution was spin-coated at 3500 rpm using a spin coater (WS-400B-6NPP/LITE, Laurell Technologies Corporation, US) for 30 seconds onto a silicon wafer with an anchoring layer of PEI polymer, followed by precipitation in HPLC

water. The cotton film was then immersed in a fresh batch of HPLC water for 1 hour and another 3 hours in another fresh batch of HPLC water. It was finally dried in a desiccator and ready for adhesion measurement.

3.2.3 Characterisation of Cotton Films

3.2.3.1 Ellipsometry

A spectroscopic ellipsometer (UVISEL, Horiba Jobin Yvon Ltd., UK) was employed to measure the thicknesses of silicon oxide layer on silicon wafer, PEI polymer film and cotton film. An image of an ellipsometer, which consists of a light source, polarizer, analyser and detector, is presented in Figure 3.8. The experimental data obtained was processed by DeltaPsi2 v2.0.8 software for the exact thicknesses of films. The thickness of each film was measured at 5 random locations, and the mean value gives the thickness of each film.

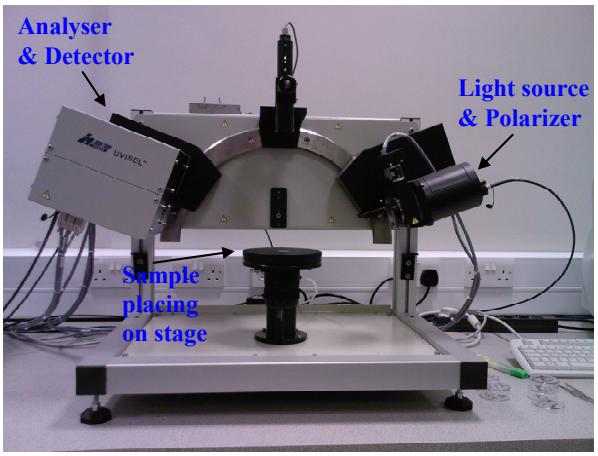

Figure 3.8 A picture of an ellipsometer.

3.2.3.2 Contact Angle Measurement

The wetting behaviour of water on cotton film was characterised using a contact angle measurement apparatus equipped with a charge coupled device camera (KP-M1E/K, Hitachi). The experiments were performed at room temperature of 25 ºC. A drop of HPLC water, approximately 1 μL in volume, was placed on the centre of a piece of cotton film using a syringe. The profile of water drop on the cotton film was visualised with a side view camera within 1 minute in order to obtain the equilibrium contact angle. 3 measurements were performed on each cotton film sample. The image was subsequently analysed with First Ten Angstroms video analysis software v1.96 to determine the contact angle; this helped to establish the hydrophilic/hydrophobic nature of cotton films.

3.2.3.3 X-ray Photoelectron Spectroscopy (XPS)

The cotton films were also analysed using a X-ray photoelectron spectrometer (Escalab 250 system, Thermo VG Scientific, UK) to ensure the cotton film was free from residual solvent. The instrument was equipped with Avantage v1.85 software, which was available in School of Physics and Astronomy at The University of Leeds. It operates under a pressure of ~5×10^{-9} mbar. An Al Kα X-ray source was used, which provided a monochromatic X-ray beam with incident energy of 1486.68 eV. The cotton film area of 0.2 mm^2 was analysed. A pass energy of 150 eV over a binding energy range of -10 to 1200 eV was applied to obtain low-resolution survey spectra with 1 eV increments. Each spectrum acquired was based on the average of three scans. A pass energy of 20 eV over a binding energy range of 28 eV and centring on the binding energy of the element being examined was applied to obtain a high resolution spectra with an increment of 0.1 eV. The elements being examined and their corresponding range of

binding energy are obtained from Briggs & Seah (1996) and listed in Table 3.3. Since cotton is mainly composed of cellulose, the examined elements are the constituent materials of cellulose, PEI and NMMO; all of these were used to generate cotton films. The chemical structures of the materials are shown in Figure 3.9. The recorded XPS peaks were analysed using the XPS software (Avantage software). In case solvent residues were present on the cotton films, the individual peak would appear between the binding energy ranges in the photoelectron spectrum, which represented the specific element originated from the solvent.

Table 3.3 Summary of binding energy range of elements from the materials used to generate cotton films.

Materials	Constituent elements	Electron orbital	Binding energy (eV)	Binding energy range (eV)
PEI	**C**	1s	287	272-300
	N	1s	402	388-416
Cellulose	**C**	1s	287	272-300
	O	1s	531	517-545
NMMO	**C**	1s	287	272-300
	O	1s	531	517-545
	N	1s	402	388-416

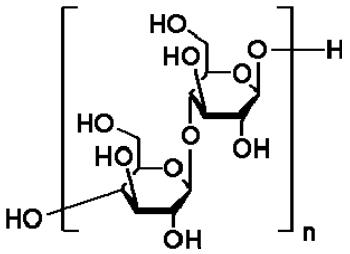

Cellulose

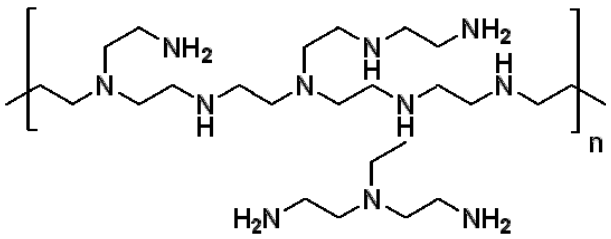

Poly(ethyleneimine) (PEI)

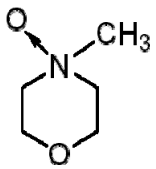

N-Methylmorpholine *N*-oxide (NMMO)

Figure 3.9 The chemical structures of the materials from which the elements were examined by XPS.

3.2.3.4 Zeta Potential

The zeta potential of cotton powder and MF microcapsules in the surfactant SDBS solution were characterised using a Zetamaster (ZEM 5004, Malvern Instruments Ltd., UK). The liquid layer surrounding the particle exists as two parts: an inner region (stern layer) where the ions are strongly bound to the particles and an outer (diffuse) region where they are less firmly associated. Within the diffuse layer there is an abstract boundary inside which the ions and particles form a stable entity. Those ions beyond the boundary stay with the bulk dispersant. The potential at this boundary (surface of hydrodynamic shear) is the zeta potential (Malvern, 2009). It is resulting effect of particle and liquid medium as a joint system. Particles with positive or negative surface charges can have negative zeta potential, since it also depends on liquid medium (Malvern, 1996). Zeta potential is often termed "a remote effect of surface charge", but surface charge requires other technique for the measurement. The zeta potentials of MF microcapsules or cotton powder in the surfactant solution including its magnitude as well as signs (positive/negative) were measured at varying pH, in order to determine their interactions in the surfactant solution (charge related) as well as validating the adhesion measurement results from other techniques, such as atomic force microscopy. The pH of MF microcapsules in suspension of 0.2 mM SDBS surfactant solution was separately adjusted from 3 to 12 and then immediately tested by the Zetamaster. The tests were performed at 25 ºC and the measurement at each pH was repeated 10 times. The same procedures were also applied to measure the zeta potential of cotton powder in suspension of 0.2 mM SDBS surfactant solution at pH from 3 to 12.

3.2.4 Measurement of Adhesive Force - Atomic Force Microscopy (AFM)

3.2.4.1 Equipment

There were two atomic force microscopes, D3100 AFM & MultiMode AFM (Digital Instruments, Santa Barbara, CA) available to carry out the experiments at The University of Birmingham. These two AFMs shared a same NanoScope III controller. The horizontal stage movement range of D3100 AFM is much wider compared with that of MultiMode AFM, hence, the former was chosen for force measurement under ambient condition between single MF microcapsules/microparticles and cotton films as well as imaging the surface of cotton films. Alternatively, MultiMode AFM was used to measure the adhesive force between single MF microcapsules/microparticles and cotton films in various liquid media with different concentrations and pH. Nanoscope III v5.12 software (Veeco, Santa Barbara, US) was used to acquire force data in real time as well as for capturing images and offline image analysis. Nanoscope III v6.12 software (Veeco, UK) was utilized to export each set of AFM force data manually into text format; the data was subsequently analysed using Microsoft Excel.

3.2.4.2 Imaging Cotton Films

Tapping mode was selected to scan cotton films, MF microcapsules and MF microparticles. The scan rate applied for imaging was 1.0 Hz at all times and the images obtained had a resolution of 256×256 pixels. Under the tapping mode, phosphorus (n) doped silicon cantilevers with a spring constant of 40 Nm^{-1} (Model RTESP, Veeco, France) were used to obtain the topographic view and RMS roughness of cotton films. The silicon rectangular

Olympus cantilevers with a spring constant of 2 Nm^{-1} (Model AC240TS, Asylum Research, UK) were used to scan the surface of MF microcapsules & MF microparticles for their RMS surface roughness. The AC240TS cantilever was chosen because its tip locates at the apex of the cantilever; this helps to locate the exact position of the microparticle surface being scanned. The distance between the cantilever tip and end of cantilever was defined as the tip set back (TSB), as shown in Figure 3.10. The TSB distance of the RTESP cantilever, according to manufacturer, ranged from 5 μm to 25 μm. This induced uncertainty when the exact location of the surface of microparticle needs to be found to start the scanning procedures. The difference in tip location between these two types of cantilevers is illustrated in Figure 3.10.

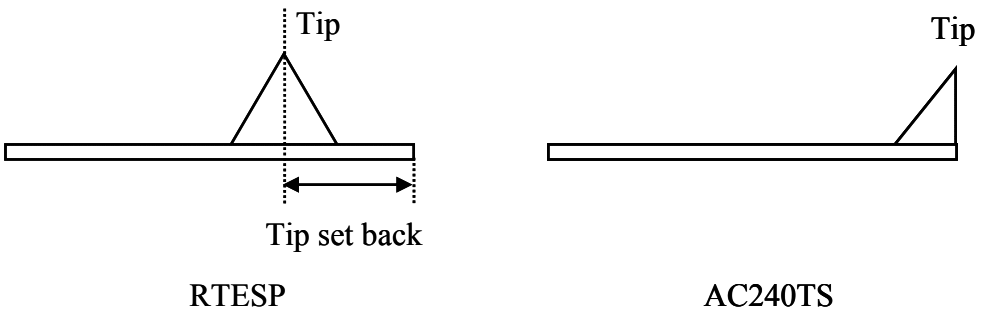

Figure 3.10 Schematic diagrams to illustrate the difference in tip location between the two types of cantilevers (side view) – RTESP & AC240TS.

3.2.4.3 Attachment of Single MF Microcapsule/Microparticle onto Cantilever

Two types of cantilevers were used for the adhesive force measurements: tipless rectangular silicon cantilever (Length 90 μm; Width 35 μm) (Model NSC12, MikroMasch, Estonia) and silicon nitride V-shape cantilever (Length 315 μm; Width 18 μm) (Model MLCT, Veeco, France). The MLCT cantilevers were much softer and more sensitive compared to the NSC12

cantilevers; hence, the former offered a higher resolution. The detailed procedures to calibrate spring constants of such two types of cantilevers are presented in Appendix A.

A colloid probe was formed when a single MF microcapsule was attached to a tipless cantilever with a two-component epoxy glue (Araldite Rapid, Bostik Findley Ltd., UK). The above procedure was completed with the use of D3100 AFM. A fresh sample of MF microcapsules in suspension was diluted with distilled water, and dried on a piece of glass slide prior to attachment. A little drop of mixed epoxy glue was placed on an empty location of the glass slide with microcapsules and spread out using a glass probe. By varying the horizontal movement setting of the stepping motor in D3100 AFM, a tipless cantilever held by a piezo was positioned on top of the epoxy glue, and lowered down gradually to come into contact with the glue before it was carefully dragged along the surface to a clean area to scrape off any excessive glue. The cantilever was then moved on top of a selected single microcapsule and then lowered down slowly until it touched the surface of the microcapsule, which was normally indicated by a change in output signal of the piezo. Furthermore, the contact between the microcapsule and cantilever could also be indicated by the total distance the stepping motor had moved at the downward direction, which should be approximately equal to the focusing distance between the cantilever and the glass slide (~1 mm) minus the microcapsule's diameter. Same procedures were applied to attach single MF microparticle to the cantilever. Figure 3.11 is an ESEM image showing a MF microparticle of 11.9 μm in diameter attached to a tipless cantilever. The image confirms that there was no glue spreading over the surface of the microparticle where adhesion measurement takes place, but less amount of glue can be applied next time.

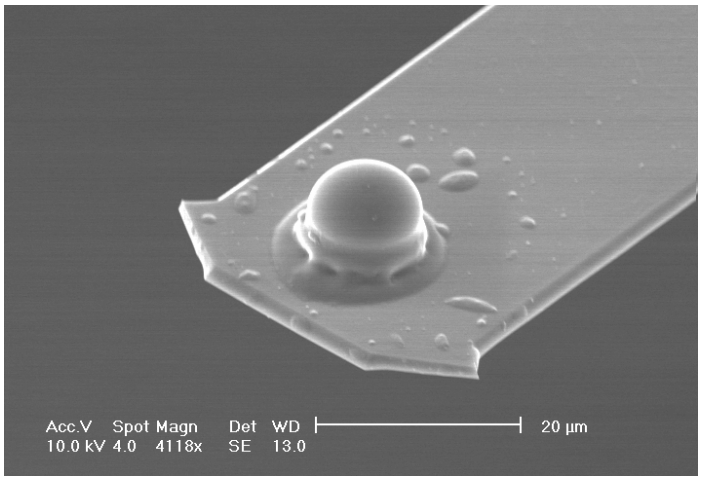

Figure 3.11 An ESEM image showing a microparticle (diameter=11.9 µm) attached to a tipless cantilever.

3.2.4.4 Experimental Conditions for Adhesive Force Measurement

Contact mode was selected for adhesive force measurements in both D3100 AFM and MultiMode AFM. For the AFM experiments performed under ambient condition, the room temperature and air RH were recorded using a thermo-hygrometer (DT-615, ATP Instrumentation Ltd., UK). The maximum ramp size (Z scan range) of D3100 AFM and MultiMode AFM was 2.757 µm and 1.903 µm, respectively. Ramp size is the distance the piezo approaches or retracts. A scan rate of 1 Hz means the piezo completes a cycle of extension and retraction within a second. Hence, piezo approaching speed is calculated by multiplying twice of ramp size to the scan rate. A typical scan rate used in the AFM force measurement is 0.1-2.0 Hz (Fritz *et al.*, 1997). As a result, a scan rate of 0.5 Hz was used for all the force measurements in both D3100 AFM and MultiMode AFM, except for scan rates that were varied in the cases to study the effect of probe approaching speed on the adhesion. Since approaching speed also depends on the use of ramp size, the use of speed could be different whilst employing D3100 AFM or MultiMode AFM, even though the same scan rate

of 0.5 Hz was used. The details of scan rates and speeds are specified in Chapter 7. The force measurement in the liquid environment using MultiMode AFM was always performed 0.5 hr to 1 hr after the fluid cell was filled with the liquid media, in order to allow the liquid system to be stabilised, which can be indicated by the end of flashing signal of photo detector.

4. CHARACTERISATION OF THE MECHANICAL STRENGTH PARAMETERS OF MF MICROCAPSULES PREPARED USING VARIOUS FORMULATIONS

In this chapter, the morphology, size distribution and wall thickness of MF microcapsules are characterised using different measurement techniques, such as environmental scanning electron microscopy (ESEM), Malvern particle sizing and transmission electron microscopy (TEM). In addition, micromanipulation was employed to perform a series of tests, including compression and holding, loading and unloading and compression to rupture on single MF microcapsules to study their visco-elastic properties, elastic limit and mechanical strength. Mechanical strength parameters that are commonly used to describe the mechanical strength of microcapsules are studied in this chapter, where their applicability and limitation are discussed. Furthermore, factors that are able to influence the mechanical strength of microcapsules were investigated by studying microcapsules which had additional coating, different core/capsule ratios in weight percentage, different components added into the microcapsule slurry or microcapsule core contents as well as varying pH of microcapsule suspending liquids. All the investigated microcapsules were supplied by Procter & Gamble.

4.1 Morphology of MF Microcapsules

An ESEM image of MF microcapsules from a slurry sample is presented in Figure 4.1. Although MF microcapsules from the slurry tended to agglomerate together, the outline of individual MF microcapsules is visible and appears in spherical shapes with a relatively smooth surface. It was observed that single MF microcapsules could easily be separated from

each other once being suspended in water. Therefore, tests such as micromanipulation can be employed to characterise the mechanical strength of single MF microcapsules.

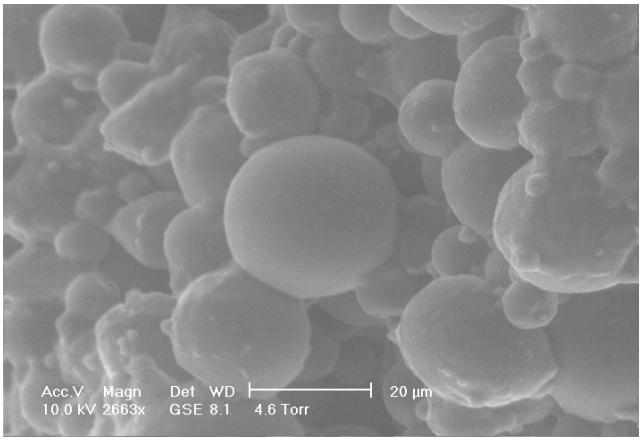

Figure 4.1 An ESEM image of microcapsules which were produced using an in-situ polymerisation technique.

4.2 Size Distribution of MF Microcapsules

A size distribution graph of another MF microcapsule sample (different from the sample used in Chapter 4.1) is presented in Figure 4.2, which was obtained from Malvern particle sizing. The MF microcapsules were produced by an in-situ polymerisation technique and the detailed steps of this technique are outlined in Figure 3.1. The curve shows the size of microcapsules in a given sample ranged from 11 μm to 90 μm. The difference in size of microcapsules was because the energy dissipation rate was not homogeneous in the emulsification step of in-situ polymerisation technique. Microcapsules with smaller size distribution can be made by techniques such as membrane emulsification (Charcosset *et al.*, 2004). The volume weighted mean diameter, d_{43}, of this microcapsule sample was measured by Malvern particle sizing to be 37.22±0.03 μm. The mean size of microcapsules in a sample produced by the in-situ

polymerisation technique can be changed by varying the agitation speed during the encapsulation process (Hwang *et al.*, 2006).

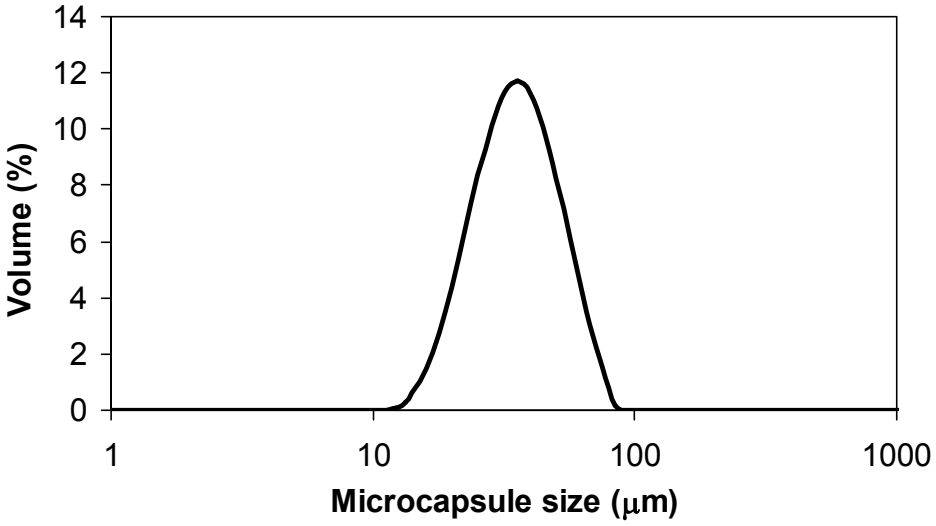

Figure 4.2 Size distribution of a typical MF microcapsule sample produced by in-situ polymerisation. The core/capsule ratio of the MF microcapsules was 80wt.% and the polymerisation time used was 4 hours.

4.3 Wall Thickness of MF Microcapsules

MF microcapsules of one sample had a core content of 80wt.% and their volume weighted mean diameter was measured to be 34.16 μm by Malvern particle sizing. The specific densities of MF wall and perfume oil core were 1.400 and 0.925 respectively (Dihora, 2006). Based on these figures, the wall thickness of MF microcapsules in a given sample is estimated to be 850 nm if all the MF input was used up for formation of the capsule walls. In order to demonstrate whether the core/capsule ratio can be used to estimate the wall thickness of microcapsules, MF microcapsules were prepared, sectioned and examined under TEM based on the procedures described in Chapter 3.1.5 to determine their real wall thickness. A typical ultrathin section of a MF microcapsule is presented in Figure 4.3 which clearly illustrates the

wall of the microcapsule. At Point A & B, the wall thickness is 299 nm and 127 nm, respectively. This implies that the wall of microcapsule is not uniform. Applying image analysis and Equation 3.1, the mean wall thickness of this MF microcapsule section was found to be 220 nm and the diameter of this particular microcapsule section is 26.9 μm.

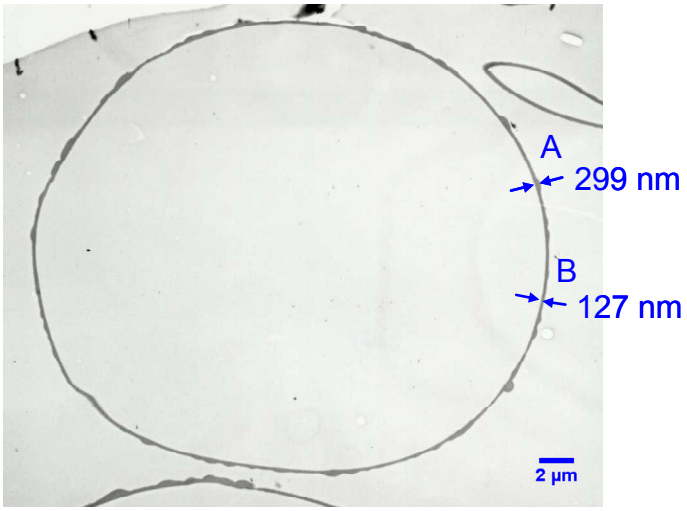

Figure 4.3 An ultrathin section of a MF microcapsule. The diameter of this microcapsule section is 26.9 μm and its wall thickness is 220 nm.

There are in total 39 random sliced sections of MF microcapsules examined. The mean wall thickness with and without correction by the model developed by Smith *et al.* (2000a) and their respective diameters are tabulated in Table 4.1. The mean corrected wall thickness of microcapsules from the given sample is 175 nm. The value is much lower than the figure estimated using the data of core/capsule ratio. This indicates that not all the MF polymer precondensate was used for the formation of MF wall. Hence, the use of core/capsule ratio might not accurately determine the real wall thickness of MF microcapsules.

Table 4.1 Summary of results from image analysis of TEM pictures with and without correction for random slicing.

	Diameter of microcapsule sections (μm)	Wall thickness of microcapsule sections (nm)	Corrected diameter of microcapsules (μm)	Corrected wall thickness of microcapsules (nm)
Averaged values	24.4±2.8	287±18	36.4±4.2	175±11

4.4 Visco-elastic Behaviour of MF Microcapsules

The typical compression-holding data of a single MF microcapsule is illustrated in Figure 4.4. A MF microcapsule of 17.9 μm in diameter was compressed to a final deformation of 7% and 13% at point A and B respectively and held for approximately 10 seconds. As can be seen, there is no significant force relaxation at the final deformation of 7%, suggesting that the microcapsule possessed no visco-elastic characteristics up to this deformation. On the other hand, slight force relaxation was observed at the deformation of 13% indicating a weakly visco-elastic behaviour the microcapsule exhibited, which is in agreement with the findings of Sun & Zhang (2001). The weakly visco-elastic behaviour could be associated with the transporting of viscous perfume oil in the interior of microcapsule as a result of mechanical loading. The overlapping of the loading curve implies the elastic behaviour dominated, which is discussed in more details in the following section. There were in total 34 MF microcapsules tested from a given sample made by in-situ polymerisation. No visco-elastic behaviour was observed at a mean deformation of 7±1%, but weakly visco-elastic behaviours were observed at a further mean deformation up to 12±2%.

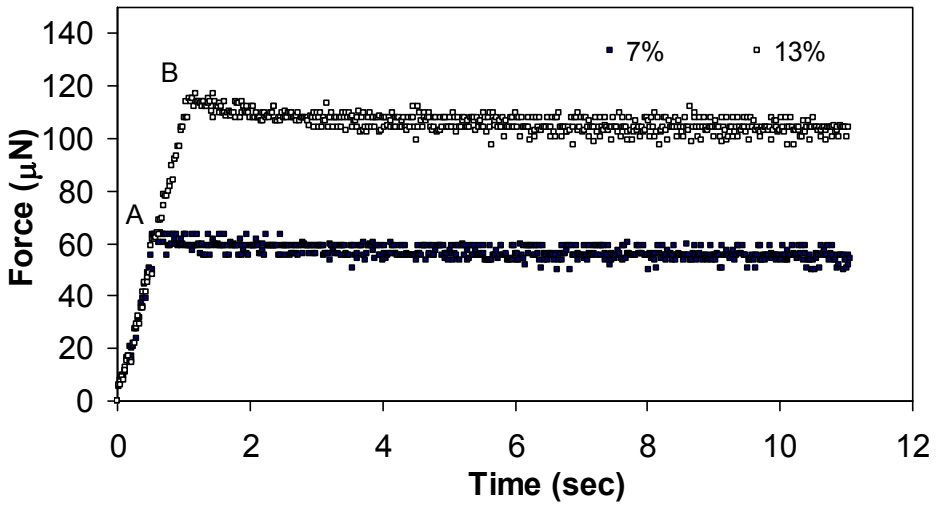

Figure 4.4 Typical compression-holding data for a single MF microcapsule (diameter=17.9 μm) compressed to a deformation of 7% and 13% respectively and then held for approximately 10 seconds.

4.5 Elastic Limit of MF Microcapsules

Loading and unloading experiments were conducted to determine the elastic limit of the MF microcapsules as described in Chapter 3.1.6.2. A MF microcapsule of 10.5 μm in diameter from a given sample, which was produced by an in-situ polymerisation technique, was compressed to a final deformation of 13% and then immediately released. In Figure 4.5, the curves denoting force imposed on the microcapsule during loading and unloading are closely matched; this suggests the hysteresis is not obvious and the MF microcapsule exhibited elastic behaviour at a deformation up to 13%. The same microcapsule was further compressed to a final deformation of 20% and then released as shown in Figure 4.6. There was hysteresis observed, since the force imposed on the microcapsule reached zero before the microcapsule resumed to its original diameter before compression. This therefore implies that the MF microcapsule exhibited plastic behaviour at the deformation of 20%. By following the

procedures detailed above, the mean elastic limit was found to be 15±1% based on the testing of 32 microcapsules from the given sample which had a mean deformation at rupture of 24±3%. The obtained elastic limit is slightly lower than that of MF microcapsules investigated by Sun & Zhang (2001) (19±1%). This may be due to the use of different core materials, which was a 10:1(w/w) mixture of partially hydrogenated terphenyls and kerosene used by Sun & Zhang (2001) and perfume oil used in this work. The identified elastic limit enables the intrinsic mechanical property, such as the elastic modulus of the microcapsule, to be determined by modelling the elastic compression data; the detailed results are presented in Chapter 6.

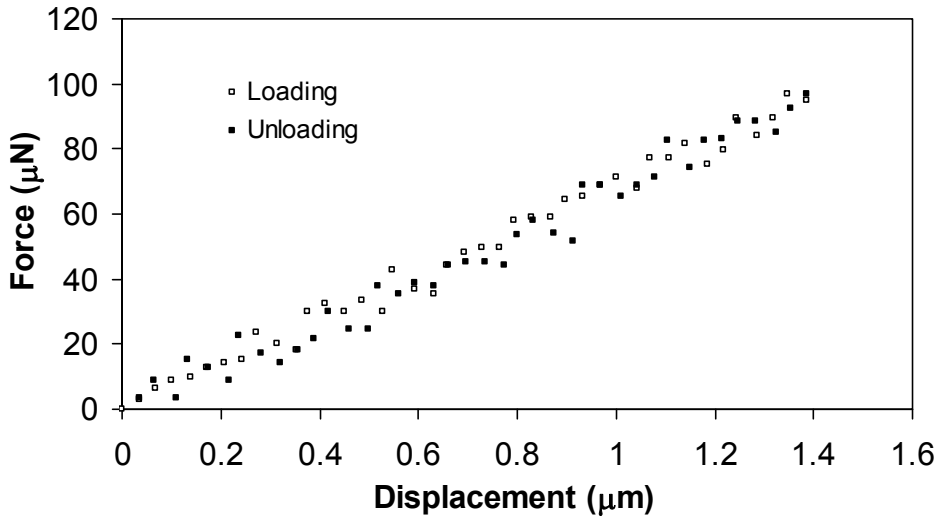

Figure 4.5 Typical loading and unloading data for a MF microcapsule (diameter=10.5 μm) compressed to a final deformation of 13%.

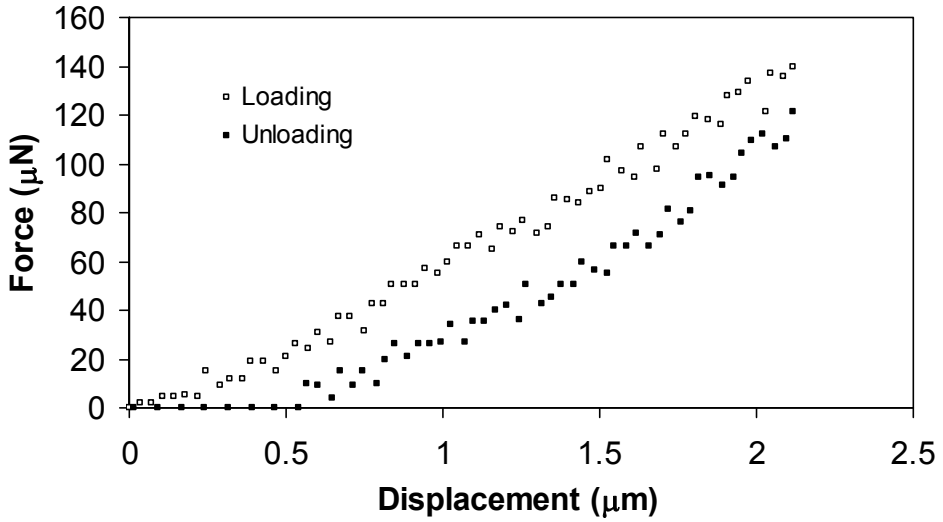

Figure 4.6 Typical loading and unloading data for a MF microcapsule (diameter=10.5 μm) compressed to a final deformation of 20%.

4.6 Mechanical Strength of MF Microcapsules

A few mechanical property parameters of microcapsules listed below can be obtained and derived using the rupture test of micromanipulation:

- Rupture force
- Deformation at rupture
- Nominal rupture stress
- Nominal wall tension

Only the above parameters are interested in this work, and other parameters such as fracture energy (Kinloch & Taylor, 2006) which can be calculated from the measured fracture toughness and modulus are not discussed here. The mechanical strength of microparticles is relevant to the end-use applications, which was represented by rupture force (Zhang *et al.*, 1999b) and nominal rupture stress (Xue & Zhang, 2009). In the following sections, the

applicability and limitations of the listed parameters to describe the mechanical strength of MF microcapsules are discussed in detail.

4.6.1 Compression of Single Microcapsules to Rupture

Figure 4.7 shows a typical relationship between the force being imposed on a single MF microcapsule and sampling time. Curve AB corresponds to the transducer probe moving in the air; as probe had not yet touched the microcapsule, the force being imposed on the microcapsule remained zero. At point B, the probe started to touch the microcapsule, and the force being imposed on the microcapsule increased until point C at which the microcapsule ruptured. As a result, the force being imposed on the microcapsule reduced to point D. The probe continued to move forward to compress the debris of the microcapsule until it cannot advance any more, which resulted in a large amount of force being induced shown from Point E. From this curve, the rupture force of the microcapsule can therefore be determined, which is the *y*-axis value of point C, equal to 0.18 mN. Rupture forces of microcapsules can be used as an important parameter to compare the mechanical strength of microcapsules that have similar diameters (Sun & Zhang, 2001). It is worth pointing out here that in order to use rupture force to compare the mechanical strength of microcapsules, microcapsules not only need to be have similar/same diameters, but also need to possess similar deformation at rupture, which is discussed in detail in the following sections.

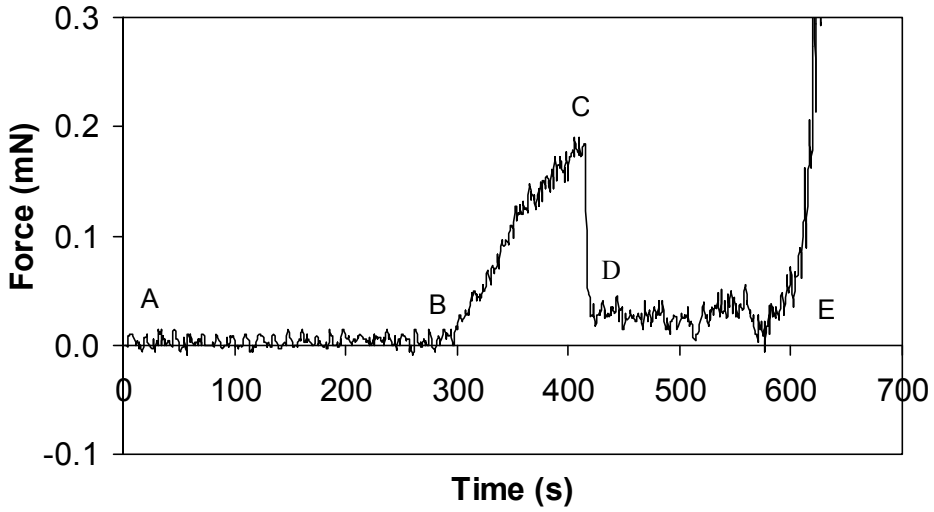

Figure 4.7 A typical relationship between the force being imposed on a single MF microcapsule and sampling time.

As the probe travelling speed was calibrated to be 2 μm/s, time at *x*-axis of Figure 4.7 can be simply converted to probe displacement by applying Equation 3.3, as presented in *x*-axis of Figure 4.8. The compliance of compression probe was calibrated to be 0.63 μm/mN, based on the procedures described in Chapter 3.1.6.5. Moreover, the figure also shows this microcapsule was ruptured at the displacement of 4.3 μm (the value of *x*-axis at point C). The initial diameter of the microcapsule was 12.2 μm, which was obtained from the image captured by the side view camera.

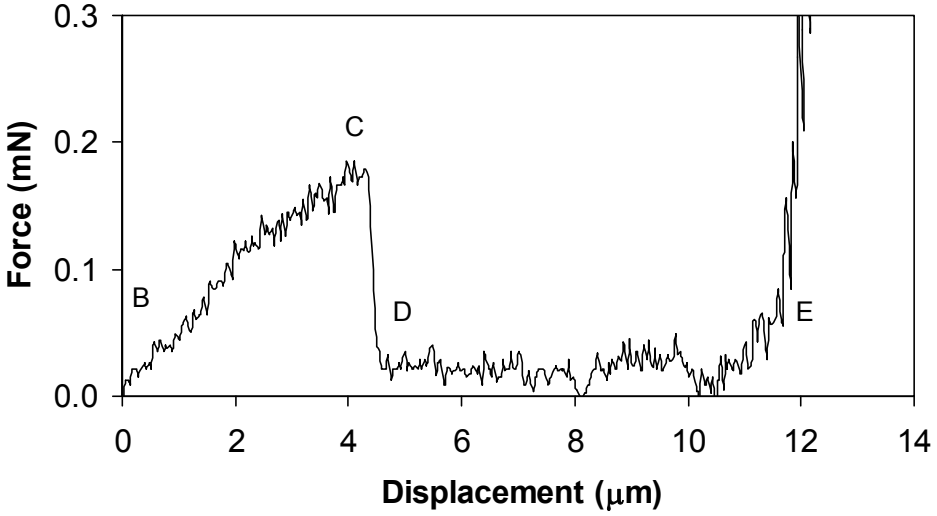

Figure 4.8 Relationship between the force imposed on the microcapsule and probe displacement.

The deformation at rupture of this microcapsule is the ratio between the displacement at rupture and the initial diameter of the microcapsule, which is 35% for this microcapsule and is one of the very important mechanical property parameters of microcapsules. For two microcapsules, if one microcapsule ruptures at a significantly smaller deformation, this shows the microcapsule is more brittle. In contrast, if the other microcapsule ruptures at a much larger deformation, this suggests the microcapsule is more flexible. If two microcapsules have similar sizes, deformation at rupture and rupture forces, they then have comparable mechanical strength. However, if two microcapsules have similar size and rupture force but significant different deformation at rupture. It is obvious that the microcapsule with smaller deformation at rupture has greater rupture stress and hence possesses greater mechanical strength. However, the use of sole knowledge of size and rupture force could lead to the wrong conclusion being drawn.

The nominal rupture stress of the microcapsule is the ratio between the rupture force and the initial cross-sectional area of the microcapsule, which is calculated to be 1.5 MPa in this case. The nominal rupture stress is very useful to determine the mechanical strength of microparticles, since this parameter may represent the mechanical strength of microcapsules (Yap *et al.*, 2008). Nominal rupture stress can be used to compare the mechanical strength of microcapsules with same/similar deformation at rupture. The combined knowledge of deformation at rupture and nominal rupture stress may be used to decide the mechanical strength of microcapsules, which may be classified as strong/brittle, strong/flexible, weak/brittle and weak/flexible. The real rupture stress of microcapsules can be determined by applying the appropriate mathematical models; the details are presented in Chapter 6. The obtained mechanical property parameters of single microcapsules can be used to compare the mechanical strength of microcapsules within a sample or between samples prepared with various formulations and processing conditions. A parameter of nominal wall tension, T_R, is introduced and defined in Equation 4.1:

$$T_R = \frac{F_R}{\pi D_m} \tag{4.1}$$

where, F_R is rupture force of a single microcapsule and D_m is diameter of a single microcapsule before compression. The nominal wall tension, T_R, is interpreted as tension or stretch of wall at rupture. The nominal wall tension is based on the assumption that microcapsules have uniform wall thickness. Nominal wall tension is derived from the expression of the dimensionless force, y, in Equation 2.6, where the dimensionless curve is independent of microcapsules' size (Wang *et al.*, 2004). Due to such unique characteristics, nominal wall tension is proposed in this work to compare the mechanical strength of microcapsules in two samples with different mean size.

4.6.2 Mechanical Property Parameters of Microcapsules within a Sample

50 MF microcapsules from a typical sample were tested using micromanipulation and their mechanical property parameters are presented here. The relationship between the rupture force and diameter of single MF microcapsules in a typical sample is displayed in Figure 4.9. It shows, in general, the rupture force increases with the increase of microcapsule diameter; this trend was also reported by Sun & Zhang (2001). In this sample, microcapsule sizes range from 8.7 μm to 64.3 μm, and their rupture forces measured mainly fall into the range of 0.1 mN – 1.2 mN.

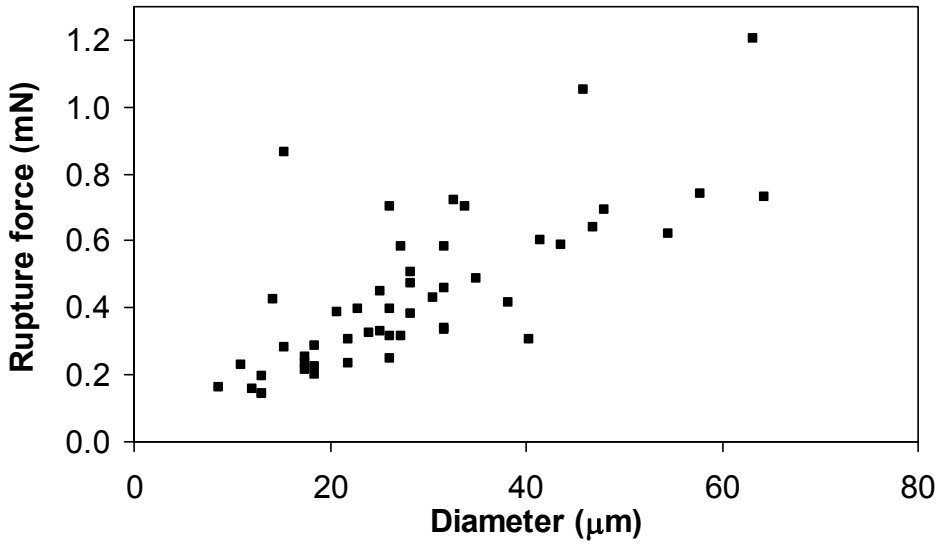

Figure 4.9 A typical graph illustrating the relationship between the rupture force and diameter of single MF microcapsules within a sample.

As shown in Figure 4.10, most of the data points denoting the deformation of microcapsule at rupture fall into the region of 7% to 30%, except for two microcapsules that were ruptured at

approximately 40%. This suggests that the deformation at rupture for majority of microcapsules in a given sample does not change with diameter significantly.

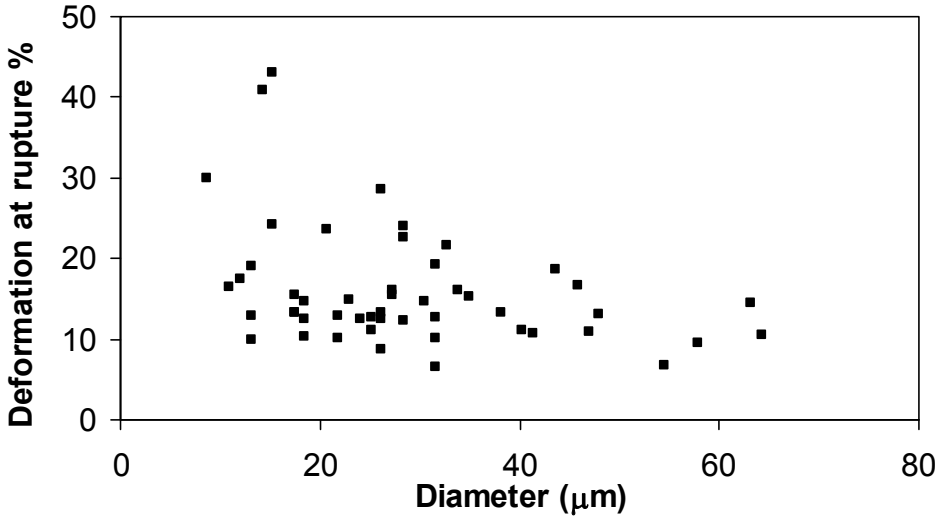

Figure 4.10 A typical graph illustrating the relationship between the deformation at rupture and diameter of single MF microcapsules within a sample.

The nominal rupture stress of microcapsules was calculated and results are shown in Figure 4.11. Overall, the nominal rupture stress decreases with diameter. In other words, large microcapsules may be ruptured more easily than small ones in processing equipment or at end-use applications. It is apparent that nominal rupture stress is size dependent. Hence, nominal rupture stress is not appropriate to compare the mechanical strength of two microcapsule samples which have different mean sizes; this has not been addressed in other literatures. Therefore, the parameter of nominal wall tension is required to be applied in this case.

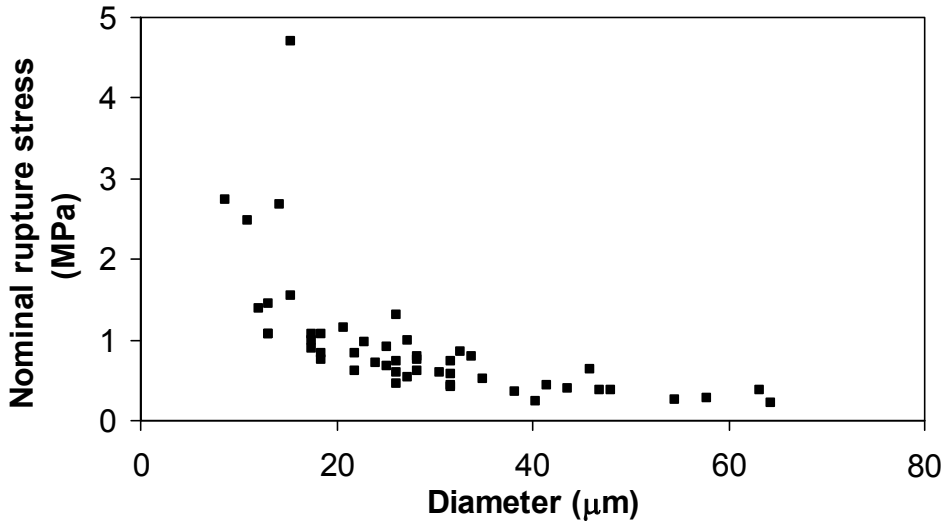

Figure 4.11 A typical graph illustrating the relationship between the nominal rupture stress and diameter of single MF microcapsules within a sample.

The relationship between the nominal wall tension and diameters of microcapsules within a sample is illustrated in Figure 4.12. It is clear that the nominal wall tension of all the microcapsules do not change significantly with the variation of sizes except for an outlier which had a nominal wall tension of 18.0 N/m at a diameter of 15.3 μm. The mean wall tension of MF microcapsules in this sample is 5.1 N/m and the three times of standard error is equal to 1.0 N/m. The nominal wall tension of this particular microcapsule (18.0 N/m) is significantly beyond the upper confidence limit (6.1 N/m) of 99% confidence interval and it is therefore confirmed as an outlier. According to the statistical analysis, this microcapsule's outlier status is also shown in the previous Figure 4.9 - Figure 4.11. The relationship between the nominal wall tension and diameter of MF microcapsules in the given sample in Figure 4.12 further proves the findings of Lardner & Pujara (1980) that the wall tension is size independent. Hence, the mean value of nominal wall tension can be used to compare the mechanical strength of microcapsules for samples with different mean sizes.

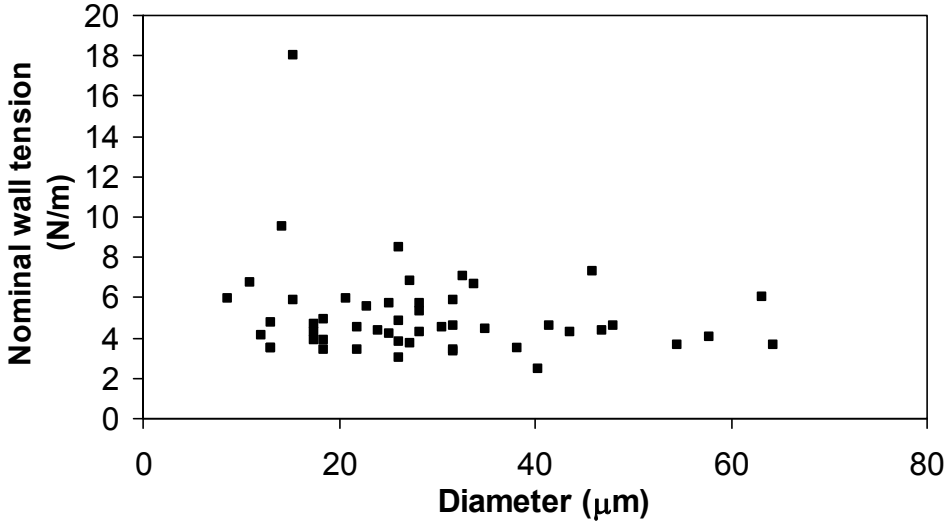

Figure 4.12 A typical graph illustrating the relationship between the nominal wall tension and diameter of single MF microcapsules within a sample.

4.6.3 Mean Mechanical Property Parameters of Microcapsules with Different Mean Diameters

Three samples of MF microcapsules were made using the same formulations, and the only difference between them is mean size of each sample. Their respective micromanipulation results are summarized in Table 4.2 using the analysis methods described above. The values in each cell represent the mean value and the twice standard errors. All the mean diameters of MF microcapsules, which were obtained from micromanipulation, refer to number mean diameter d_{10}. The mean diameters of microcapsules from sample D10, D15 and D30 as shown in Table 4.2, which were obtained from micromanipulation test, are 11.3 ± 0.6 μm, 18.4 ± 1.4 μm and 37.2 ± 2.2 μm respectively. It is shown in Table 4.2 that the mean rupture force of microcapsules in a sample increased with a greater mean diameter. However, the mean deformation at rupture did not seem to vary. The mean nominal rupture stress decreased

significantly with increasing mean size of microcapsules. This means microcapsules with greater mean size are weaker.

Table 4.2 Mean mechanical property parameters of microcapsules in various samples with different mean sizes.

Sample Name	Diameter (μm)	Number of capsule tested	Rupture force (mN)	Deformation at rupture (%)	Nominal rupture stress (MPa)	Nominal wall tension (N/m)
D10	11.3±0.6	55	0.13±0.01	25±2	1.4±0.2	3.8±0.3
D15	18.4±1.4	50	0.21±0.03	24±3	1.0±0.2	4.0±0.7
D30	37.2±2.2	60	0.37±0.08	20±3	0.4±0.2	3.4±1.0

If two parameters are compared and their mean values plus their respective range of twice standard errors are overlapping, such as the mean nominal wall tension of sample D10 (3.8±0.3 N/m) and D15 (4.0±0.7 N/m), a statistic *t* test is required to test whether one is significantly greater than the other one or there is no significant difference between them. The detailed procedures of *t* test are described in Appendix B. The statistic *t* test is applied to the results in this work when similar cases like nominal wall tension of sample D10 and D15 are encountered.

The statistic *t* test was performed on the mean nominal wall tension of each sample in Table 4.2; it was found that no significant difference is between the mean wall tension of microcapsules of the 3 samples with 95% confidence. This implies that these samples had the similar mechanical strength if microcapsules with the same size were compared. The results make sense since the only difference between the samples is the difference in size and no other formulation or processing parameters were varied. The obtained data studies the relationship between the particle size and their mechanical property parameters, which is beneficial to

formulate the microcapsules with a desirable mechanical strength to be able to release the perfume oil when required.

4.6.4 Additional Coating

4.6.4.1 Starch Coating

After MF microcapsules were produced using the *in-situ* polymerisation technique, they were coated with a layer of starch by Procter & Gamble. The details of starch and coating procedures were not specified by company due to confidentiality. Their mechanical strength was then tested using micromanipulation and compared with those without coating. Mean diameters shown in Table 4.3, which are based on randomly selected 30 microcapsules from each sample, are less accurate to represent the mean size of whole sample than other techniques such as Malvern mastersizing, which is able to measure larger number of microcapsules when compared to micromanipulation. The mean deformation at rupture of the starch-coated microcapsules is 13±11% which is much lower than that of microcapsules without coating (37±5%). This is probably due to the brittleness of starch material in turn increases the brittleness of microcapsules, which results in the lower deformation at rupture of starch-coated microcapsules.

Table 4.3 Mean mechanical property parameters of microcapsules without and with starch coating.

Samples	Diameter (μm)	Rupture force (mN)	Deformation at rupture (%)
Without coating	23.4±2.9	1.6±0.3	37±5
Starch coating	22.3±5.2	2.1±0.7	13±11

Since the mean sizes of these 2 samples are not significantly different, only mean nominal rupture stress was calculated, as shown in Figure 4.13. The *t* statistic test shows that the

nominal rupture stress of microcapsules with starch coating (6.7±3.5 MPa) does not significantly differ from that without coating (5.4±2.0 MPa). However, it is also noticed that both mean nominal rupture stress have relatively large standard errors. In addition, the deformation at rupture of starch-coated microcapsules is significantly smaller, which leads to the contact area of microcapsules at rupture were different. As such, appropriate mathematical models are required; see Chapter 6 to determine the real rupture stress of microcapsules with and without starch coating in order to compare their mechanical strength.

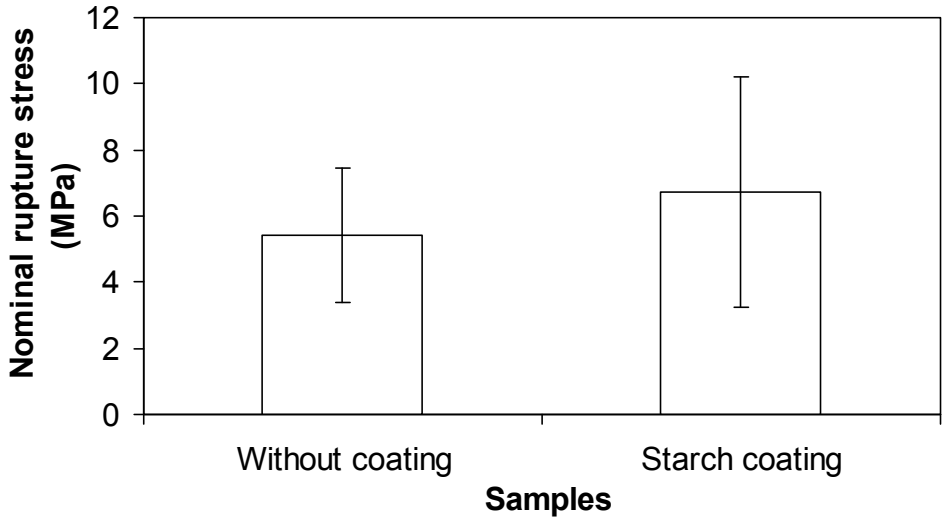

Figure 4.13 Mean nominal rupture stress of microcapsules without and with starch coating.

4.6.4.2 Silicate Coating

Silicate was also used to provide an additional layer of coating around single microcapsules. The mechanical strength of silicate-coated microcapsules was tested and compared with those without the additional coating. 50 microcapsules from each sample were tested; unless otherwise stated, the number of microcapsules tested for each sample is 50 for the results obtained from micromanipulation. The mean mechanical property parameters of

microcapsules are presented in Table 4.4. The mean diameter of tested microcapsules without and with silicate coating is 6.8±0.8 μm and 11.4±1.0 μm, respectively. The mean deformation at rupture of microcapsules with coating is 14±2%, whilst the microcapsules without coating has a mean deformation at rupture of 39±5%. This indicates the microcapsules with a coating of silicate were more brittle than those without.

Table 4.4 Mean mechanical property parameters of microcapsules without and with silicate coating.

Samples	Diameter (μm)	Rupture force (mN)	Deformation at rupture (%)	Nominal rupture stress (MPa)
No coating	6.8 ± 0.8	0.05 ± 0.01	39±5	1.7±0.4
With coating	11.4 ± 1.0	1.50 ± 0.34	14±2	18.8±5.2

The mean nominal rupture stress of microcapsules coated with silicate (18.8±5.2 MPa) is much greater in comparison to that without silicate coating (1.7±0.4 MPa) for the microcapsules tested. Because the mean sizes of microcapsules are significantly different between the two samples, nominal rupture stress is not used here to compare their mechanical strength. In Figure 4.14, the wall tension of microcapsules with silicate coating (44.9±9.9 N/m) is significantly greater than that without coating (2.5±0.4 N/m). This implies that microcapsules with silicate coating were much stronger than those with the same size but without coating. This is due to the formation of a protective silicate layer. Mathematical modelling is applied in Chapter 6 to determine the real rupture stress of microcapsules, which takes the deformation at rupture into consideration. Overall, it can be concluded that the addition of silicate coating around microcapsules can make them more brittle and much stronger than those without. The results present a new direction to increase the mechanical strength of microcapsules if required.

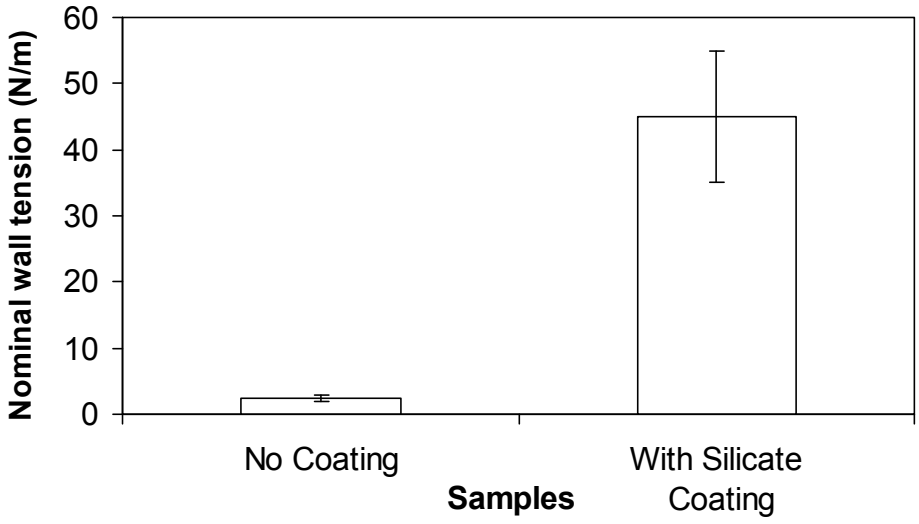

Figure 4.14 Mean nominal wall tension of microcapsules without and with silicate coating.

4.6.5 Variation of Core/Capsule Ratio

The effect of core/capsule ratio in weight % (wt.%) on the mechanical strength of microcapsules is studied here. There are in total 3 pairs of microcapsule samples being tested. Each pair consists of 2 samples which were produced under the same processing conditions; the only difference is core/capsule ratio. Since the mean sizes are different between 2 samples of each pair, nominal wall tension is applied to compare the mechanical strength of microcapsules. For microcapsules in sample pair 1, as shown in Table 4.5 (a), the mean nominal wall tension of microcapsules with 85wt.% core/capsule ratio is 15.2±4.6 N/m, which is significantly greater than that of microcapsules with 95wt.% core/capsule ratio (5.4±1.3 N/m). This is expected since microcapsules with lower core/capsule ratio in wt.% have relatively thicker wall than those with higher core/capsule ratio. For the same size, the thicker wall leads to higher strength. Zhang & Wang (2009) also reported that the release rate of core content studied using anti-osmosis tests increases with the increasing core/capsule ratio of

melamine formaldehyde microcapsules, which was due to the thinner wall of microcapsules. The results of the other 2 pairs of microcapsule samples with "85wt.% vs. 95wt.%" and "85wt.% vs. 92wt.%" core/capsule ratio in Table 4.5 (b) & (c) agree well with the above findings that lower core/capsule ratio results in significantly greater nominal wall tension, which leads to higher mechanical strength of microcapsules. There is not an obvious relationship between the deformation at rupture % and the core/capsule ratio, based on the results of 2 microcapsule samples of each pair. The 3 pairs of samples were from different batches and no information was available to confirm the detailed processing conditions between batches. Therefore, the results between the 3 pairs of samples are not directly compared here.

Table 4.5 Mean mechanical property parameters of microcapsules with different core/capsule ratios.

(a) Sample pair 1: 85wt.% vs. 95wt.%

Sample pair	Core/capsule ratio (wt.%)	Diameter (μm)	Rupture force (mN)	Deformation at rupture (%)	Nominal rupture stress (MPa)	Nominal wall tension (N/m)
1	85	13.0±0.9	0.5±0.1	39±6	5.5±1.9	15.2±4.6
	95	14.5±0.9	0.2±0.1	44±6	1.6±0.4	5.4±1.3

(b) Sample pair 2: 85wt.% vs. 95wt.%

Sample pair	Core/capsule ratio (wt.%)	Diameter (μm)	Rupture force (mN)	Deformation at rupture (%)	Nominal rupture stress (MPa)	Nominal wall tension (N/m)
2	85	30.5±2.1	0.62±0.04	23±1	0.9±0.1	6.6±0.3
	95	21.2±1.8	0.21±0.02	30±3	0.7±0.1	3.3±0.4

(c) Sample pair 3: 85wt.% vs. 92wt.%

Sample pair	Core/capsule ratio (wt.%)	Diameter (μm)	Rupture force (mN)	Deformation at rupture (%)	Nominal rupture stress (MPa)	Nominal wall tension (N/m)
3	85	13.9±1.0	0.31±0.05	41±5	2.28±0.23	7.3±1.2
	92	12.8±0.8	0.05±0.01	18±2	0.44±0.02	1.3±0.1

4.6.6 Addition of Different Components into MF Microcapsule Slurry

4.6.6.1 β-keto Butyramide (BKB)

Formaldehyde plays an important role in the encapsulation of MF microcapsules. Molar ratio of melamine/formaldehyde proved to have significant effect on the molecular structure of microcapsule; higher amount of formaldehyde leads to greater cross-linking of microcapsule walls, and hence microcapsules become stronger (Luo *et al.*, 2007). However, the amount of excess formaldehyde in the MF microcapsule slurry needs to be controlled due to its carcinogen nature; they are normally un-reacted formaldehydes or from hydrolysis of MF over the time. It was reported in the patent EP1991648 (Fossum *et al.*, 2008) that β-keto Butyramide (BKB), also called acetoacetamide, can act as a scavenger to reduce the level of free formaldehyde in MF microcapsule slurry; tests were conducted here to investigate the mechanical strength of microcapsules before and after the addition of BKB into the microcapsule slurry. BKB was added at the room temperature of 25 ºC after microcapsules were made. The surface morphology of both types of microcapsules were observed using EMEM and the images presented in Figure 4.15 show that they have relatively smooth surfaces.

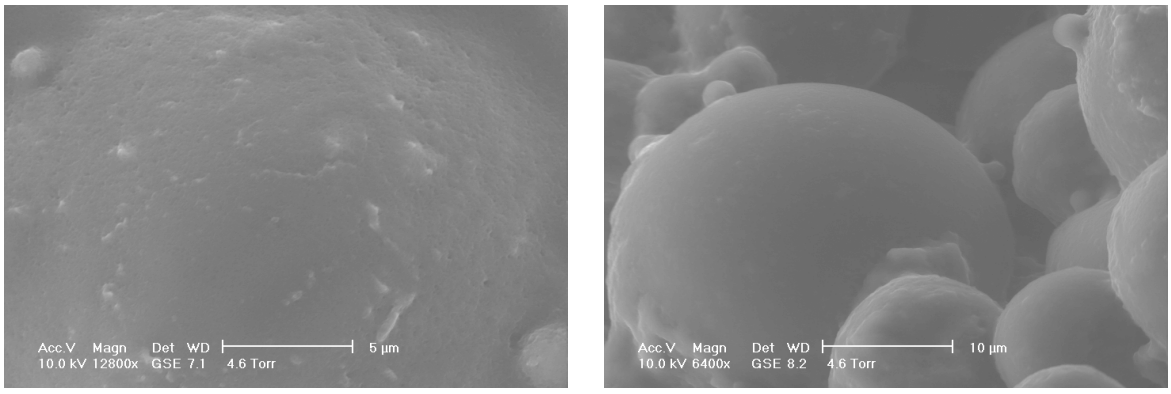

(a) Without BKB **(b) With BKB**

Figure 4.15 The ESEM images of microcapsules in the slurries (a) without BKB and (b) with BKB.

Microcapsules in the samples without and with BKB had number mean diameters of 15.6±1.7 μm and 13.9±1.3 μm respectively. Microcapsules in the slurry containing no BKB had a rupture deformation of 36±5%, which is almost twice of those containing BKB (15±3%). This indicates that microcapsules became more brittle after the addition of BKB. For the microcapsules investigated, their nominal rupture stress decreased from 2.9±1.0 MPa to 0.9±0.2 MPa after the addition of BKB.

Table 4.6 Mean mechanical property parameters of microcapsules without BKB and with BKB.

Samples	Diameter (μm)	Rupture force (mN)	Deformation at rupture (%)	Nominal rupture stress (MPa)
No BKB	15.6±1.7	0.39±0.09	36±5	2.9±1.0
With BKB	13.9±1.3	0.11±0.02	15±3	0.9±0.2

In order to study the effect of BKB on the mechanical strength of microcapsules, their respective nominal wall tension which eliminates the influence of size is presented in Figure 4.16. The nominal wall tension of microcapsules in the slurry without BKB is significantly greater than those with BKB. This implies that BKB is able to lower the mechanical strength of microcapsules and also renders them more brittle. This is probably because the melamine and formaldehyde crosslinking reaction was reversible. Although BKB was added at 25 ºC,

the hydrolysis of crosslinking can take place when melamine formaldehyde is exposed to water (Bauer, 1986; Gerlock, 1986). The reduction in the concentration of free formaldehyde by BKB probably disturbed the original reaction equilibrium and favoured the reverse reaction, which may subsequently reduce the degree of MF polymer crosslinking and then lead to weaker walls of microcapsules and lower nominal wall tension.

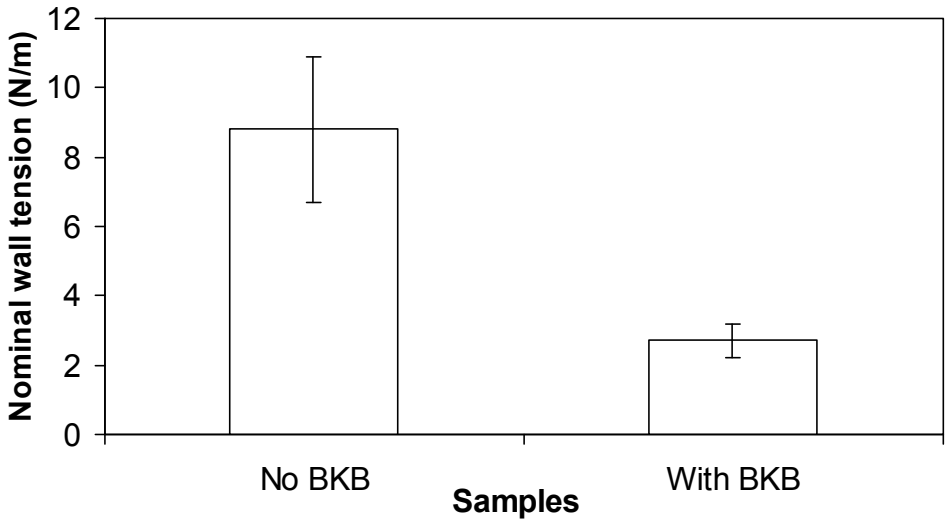

Figure 4.16 Mean nominal wall tension of microcapsules without BKB and with BKB.

4.6.6.2 Xanthan Gum, $MgCl_2$ and Biocide

Additional components including suspending agents of xanthan gum, $MgCl_2$ and biocide of methyl and benzisothiazolinone (MBS) were added into the produced microcapsule slurry by the Procter & Gamble to increase the viscosity of slurry and prevent microcapsules from floating to the top surface, which was due to the smaller density of encapsulated perfume oil than water. Such microcapsule sample was named "structured" sample. In contrast, the microcapsule sample without the addition of additional components was named "unstructured" sample. Malvern particle sizing results reveal that structured and unstructured microcapsule

sample have volume weighted mean diameters of 54.08±5.51 μm and 27.23±0.03 μm respectively. It was found that the former had approximately twice the mean size of the later after the introduction of the additional components and also had much larger standard errors. This can be explained by a microscopic image of suspended microcapsules in water from the structured sample (Figure 4.17), in which some single microcapsules aggregated together to form clusters due to the addition of extra components. Single microcapsules cannot be easily separated from the clusters even after being dispersed in the water and shaken vigorously, and then mixed at the agitation speed of 2000 rpm by Malvern particle sizing. On the contrary, microcapsules from unstructured sample appeared individually once being dispersed in water (microscopic image not shown). As a result, the Malvern measurement obtained can not represent the real mean size of single microcapsules in the structured sample.

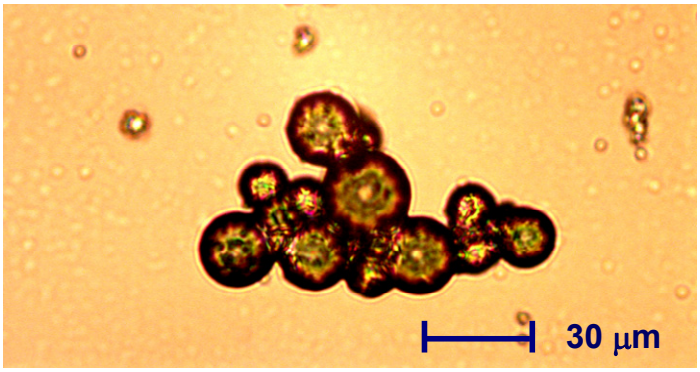

Figure 4.17 An optical microscopic image of microcapsules suspended in water from the structured sample.

The micromanipulation results of 30 microcapsules from each of structured and unstructured samples are summarized in Table 4.7. Both samples have rather similar mean deformation at rupture %. The mean nominal rupture stress of the structured and unstructured microcapsules is 2.3±0.4 MPa and 4.5±1.6 MPa respectively.

Table 4.7 Mean mechanical property parameters of microcapsules in the structured and unstructured samples.

Samples	Diameter (μm)	Rupture force (mN)	Deformation at rupture (%)	Nominal rupture stress (MPa)
Structured	30.5±2.0	1.5±0.1	19±3	2.3±0.4
Unstructured	24.8±3.2	1.5±0.3	17±3	4.5±1.6

However, it is noticed that the mean size of tested microcapsules in the unstructured sample is approximately 6 μm smaller than the structured ones. As mentioned previously, the size also has an influence on the nominal rupture stress. Hence, nominal wall tension of structured and unstructured microcapsules is compared and shown in Figure 4.18. The results of *t* statistic test suggest the wall tensions of microcapsules in the structured sample are smaller than those in unstructured ones. Since the majority of microcapsules in the structured sample were aggregated, the single microcapsules being tested were a small amount of the whole sample and therefore cannot fully represent the mechanical strength of microcapsules. Hence, the obtained results should be treated with caution. Furthermore, the purpose of adding the additional components was to thicken the microcapsule slurry and no evidence suggested such components could weaken the MF wall. Theoretically, no significant difference should be between the mean nominal wall tension of microcapsules in the two samples. As a result, further work is required to find a way to test the mechanical strength of those microcapsules which were in aggregation to reflect the real and unbiased mechanical strength of microcapsules in the structured sample.

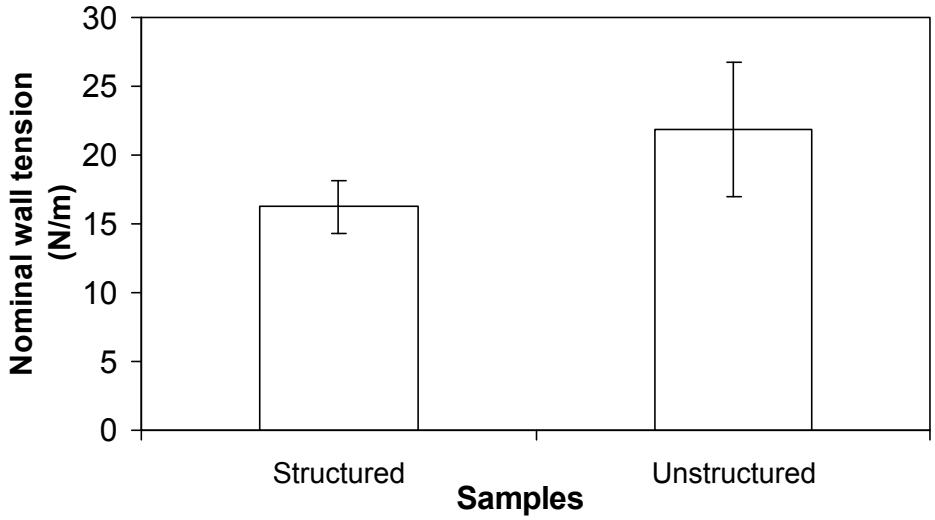

Figure 4.18 Mean nominal wall tension of microcapsules in the structured and unstructured samples.

4.6.6.3 Elvax Polymer

It has been found that the incorporation of hydrophobic polymers, such as elvax polymer which is a copolymer of ethylene and vinyl acetate, into the perfume oil as the core of MF microcapsules can improve stability by thickening the core and slowing the diffusion of the fragrance from the core, as shown in the patent US7491687 (Popplewell *et al.*, 2009). In order to investigate the addition of elvax polymers on the mechanical strength of microcapsules, micromanipulation tests were performed on two microcapsule samples which were produced under the same processing condition. The only difference is that the core contents of microcapsules in the 2 samples are composed of 0% and 10% elvax polymers respectively; the rest of core contents other than the elvax polymers are perfume oil only.

30 microcapsules from each of the samples were tested and their mean mechanical property parameters are shown in Table 4.8. It is shown that microcapsules containing 10% elvax

polymer are more brittle than those without the polymer, since their mean deformation at rupture (15±2%) are much lower in comparison to that of microcapsules containing no elvax polymer (32±3%). It was shown in the results of *t* statistic test that no significant difference is between the mean nominal rupture stress of microcapsules with 0% (3.4±1.0 MPa) and 10% elvax polymer (2.4±0.4 MPa).

Table 4.8 Mean mechanical property parameters of microcapsules containing no and 10% elvax polymer.

Samples	Diameter (μm)	Rupture force (mN)	Deformation at rupture (%)	Nominal rupture stress (MPa)
No elvax	19.9±2.2	0.8±0.1	32±3	3.4±1.0
10% elvax	25.5±3.1	1.1±0.1	15±2	2.4±0.4

Due to the size difference between the tested microcapsules, nominal wall tension is plotted in Figure 4.19 to evaluate the sole effect of elvax polymer on the mechanical strength of microcapsules. The results of *t* statistic tests indicate that the nominal wall tension for microcapsules with 0% & 10% elvax polymer have no significant difference. This is reasonable since the role of elvax polymer is to thicken core contents. The only difference between these microcapsule samples is the composition of core contents, whilst other parameters, such as core/capsule ratio, that are known to affect the mechanical strength of microcapsules remain the same.

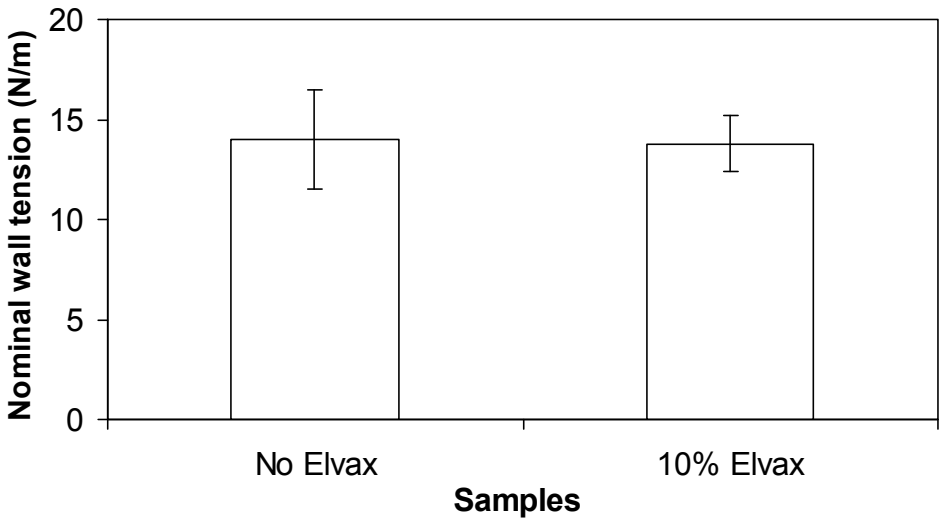

Figure 4.19 Mean nominal wall tension of microcapsules containing no and 10% elvax polymer.

4.6.7 Variation in pH of MF Microcapsule Suspending Liquid

The final pH of detergents, into which MF microcapsules are incorporated, could be different from the pH of microcapsules at formulation. It is therefore important to investigate the influence of pH on the mechanical strength of MF microcapsules. As a result, MF microcapsules in water suspension at a range of pH from 2 to 11 were studied here. The microcapsules dispersed in water had a pH of 6 and a volume weighted mean diameter of 27.55±0.03 μm from the measurement of Malvern particle sizing. Their mechanical strength was tested by micromanipulation. The pH of microcapsules in water suspension was then adjusted to pH 2 and pH 11 using 10wt.% HCl solution and 10wt.% NaOH solution respectively. The microcapsules remained at such two pH conditions for a duration of 25 hours before they were tested by Malvern particle sizing and micromanipulation. The volume weighted mean diameters of microcapsules at pH 2 and pH 11 were 28.06±0.02 μm and 28.15±0.03 μm. It appears that the size measured at pH 2 and 11 was approximately 0.60 μm

greater than that at pH 6. Experiments were conducted earlier to study the repetivity of the Malvern measurement results. A repetitive measurement of microcapsules in a given sample with a volume weight mean diameter of 16.99 μm suggested that the repeated results could be 0.45 μm different from the original one due to the sampling of microcapsules. Therefore, the mean size of MF microcapsules at varying pH was considered as no significant change. This finding was confirmed with their size distribution presented in Figure 4.20, which indicates that the size distribution of microcapsules does not change significantly with varying pH. This implies that pH ranging from 2 to 11 had no significant influence on the size of microcapsules for the investigated duration.

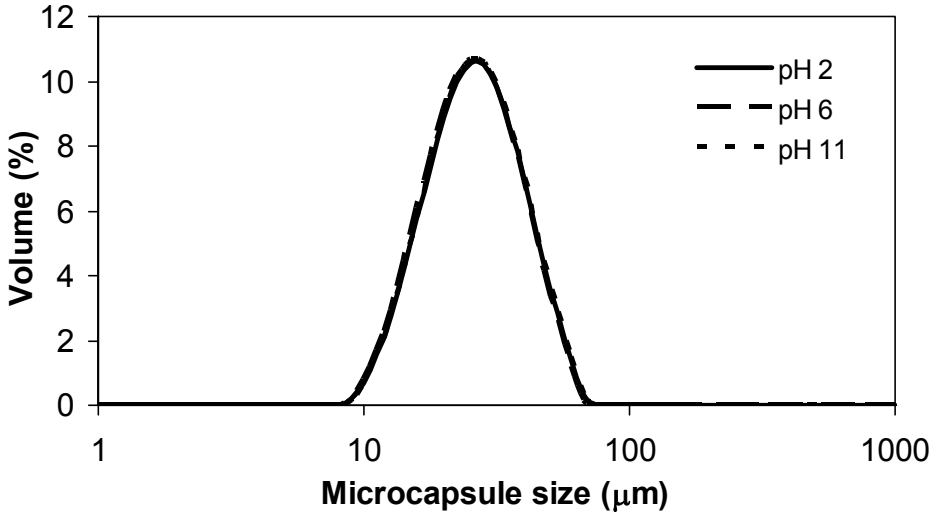

Figure 4.20 Size distribution of microcapsules that were in water suspension and at varying pH.

The mean mechanical property parameters of MF microcapsules which were in water suspension and at varying pH are presented in

Table 4.9. The deformation at rupture of microcapsules at pH 2, 6 and 11 is 39±5%, 37±6% and 37±5% respectively. This suggests that varying pH for the given duration did not make

microcapsules more flexible or brittle. No significant difference is between the nominal rupture stress of tested microcapsules at different pH, according to the *t* statistical test results.

Table 4.9 Mean mechanical property parameters of microcapsules that were in water suspension and at varying pH.

Sample pH	Diameter (μm)	Rupture force (mN)	Deformation at rupture (%)	Nominal rupture stress (MPa)
2	27.1±2.3	1.6±0.4	39±5	3.3±1.1
6	26.6±2.4	2.1±0.4	37±6	4.6±1.4
11	26.4±2.5	2.1±0.6	37±5	4.1±0.9

In Figure 4.21, the mean nominal wall tension of microcapsules at various pH is presented and the results of *t* statistic test show that no significant difference is between the 3 microcapsule samples. This indicates that the mechanical strength of microcapsules is not affected by varying pH from 2 to 11 for a duration of 25 hours. Although hydrolysis of MF can take place under the acidic condition (Bauer, 1986), the obtained results here implied that the MF wall was not weaken at pH 2 after a period of 25 hours. This is consistent with the finding of Gao *et al.* (2001) that MF can not be dissolved at pH higher than 1.7. Gao *et al.* (2001) suggested this was because the rate of crosslinking was higher than the rate of hydrolysis, based on the measurement results of infrared spectra of MF treated with HCl with different pH values. The obtained results here are useful to the development of detergent products at varying pH for the laundry process which requires the contribution of MF microcapsules.

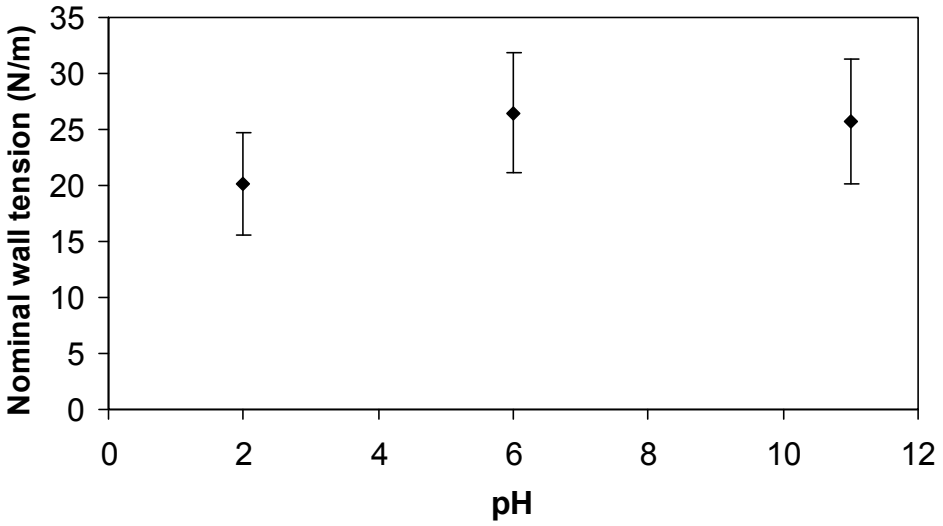

Figure 4.21 Effect of pH on the nominal wall tension of microcapsules.

4.7 Conclusions

MF microcapsules in a given sample, which was produced by an in-situ polymerisation technique and contained perfume oil, were found to be spherical and had a relatively smooth surface from their ESEM images. The mean wall thickness of MF microcapsules in a sample was calculated to be 850 nm, based on their core/capsule ratio of 80wt.%; this is not consistent with the TEM results that mean wall thickness of MF microcapsules within the same sample was found to be 175±11 nm. This over-estimation on wall thickness may be partly due to an incomplete use of MF polymer pre-condensate during formation of microcapsules. Furthermore, MF microcapsules exhibited no visco-elastic property at a mean deformation of 7±1%, but showing weakly visco-elastic behaviour at a further mean deformation up to 12±2%. The elastic limit of MF microcapsules in a sample which had a rupture deformation of 24±3% was found to be 15±1%.

In a given sample, it was revealed that the rupture force of MF microcapsules increased with an increase in diameter; this is consistent with the trend observed by Sun & Zhang (2001). The deformation at rupture, which can be used to evaluate the brittleness of microcapsules, does not seem to change significantly. The nominal rupture stress of microcapsules decreases with an increase in diameter; this is also in agreement with the results obtained by Xue & Zhang (2009). Such trends were also applicable to microcapsules with different mean sizes between samples. Mechanical strength parameters including rupture force and nominal rupture stress can be used to compare the mechanical strength of microcapsules but with some limitations. Rupture force and nominal rupture stress can be applied to microcapsules which have similar diameters and comparable deformation at rupture. Another mechanical property parameter, nominal wall tension, which was derived from the dimensionless force curve (Wang *et al.*, 2004) and is independent of size, was introduced to compare the mechanical strength of MF microcapsules with various formulations.

The factors that can influence the mechanical strength of microcapsules have been identified. For example, the reduction in size increased the nominal rupture stress of microcapsules. The increase in core/capsule ratio reduced the nominal wall tension of microcapsules. Addition of silicate or starch coating can make microcapsules more brittle. The nominal rupture stress of starch-coated microcapsules had relatively large standard errors and significant different rupture deformation before and after coatings, mathematical models are applied in Chapter 6 to determine their rupture stress in order to compare their mechanical strength. Microcapsules with silicate coating had much higher nominal wall tension. The β-keto Butyramide (BKB), which was added into the microcapsule slurry to reduce the amount of free formaldehyde, was

found to reduce the nominal wall tension of microcapsules. It was suggested that the lower concentration of free formaldehyde favours the reverse reaction and caused the reduction of crosslinking of MF polymer. Future work involves applying TEM to measure the wall thickness of such microcapsules to confirm the finding. Microcapsules in the slurry, which was added with a combination of xanthan gum, $MgCl_2$ and biocide to increase the viscosity, were found to have lower nominal wall tension. Further work is required to confirm the finding, since the test results were based on small part of single microcapsules and cannot fully represent the mechanical strength of majority of microcapsules which were in aggregation. MF microcapsules with core contents comprising 10% elvax polymer were found to have no significant different nominal wall tension than those without elvax polymer. Furthermore, the interpreted micromanipulation results suggest that the nominal wall tension of microcapsules did not differ significantly, after they were suspended in water with a pH range of 2 to 11 for a duration of 25 hours. It is of interest for the future work to study the influence of such pH range on the mechanical strength of microcapsules for a period longer than 25 hours.

In conclusion, micromanipulation is a very powerful tool to characterise the mechanical strength of microcapsules. The factors including size, core/capsule ratio as well as the variation in formulation which are capable of influencing the mechanical strength of microcapsules have been discussed in this chapter. The obtained results are very useful for the production of microcapsules which are required to possess different mechanical strength for a variety of industrial applications.

5. EFFECT OF PREPARATION AND PROCESSING CONDITIONS ON THE MECHANICAL STRENGTH OF MF MICROCAPSULES

The variation in the preparation and processing conditions of microcapsules is vast in the process industry. In this chapter, micromanipulation was employed to study the mechanical strength of MF microcapsules which were supplied by Procter & Gamble and with different preparation and processing conditions, such as polymerisation time and temperature, and production scale (lab, pilot plant and full scales). The effect of heat treatment on the mechanical strength of microcapsules is also investigated. As well as supplied in slurry form, end-use products incorporated with microcapsules are often required to undergo drying prior to delivery. Therefore, the mechanical strengths of microcapsules dried using different methods (oven drying, spray drying and freeze drying) are also compared here. The effect of fluidised bed drying on the mechanical strength of microcapsules in the agglomerates was also investigated. In addition, the mechanical strength of microcapsules, which are in the slurry, dried by ambient air and rehydrated, is also studied in this chapter.

5.1 Polymerisation Time and Temperature

5.1.1 Polymerisation Time

The in-situ polymerisation method described in Chapter 3 was modified to study the impact of polymerisation time on the mechanical strength of formed microcapsules. In total, 3 MF microcapsule samples were produced with different lengths of polymerisation time; that is 2, 4 and 6 hours. The temperature was maintained at 65 ºC throughout the period of

polymerisation. The samples were subsequently tested using micromanipulation to investigate the influence of polymerisation time on their mechanical strength and the results are presented in Table 5.1.

Table 5.1 Mean mechanical property parameters of microcapsules produced using different lengths of polymerisation time.

Polymerisation time (hour)	Diameter (μm)	Rupture force (mN)	Deformation at rupture (%)	Nominal rupture stress (MPa)
2	13.4±1.1	0.047±0.007	26±4	0.45±0.12
4	15.7±1.2	0.059±0.005	18±2	0.38±0.06
6	12.6±1.3	0.073±0.010	25±4	0.85±0.22

Among the 3 samples, the microcapsules made with 6 hours polymerisation seemed to have the highest mean nominal rupture stress. It was noticed that the mean size of tested microcapsules from micromanipulation measurement was slightly different due to random selection of 30 microcapsules per sample. Since size also can influence the mechanical strength of microcapsules, the mean nominal wall tension of microcapsules at rupture was also determined for each sample as shown in Figure 5.1, which is independent of size and can be used to compare the mechanical strength of microcapsules here. The *t* statistic test results revealed that no significant difference was between the mean nominal wall tension of microcapsules with 2 and 4 hours polymerisation time, and microcapsules made with 6 hours polymerisation time had significantly higher nominal wall tension than the former two microcapsule samples made with shorter polymerisation time. Overall, the findings here indicate that the polymerisation time of 6 hours seemed to produce strongest microcapsules for the conditions investigated. This is probably because the longer polymerisation time leads to higher degree of crosslinking of MF wall, and hence microcapsules with 6 hours

polymerisation time had the highest nominal wall tension. Further work can involve measuring wall thickness of microcapsules to validate this finding as well as exploring the kinetics of polymerisaiton reaction. Future experiments may include the comparison of mechanical strength of microcapsules with longer polymerisation time at a constant temperature of 65 ºC, e.g. 24 hours. Results would help to determine whether such long polymerisation time offers any benefit in enhancing the mechanical strength of microcapsules.

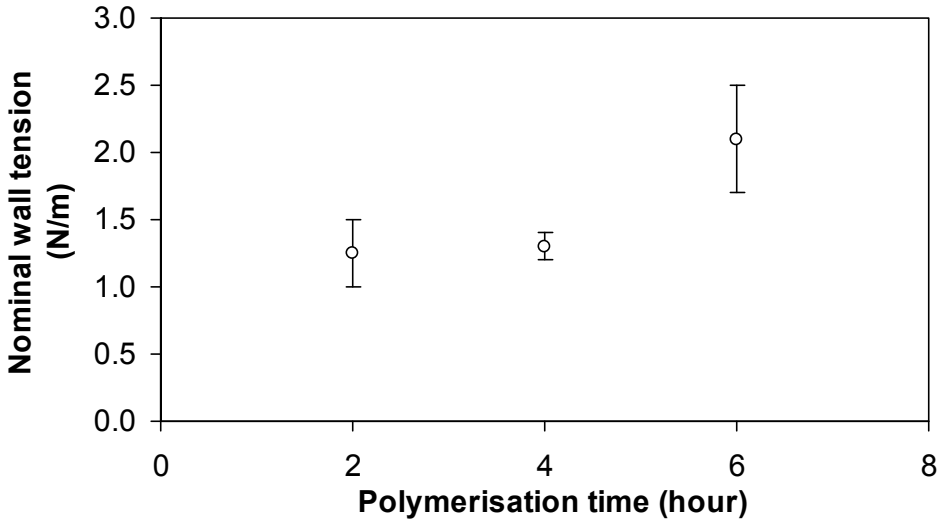

Figure 5.1 Mean nominal wall tension of microcapsules produced using different lengths of polymerisation time.

5.1.2 Polymerisation Time and Temperature

Microcapsules in one sample were encapsulated by allowing the polymerisation of MF wall to last for 2 hours at 65 ºC, whilst the duration of polymerisation for producing microcapsules in the other sample is 24 hours. The 24-hour period was split into an initial 8-hour at 65 ºC and an additional 16-hour at 85 ºC. All other processing parameters used to encapsulate the microcapsules of these 2 samples were kept the same. These 2 samples were treated and supplied by the company with the described processing conditions. It is worth pointing out

that both polymerisation time and temperature were varied for the 2nd sample, which makes it difficult to single out the sole effect of increase in polymerisation time or temperature on the mechanical strength of microcapsules. Therefore, this point needs to be taken note for the further work on designing microcapsules for the analysis.

Size measurement made using Malvern particle sizing shows that these 2 samples had similar volume weighted mean diameters of 12.76±0.02 μm and 12.60±0.01 μm. The shape of their size distribution curves in Figure 5.2 is similar; both samples in terms of volume % of size distribution have a large peak and a much smaller peak centring on 13.2 μm and 1.2 μm respectively. It is therefore suggested that prolonging the polymerisation time and increasing the temperature did not lead to an increase in the microcapsule mean size, which is expected since the size of microcapsules should be dominated by the droplets generated in the stage of emulsification.

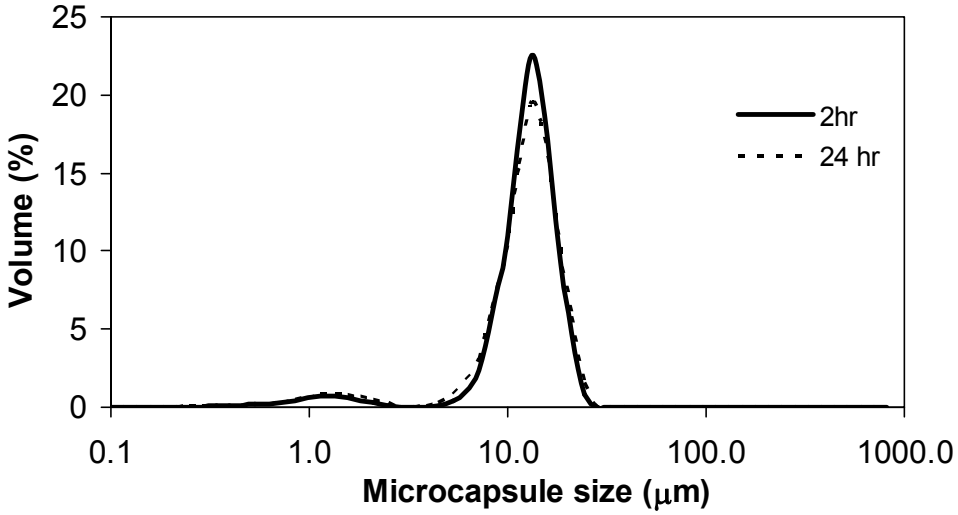

Figure 5.2 Size distribution of microcapsules with different lengths of polymerisation time and temperature.

Micromanipulation tests were also conducted for the study of the impact of polymerisation time & temperature on the mechanical strength of microcapsules. The number mean diameters of 50 microcapsules from each sample were 14.3±0.8 μm and 11.3±0.6 μm, as shown in Table 5.2. It is apparent that microcapsules from the sample prepared with longer polymerisation time and higher temperature had a larger mean rupture force of 0.260±0.072 mN, an 8-fold increase from that of microcapsules with shorter polymerisation time and lower temperature, even though microcapsules in the former sample chosen for micromanipulation test had a slightly smaller mean diameter.

Table 5.2 Mean mechanical property parameters of microcapsules from samples with different polymerisation time & temperature.

Polymerisation conditions of samples	Diameter (μm)	Rupture force (mN)	Deformation at rupture (%)	Nominal rupture stress (MPa)
2 hours at 65 ºC	14.3±0.8	0.027±0.003	8±1	0.19±0.04
8 hours at 65 ºC & further 16 hours at 85 ºC	11.3±0.6	0.260±0.072	42±3	2.71±0.72

The results also reveal the shorter polymerisation time and lower polymerisation temperature produced more brittle microcapsules, since their mean rupture deformation (8±1%) is approximately one fifth of that with lengthier polymerisation time and higher temperature (42±3%). Further study needs to be conducted to understand the reason why a significant difference is between the deformations at rupture of microcapsules. Furthermore, it was also shown that microcapsules with longer polymerisation time and higher temperature had significantly higher nominal rupture stress than the ones with shorter polymerisation time and lower temperature. Since the number mean diameters of microcapsules tested using micromanipulation differed by approximately 3 μm, the mean nominal wall tension was

calculated and is shown in Figure 5.3. The results suggested microcapsules had significantly higher nominal wall tension whilst they were polymerised for a first 8 hours at 65 ºC and a further 16 hours at 85 ºC. Hence, it was demonstrated that microcapsules prepared with longer polymerisation time and higher temperature possessed higher mechanical strength.

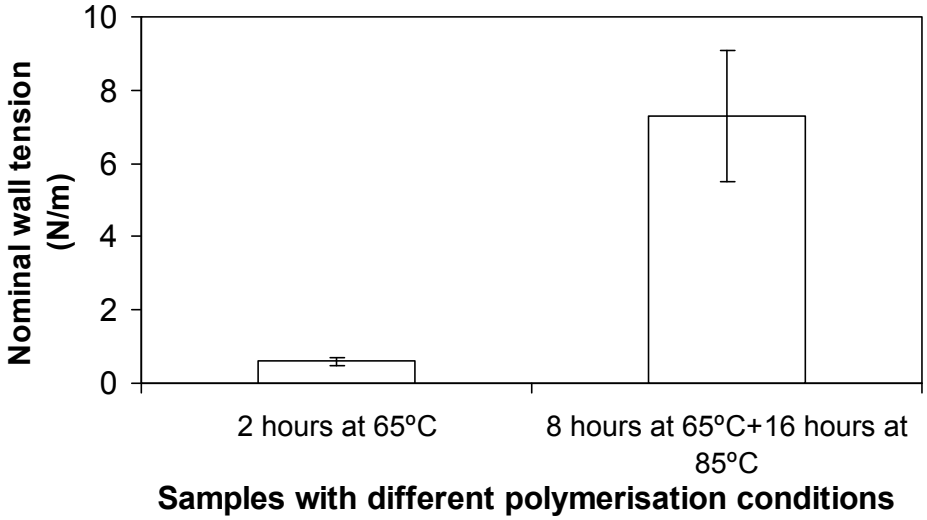

Figure 5.3 Mean nominal wall tension of microcapsule samples with different lengths of polymerisation time and temperature.

MF microcapsules made using longer polymerisation time and higher temperature had significantly higher nominal wall tension. This might be because higher polymerisation temperature accelerated the polymerisation reaction. In addition, the longer polymerisation time could also help to create a higher degree of crosslinking. This in turn resulted in production of higher cross-linking of MF wall. Chemical cross-linking reduces the free volume by bringing adjacent polymer chains close together (Ward & Hadley, 1993). As such, the resulting microcapsules had walls with less free volume and were mechanically stronger. Further work is required to measure the wall thickness of microcapsules from such two samples to validate the higher degree of cross-linking for microcapsules with longer

polymerisation time and temperature. It is also worth to explore the kinetics of polymerisation reaction in the further work. It would be of interest for future studies to investigate the sole influence of polymerisation time or temperature on the mechanical strength of microcapsules, by varying polymerisation time alone (up to 24 hours) at a constant temperature of 65 ºC and comparing with microcapsules prepared at a constant temperature of 85 ºC but keeping the 24 hour polymerisation time. It is noticed that microcapsules in the two samples studied in Chapter 5.1.1 and 5.1.2 were both produced with the same polymerisation duration and temperature (2 hours at 65 ºC). They were however supplied from different batches and dates, and the chemicals added by the supplier at the post-process could be different between batches. Therefore, the mechanical strengths of microcapsules from these two samples are not directly compared here.

5.2 Production Scale

It is of great importance to ensure the microcapsules produced at full scale (e.g. factory production) possess matching mechanical strength as those made at pilot plant and lab scale, hence, the polymerisation time and temperature must be maintained. Lab, pilot plant and full scale are defined according to the quantity of microcapsules being produced in one batch; that is 1 kg, 100 kg and 8000 kg respectively. The effect of adopting different production scales of encapsulation on the mechanical strength of microcapsules was investigated and the results are presented in this section.

Microcapsules prepared in all scales (lab, pilot plant and full scale) were measured using Malvern particle sizing; their volume weighted mean diameters were 9.00±0.01 μm, 14.4±0.02

μm and 13.5±0.02 μm respectively. It is an interesting finding that the mean size of microcapsules manufactured in lab scale is approximately 5 μm smaller than those produced in larger scales, but there is no significant difference in mean size between microcapsules manufactured in pilot plant and full scales. This suggests that the agitation speed used in the emulsification step in pilot plant and full scale was slower than what it should be, since the size of microcapsules produced depends critically on the stirring speed (Sgraja *et al.*, 2008). The use of higher speed generally leads to production of smaller oil droplets. As a result, smaller microcapsules are made after small oil droplets are surrounded by MF wall material and polymerised. The results show that the encapsulation process was not properly scaled up by the manufacturer. Moreover, the size distribution of 3 microcapsule samples is presented in Figure 5.4, which indicated microcapsules made in lab scale had the narrowest size distribution among all.

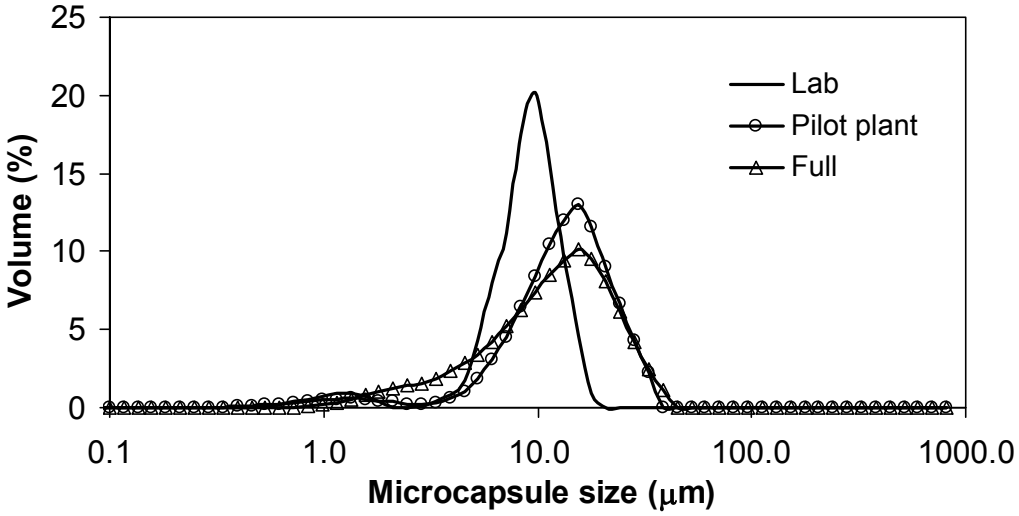

Figure 5.4 Size distribution of microcapsules produced at different scales.

50 microcapsules from every sample produced at lab, pilot plant and full scales were tested using micromanipulation and had number mean diameters of 11.3±0.6 μm, 12.6±1.0 μm and

13.5±0.9 μm respectively. The mean rupture forces of microcapsules produced at different scales is shown in Figure 5.5. It is found that the mean rupture force of microcapsules prepared in lab scale (0.13±0.01 mN) are significantly greater than those manufactured at pilot plant scale (0.03±0.01 mN) and full scale (0.015±0.002 mN), even though the statistic *t* test suggested the mean diameters of the former microcapsules tested by micromanipulation had smaller mean size than the latter two. It implies that production scales of microcapsules had a significant impact on the mechanical property parameters of microcapsules, such as rupture force.

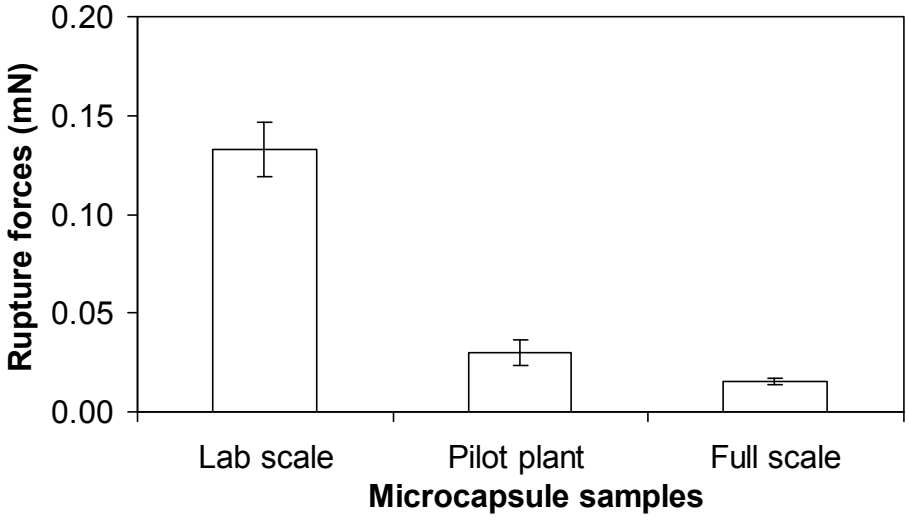

Figure 5.5 Mean rupture forces of 3 microcapsule samples manufactured at different scales.

To understand the influence of production scale on the mechanical strength of microcapsules in greater depth, the graphs showing the detailed rupture forces of single microcapsules manufactured at different scales are plotted in Figure 5.6. It is clear from Figure 5.6 (a) that the rupture force of microcapsules prepared in lab scale increases with the increase of microcapsule diameter on average. However, the increasing trend of rupture force with diameter is less significant for microcapsules produced at pilot plant scale, see Figure 5.6 (b).

And finally, the rupture force of microcapsules manufactured at full scale does not seem to change with diameter, as shown in Figure 5.6 (c).

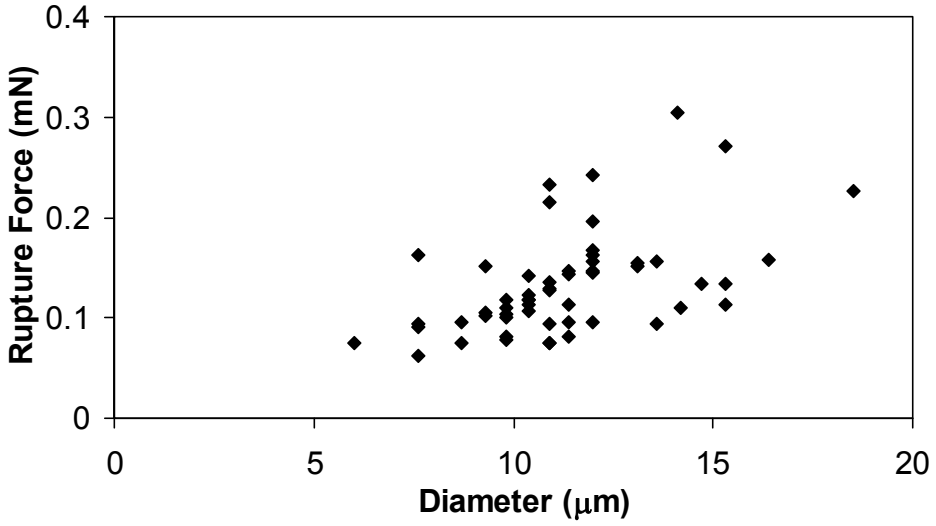

(a) Lab scale.

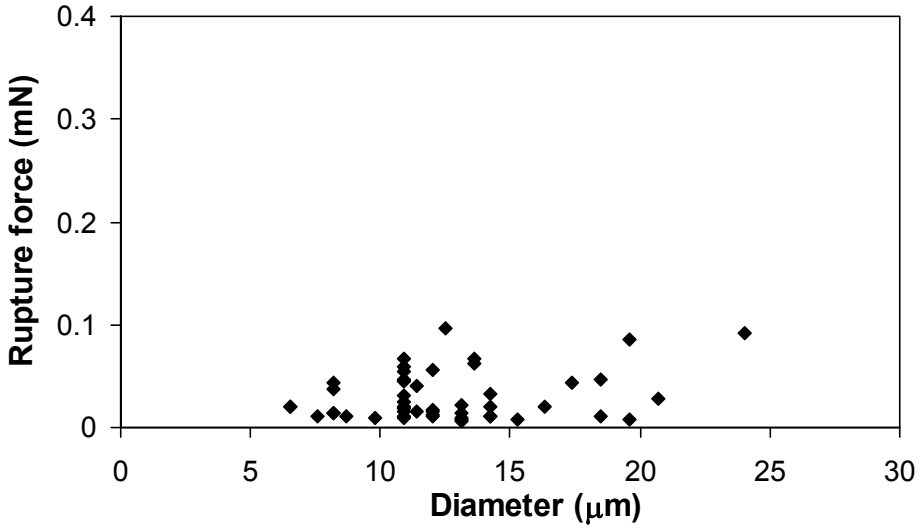

(b) Pilot plant scale.

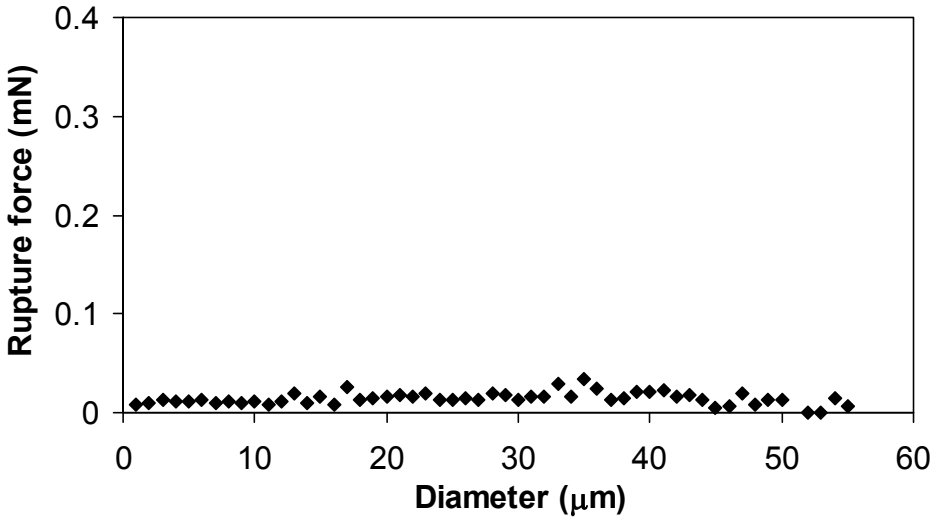

(c) Full scale.

Figure 5.6 Rupture forces of microcapsules manufactured at different scales.

The mean deformation at rupture for microcapsules made at lab, pilot plant and full scales was 25±2%, 21±3% and 14±2%, respectively. They indicate that microcapsules manufactured at full scale were the most brittle. The mean nominal rupture stress of microcapsules manufactured in lab scale was found to be the greatest (1.4±0.2 MPa) among all, as illustrated in Figure 5.7. The mean nominal rupture stress for microcapsules produced in pilot plant and full scale was 0.3±0.1 MPa and 0.1±0.0 MPa respectively.

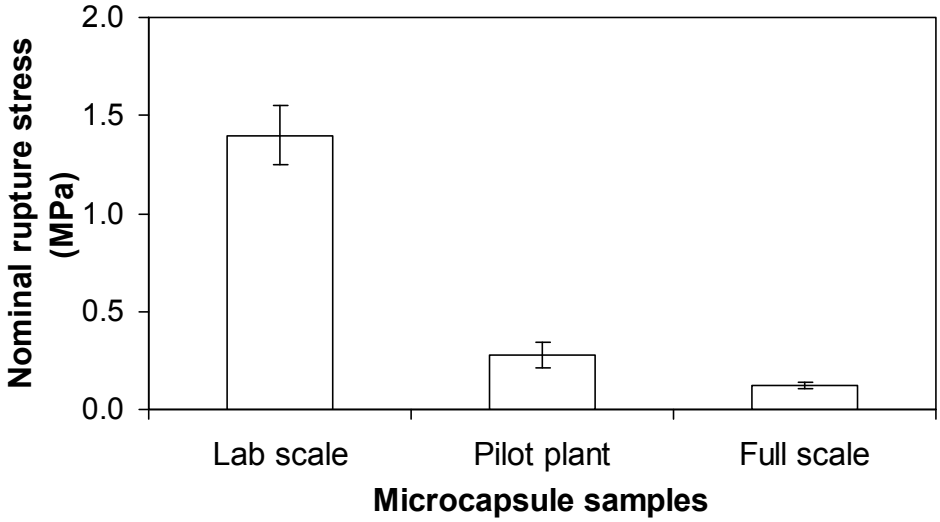

Figure 5.7 Mean nominal rupture stress of 3 microcapsule samples manufactured at different scales.

The comparison of mean nominal wall tension of microcapsules made in different scales as illustrated in Figure 5.8 also shows the same trend as in Figure 5.7. Hence, it is revealed that microcapsules of a given size produced in smaller scale (lab scale) tended to possess greater nominal wall tension in comparison to those manufactured in the larger scales (pilot plant and full scales). Moreover, the microcapsules produced in the largest scale (full scale) were most brittle and weaker. As discussed above, the smaller size of microcapsule made in lab scale was probably due to the use of high agitation speed. Smaller microcapsules are normally stronger than larger microcapsules, based on the conclusion of Chapter 4. This leads to higher nominal wall tension measured for microcapsules from lab scale. Furthermore, comparing the same size of microcapsules in different scales, microcapsules from lab scale have the highest rupture force whilst those from full scale have the lowest. This implies microcapsules from lab scale probably have thicker wall, hence, core/capsule ratio and processing conditions such as polymerisation time used in different scales are required to be checked. In order to achieve the proper scale-up, it is recommended to calculate Reynold's number for 3 different scales which

is concerned with the parameters such as density, viscosity, impeller diameter as well as agitation speed. It is essential to determine the mechanical strength of microcapsules prepared using different production scales to ensure the proper process scale-up is achieved.

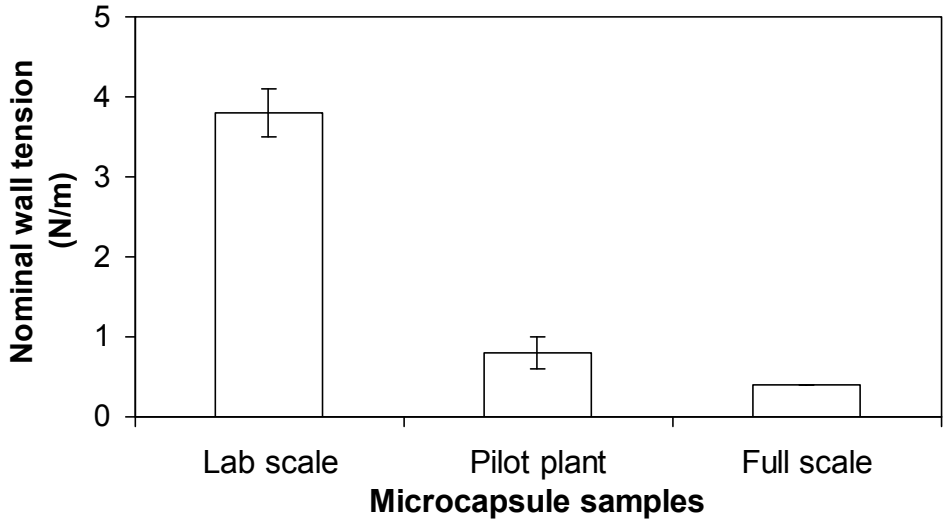

Figure 5.8 Mean nominal wall tension of 3 microcapsule samples manufactured at different scales.

5.3 Glass Transition Temperature T_g

Microcapsules were heated to 120 ºC, which is above the glass transition temperature T_g of MF shell material (97 ºC), and then cooled down to room temperature in order to reduce the leakage of the core contents of microcapsules. The speeds of heating and cooling are not specified by the company that supplied the samples. The duration of microcapsules stayed at 120 ºC was also not given. The glass transition temperature of 97 ºC for MF material was provided by Burdis (2009). T_g can be measured using a differential scanning calorimetry (DSC) technique which detects a characteristic change in specific heat at T_g (Roos & Karel, 1991). It is of interest to see how the heat treatment affected the mechanical strength of

microcapsules. 30 microcapsules from each of two samples (before and after the heat treatment) were tested using micromanipulation. Their mechanical property parameters are presented in

Table 5.3. It shows that the heat treatment caused a decrease in the mean rupture force of the microcapsules, whilst the size and deformation at rupture did not change significantly.

Table 5.3 Mean mechanical property parameters of microcapsules before and after heat treatment.

Samples before and after heat treatment	Diameter (μm)	Rupture force (mN)	Deformation at rupture (%)
Before	26.3±2.4	1.6±0.3	24±3
After	27.3±2.8	0.9±0.1	20±2

As illustrated in Figure 5.9, the mean nominal rupture stress of microcapsule before heat treatment (3.1±0.5 MPa) is approximately twice of that of microcapsules after heat treatment (1.6±0.3 MPa). This implies that microcapsules became weaker after heat treatment. During heat treatment, semi-crystalline or amorphous material could transform from glassy state to rubbery state when they are heated to or above T_g. In glassy state, the molecules within the material may only have a slight vibration, but they can wiggle around once heated to the rubbery state. Therefore, polymers in rubbery state have less cross-linking in comparison to those in glassy state (Ashby & Jones, 2005). The wall material of microcapsules in the rubbery state involves more free volume in the polymer matrix in comparison to that in the glassy state; this free volume in turn reduced wall density and weakened the wall (Partanen *et al.*, 2005). Furthermore, the collapse of the structure may take place if the material matrix is transformed into the rubbery state, which results in the weakening of material matrix above T_g (Roos and Karel, 1993).

Roos & Karel (1991) presented a diagram titled "physical state of materials" which described the change of material states at slow or rapid cooling/heating in detail. Polymers are normally semi-crystalline which exhibit the properties of both amorphous and crystalline (Roesler *et al.*, 2007). Crystalline polymers which are at high temperature can crystallize during slow cooling, whilst amorphous polymers which are at high temperature can enter rubbery state during cooling or directly reach glassy state at rapid cooling. Since the detailed speeds of cooling or heating process are not clear, further work is required to correlate the process conditions with the material states. However, the micromanipulation results imply that the polymer matrix of microcapsule wall was probably weakened during the heat treatment process. As such, the microcapsules after heat treatment were found to possess a significantly lower mean nominal rupture stress.

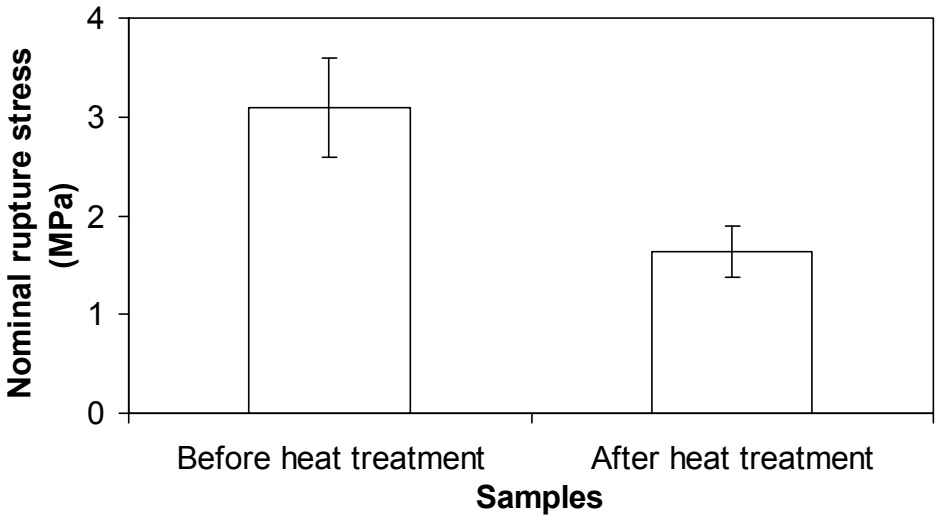

Figure 5.9 Mean nominal rupture stress of microcapsules before and after heat treatment.

5.4 Drying Methods

Microcapsules are sometimes required to undergo drying processes if the end-use products need to be delivered in dry powder form. Some types of drying methods are of special interest to industry, in particular oven drying, spray drying, freeze drying and fluidised bed drying. Their working principles, advantages and disadvantages are summarized and discussed in this chapter, and their effects on the mechanical strength of microcapsules were also investigated. Different types of drying methods were introduced and described by Nonhebel & Moss (1971); their advantages and disadvantages are summarized in Table 5.4. Oven drying is generally performed in a batch atmospheric tray dryer; drying is achieved by blowing hot air over the trays by the means of fans. Heat is supplied by steam or hot water coil heat exchangers situated inside or outside the drying compartment; alternatively, electric heating, direct heating with gas, oil or flue gas is also used. Oven drying is able to dry any material but at a higher labour cost. With spray drying process, the feed material, which is generally in liquid form, is sprayed from the top of a large chamber and comes into contact with a hot air. The liquid flow of component is then rapidly evaporated; and the remaining solid particles are separated from the air. Freeze drying is desiccation by sublimation of water vapour from its solid state in a vessel with an absolute pressure of around 1 mbar (vacuum). It is relative slow and expensive but sometimes it is the only means to achieve a satisfactory dried product. It has been applied in the industries to dry pharmaceutical products, dyes and food. In fluidised bed drying, heated gas is blown up through a bed of particulate material to be dried. The gas is distributed evenly through the small orifices to cause the fluidisation of particles. The advantage is that the breakage is smaller due to the particles are cushioned from each other by the gas stream, however, there is a limitation on the size range of 0.05-15 mm.

Table 5.4 Advantages and disadvantages of various drying methods.

Drying methods	Advantages	Disadvantages
Oven drying	• Dry almost any material	• High operating cost due to intensive labour requirement
Spray drying	• Suitable for heat sensitive material due to its quick drying time • The dried product is a finely separated and free-flowing powder. • Continuous drying of high capacity of materials	• Heat requirement is high. • Capital cost of equipment is high • The equipment requires a large amount of space
Freeze drying	• Undesirable impact on heat-sensitive materials (e.g. bacteria) can be avoided due to its low working temperature	• Drying process is slow. • Expensive due to the use of vacuum
Fluidised bed drying	• The contact between solid and drying gas is far better than any other type of drier. • Abrasion and breakage of particles are smaller due to being cushioned by gas streams.	• Heavy power cost • Materials to be dried must be suitable for fluidisation. • Limitation for materials of size 0.05-15 mm

Effect of drying methods on the mechanical strength of MF microcapsules was investigated by studying a few pairs of microcapsule samples, including microcapsules in the slurries and then dried by an oven or a spray drier or microcapsules being agglomerated first and then dried by a fluidised bed. Finally, the mechanical strength of oven dried, spray dried and freeze dried microcapsules were directly compared.

5.4.1 Slurry and Oven Drying

A MF microcapsule sample in a slurry form was placed into an oven to be dried for a period of 16 hours at 50 ºC by the company, which does not specify the drying rate as well as the slurry

concentration before and after oven drying. The MF microcapsules after being oven dried appeared as a large block instead of powder forms. 50 microcapsules from each of slurry and oven dried samples were tested using micromanipulation to compare their mechanical strength. Their mean mechanical property parameters are summarized in Table 5.5. It was found that microcapsules in the slurry form had a mean deformation at rupture of 16±2%; this was significantly reduced to 8±1% after oven drying. According to the results of *t* statistic test, no significant difference was observed in the mean nominal rupture stress of microcapsules before and after oven drying.

Table 5.5 Mean mechanical property parameters of microcapsules before and after oven drying.

Samples	Diameter (μm)	Rupture force (mN)	Deformation at rupture (%)	Nominal rupture stress (MPa)
Slurry	28.6±3.9	0.44±0.07	16±2	0.93±0.22
Oven drying	25.7±2.5	0.36±0.05	8±1	0.86±0.18

As the tested microcapsules using micromanipulation had different number mean diameters, the nominal wall tension of microcapsules was also calculated and the data are shown in Figure 5.10. The mean nominal wall tension of microcapsules in the slurry and oven dried samples was 5.1±0.7 N/m and 4.7±0.5 N/m respectively, and the *t* statistic test revealed that no significant difference was between such two values. This indicates no significant change is between the mechanical strength of microcapsules before and after oven drying. Therefore, micromanipulation results show that oven drying process can cause microcapsules to become more brittle, but does not seem to affect the nominal rupture stress or wall tension of microcapsules.

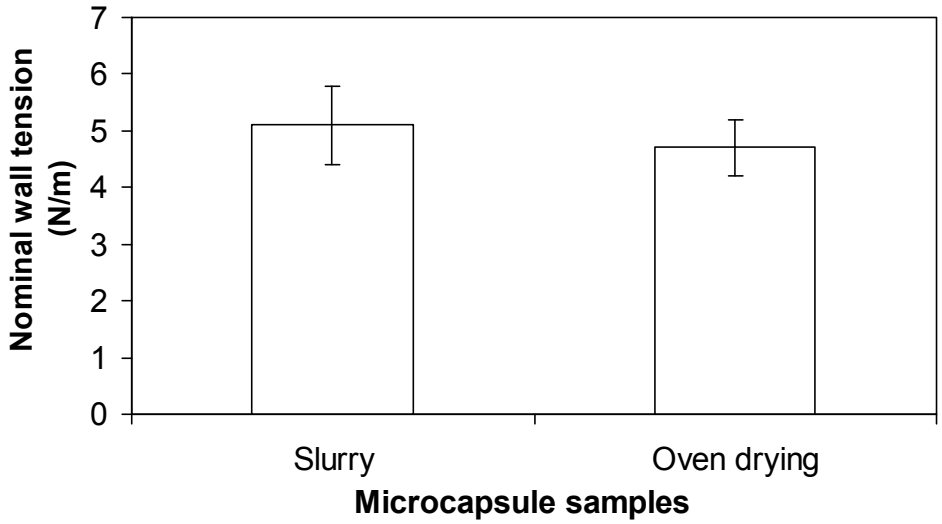

Figure 5.10 Mean nominal wall tension of microcapsules before and after oven drying.

5.4.2 Slurry and Spray Drying

MF microcapsules in a slurry sample with 80wt.% core/capsule ratio underwent a spray drying process; their mechanical strength prior to and after spray drying was subsequently tested. The slurry used for spray drying is not the same slurry used for oven drying, which is discussed in the previous section. The inlet air temperature of the spray dryer was at 200 ºC and the outlet air temperature was at 100 ºC. The retention time of microcapsules in the spray dryer was 15 seconds in a batch. The volume weighted mean diameter of microcapsules in the slurry was measured using Malvern particle sizing and was found to be 34.16±0.01 μm; their mean diameter was reduced by 3.31 μm to 30.85±0.05 μm after going through spray drying, as shown in Table 5.6. It was demonstrated in Chapter 4 that larger microcapsules were ruptured more easily than smaller ones in a given sample. This could be because some weak microcapsules (in general large) may have been ruptured during the spray drying process. It is understandable that the feed material, such as microcapsules here, was sprayed from the top

into the chamber of spray dryer at a certain speed, this could result in microcapsules hitting the chamber wall and then ruptured. Consequently, the mean size of microcapsules after spray drying was smaller.

Table 5.6 Mean diameters of microcapsules in slurry and spray drying forms measured using Malvern particle sizing.

Samples	Core/capsule ratio (wt.%)	Volume weighted mean diameter (μm)	Difference in volume weighted mean diameter (μm)
Slurry	80	34.16±0.01	3.31
Spray drying	80	30.85±0.05	

A total of 50 microcapsules from each of the slurry and spray dried samples were tested using micromanipulation and the results are presented in Table 5.7; their number mean diameter was 29.2±1.7 μm and 28.4±2.5 μm and the mean rupture force was 0.7±0.1 mN and 0.9±0.1 mN, respectively. The deformation at rupture for microcapsules in slurry form was 29±4%, which was comparable to that of microcapsules after spray drying (25±2%). The mean nominal rupture stress was calculated to be 1.3±0.3 MPa for microcapsules in slurry and 1.8±0.4 MPa for spray dried microcapsules based on the tested microcapsules. The statistic *t* test suggested that microcapsules after spray drying had significantly greater mean nominal rupture stress than those before spray drying with 95% confidence.

Table 5.7 Mean mechanical property parameters of microcapsules (80wt.% core/capsule ratio) in slurry and spray drying forms.

Microcapsule samples	Diameter (μm)	Rupture force (mN)	Deformation at rupture (%)	Nominal rupture stress (MPa)
Slurry	29.2±1.7	0.7±0.1	29±4	1.3±0.3
Spray drying	28.4±2.5	0.9±0.1	25±2	1.8±0.4

The mean nominal wall tension of microcapsules in such two samples is shown in Figure 5.11, and *t* statistic test also revealed that microcapsules after spray drying had significantly higher nominal wall tension (11.0±1.4 N/m) than those before drying (8.5±1.5 N/m). The higher mean nominal wall tension of microcapsules in spray dried sample could be attributed to the weaker microcapsules tended to be ruptured more easily during spray drying; as such, the remaining microcapsules in the spray dried sample, which were stronger, showed a higher mean mechanical strength. The findings provide a useful guide for the industries on the production of spray dried microcapsules with desirable mechanical strength.

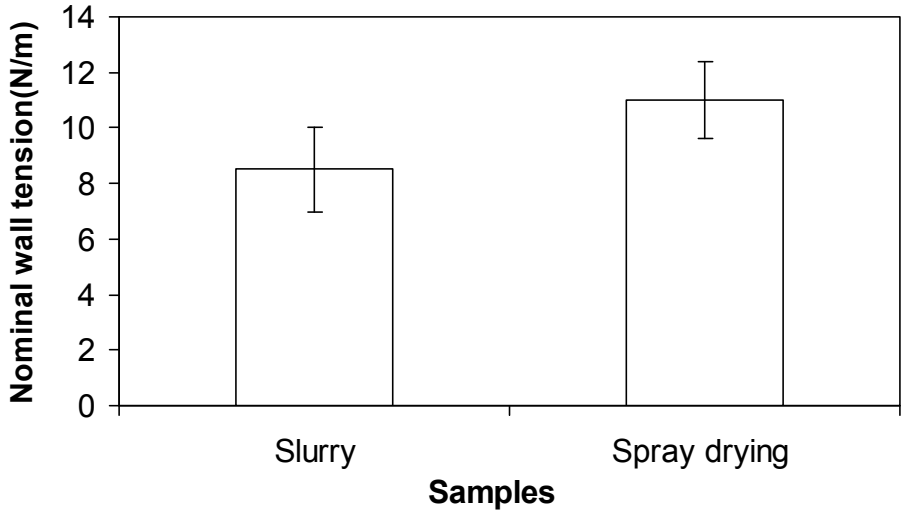

Figure 5.11 Mean nominal wall tension of microcapsules from a slurry sample and their spray drying form (80wt.% core/capsule ratio).

The other MF microcapsule sample with 85wt.% core/capsule ratio in slurry and after being spray dried were also tested by Malvern particle sizing and micromanipulation to confirm the above finding regarding on the effect of spray drying. The volume weighted mean diameter of spray dried microcapsules was also found to be 3.36 μm smaller than that of microcapsules in

slurry, as shown in Table 5.8. The result that the spray dried microcapsules had smaller mean size than those in slurry is consistent with the above findings of microcapsules with 80wt.% core/capsule ratio.

Table 5.8 Mean diameters of microcapsules in slurry and spray drying forms measured using Malvern particle sizing.

Samples	Core/capsule ratio (wt.%)	Volume weighted mean diameter (μm)	Difference in volume weighted mean diameter (μm)
Slurry	85	41.89±0.01	3.36
Spray drying	85	38.53±0.07	

The mean mechanical property parameters of microcapsules with 85wt.% core/capsule ratio in slurry and spray drying forms are summarized in Table 5.9. The number mean diameter of 50 microcapsules from each of slurry and spray dried samples was 36.3±1.8 μm and 30.9±3.1 μm respectively. Their mean rupture force was 0.65±0.04 mN and 0.84±0.10 mN and their deformation at rupture was 17±2% and 30±3%, respectively. The mean nominal rupture stress of microcapsules in the slurry (0.7±0.1 MPa) was evidently lower than that in spray dried samples (1.4±0.2 MPa).

Table 5.9 Mean mechanical property parameters of microcapsules (85wt.% core/capsule ratio) in slurry and spray drying forms.

Microcapsule samples	Diameter (μm)	Rupture force (mN)	Deformation at rupture (%)	Nominal rupture stress (MPa)
Slurry	36.3±1.8	0.65±0.04	17±2	0.7±0.1
Spray drying	30.9±3.1	0.84±0.10	30±3	1.4±0.2

In addition, the mean nominal wall tension at rupture was also calculated to compare the mechanical strength of microcapsules and the data is presented in Figure 5.12. Microcapsules in the slurry form had significantly lower nominal wall tension than those after spray drying. The results imply that spray dried microcapsules had a higher mechanical strength in comparison to those in slurry form with similar mean diameter. It is demonstrated again that microcapsules in the slurry sample was weaker than those in spray dried sample; this is in good agreement with the above findings of microcapsules with 80wt.% core/capsule ratio.

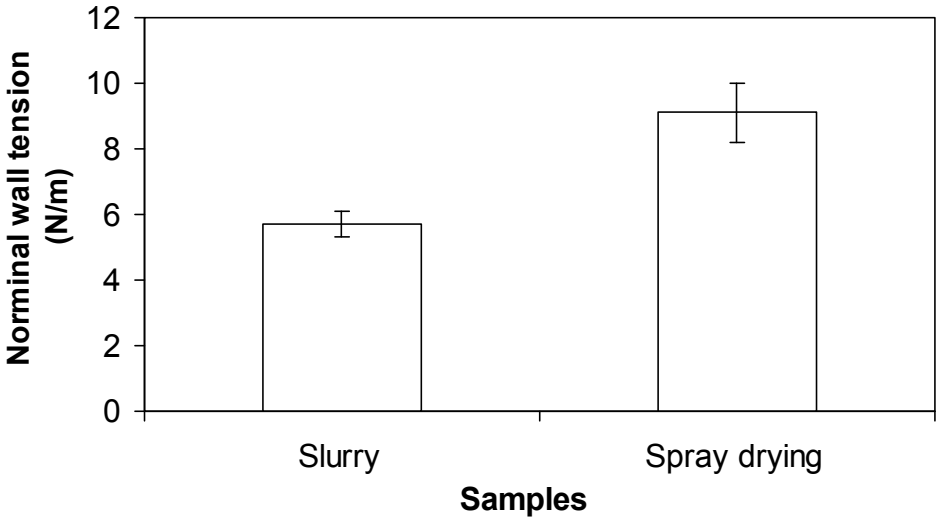

Figure 5.12 Mean nominal wall tension of MF microcapsules (85wt.% core/capsule ratio) from their slurry and spray drying forms.

5.4.3 Slurry and Fluidised Bed Drying

Microcapsules are sometimes required to form agglomerates first and subsequently dried in a fluidized bed in order to be applied in the end-use products. A MF microcapsule sample in slurry form was mixed with the binder to form the aggregates and then dried in a fluidized bed for 8 minutes at 150 ºC. The binder is a kind of cellulose and had no reactions with microcapsules according to the supplier. Micromanipulation tests were performed on 30

microcapsules from each of the samples in the form of slurry and dry agglomerates to evaluate the effect of fluidized bed drying on the mechanical strength of microcapsules which are in the form of agglomerates. Their respective mean mechanical property parameters are presented in Table 5.10. The mean diameters of tested microcapsules in slurry and after fluidized bed drying are 27.1±3.0 μm and 25.1±2.8 μm, and their mean deformations at rupture are 31±4% and 37±4% respectively.

Table 5.10 Mean mechanical property parameters of microcapsules in slurry and agglomerates by fluidized bed drying.

Samples	Diameter (μm)	Rupture force (mN)	Deformation at rupture (%)	Nominal rupture stress (MPa)
Slurry	27.1±3.0	1.8±0.4	31±4	3.7±1.1
Fluidized bed drying	25.1±2.8	1.7±0.3	37±4	4.3±1.3

The statistic *t* test reveals that no significant difference is between the nominal rupture stress of microcapsules in the slurry and dry agglomerates. After the effect of size is considered, the nominal wall tension of microcapsules in each sample is plotted in Figure 5.13. The results of *t* statistic test indicate that there is also no significant difference between the nominal wall tension of microcapsules in slurry and dry agglomerates. The results demonstrate that the microcapsules remained comparable mechanical strength between in the slurry and after fluidised bed drying in the agglomerates form. This implied that microcapsules in agglomerates were not damaged during the fluidised bed drying. This may be attributed to the characteristics of fluidised bed drying that microcapsule agglomerates were cushioned by gas stream, unlike spray drying process which can cause microcapsules to be damaged due to

hitting the chamber wall. The findings should be very beneficial to the industry on understanding the mechanical strength of microcapsules before and after drying.

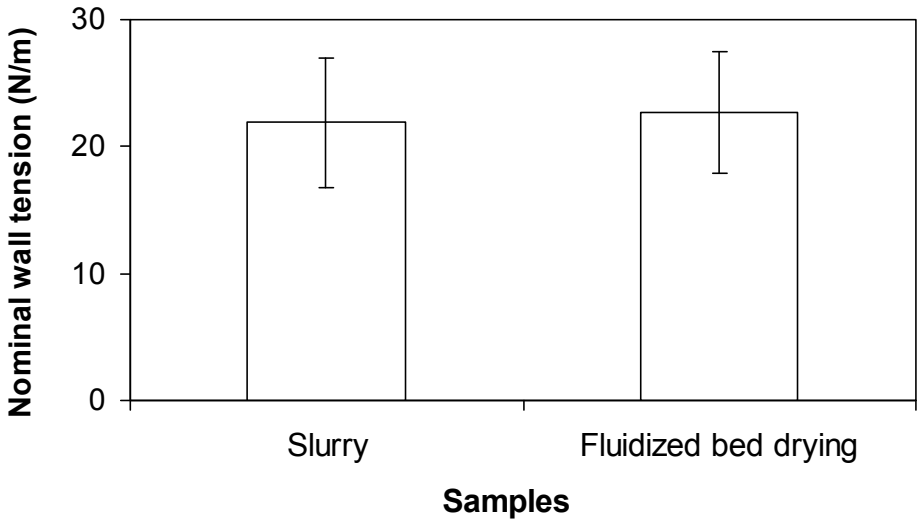

Figure 5.13 Mean nominal wall tension of microcapsules in slurry and agglomerates by fluidized bed drying.

5.4.4 Oven drying, Spray Drying and Freeze Drying

Microcapsules in slurry were dried using oven drying, spray drying and freeze drying respectively before they were characterized by ESEM, Malvern particle sizing and micromanipulation to investigate the effect of drying on their mechanical property parameters. The oven drying time was 3 days at a constant temperature of 50 ºC. The drying temperature and duration of spray drying are the same as those specified in Chapter 5.4.2. Freeze drying was conducted at -50 ºC for a duration of 24 hours. Since the original slurry sample was not available, it was not tested here. It is shown in Figure 5.14 (a) that oven dried microcapsules appear to be blended into a large block instead of free powder form, which is consistent with the observation of oven dried microcapsules studied in Chapter 5.4.1. Furthermore, there were many pores on the surface of the block which might be attributed to the evaporation of water

leaving the microcapsule slurry. Since the whole sample remained stationary in the tray during drying due to the mechanism of oven drying, the excess uncross-linked polymers in the slurry in turn formed a block. This indicates that oven drying method is not effective in terms of drying microcapsules to powder forms. In contrast, spray dried and freeze dried microcapsules had a free-powder appearance based on the ESEM images shown in Figure 5.14 (b) & (c), respectively. Collapsed microcapsules were observed in the spray dried sample.

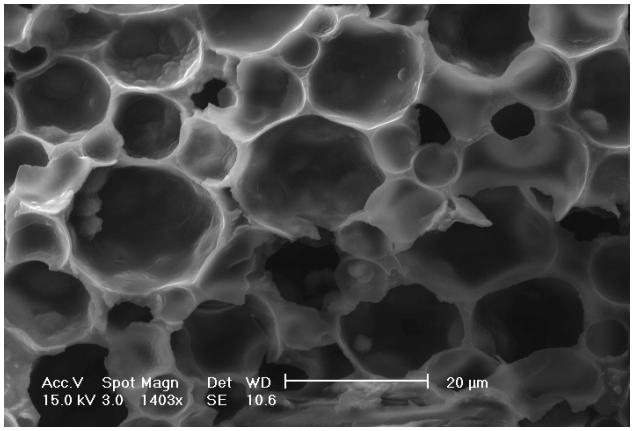

(a) Oven drying

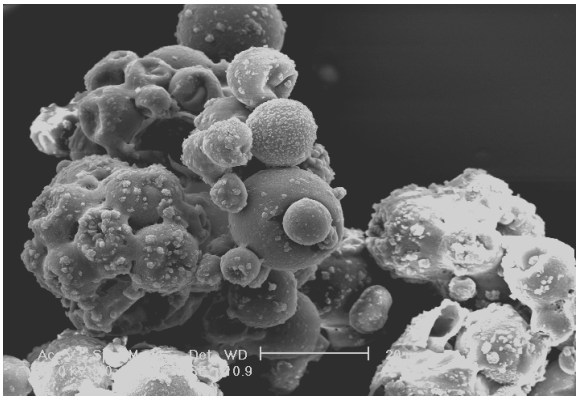

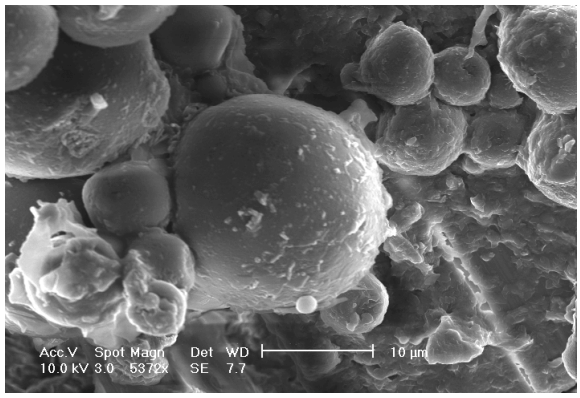

(b) Spray drying **(c) Freeze drying**

Figure 5.14 ESEM images of microcapsules after (a) oven drying (b) spray drying and (c) freeze drying.

Malvern measurement results show that oven dried microcapsules have a highest volume weighted mean diameter of 25.27±6.23 μm among all samples. However, their size distribution curves in Figure 5.15 indicate that some microcapsules from oven dried sample fall into a much larger size range of 80–250 μm; this is not observed in the other 2 samples. This suggests that the recommended agitation speed 2000 rpm used for conventional size measurement (Malvern, 2007) was not high enough to separate all single microcapsules from the block as illustrated in the ESEM image. This is supported by visual observation of microcapsule aggregates in the sample dispersion unit of the Malvern Mastersizer. The presence of aggregates resulted in the different mean size obtained from each measurement of oven dried microcapsules, which was reflected on the relatively large standard errors of the obtained mean size (25.27±6.23 μm), as shown in Table 5.11. As a result, the mean size obtained using Malvern particle sizing does not represent the actual size of oven dried microcapsules. In contrast, the measurement made on the spray dried and freeze dried microcapsules shows that their volume weighted mean diameters were 16.90±0.02 μm and 17.58±0.03 respectively. Such two mean sizes are considered as no significant difference, since the slight difference of 0.68 μm could arise from sampling of microcapsules from their original batch.

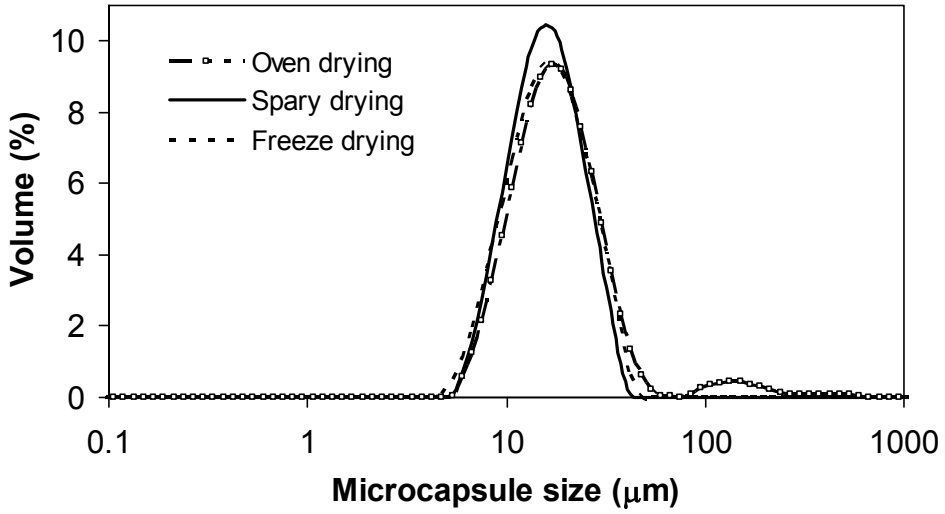

Figure 5.15 Size distribution of microcapsules after oven drying, spray drying and freeze drying.

Table 5.11 Malvern particle sizing measurement of mean sizes of microcapsules treated by different types of drying.

Samples	Volume weighted mean diameter (μm)
Oven drying	25.27±6.23
Spray drying	16.90±0.02
Freeze drying	17.58±0.03

Mean diameters of 50 individual microcapsules from each of oven dried, spray dried and freeze dried samples were obtained using micromanipulation, and they were 15.8±1.2 μm, 15.4±1.7 μm and 19.4±1.8 μm respectively. Micromanipulation results indicate that the oven and freeze dried microcapsules were more brittle, since their deformations at rupture were 13±2% and 15±2% respectively which is smaller than that of spray dried microcapsules (24±4%) as shown in Figure 5.16.

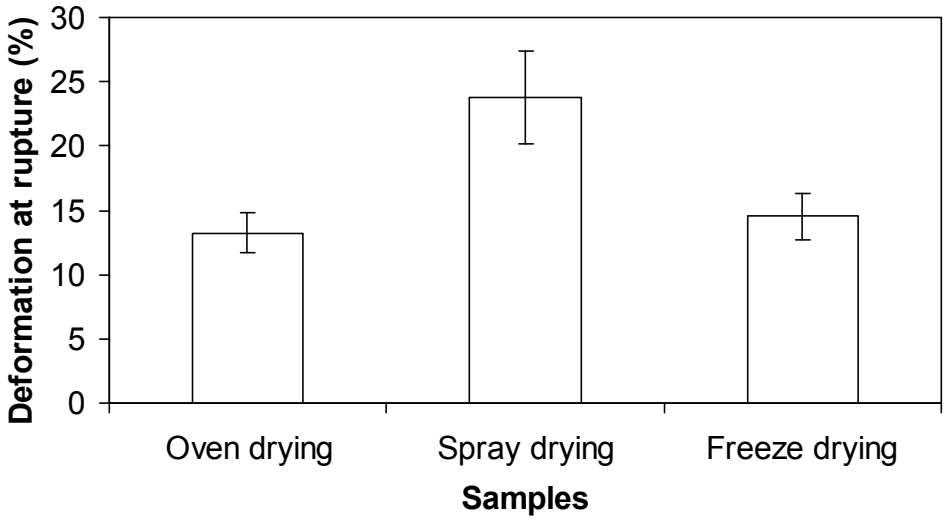

Figure 5.16 Deformation at rupture of microcapsules treated by different types of drying.

In Figure 5.17, spray dried microcapsules have the highest mean nominal rupture stress of 2.6±0.9 MPa; this is approximately twice of those from oven drying and freeze drying with 1.3±0.2 MPa and 1.1±0.3 MPa respectively.

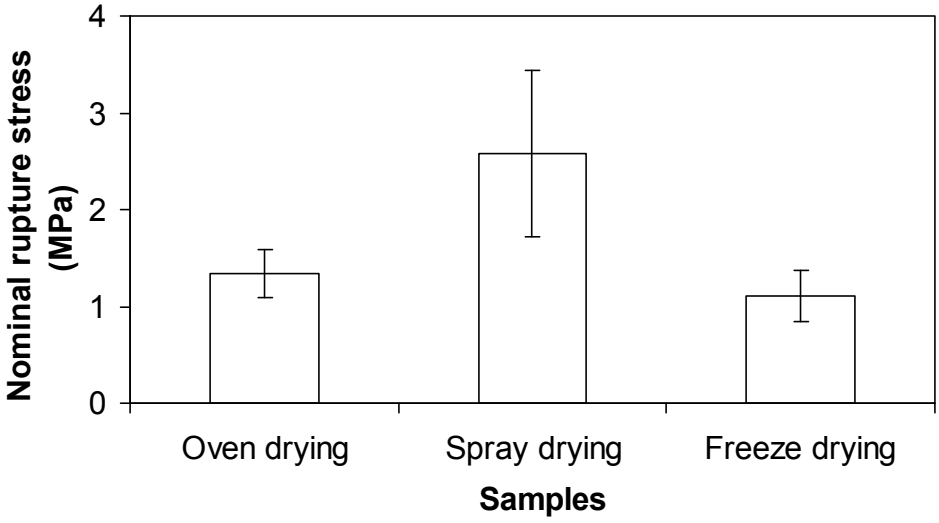

Figure 5.17 Mean nominal rupture stress of microcapsules treated by different types of drying.

In Figure 5.18, the mean nominal wall tension for microcapsules dried using oven drying, spray drying and freeze drying methods is 4.6±0.6 N/m, 7.0±1.5 N/m and 4.3±0.6 N/m respectively. The statistic *t* test indicated that the spray dried microcapsules have a significantly higher nominal wall tension than those undergoing oven drying and freeze drying; in addition, no significant difference is between the nominal wall tension of oven dried and freeze dried microcapsules. This implies that the spray dried microcapsules have an apparent higher mechanical strength than the other 2 types of dried microcapsules. The obtained results are consistent with the above findings that the oven dried microcapsules had comparable mechanical strength as their slurry forms and the spray dried microcapsules appeared stronger than their slurry form.

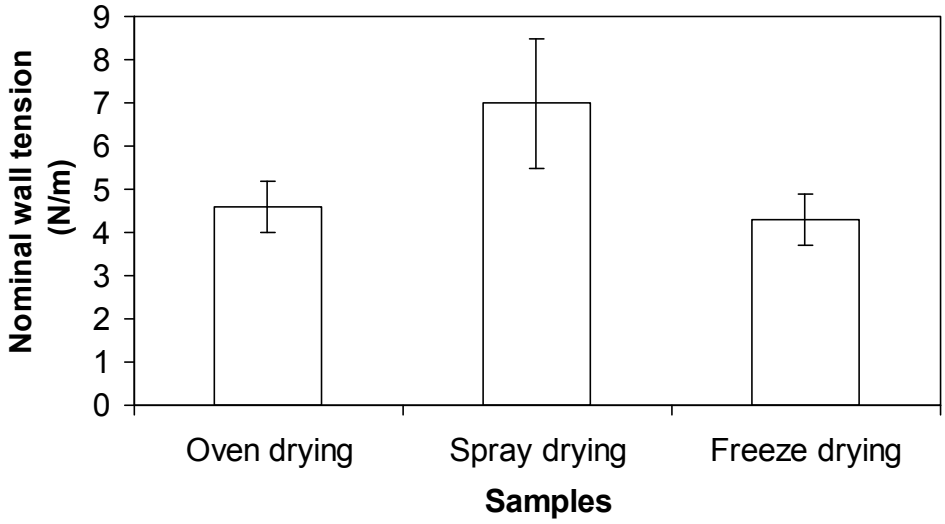

Figure 5.18 Mean nominal wall tension of microcapsules treated by different types of drying.

As discussed above, the higher nominal wall tension of spray dried microcapsules might be attributed to the process of spray drying which allowed the microcapsules to have a higher chance of hitting the chamber wall of spray dryer, which in turn could result in the breakage of some weaker MF microcapsules. The measurement made here reflects the mechanical

property parameters of the stronger microcapsules that remained intact. Hence, if the mechanical strength of microcapsules is required to remain no significant change before and after drying, spray drying is not suitable for drying such microcapsules; in contrast, oven drying or freeze drying method is more appropriate. In order to understand the effect of drying on the wall material, thermal behaviour of MF wall can be studied in the further work by measuring their glass transition temperature before and after various types of drying. Further work can also include studying the porosity of microcapsule surface after various types of drying.

5.5 Air Drying and Rehydration

It is of interest whether the mechanical strength of microcapsules is affected after being naturally dried in the atmospheric air for a long period of time and then rehydrated. Hence, micromanipulation tests were conducted to test 30 microcapsules from each of the 3 samples at 3 different stages: microcapsules in slurry, dried in air for 16 hours and then rehydrated. Microcapsules in water suspension were placed on a piece of glass slide to air dry for 16 hours prior to test. Rehydrated microcapsules were prepared by a 16-hour air drying and subsequently wetted with water; test started as soon as the water on the slide evaporated for single microcapsules to emerge. The air temperature in the room was at 25±1 ºC. The obtained micromanipulation results are summarized in Table 5.12.

Table 5.12 Mean mechanical property parameters of microcapsules in the slurry, after air drying and rehydration.

Samples	Treatment	Diameter (μm)	Rupture force (mN)	Deformation at rupture (%)	Nominal rupture stress (MPa)
A1	In slurry	26.7±3.3	0.4±0.2	18±4	0.7±0.2
	Air drying	29.6±3.4	0.5±0.2	16±4	0.7±0.2
	Rehydration	24.9±4.3	0.4±0.2	17±4	0.8±0.2
A2	In slurry	23.4±2.9	1.6±0.3	37±5	5.4±2.0
	Air drying	19.3±2.3	1.8±0.4	48±5	6.9±1.5
	Rehydration	24.6±3.0	1.5±0.2	40±5	4.6±1.4
A3	In slurry	19.8±1.6	0.14±0.02	22±4	0.5±0.1
	Air drying	15.7±2.5	0.12±0.02	16±4	0.9±0.3
	Rehydration	17.2±2.3	0.14±0.03	22±5	0.8±0.2

No significant difference in deformation % at rupture is observed for all the samples (A1, A2 and A3) at different stages. The mean nominal rupture stress of microcapsules in the slurry, after 16-hour air drying and rehydration for each of samples were also calculated. However, the slight difference in number mean diameters of microcapsules at each stage is due to the random selection of microcapsules for the micromanipulation test. Since the size can influence the microcapsules' mechanical strength, the mean nominal wall tension of each sample, which can eliminate the effect of size of microcapsules, is determined and shown in Figure 5.19. The *t* statistic test results show that no significant difference is between the mean nominal wall tension of microcapsules in all the samples at different stages of treatment. This suggests that the mechanical strength of microcapsules is not significantly affected after being naturally dried in the atmospheric air for a long period of time and then rehydrated.

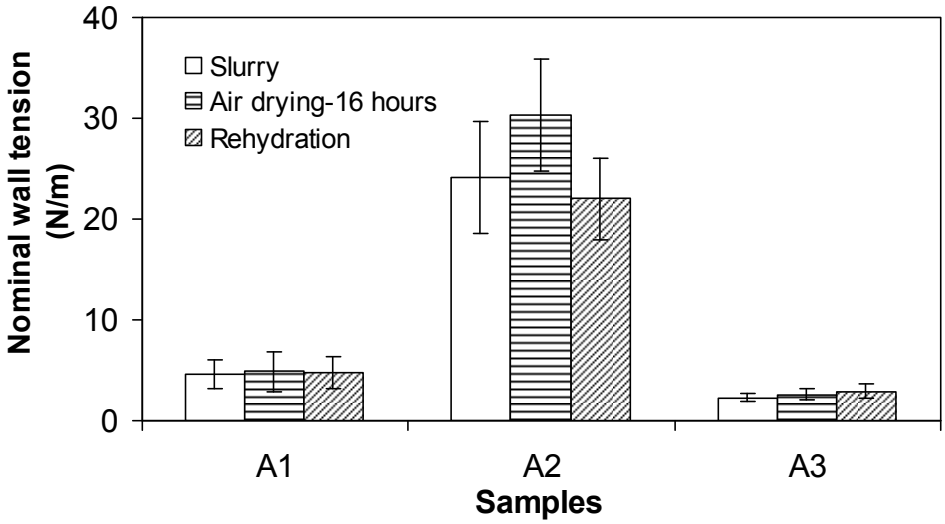

Figure 5.19 Mean nominal wall tension of microcapsules in the slurry, after air drying and rehydration.

5.6 Conclusions

Micromanipulation measurements show that no significant difference is between the nominal wall tension of microcapsules made using the polymerisation time of 2 hours and 4 hours at a constant temperature of 65 ºC. However, increasing the amount of polymerisation time to 6 hours at the same constant temperature of 65 ºC significantly increased the nominal wall tension of microcapsules. Microcapsules produced using 8 hours' polymerisation time at 65 ºC and a further 16 hours at 85 ºC were stronger in comparison to those polymerised for 2 hours at 65 ºC. This points out the combination of much prolonged polymerisation time & elevated temperature is able to strengthen microcapsules. Tests by Malvern particle sizing revealed that microcapsules manufactured in pilot plant and full scales had larger volume weighted mean diameters than those produced in lab scale, which was probably attributed to the use of slower agitation speed in pilot plant and full scales than it should be. Moreover, microcapsules prepared in lab scale possessed the highest mean nominal wall tension. Therefore, it is critical

to scale up the process properly so that microcapsules produced at different scales can bear comparable mechanical strength. Micromanipulation results also showed that heat treated microcapsules, which were heated to 120^0C (above the glass transition temperature T_g of MF shell material 97 ºC) and then cooled down to room temperature, had significantly lower mean nominal rupture stress than their original form. It was suggested that this was due to the weakening of MF wall in the heat treatment.

In the studies of effect of various drying methods on the mechanical strength of microcapsules, oven dried microcapsules were found to become more brittle, but their mean nominal rupture stress and nominal wall tension did not change significantly from those in the slurry form. Furthermore, micromanipulation results showed the spray dried microcapsules had greater mean nominal rupture stress and nominal wall tension than those before spray drying. This was probably due to the breakage of weak microcapsules (in general large) during the spray drying process. This is also supported by the results that the mean size of microcapsules after spray drying was approximately 3 μm smaller than those before spray drying. In contrast, microcapsules in agglomerates after fluidised bed drying were found to have no significant change in nominal rupture stress or nominal wall tension. In the direct comparison of microcapsules from a same slurry batch and treated by various drying methods, freeze dried and spray dried microcapsules were found to be easier to measure using Malvern particle sizing, since the microcapsules remained well dispersed. Oven dried microcapsules however tended to aggregate. In terms of mechanical strength, the mean nominal wall tension of spray dried microcapsules was significantly greater in comparison to those prepared using oven and freeze drying, and no significant difference was found between the mean nominal

wall tension of microcapsules treated using the latter two drying methods. The oven and freeze dried microcapsules were also found to be more brittle than the spray dried microcapsules. Finally, the test results also demonstrated that no significant difference is between the mean nominal wall tension of microcapsules in every stage of treatment including in slurry, air drying for a duration of 16 hours and then rehydrated. The findings should be very useful to the industries for the application of MF microcapsules to the end-use products.

6. DETERMINATION OF YOUNG'S MODULUS AND RUPTURE STRESS OF SINGLE MF MICROCAPSULES BY MODELLING

It was demonstrated in Chapter 4 & 5 that micromanipulation is a very powerful technique to provide a large amount of mechanical property parameter data, such as rupture force or displacement at rupture, which however do not represent the intrinsic mechanical properties of microcapsules since they all depend on size. Therefore, in this chapter, Hertz model (Johnson, 1985) and Finite Element Analysis (FEA) (Nguyen *et al.*, 2009a) were employed to fit the compression data of MF microcapsules to determine their intrinsic mechanical properties, such as Young's modulus. The modulus obtained from respective models was interpreted and the possible relationship between the modelled results was also established, and the details are presented.

Moreover, the use of nominal rupture stress of microcapsules which is calculated from ratio of rupture force to initial cross-sectional area of microcapsules to determine the mechanical strength of microcapsules has some limitations, as discussed in Chapter 4. The data of compressive force and contact diameters provided in the literature (Stenson *et al.*, 2008) were applied to determine the real contact pressure of single microcapsules during compression so as to validate the assumption of Johnson's solid plastic model. Hertz model combined with Johnson's plastic model was applied to microcapsules that were previously studied in Chapter 4 and had significantly different deformation at rupture, to determine the contact area between a single microcapsule and the force probe as well as the contact pressure during compression. The modelling procedures were described in detail in this chapter. As such, the mechanical strength of microcapsules based on the real rupture stress can be acquired and compared with

the findings obtained using nominal rupture stress in Chapter 4, which should be very useful to interpretation of the data and understanding how to determine the mechanical strength of microcapsules under various conditions.

6.1 Young's Modulus of MF Microcapsule

6.1.1 Hertz Model

As reviewed in Chapter 2, Hertz model has been successfully applied to determine the Young's moduli of single microspheres (Liu *et al.*, 1998; Muller *et al.*, 2005; Ding *et al.*, 2008; Yap *et al.*, 2008) and microcapsules as a whole identity, although they have a core/shell structure (Ju *et al.*, 2005). Hertz model was also applied here to the compression data of MF microcapsules. To apply the Hertz model, the surface of microcapsules was assumed to be continuous, non-conforming and frictionless and the strain of microcapsules was small (Johnson, 1985). The material of microcapsules was assumed to be incompressible (ν_P=0.5). The assumptions of Hertz model were applied to all the microcapsules, the data of which were fitted with Hertz model in this chapter.

Figure 6.1 presents the loading and unloading data of a MF microcapsule, which had a diameter of 12.6 μm and was compressed to a final deformation of 10% and then the load was lifted. δ in the x-axis of Figure 6.1 refers to the axial half of total compressive displacement of single microcapsules and also denotes the same meaning in the rest of chapter. The hysteresis between the loading and unloading data is not significant; therefore, this microcapsule exhibited an elastic behaviour at the deformation of 10%. Since the deformation is small and

lower than 10% strain, Equation 2.2 of Hertz model (Johnson, 1985) can be applied to the loading data to study the elastic behaviour, as illustrated by a solid line in Figure 6.1. Other models, such as Tatara model (Tatara *et al.*, 1991) reviewed in Chapter 2, are normally applied to microparticles with a large elastic strain (>15%) (Liu *et al.*, 1998) and was therefore not used here.

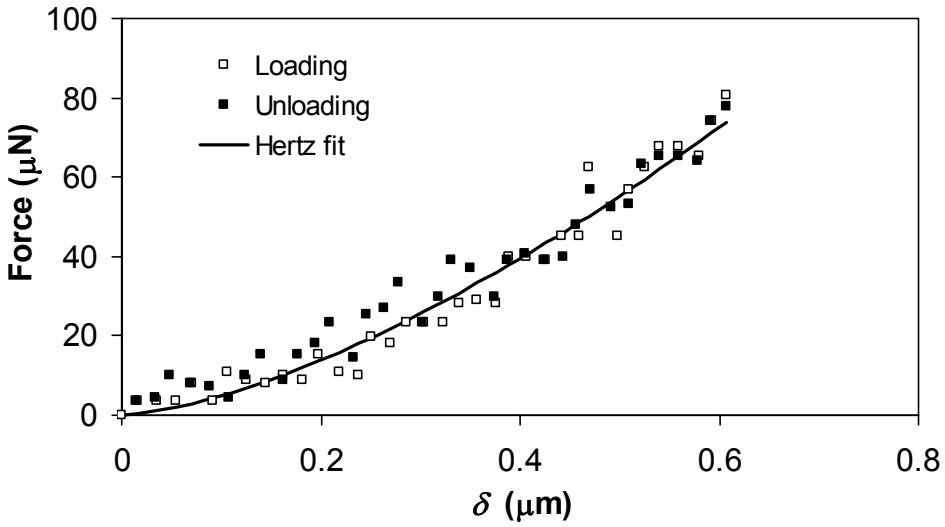

Figure 6.1 Loading and unloading data of compressing a single MF microcapsule (diameter=12.6 μm) to a final deformation of 10%. The solid line is the best fit of Hertz model to the loading data.

The Hertz fitting is normally presented in a linear form as illustrated in Figure 6.2. The linear line is the best fit of Hertz model and the correlation coefficient is 0.96. The Young's modulus of this MF microcapsule can be determined from the slope of the linear line and was found to be 35 MPa. The Hertz model was then applied to a total of 32 MF microcapsules in a sample up to 10% elastic deformation by applying the above fitting procedures. This sample (mean diameter=13.6±0.9 μm) was previously studied in Chapter 4.5 to obtain their elastic limit (15±1%) using the loading-unloading experiments. The mean Young's modulus of MF microcapsules was determined to be 32±4 MPa. Hertz model not only fitted well with the

elastic loading data of microcapsules up to 10% deformation for all the 32 microcapsules in the sample, but also gave good fitting to their respective loading data up to their elastic limit of 15±1% (data not shown). The good fitting of Hertz model to the elastic loading data of MF microcapsules demonstrates that besides loading-unloading experiments Hertz model can also be used to describe the elastic behaviour of microcapsules. Since microcapsules prepared using different formulations could have different elastic limits, Hertz model can sometimes be used to estimate the elastic limit when the data of loading-unloading experiments is not available.

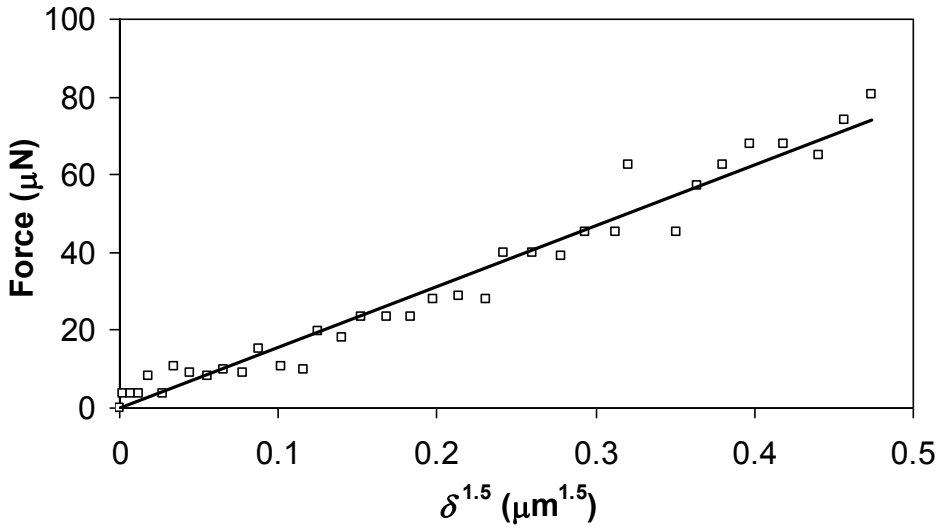

Figure 6.2 The linear fit of Hertz model (solid line) to the loading data shown in Figure 6.1.

Ju *et al.* (2005) found that the Young's modulus of a 65 μm urea-formaldehyde biomimetic microcapsule is 0.987 MPa; however, the elastic limit as well as the adequacy of using the Hertz model to fit their compression data of microcapsules was not given. Therefore, the predicted Young's moduli of microcapsules in such two cases are not directly compared here. Hertz model was derived from the contact mechanics theory, and it is worth noting that the Young's modulus determined from Hertz model represents the modulus of whole

microcapsule. In the following section, other models which consider the core/shell structure of microparticles were utilized to determine the Young's modulus of MF microcapsule wall material.

6.1.2 Finite Element Analysis (FEA)

Finite element analysis (FEA) and a simple linear elastic model were applied to the compression data of MF microcapsules by Dr. Bac Nguyen from The University of Birmingham to develop a dimensionless force-deformation curve, which was proven in the literatures to be able to determine the Young's modulus of wall material of microparticles with a core/shell structure (Lardner & Pujara, 1980; Liu *et al.*, 1996; Wang *et al.*, 2004). The procedures of applying FEA are described in detail in Nguyen *et al.* (2009a). The wall of microcapsule and the perfume oil in the core were both taken to be incompressible. This means the Poisson's ratio of the microcapsule, ν_P, is equal to 0.5. The wall of microcapsule was also assumed to be homogeneous and was described as isotropic linear elastic material with Hookean behaviour. The contact between the compression probe and the microcapsule wall was assumed to be frictionless. The equation developed from FEA to describe the dimensionless force-deformation curve of MF microcapsules is shown in Equation 6.1:

$$y = 3.884x^3 + 0.6676x^2 + 0.007x \qquad (6.1)$$

where x is the fractional deformation and y is the dimensionless force. The expressions of factional deformation and dimensionless force presented in Equation 2.5 and 2.6 include the term of initial stretch ratio λs. Since microcapsules unlike some biological cells were not

inflated before being compressed, λs is equal to 1 for microcapsules. Therefore, Equation 2.5 is converted to Equation 6.2:

$$x = \frac{X}{r_0} \tag{6.2}$$

Similarly, Equation 2.6 becomes Equation 6.3 as follows:

$$y = \frac{F}{Ehr_0} \tag{6.3}$$

In Figure 6.3, fractional deformation, x, and dimensionless force, y, were featured as x-axis and y-axis of the developed dimensionless force curve (solid line) respectively. The dimensionless curve was fitted to the loading data of compressing the same 12.6 μm microcapsule at a deformation of 10% using the least-squared method, which had been fitted above by Hertz model as presented in Chapter 6.1.1. The correlation coefficient of curve fitting is 0.95. The product of Young's modulus of MF microcapsule wall (E_w) and wall thickness of MF microcapsule (h), $E_w h$, was found to be 1320 Nm^{-1}. The mean wall thickness of MF microcapsules measured by TEM as presented in Chapter 4 is 175 nm. The TEM results suggested that no significant difference was between the apparent wall thickness of the ultrathin MF microcapsule sections, hence, mean wall thickness of 175 nm was applied to every microcapsule, and the Young's modulus of MF microcapsule wall was then determined to be 8 GPa.

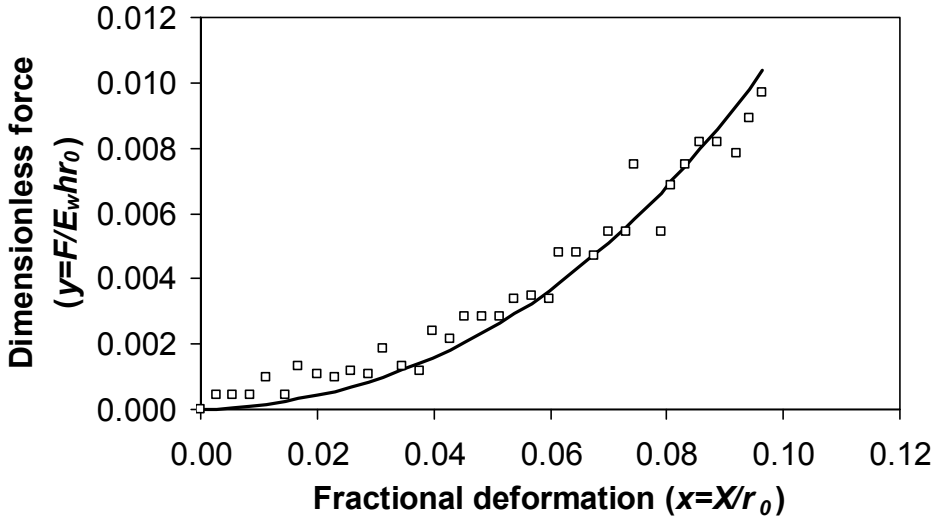

Figure 6.3 Fitting a dimensionless force curve developed by FEA (solid line) to the loading data of compressing the single 12.6 μm MF microcapsule described in Figure 6.1 to a final deformation of 10%.

The procedures of fitting the dimensionless curve to the loading data were applied to the same 32 microcapsules which were previously used for Hertz analysis. The mean Young's Modulus of MF microcapsule wall was found to be 8±1 GPa. The obtained result was in good agreement with the suggestion of Ashby & Jones (2005) that all polymers, if really solid, should have moduli above the lowest level of 2 GPa. The determined modulus was also in the same order of magnitude as the findings of Keller & Sottos (2006), who claimed that the Young's modulus of poly(urea-formaldehyde) microcapsule wall material had a mean value of 3.7 GPa. Keller & Sottos (2006) employed an analytical approach (Lardner & Pujara, 1980; Liu *et al.*, 1996; Wang *et al.*, 2004) to determine the Young's modulus of microcapsule wall. It is also demonstrated that the Young's modulus of MF microcapsule wall material is greater than that of poly(urea-formaldehyde) microcapsules. This is consistent with the finding of Sun & Zhang (2002) that MF microcapsules on average had higher mechanical strength than the same size of urea-formaldehyde microcapsules. The results here have demonstrated that finite

element modelling is as effective as numerical simulations to determine the intrinsic mechanical properties of microcapsules, such as Young's modulus. This approach can also be applied to other types of microcapsules to obtain their mechanical properties.

6.1.3 Comparison of Young's Modulus Determined from Hertz Model & FEA

As discussed above, E_c obtained from Hertz model represents Young's modulus of whole MF microcapsule, and E_w determined from the dimensionless curve using FEA stands for Young's modulus of MF microcapsule wall material. E_c and E_w determined from both models were based on the data of the same 32 MF microcapsules in a given sample. The modelled results are plotted in Figure 6.4 to establish a correlation between E_c and E_w. If there were a proven connection between them, the developed equation could be used to predict one of the parameters when the other one is known. In Figure 6.4, a linear relationship was found between E_c and E_w. The slope of the trend line was then correlated to the wall thickness h and diameter of each microcapsule D_m. The relationship between E_c and E_w may be described by Equation 6.4:

$$E_c = (0.32 \pm 0.01)\frac{h}{D_m}E_w \qquad (6.4)$$

In theory, the value of E_c should be the same as E_w whilst diameter of a microcapsule is equal to twice of their wall thickness. In other words, the coefficient in Equation 6.4 should ideally be equal to 2 rather than 0.32±0.01. However, when modelling the microcapsule using the finite element approach, no bending effects were considered for the wall of microcapsule. This was because the wall thickness of microcapsule was significantly smaller than the diameter. It

should be noted that this approach can generally be applied to a microparticle whose ratio of initial wall thickness to radius $\hat{\tau}$ is less than 0.133 (Nguyen, 2009b). This is to say that Equation 6.4 becomes valid when $\hat{\tau} < 0.133$. The $\hat{\tau}$ for MF microcapsules studied here was equal to 0.027±0.002, which is smaller than 0.133. The $\hat{\tau}$ used here was also smaller than the $\hat{\tau}$ value 0.037±0.002 used by Smith *et al.* (2000b), which applied FEA to determine the Young's modulus of yeast cell. Since finite element approach can not be applied to the microparticles with $\hat{\tau}$ greater than 0.133, the coefficient obtained here is not directly compared with the ideal coefficient of 2.

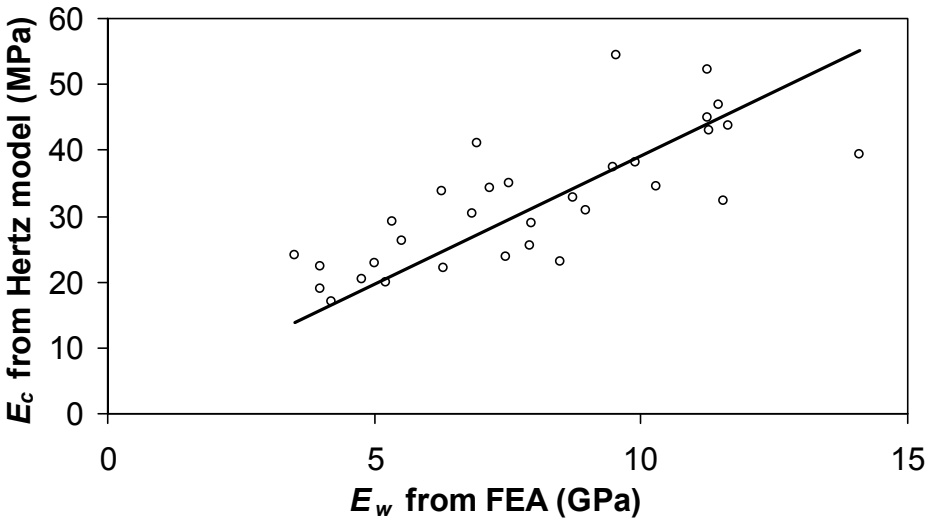

Figure 6.4 Relationship between Young's modulus E_c predicted from Hertz model and E_w from FEA. Solid line is a linear trend line.

6.2 Rupture Stress of Single MF Microcapsules during Compression

As described in Chapter 4, nominal rupture stress is calculated using the initial cross-sectional area. In reality, this is however not the real rupture stress of single microcapsules. Because microcapsules rupture at relative deformations, and the contact area at rupture is not

necessarily equal to the initial cross-sectional area. As discussed in Chapter 4, nominal rupture stress can be used to compare the mechanical strength of microcapsules which have similar deformation at rupture. For the microcapsules with significantly different deformations at rupture, the real rupture stress of microcapsules, which was calculated from the data of contact area at rupture and rupture force, becomes a critical parameter to evaluate the mechanical strength of microcapsules. Rupture force can simply be measured by micromanipulation as previously discussed. Modelling methods such as Hertz model were applied to the micromanipulation rupture data of single MF microcapsules to determine their contact area during compression as well as their real rupture stress. With the contact area estimated by appropriate modelling, the rupture stress obtained could truly reflect the mechanical strength of microcapsules.

6.2.1 Contact Stress of Single MF Microcapsules during Compression

It was reported that the compression test by nanomanipulation was able to measure the contact diameters of yeast cells (Ren *et al.*, 2008) and MF microcapsules (Stenson *et al.*, 2008) in an environmental scanning electron microscope. However, the contact diameters of microcapsules during compression were not measured in the current work due to the limited resolution of the optical microscope used in the micromanipulation rig for microcapsules smaller than 100 μm. Therefore, modelling method such as Hertz model was applied to determine the contact diameters of single microcapsules during compression.

During the loading phase, the contact regions between the particle and the two glass surfaces are flattened, which results in the formation of a circular contact area with radius, a_h. For small

strain of elastic behaviour, if Equation 2.2 of Hertz model can be fitted to the compression data of microcapsule, it can also relate the contact radius, a_h, to the axial half of the total compressive displacement, δ, and radius of microparticle, R, as shown in Equation 6.5 (Adams *et al.*, 2004).

$$\delta = \frac{a_h^{\,2}}{R} \tag{6.5}$$

The contact stress of a microcapsule during compression, σ_h, can be obtained from the compressive force, F, and the contact radius, a_h, determined from Hertz model, as shown in Equation 6.6:

$$\sigma_h = \frac{F}{\pi a_h^{\,2}} \tag{6.6}$$

where, F is compressive force imposed on a microcapsule.

Equation 2.2 of Hertz model was fitted to the loading data of compressing a single MF microcapsule (diameter=11.0 μm) which had a rupture deformation of 67%, as illustrated in Figure 6.5. The loading data of this microcapsule was obtained from Stenson *et al.* (2008). Hertz model appeared to fit the loading data up to 58% of deformation as denoted by Point D. It was reported that Hertz model is generally valid up to 10% strain of microparticles, which is equivalent to 30% deformation of microparticles (Wang *et al.*, 2005; Yan *et al.*, 2009). It is therefore a coincidence that Hertz model in this case also fitted the loading data of plastic deformation which is beyond 30% deformation. It was demonstrated in Chapter 6.1.1 that Hertz model can be as effective as applying loading-unloading experiments to study the elastic behaviour of microcapsules. As a result, the elastic limit of this microcapsule is 30%, as

denoted by Point B in curve AB. The correlation coefficient of Hertz fitting up to 30% deformation is 0.97.

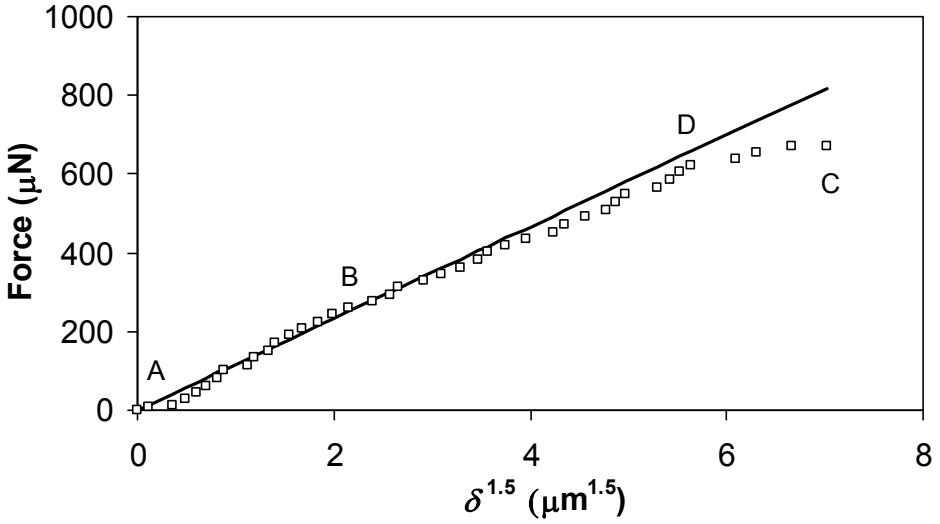

Figure 6.5 The linear fit of Hertz model to the loading data of compressing a single MF microcapsule (diameter=11.0 μm) to a final rupture deformation of 67%. Hertz model was fitted to the loading data up to 30% deformation.

According to characteristics of MF microcapsules studied in Chapter 4, curve BC in Figure 6.5 represents the plastic behaviour of microcapsule (deformation between 30% and 67%). In Johnson's solid plastic model, the contact pressure (stress) in the plastic region was assumed to be constant (Johnson, 1985). Since the compressive force and contact diameters during compression of this MF microcapsule (diameter=11.0μm) is readily available from Stenson et *al.* (2008), the contact stress of such microcapsule during compression from 0% to a final deformation of 67% was calculated here and presented in Figure 6.6 to validate the assumption in Johnson's solid plastic model. The contact stress during elastic deformation in curve AB of Figure 6.5 corresponds to the circle line AB in Figure 6.6. Similarly, the plastic deformation of curve BC in Figure 6.5 corresponds to the triangle line BC in Figure 6.6. The

solid line only indicates the trend of contact stress in the plastic deformation. The slope of such trend line was equal to be 0.09±0.02 by applying SigmaPlot software. The results suggest that the contact stress in the plastic region does not change significantly, and this agrees with the assumption of Johnson's solid plastic model. By applying the theory of constant stress in plastic region, the contact stress at Point B is equal to the contact stress at Point C. This indicates that Hertz model combined with Johnson' plastic model can be used to determine the contact diameters of microcapsules during compression as well as calculating the rupture stress of microcapsules.

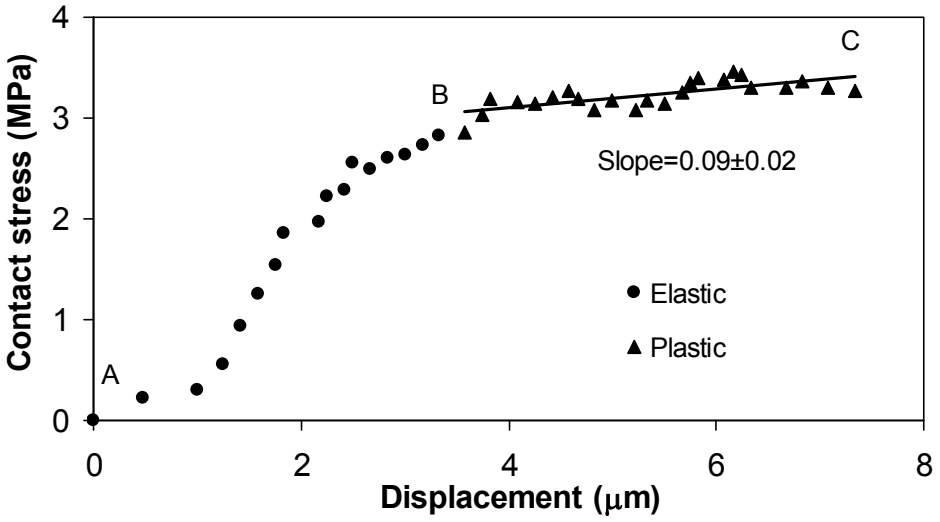

Figure 6.6 Contact stress of a single MF microcapsule (diameter=11.0 μm) during compression from 0% to a final rupture deformation of 67%, calculated based on the data from nanomanipulation. The solid line only indicates the trend.

It should be noted that the contact diameter of MF microcapsule reported by Stenson et al. (2008) had an initial contact diameter of 5 μm before compression experiment started. This is attributed to the nature of nanomanipulation test that the microcapsule was deposited in a vertically erected glass slide in the environmental scanning electron microscope (Ren *et al.*,

2007) which resulted in an initial contacting of microcapsule to the slide. Hence, the contact diameters determined by Hertz model are not directly compared with the contact diameter data of Stenson *et al.* (2008).

Literatures concerning the measurement of contact diameters of microcapsules are very limited; as a result, Johnson's plastic model was only validated with one microcapsule's data. It is of great importance to validate the model with experimental data. Future works are required to obtain more data on the contact diameters of single microcapsules during compression to validate such model. It can be achieved by applying nanomanipulation (Stenson *et al.*, 2008) if the diameters of microcapsules are around 10 μm. If microcapsules have larger sizes ranging from 60 μm to 120 μm, a sensitive microscope visualisation instrument can be applied (Liu *et al.*, 2002). Nguyen *et al.* (2009a) found the modelling results, which were obtained by applying FEA to a visco-elastic material model, are in good agreement with both contact diameters and central lateral extension of a single alginate microsphere (102 μm) during compression. FEA offers the advantage of modelling different constitutive equations which describe the elastic and plastic models. Hence, future works can involve applying FEA and some other plastic models to microparticles with core/shell structure, such as microcapsules, to determine the contact diameters of single microcapsules during compression, which can be validated using experimentally measured contact diameters of single microcapsules during compression.

6.2.2 Application of Hertz and Johnson's Plastic Models to the Compression Data of MF Microcapsules

6.2.2.1 Microcapsules with & without Starch Coating

Since the assumption of Johnson's plastic model that contact stress is constant in the plastic region was demonstrated to be valid, Hertz and Johnson's plastic model were then applied to a few MF microcapsule samples which were discussed in Chapter 4 to obtain their real rupture stress and re-examine the conclusions drawn in Chapter 4. As mentioned previously, it should be demonstrated that Hertz model can well fit the loading data of microcapsules at a small strain before Equation 6.5 derived from Hertz model can be applied to determine the contact radius a_h of single microcapsules during compression.

Hertz model was therefore fitted to the loading data of compressing a single microcapsule with starch coating (diameter=15.0 μm) at a final rupture deformation of 6%, which is shown in Figure 6.7. The micromanipulation data of starch-coated microcapsules was summarized in Chapter 4. The solid line is the best fit of Hertz model and the correlation coefficient is 0.98. The results indicate that this microcapsule had an elastic deformation up to rupture and can be fitted by Hertz model. Therefore, Equation 6.5 of Hertz model was applied to estimate the contact area at rupture for this microcapsule. As a result, the rupture stress of this microcapsule could be determined.

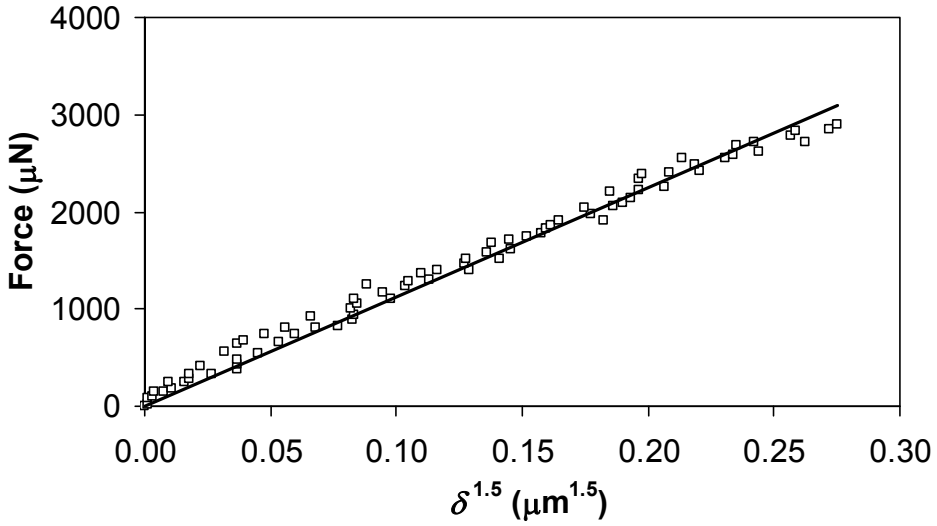

Figure 6.7 The linear fit of Hertz model (solid line) to the loading data of compressing a single MF microcapsule (diameter=15.0 μm) with starch coating at a final rupture deformation of 6%.

As discussed in Chapter 4, microcapsules without starch coating had larger rupture deformation and were less brittle. A MF microcapsule without starch coating (diameter=18.0 μm) ruptured at a deformation of 34%. Equation 2.2 of Hertz model was fitted to the loading data of this microcapsule, and the result is shown in Figure 6.8. The solid line is the best fit of Hertz model. It is clearly shown in Figure 6.8 that the solid line diverges from the experimental data at Point A of 7% deformation. The correlation coefficient for the Hertz model to fit the data to 7% deformation is 0.97. As demonstrated in Chapter 6.1.1, application of Hertz model is an alternative means to determine the elastic limit of single microcapsules besides loading-unloading experiment. Therefore, the results here indicate that this microcapsule had an elastic limit of 7%. This means the plastic deformation of this microcapsule took place after 7% deformation. By applying Johnson's plastic solid model that contact stress is constant in the plastic region, the rupture stress of this microcapsule at the rupture deformation of 34% or the contact stress at plastic deformation was then equivalent to

the contact stress at 7% elastic deformation. The rupture stress was calculated by using compressive force at 7% deformation dividing by contact area at 7% deformation, whilst the contact radius at 7% deformation can be determined by applying Equation 6.5.

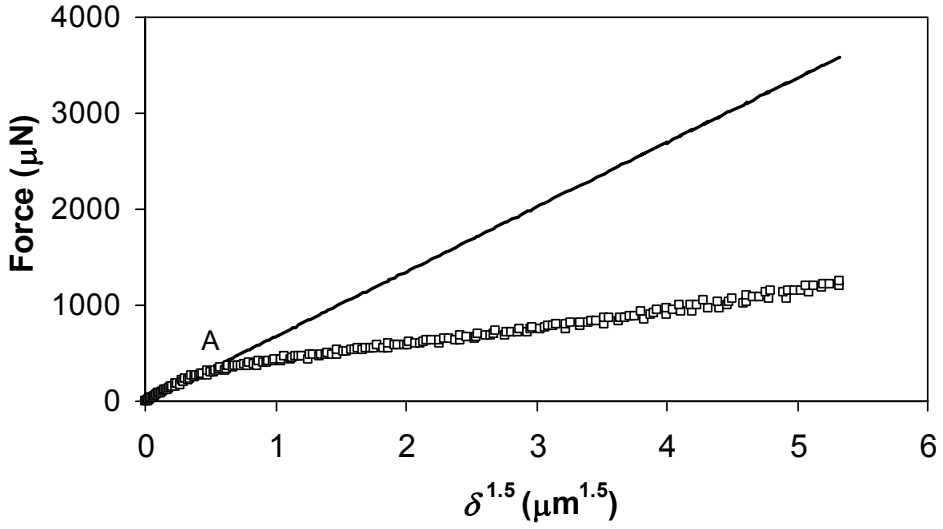

Figure 6.8 The linear fit of Hertz model (solid line) to the loading data of compressing a single MF microcapsule (diameter=18.0 μm) without starch coating up to a final rupture deformation of 34%. Hertz model can be fitted to a deformation of 7%.

The above approach of employing Hertz and Johnson's model to determine the rupture stress of individual microcapsules was applied to 10 microcapsules from each of samples with or without starch coating, which had respective small and large deformations at rupture. Hertz model was able to fit the loading data of starch-coated microcapsules up to 6±3% deformation and that of microcapsules without coating up to 12±7%. Such two values determined by Hertz model were therefore elastic limits of the respective samples. Their mean rupture stress was calculated, and the data is presented in Figure 6.9. The results clearly suggest the mean rupture stress of microcapsules with starch coating (102±55 MPa) is significantly greater than those

without coating (18±7 MPa). This implies that the use of starch coating is able to increase the mechanical strength of microcapsules.

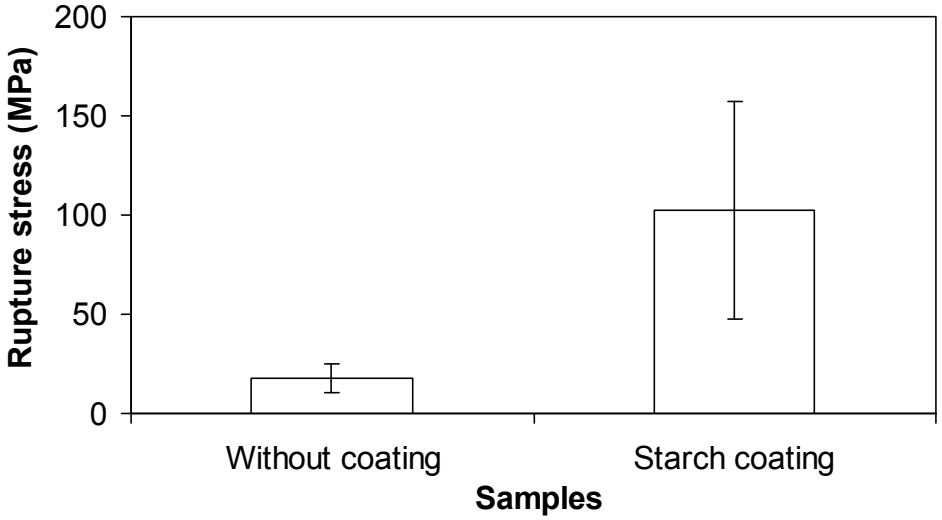

Figure 6.9 Mean rupture stress obtained by applying Hertz model and Johnson's plastic model for microcapsules without and with starch coating.

The *t* statistic test conducted in Chapter 4 suggested that no significant difference was between the nominal rupture stress of microcapsules with starch coating (6.7±3.5 MPa) and without coating (5.4±2.0 MPa) which however both had relatively large standard errors. As shown in Chapter 4, the mean deformation at rupture differed significantly between such two samples, which were 13±11% for starch-coated microcapsules and 37±5% for microcapsules without coating. Nominal rupture stress should ideally be applied when microcapsules rupture at similar deformations. The modelling results show that the real rupture stress of starch-coated microcapsules was significantly higher in comparison with that of microcapsules without coating. Microcapsules with starch coating were therefore stronger. This is probably because starch coating around microcapsules in fact adds another layer of wall to the microcapsules. As such, higher force is required to not only rupture MF wall but also starch coating which

leads to the higher strength of microcapsules. The modelling result highlights the importance of interpreting the data of nominal rupture stress with caution. The acquired results have demonstrated that the real rupture stress determined from modelling is very effective to validate the findings based on comparison of nominal rupture stress of microcapsules which have relatively large standard errors, as well as microcapsules have significantly different rupture deformations.

6.2.2.2 Microcapsules with & without Silicate Coating

The Hertz elastic model and Johnson's plastic model were also applied to compression data of 10 microcapsules from each of samples with or without silicate coating to obtain the rupture stress of single microcapsules. It was found in Chapter 4 that microcapsules with silicate coating was more brittle than those without, since the former had a deformation at rupture of 14±2% compared to 39±5% the latter had. Utilizing the procedures presented above, the modelling results reveal that Hertz model can fit the loading data of silicate-coated microcapsules up to 11±3% and 19±5% for microcapsules without coating. The mean rupture stress of these two samples is shown in Figure 6.10. It is clear that the rupture stress of microcapsules with silicate coating (212±117 MPa) is significantly higher than those without coating (3.1±0.8 MPa). This agrees with the finding in Chapter 4 that nominal rupture stress of silicate-coated microcapsules (18.8±5.2 MPa) is significantly greater than those without coating (1.7±0.4 MPa). The standard errors of nominal rupture stress of microcapsules studied here is relatively small. It is worth noting both rupture stress obtained were greater than their respective nominal rupture stress due to the use of contact area. The results demonstrate that the use of rupture stress to compare the rupture strength of microcapsules can get the similar

results as those from employing nominal rupture stress with relatively small standard errors. The difference is that use of rupture stress can magnify the difference between samples in comparison with adopting nominal rupture stress. It is understandable that rupture stress determined by modelling can reflect the real rupture strength of microcapsules, but it takes longer time to apply modelling and might not be suitable for the industries which demand efficiency. The results here have shown that nominal rupture stress can be applied to accurately compare the mechanical strength of microcapsules with significantly different deformation, as long as the standard errors are relatively small. The findings should be very useful for the industries to not only quickly but also correctly compare the mechanical strength of microcapsules using nominal rupture stress. It was noted that the rupture stress of microcapsules with silicate coating is approximately 70 times of microcapsules without coating, whilst it was around 6 times for microcapsules with and without starch coating. This could be attributed to that silicate coating is much thicker than that of starch coating. As such, further work is required to measure and compare the thickness of such two coatings.

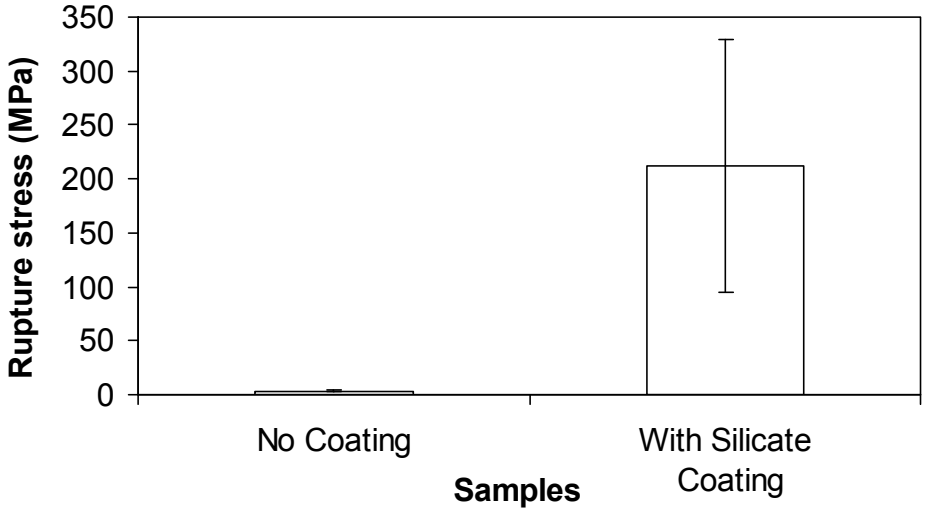

Figure 6.10 Mean rupture stress obtained by applying Hertz model and Johnson's plastic model for microcapsules without and with silicate coating.

6.3 Conclusions

It can be concluded that Hertz model was able to describe elastic deformation of MF microcapsules and to determine the Young's modulus of microcapsule E_c, which was found to be 32±4 MPa; however, it represents the modulus of whole microcapsule. The results also demonstrated that FEA with elastic material model has allowed the loading data of MF microcapsules to be fitted with good agreement. The obtained Young's modulus E_w corresponds to the modulus of microcapsule wall material, which was found to be 8±1 GPa and was in the same order of magnitude as that suggested in the literature using an analytical approach (Keller & Sottos, 2006). The FEA method can therefore be applied to other microcapsules in order to determine the Young's modulus of microcapsule wall material. A correlation describing the relationship between E_c and E_w was developed based on the modelled results, wall thickness and diameters of microcapsules.

The contact stress of a MF microcapsule during compression was calculated by applying the compressive force and the corresponding contact diameters of a single MF microcapsule provided by Stenson *et al.* (2008), which were measured by nanomanipulation in an environmental scanning electron microscope. It was demonstrated that the obtained contact stress is in good agreement with the assumption of Johnson's solid plastic model that contact stress in the plastic deformation region remains constant.

Hertz model together with Johnson's plastic model were therefore adopted to apply on the compression data of 4 microcapsule samples previously discussed in Chapter 4. It was found

that the use of nominal rupture stress with relatively small standard errors can reach the same conclusion as employing the modelled rupture stress in terms of comparing the mechanical strength of microcapsules with significantly different rupture deformation. The application of rupture stress simply magnifies the difference between samples in comparison with nominal rupture stress. Johnson's plastic model is required to be further validated using the measured contact diameters which can be obtained from nanomanipulation (Stenson *et al.*, 2008), if the sizes of microcapsules are around 10 μm. Alternatively, a sensitive microscope visualisation instrument can be employed for microcapsules with sizes ranging from 60 μm to 120 μm (Liu *et al.*, 2002). It is always important to validate the model directly using the experimental data. Moreover, other modelling methods such as FEA combined with other plastic models can be developed to determine the contact diameters of microparticles with core/shell structure like microcapsules. The modelled contact diameters can then be validated using the experimentally measured contact diameters of single microcapsules during compression. Rupture stress of microcapsules by modelling is very useful either to determine or validate the mechanical strength of microcapsules. This should be very beneficial to different industrial sectors which have used or intend to use microcapsules in a wide range of products including detergents.

7. ADHESIVE FORCE MEASUREMENT

The interaction between MF microcapsules and dry or detergent solution soaked cotton fabrics is of particular interest to the industry for their commercial applications. An AFM 3-D surface image of a strand of cotton fibre with a root mean square (RMS) roughness of 21.9 nm over an area of 4 μm^2 is shown in Figure 7.1. There were totally 4 such locations (each with an area of 4 μm^2) of the cotton fibre scanned and the mean RMS roughness obtained is 17.6±3.2 nm. It depicts the rough and inconsistent surface of the single cotton fibre, which could hinder the force measurement or even damage the delicate AFM cantilever. As a result, cotton films were regenerated by dissolving cotton powder/fabrics to replace cotton fibres for the adhesion studies. In this chapter, the characterisation of cotton films including their roughness, thickness, hydrophilic property and purity are presented. Moreover, the interaction between MF microcapsule/microparticle and cotton films under ambient condition or in the detergent/surfactant solutions is also studied.

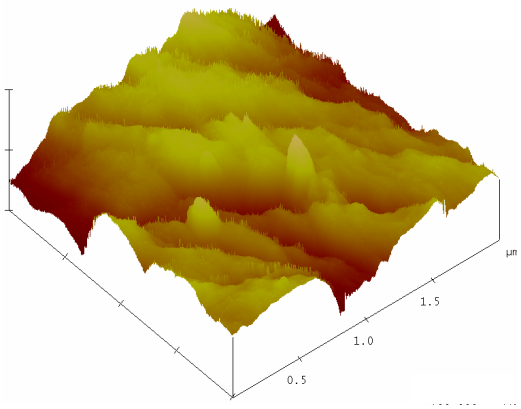

Figure 7.1 AFM 3-D surface image of a single cotton fabric fibre with a scan area of 2µm×2µm. The RMS roughness of the fibre shown here is 21.9 nm and the data scale is 100 nm.

7.1 Characterisation of Cotton Films

Cotton films generated using the procedures described in Chapter 3.2.2 were characterised using various techniques. Surface images and the results regarding the thickness, contact angle and purity of cotton films are presented in this section.

7.1.1 Atomic Force Microscopy (AFM) Imaging

7.1.1.1 PEI Polymer Layer

According to generation procedures of a cotton film, a substrate silicon wafer first needs to be treated with 10% NaOH solution before being coated with an anchoring PEI polymer layer. Between each step of the procedures, the films were imaged using AFM. The typical images of silicon wafer, silicon wafer treated by 10% NaOH solution and PEI film are illustrated in Figure 7.2 and their RMS surface roughness is 0.3 nm, 0.3 nm and 0.4 nm respectively, based on a scan area of 5μm×5μm. By scanning 3 locations per film, the mean RMS roughness for silicon wafer was found to be 0.4±0.1 nm and the mean roughness became 0.37±0.01 nm after being treated with 10% NaOH solution. The mean roughness of the film was 0.371±0.005 nm after it was coated with PEI polymer. The topography images and low RMS roughness level indicate that these 3 films have much smoother surface with respect to the single cotton fibre. The repeated experiments demonstrated that elimination of either NaOH treatment or anchoring PEI polymer layer would result in the cotton film not being able to adhere to the silicon substrate. It may be because that the silicon wafer has a native silicon oxide layer on the surface and the high pH value of NaOH solution converts the Si-OH bond on silicon surface to Si-O-, or a Si-O-Si bond to Si-O- and Si-O-, enabling the silica to adsorb more

polymers. The importance of including the two steps was also stressed by Gunnars *et al.* (2002). It was stated that the mechanism of the anchoring polymer is not exactly known, however, an anchoring polymer layer is necessary in order to attach the cotton film to the wafer.

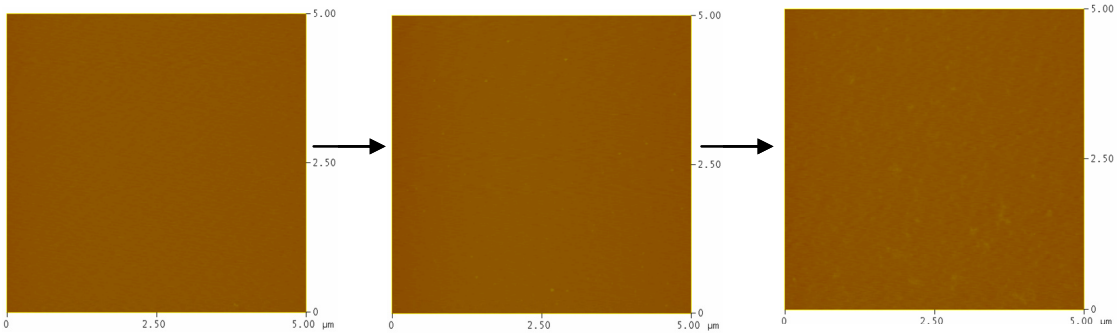

(a) **(b)** **(c)**

Figure 7.2 AFM topography images of (a) Bare silicon wafer (RMS=0.3 nm); (b) Silicon wafer after being treated with 10% NaOH solution (RMS=0.3 nm); (c) PEI polymer layer (RMS=0.4 nm). The data scale is 100 nm.

7.1.1.2 Cotton Films

It was found that only 0.2 g cotton fibre bundles that were cut into pieces could be completely dissolved in 25 g NMMO solution with respect to 0.5 g dissolvable wood pulps suggested by Notley *et al.* (2006). In contrast, as much as 0.5 g cotton powder was found to be completely dissolved in the same amount of 25 g NMMO solution. If the same amount of time is used to dissolve 0.5 g cotton fibre or powder, only less than half amount of 0.5 g cotton fibre can be completely dissolved in comparison to all 0.5 g cotton powder. With the amount of employed time extended, NMMO solution was found evaporated away before the remaining fibres were completely dissolved. This could be due to the difference between the compositions of cotton fibres and cotton powder. According to the supplier (Sigma-Aldrich, UK), the cotton powder

was composed of cellulose except the presence of a less than 10 ppm metal traces. On the other hand, cotton fibre is composed of 95% cellulose and the other 5% are protein, ash, wax, sugar, organic acids and other chemical compounds (Wakelyn *et al.*, 2006).

Another reason could be that cotton powder has smaller sizes (mean width 20 μm) compared with cotton fibre bundles with the mean width around 200 μm. Cotton fibre bundles consist of various woven single strands of fibres; they were still tightly woven with each other even though being cut into pieces. As a result, cotton powder has larger specific surface area than cotton fibre bundles in contact with NMMO solution. Consequently, within the same amount of given time, 0.5 g cotton powder could be completely dissolved before all the NMMO solution was evaporated in comparison to 0.2 g cotton fibre bundles. Therefore, the concentrations of cotton fabrics & cotton powder in NMMO solution with a latter addition of DMSO solvent were 0.2wt.% and 0.5wt.%, respectively. Further work can involve studies on reduction of evaporation rate to allow 0.5 g cotton fibre to be completely dissolved.

The films prepared from cotton fibres and cotton powder were characterised using AFM to study the material distribution of cotton on the film surfaces and to measure their roughness. Figure 7.3 and Figure 7.4 give typical topography and 3-D surface images of cotton films generated from cotton fabric fibres and cotton powder at a scan area of 5μm×5μm. Their RMS roughness for the presented typical images is 5.5 nm and 5.2 nm, respectively. Their mean RMS roughness for cotton films prepared from fabric and powder is 5.5±0.1 nm and 5.1±0.2 nm, based on scanning results of 3 locations on each film. This shows that a comparable roughness of cotton films generated from cotton fibres or powder can be obtained, even

though their concentrations in solvents were different. It agreed very well with the findings of Falt *et al.* (2004) that the increase in concentration of cellulose solution only contributes to thicker cellulose films and has no influence on the surface roughness. Since the surface roughness of such two types of films is similar, cotton powder was chosen as the solute in further work; not only the cellulose concentration of 0.5wt.% specified by Gunnars *et al.* (2002) and Notley *et al.* (2006) was allowed, but also thicker films can be produced. For the following sections, unless otherwise mentioned, all the cotton films are referred to films generated from cotton powder.

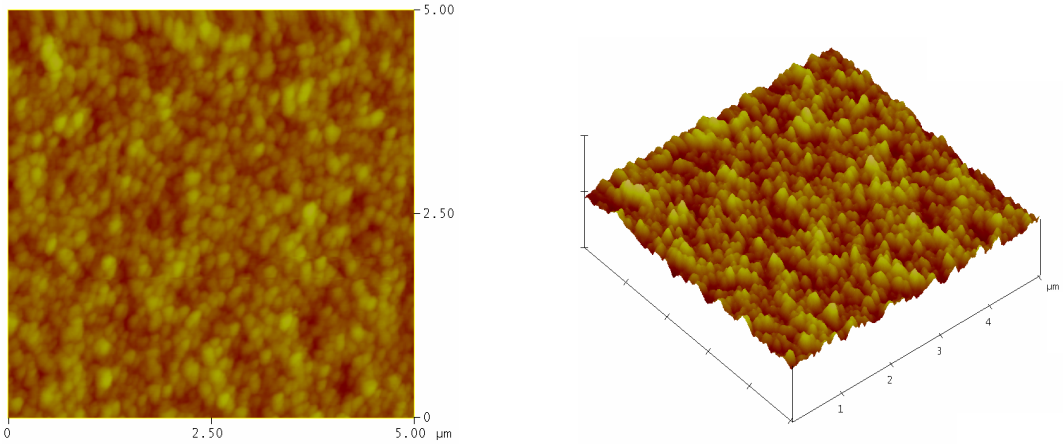

(a) **(b)**

Figure 7.3 AFM (a) topography image (b) 3-D surface image of a dry cotton film generated from cotton fabrics (scan area 5µm×5µm) and cotton concentration in solution is 0.2wt.%. The RMS roughness of the cotton film shown here is 5.5 nm and the data scale is 100 nm.

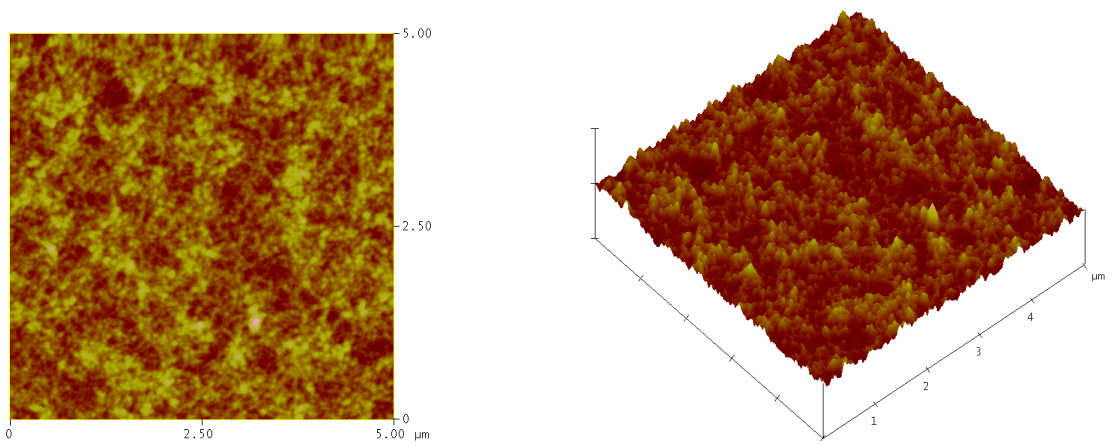

(a) **(b)**

Figure 7.4 AFM (a) topography image (b) 3-D surface view of a dry cotton film generated from cotton powder (scan area 5µm×5µm) and cotton concentration in solution is 0.5wt.%. The RMS roughness of the film shown here is 5.2 nm and the data scale is 100 nm.

7.1.2 Ellipsometry

Ellipsometry was employed to measure the thickness of respective layers of films during generation of cotton films. The film thickness was obtained by measuring 5 individual and visibly defect-free locations across the film, and the mean thickness of each film and the twice standard errors are presented in Table 7.1. The mean thicknesses of the native silicon oxide layer on the silicon wafer surface (after being treated with 10% NaOH solution), PEI polymer film and cotton film are 2.5 ± 0.4 nm, 0.9 ± 0.2 nm and 13.1 ± 2.5 nm, respectively. The thickness of cellulose film generated from dissolving pulp solution and using the same type of PEI polymer was reported to be around 30 nm by Aulin *et al.* (2008), which is approximately twice of that of cotton film generated from cotton powder solution. According to Falt *et al.* (2004), the thickness of cellulose film increases with the concentration of cellulose solution. As the concentration of dissolving pulp solution was not specified by Aulin *et al.* (2008), the

thickness of cellulose films prepared from wood pulp and the thickness of cotton films prepared from cotton powder are therefore not directly compared here.

Table 7.1 Thickness of silicon oxide layer on bare silicon wafer (after being treated with 10% NaOH solution), PEI polymer film and cotton film.

Location	SiO_2	PEI	Cotton
1	2.1	0.7	13.5
2	2.8	0.7	15.7
3	2.9	0.9	15.4
4	2.5	1.2	10.4
5	2.0	0.9	10.7
Mean (nm)	2.5 ± 0.4	0.9 ± 0.2	13.1 ± 2.5

7.1.3 Contact Angle Measurement

The results of contact angle measurement show that the contact angle, θ, between a drop of water and cotton film is 33º, as illustrated in Figure 7.5. It is within the range of contact angles suggested by Gunnars *et al.* (2002) for pure cellulose. As reviewed in Chapter 2.5.2.2, the contact angle between a hydrophilic surface and a water droplet is less than 90º; the cotton film is therefore hydrophilic. This implies that, in an ambient environment with a relatively high RH, the adhesive force between cotton films and the other hydrophilic surface could be mainly capillary force (Jones *et al.*, 2002).

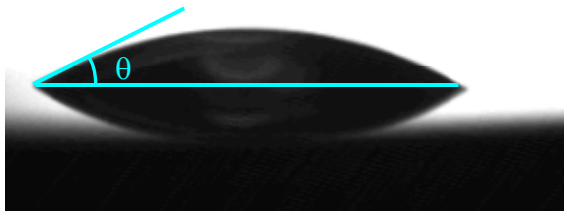

Figure 7.5 Optical photograph of a drop of water on a cotton film for measuring the contact angle, which is 33º in this case.

7.1.4 X-ray Photoelectron Spectroscopy (XPS)

A survey XPS scan was performed on a cotton film and the results shown in Figure 7.6 are based on the average of 3 scans. The cellulose of cotton film consists of C, O & H elements, therefore, the distinctive O 1s and C 1s peaks can be observed from the spectra. The H peaks are missing in the spectra, but this is expected as the XPS technique is not able to detect H element (Nefedov, 1988).

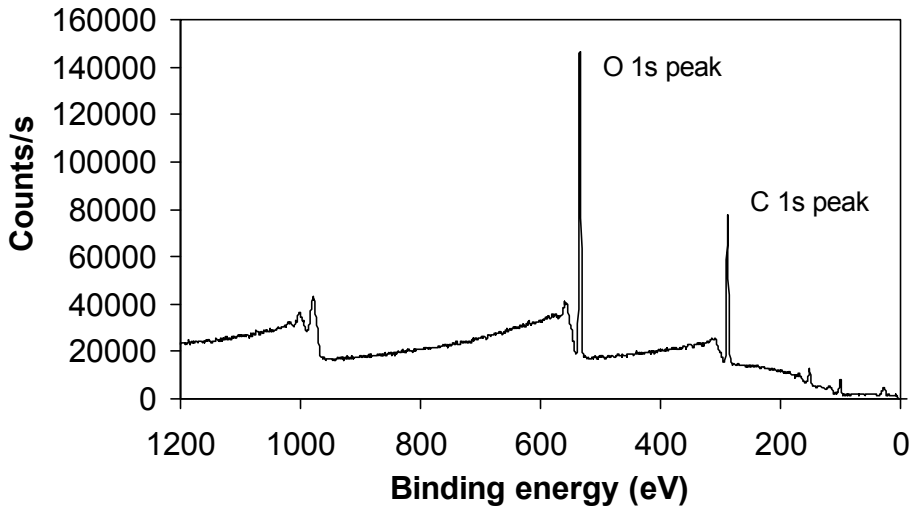

Figure 7.6 Survey XPS spectra for a cotton film.

In order to ensure there is no solvent residue on the film, the detailed scan was undertaken and concentrated on the range of binding energy of the element originated from the solvent. As illustrated in Chapter 3.2.3.3, NMMO solvent consists of N element with a binding energy of 402 eV. The binding energy ranging from 390 eV to 412 eV was scanned for N 1s and the results are presented in Figure 7.7. No visibly distinctive N 1s peaks can be observed in the range of this binding energy except the baseline noise. According to Gunnars *et al.* (2002), this

indicates there is no presence of NMMO solvent on the surface of cotton film. If there were any NMMO residue on the cotton film surface, the spectra would look similar to that of PEI film (Figure 7.8) in which a distinctive N 1s peak can be identified, as PEI polymer consists of N elements.

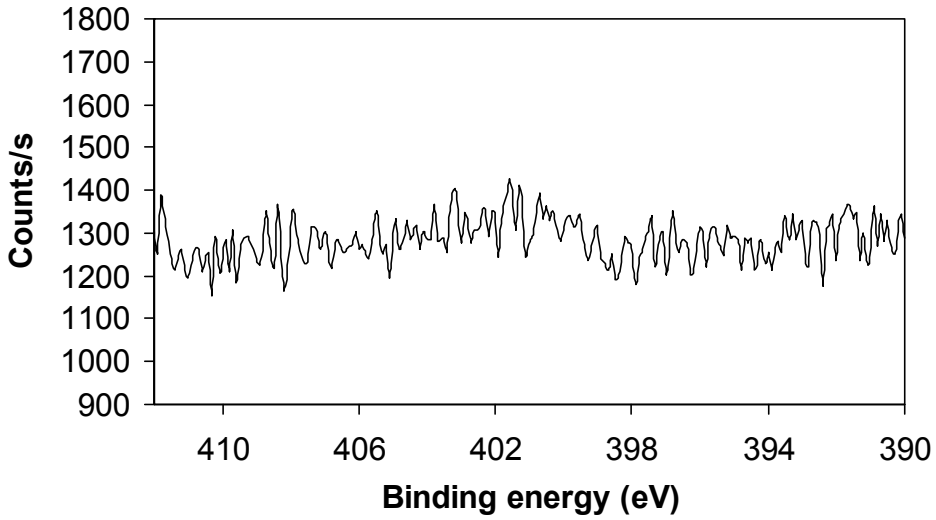

Figure 7.7 XPS spectra of N 1s for a cotton film.

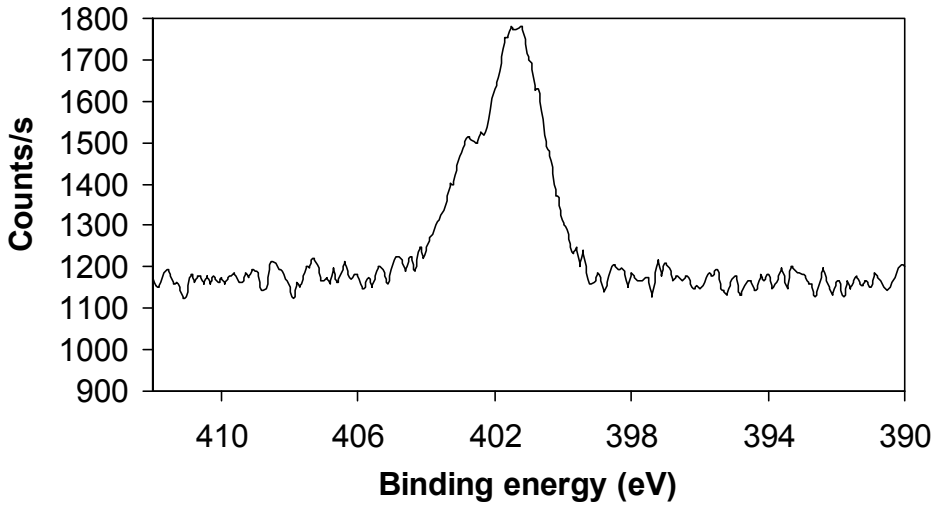

Figure 7.8 XPS spectra of N 1s for a PEI film.

7.2 Surface Roughness of MF Microcapsules and MF Microparticles

The surface roughness of MF microcapsules & MF microparticles was also characterised by AFM. Figure 7.9(a) shows an AFM image of a MF microparticle surface (diameter=12.5 μm) and its RMS roughness is 3.8 nm based on a scan area of 500nm×500nm. A larger scan area might cause an error in roughness data since the microparticle had a curved surface. The RMS roughness on an area smaller than 500nm×500nm might not be representative enough. Moreover, it is worth noting that the diameter of cantilever tip is approximately 20 nm. Hence, a resolution smaller than 20nm×20nm is unachievable. The mean RMS surface roughness of MF microparticles is 4.2±0.4 nm based on scanning images of 4 such microparticles with a mean diameter of 12.5±0.2 μm using the same scanning area as that in Figure 7.9(a). Figure 7.9(b) shows an AFM image of a MF microcapsule surface (diameter=38.2 μm). For comparison purposes, the same scan area of 500nm×500nm was again used for the microcapsule. The RMS surface roughness of MF microcapsule is 3.4 nm, as shown in Figure 7.9(b). The mean RMS surface roughness of MF microcapsules is 3.3±1.1 nm based on the same scanning area of 500nm×500nm and scanning images of 3 such microcapsules which had a mean diameter of 36.0±5.0 μm. Taking into account of standard errors, MF microparticles and MF microcapsules have a comparable surface roughness. It should be noted that the mean RMS roughness of a cotton film with a same scan area of 500nm×500nm on 3 locations of the cotton film is 4.76±0.02 nm (images not shown), which is also similar to that of MF microcapsule or microparticle.

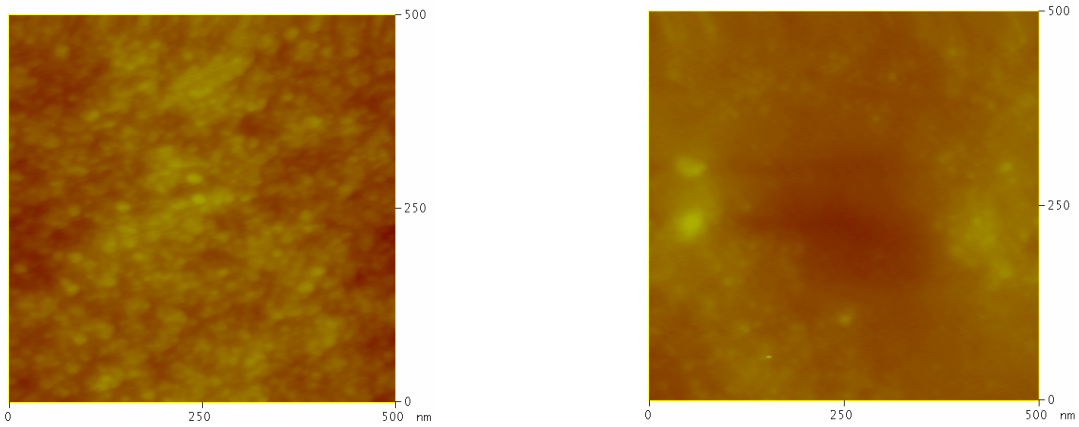

(a) **(b)**

Figure 7.9 AFM topography image of (a) a MF microparticle (12.5 μm in diameter) surface with a RMS roughness of 3.8 nm; (b) a MF microcapsule (38.2 μm in diameter) surface with a RMS roughness of 3.4 nm. Both images were based on a scan area of 500nm×500nm and the data scale is 100 nm.

7.3 Adhesion under Ambient Condition

7.3.1 Adhesion between MF Microcapsule and Cotton Fibre Bundles or Cotton Films under Ambient Condition

The experiments were performed to study the adhesion between MF microcapsule and cotton fibre bundles or cotton films under ambient condition with a RH of 46%; at the same time, the effect of piezo approaching speed on the adhesion were also investigated. A typical "Force-separation" graph describing the interacting forces between a MF microcapsule (diameter=34.8 μm) and a cotton film during the process of piezo extending and retracting is shown in Figure 7.10. As reviewed in Chapter 2.5.3.6, the force measured due to the deflection of cantilever during the extending of piezo denotes the attractive force, which is 11.7 nN here by calculating the difference in force between point A & B. Similarly, the force obtained during the retracting of piezo represents adhesive force, which is 79.6 nN based on

the difference in force between point C & D. After normalizing with the radius of MF microcapsule (radius=17.4 μm), the obtained adhesive force is 4.6 mNm^{-1}.

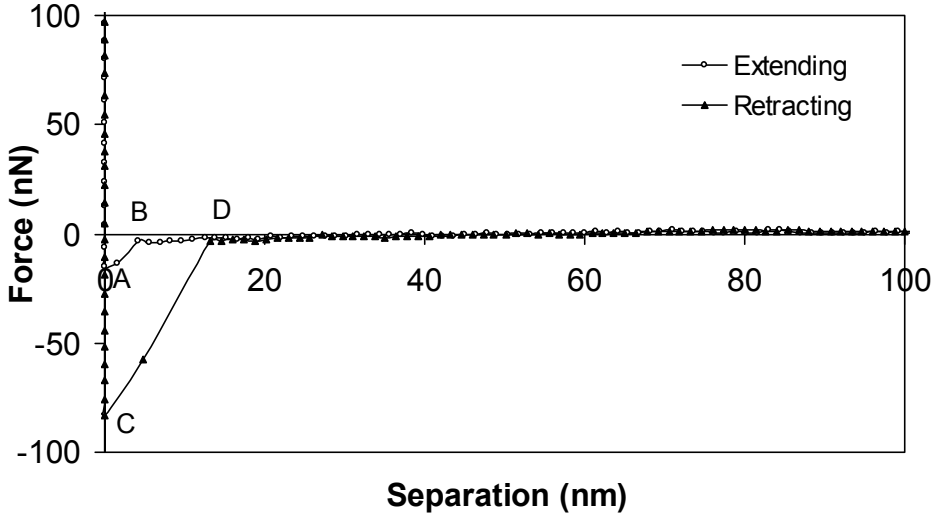

Figure 7.10 A typical graph depicting the interacting forces between a MF microcapsule (diameter=34.8 μm) and a cotton film under ambient condition with an air RH of 46% and a piezo approaching speed of 276 nms^{-1}.

Since only the adhesive force is interested here, the forces incurred during retraction were analysed and the summarized data is presented Figure 7.11. The highlighted bars denote the adhesive forces between a MF microcapsule (diameter=35.7 μm) and fibre bundles at various speeds, and the blank bars represent the adhesive forces between a MF microcapsule (diameter=34.8 μm) and cotton films. It is noted that the sizes of microcapsules used were slightly different, therefore, the adhesive forces were normalised with the radius of microcapsules for comparison. For adhesion on cotton bundles, 5 locations were chosen and 5 repeated measurements were made at each location. For adhesion on cotton films, 10 locations were chosen and 5 repeated measurements were made at each location. The scan rates used were 0.05 Hz, 0.5 Hz and 2.33 Hz, which corresponded to the piezo approaching speeds of

276 nms^{-1}, 2760 nms^{-1} and 12850 nms^{-1} respectively based on the ramp size of 2.757 μm. The detailed conversion procedures between scan rate and piezo approaching speed are described in Chapter 3.2.4.4. MF microcapsules are partly hydrophilic due to the amine groups in the chemical structure of wall material melamine formaldehyde. Moreover, the wall of MF microcapsule is also composed of copolymer acrylamide and acrylic acid as shown in Figure 3.1, which are also hydrophilic due to the hydroxyl group and amine group they bear. Cotton films are hydrophilic as well based on the results of contact angle measurement. The RH of air during the force measurement was above 40%; the adhesive force measured is therefore mainly the capillary force, as suggested by Jones *et al.* (2002).

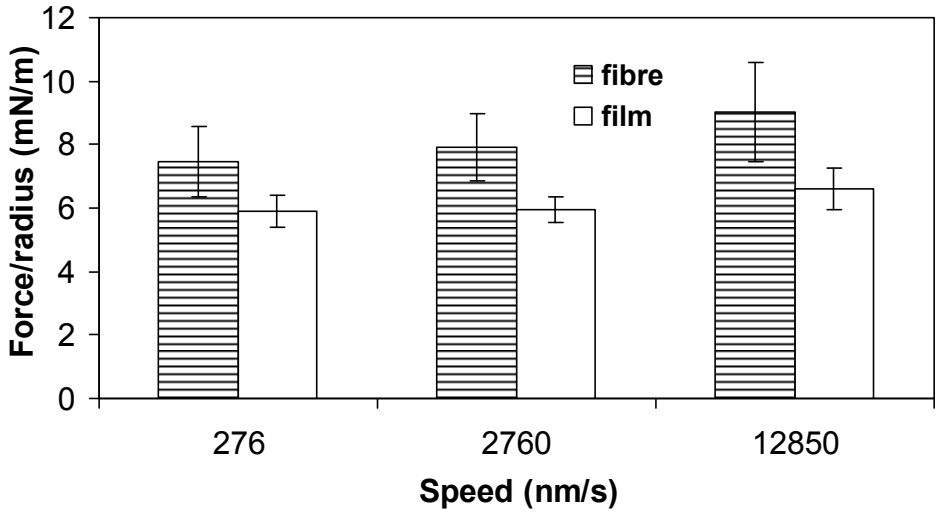

Figure 7.11 The adhesive forces (normalised with the radius of microcapsules) between MF microcapsules and cotton fibre bundles or cotton films under ambient condition (air RH 46%), measured at different piezo approaching speeds.

The standard errors of adhesive forces between the microcapsule and fibre bundles are significantly larger than that between the microcapsule and cotton films. This might be attributed to the dimension and structure of fibre bundles, which have a cylindrical shape with a diameter around 200 μm and consist of many single fibres that are often spatially dangled

out in air. As a result, the contact area between the microcapsule and the fibre might be inconsistent between each measurement. In contrast, the standard errors of adhesive forces between the microcapsule and the cotton films are much smaller, which is because cotton films were much more uniform and able to act as reliable substrates, and hence reliable adhesion measurement results can be produced. The adhesive force between the microcapsule and cotton fibre bundles is slightly greater than that when cotton bundles were replaced with cotton films. This might be again due to the structure of cotton bundles which have smaller fibres dangling out in the air to increase the contact area with the microcapsule, which in turn resulted in the formation of greater capillary force. Taking account of twice standard errors, the piezo approaching speed does not have a significant effect on the adhesive forces between the single microcapsule and fabric bundles or cotton films under ambient condition. It agrees with the suggestion of Jones *et al.* (2002) that there was no evidence that varying the speed significantly affected the pull-off force for relatively hard materials, such as cotton films studied here.

7.3.2 Adhesion between MF Microparticles/Microcapsules and Cotton Films under Ambient Condition

Figure 7.12 shows the adhesive forces between a MF microparticle/microcapsule and cotton films, measured at various piezo approaching speeds. The measurement results of MF microparticle are based on measurements at 14 different locations on cotton films for a given speed and 5 repeated measurements at each location. Similar to Figure 7.11, the speed does not show any significant effect on the adhesion between the MF microparticle/the MF microcapsule and the cotton films. As the experiments were conducted at 43% of air RH and

MF is of a hydrophilic nature, it is likely that the main mechanism of adhesion for both adhesion of MF microparticle or microcapsule is capillary force rather than that described by JKR contact mechanics theory, the latter of which is normally applicable to interpret dry contact at very low air RH. It is noted that the size of MF microparticle supplied by the manufacturer is smaller than that of MF microcapsule. The comparison can therefore be achieved by normalising with the radius of microparticle/microcapsule. Furthermore, it was revealed in the literature that there is little variation in adhesive force with particle size (Hodges *et al.*, 2002; Hodges *et al.*, 2004).

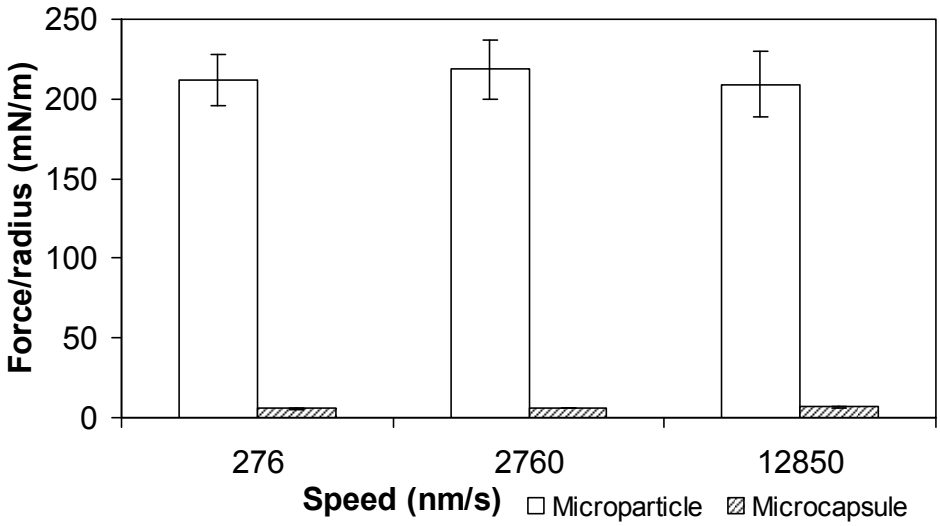

Figure 7.12 The adhesive forces (normalised with the radius of microcapsule/microparticle) between a MF microparticle (diameter=11.9 μm) / a MF microcapsule (diameter=34.8 μm) and cotton films under the ambient condition (air RH 43%), measured at different piezo approaching speeds.

Therefore, according to Equation 2.9, the maximum capillary force (θ_c=0) after being normalized with the radius of microparticle or microcapsule was predicted to be 905 mNm^{-1}. The measured normalised adhesive forces for the MF microparticle and the MF microcapsule at the speed of 276 nms^{-1} are 212±16 mNm^{-1} and 6±1 mNm^{-1}, respectively. The measured

adhesion falling well below the prediction of liquid bridge theory was also observed by others (Jones *et al.*, 2002; Hodges *et al.*, 2002). It was interpreted that the liquid bridge adhesion depends on a complex interplay of many effects, notably the geometry of surface asperities, meniscus radii (the radii of adsorbed water film), contact angles and the thickness of adsorbed water films. Furthermore, the contact angles and the adsorbed water layers are also very sensitive to the surface chemical conditions. Therefore, besides capillary force, surface chemistry and roughness are also two factors contributing to the adhesive forces.

The much elevated adhesive force measured between MF microparticle/cotton films than that between MF microcapsule/cotton films may arise from two reasons. Firstly, some perfume oils could be diffused out from the core of microcapsule and were present on the surface of microcapsule. Furthermore, MF microcapsules were produced from in-situ polymerisation technique which involves oil-water emulsion; as such the extra oil which had not been encapsulated could be still present on the surface of microcapsules. As pointed out by Schaefer *et al.* (1994), the presence of a contamination layer (e.g. volatile oils) between the sphere and substrate reduces the adhesive force. Moreover, model calculations have shown that a thin hydrocarbon contamination layer can reduce the attractive force between the two materials by about 50% (Cohen, 1992). In addition, the perfume oil is hydrophobic; as reviewed in Chapter 2.5.3.7, the degree of capillary condensation can be effectively suppressed by increasing the hydrophobicity of the contacting surfaces (Garoff & Zauscher, 2002).

Secondly, the surface chemistry of MF microcapsule surface is slightly different from that of MF microparticle, as the wall of MF microcapsule is composed of not only MF, but also acrylamide and acrylic acid and the surface MF microparticle is purely MF. The carbonyl group (C=O) in the acrylamide has a net negative charge, which could have a slight repulsive effect with the O bond in the cotton cellulose. Therefore, adhesive force of MF microcapsules with a wall composition of MF, acrylamide and acrylic acid was lower than that of MF microparticle which was composed of solely MF. The error bar represents twice standard errors of the mean adhesive force, which indicates that the adhesive force maybe varies with the locations of cotton films.

Hence, a graph showing adhesion between a MF microparticle (diameter=11.9 μm) and 4 random locations of the same cotton film (5 repeated measurements at each location) under the same ambient condition (RH 43%) is plotted in Figure 7.13. It is apparent that adhesive force is the lowest at location 3 (121±4 mNm^{-1}) and is the greatest at location 4 (180±1 mNm^{-1}). This suggests that the adhesion is influenced by the variation of locations which gave different roughness. It can be explained by the typical topography image of cotton film shown in Figure 7.4 that the cotton was not homogeneously deposited on the cotton film. As discussed above, the main adhesive force at RH greater than 40% is attributed to capillary force which also depends on factors such as surface roughness (Jones *et al.*, 2002).

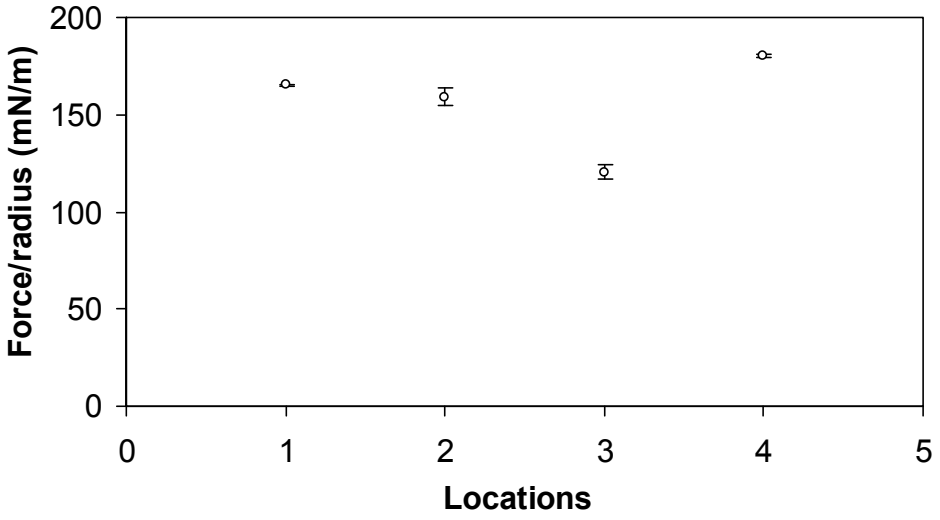

Figure 7.13 The adhesive forces (normalised with the radius of MF microparticle) between a MF microparticle (diameter=11.9 μm) and cotton films under the ambient condition (air RH 43%), measured at the piezo approaching speed of 2760 nm/s.

In order to validate the obtained adhesive forces between MF microparticle and cotton films, experiments were also conducted at 52% RH to measure the adhesive forces between a MF microparticle (diameter=9.2 μm) and a cotton film, as well as a strand of single fibre which was extracted from a cotton bundle. The single strand of cotton fibre with a dimension of 31 μm in width and 10 mm in length was fixed on a glass slide. The measurement was performed 5 times at each of 6 locations across the cotton film or single fibre with a piezo approaching speed of 2760 nms^{-1}. As shown in Figure 7.14, the adhesive forces between the MF microparticle and the cotton film/single fibre are 326±22 mNm^{-1} and 332±24 mNm^{-1}, respectively. The similarity between the two measurements again shows cotton film is a great substitute for fibre bundles. Although the adhesive force acquired in Figure 7.14 at air RH of 52% is higher than that measured at air RH of 43% in Figure 7.12, adhesion was also

influenced by variation of locations on cotton film, as shown in Figure 7.13. Therefore, such two results are not directly compared here.

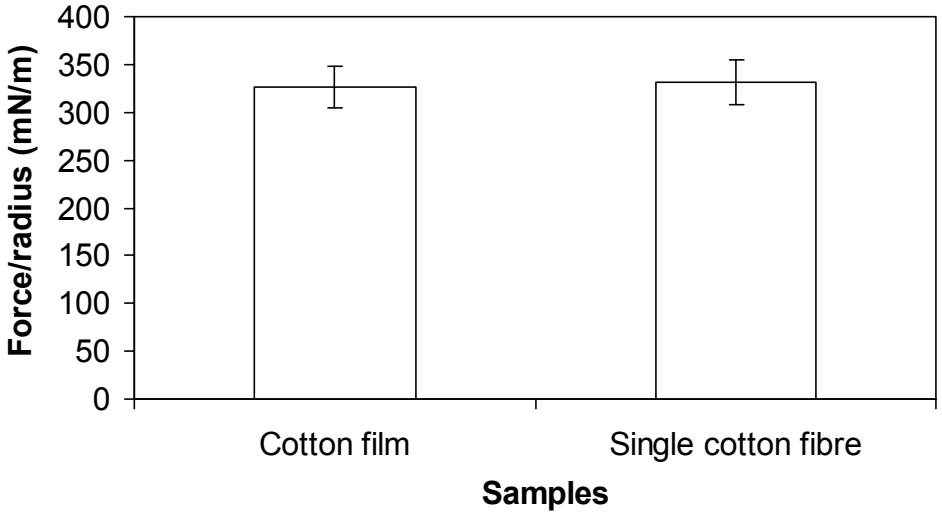

Figure 7.14 Comparison of adhesive forces between a MF microparticle (diameter=9.2μm) and a cotton film/a single cotton fibre under the ambient condition (air RH 52%).

7.4 Interaction between Single MF Microcapsules/Microparticles and Cotton Films in Liquid

The adhesion between single MF microcapsule/microparticle and cotton fibres/films under ambient conditions is studied in the above Chapter 7.3. The interaction between them in the liquid environment is studied here. Only the approach (extending) curves are discussed in the following sections according to Notley *et al.* (2006). Unless otherwise stated, the results below were based on experiments performing on at least 5 locations on the cotton films (5 measurements per location) and the typical interaction force curves are presented.

7.4.1 Interaction between MF Microcapsule and Cotton Films in Liquid

Before switching to employ MF microparticles, the interaction between a MF microcapsule (diameter=34.8 μm) and cotton films in the detergent solutions was also studied and the results are presented here. The spring constant of the cantilever used to attach this MF microcapsule was calibrated to be 7.5 Nm^{-1} using the reference cantilever method. Results showing the interaction between the microcapsule and a cotton film immersed in 1.0wt.% detergent solution are presented in Figure 7.15. The same scan rates of 0.05 Hz, 0.5 Hz and 2.33 Hz were applied. Since the maximum ramp size of MultiMode AFM was 1.903 μm, the corresponding piezo approaching speeds were 190 nms^{-1}, 1900 nms^{-1} and 8850 nms^{-1}; however, the speed does not appear to have any significant effect on the interaction in the detergent solution, which indicates that the interaction is not influenced by the hydrodynamic effect (McLean *et al.*, 2005). This is probably attributed to the large size of particle used (diameter=34.8 μm), as Vinogradova *et al.* (2001) concluded that the use of a sphere ($2R \geq 10$ μm) would be enough to suppress the hydrodynamic force contributed from the cantilever at a physically realistic range of driving speed. Since it is established that the piezo approaching speed does not show any significant effect on the interaction between the microcapsule and the cotton film in the liquid media, the piezo approaching speed of 1900 nms^{-1} corresponding to the scan rate of 0.5 Hz was applied for the further experiments, as shown in Figure 7.16 and Figure 7.17 later.

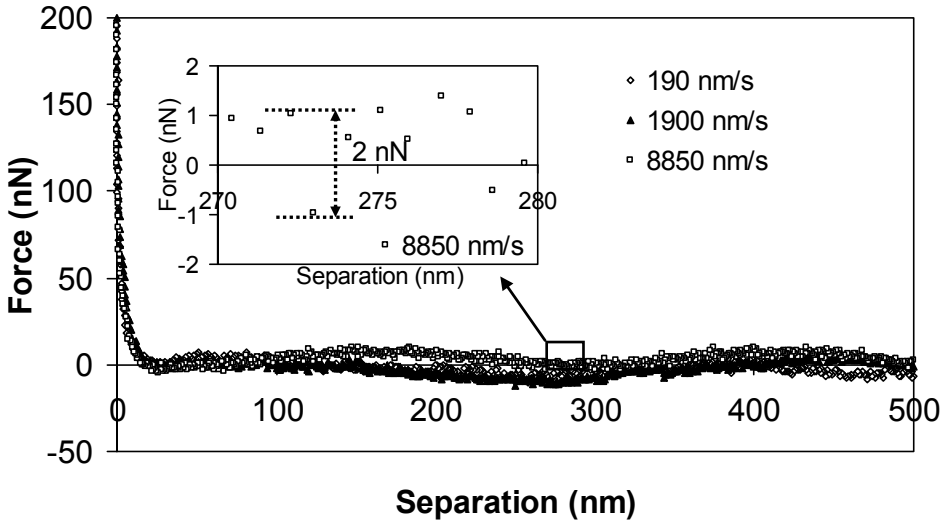

Figure 7.15 The interaction between a MF microcapsule (diameter=34.8 μm) and a cotton film immersed in 1.0wt.% detergent solution (pH=8), obtained at 3 different piezo approaching speeds. The inset figure illustrates how to determine the resolution of force curve.

The sinusoidal component in the baseline of the approach curves may be caused by the interference effect between the laser beam reflected by the cantilever and the stray light of laser beam scattered from the specimen surface. Due to the limitations of the optical focus path, the focused spot of laser beam is usually tens of micrometers in diameter, which is in the same order of the cantilever width. Furthermore, silicon material is semi-transparent; therefore, a portion of laser beam passed through the cantilever or around the sides instead of being reflected completely, which causes the formation of stray light (Huang *et al.*, 2006). Its interference can be minimized by choosing the cantilever with a high reflective material on its back.

It should be noted that the cantilever used here has a calibrated spring constant of 7.5 Nm^{-1} and is relatively stiff; and the force resolution in Figure 7.15 is 2 nN which was determined by following the method reported by Owen (2002). The force resolution is generally limited by

the thermal fluctuation and spring constant of cantilever; it can then be obtained from the baseline of force curve as illustrated in the inset graph of Figure 7.15. This method was applied to all the force graphs reported below to determine the force resolution. The cantilever with a spring constant of 7.5 Nm^{-1} was also used to study the interaction between a MF microcapsule (diameter=34.8 μm) and a cotton film immersed in water and 1.0wt.% detergent solution, as shown in Figure 7.16. No significant attractive interaction was observed from the curves based on the force resolution of 2 nN.

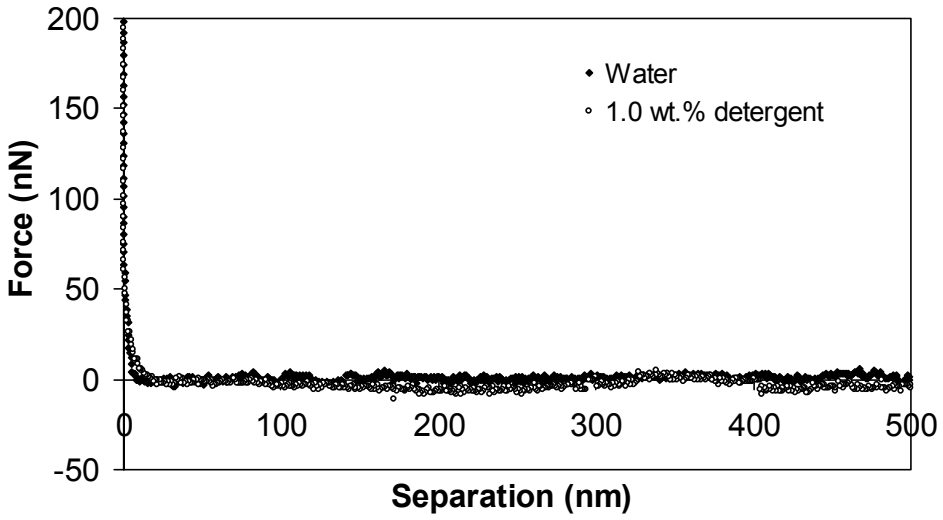

Figure 7.16 The interaction between a MF microcapsule (diameter=34.8 μm) and a cotton film immersed in water and 1.0wt.% detergent solution (pH=8).

Similarly, no significant attractive interaction was detected from the force curves showing the influence of pH on the interaction between a microcapsule (diameter=34.8 μm) and a cotton film in the detergent solution in Figure 7.17, based on the force resolution of 2 nN. Furthermore, the sinusoidal components were explicitly present on the baseline of force curve due to the use of the semi-transparent silicon cantilever (spring constant=7.5 Nm^{-1}). Therefore, this suggests that softer and more sensitive silicon nitride cantilevers coated with a reflective

material on the back need to be employed in order to measure smaller force than the current force resolution as well as eliminating the sinusoidal components, and the results are presented later.

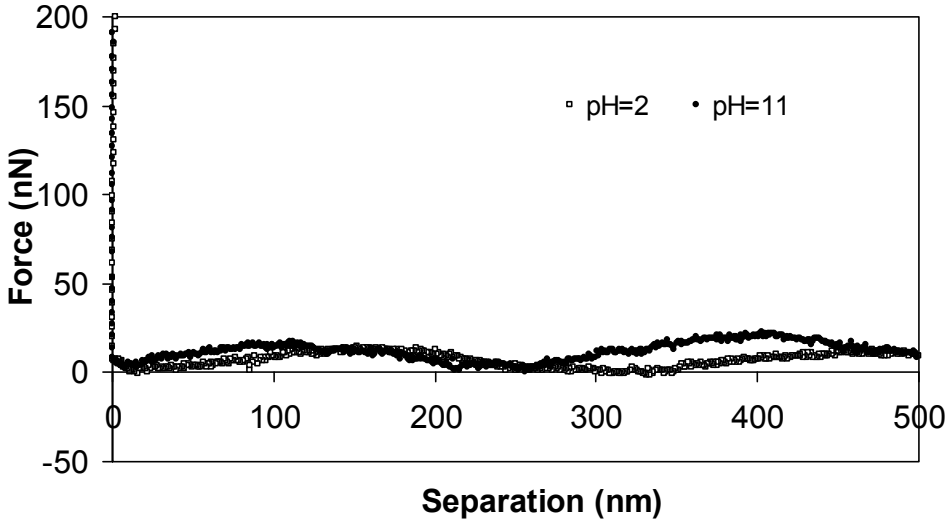

Figure 7.17 The interaction between a MF microcapsule (diameter=34.8 μm) and a cotton film immersed in 1.0wt.% detergent solution at varying pH.

7.4.2 Interaction between MF Microparticle and Cotton Films in Liquid

It was found that it was not easy to attach a single microcapsule to a tipless cantilever without rupture, using the D3100 AFM. The attachment was achieved by the procedures described in Chapter 3. However, it is very difficult to control the attachment process as there were no side-view or bottom-view cameras available. A slight overshoot of piezo movement can result in rupture of the microcapsule. Consequently, the rate of successful attachment was often less than 50%. The wall material of MF microcapsules is mainly MF. Also, MF microparticle and MF microcapsule have a similar surface roughness as demonstrated in Chapter 7.2. Moreover, MF microparticle is a rigid particle and is relatively not easy to collapse in comparison with

the soft particle like MF microcapsules. Thus, MF microparticle is ideal to substitute MF microcapsule for its ease of being attached to the cantilever. The physical appearance of MF microparticles (mean diameter=12.5 μm) is shown by an ESEM image in Figure 7.18, where the MF microparticles possess smooth surface and uniform sizes.

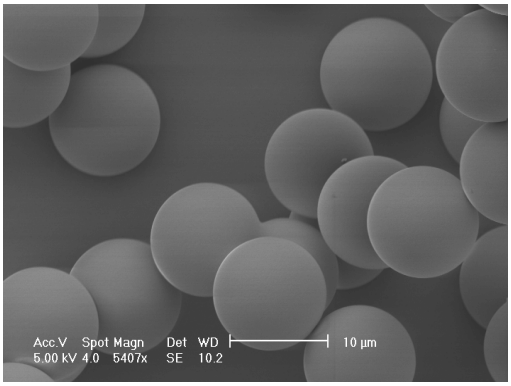

Figure 7.18 An ESEM image of MF microparticles with a mean diameter of 12.5 μm.

A selected MF microparticle (diameter=11.9 μm) was attached to a clean and unused stiff cantilever with a calibrated spring constant of 14.8 Nm^{-1}. The interaction between the microparticle and cotton films in water or 1.0wt.% detergent solution still produced the sinusoidal baseline. Furthermore, because of the use of the stiff cantilever, the detailed interaction between the MF microparticle and cotton films in water or 1.0wt.% detergent could not be distinguished clearly from the obtained graphs (data not shown), which is similar to the figures shown above. As a result, softer cantilevers were employed to act as colloidal probes by attaching a single MF microparticle. The interaction between MF microparticles and cotton films in the liquid environment are presented at the following sections in detail.

7.4.2.1 In Detergent Solution

The interaction between a MF microparticle (diameter=9.2 μm) and a cotton film in 0.15wt.% detergent solution was investigated using a softer cantilever, i.e. a silicon nitride colloid probe with a calibrated spring constant of 0.13 Nm^{-1}. 0.15wt.% detergent solution is generally used in the typical household washing. The scan rates applied were 0.5 Hz, 1.16 Hz and 3.49 Hz. The effect of speeds was re-examined to confirm the above finding based on the stiff cantilever, now that the softer and more sensitive cantilever was applied. Ramp size of 250 nm was used here in order to increase the resolution of curve. Because given a fixed number of data points to describe a curve by the AFM software, the smaller the ramp size is the higher resolution of curve it becomes. It is worth noting that the resolution of curve depending on ramp size is completely different from the resolution of force curve which is affected by the spring constant of cantilever as well as thermal fluctuation. Therefore, the corresponding piezo approaching speeds to the scan rates were 250 nms^{-1}, 580 nms^{-1} and 1745 nms^{-1}, based on the conversion procedures described in Chapter 3. Figure 7.19 shows that speed does not have significant effect on the force curve, since the shape of force curves at 3 various speeds had no significant difference. However, faster speed gives higher thermal fluctuation; which is reflected from the force resolution of 0.7 nN for the curve denoting a piezo approaching speed of 1745 nms^{-1} in comparison with 0.3 nN for 250 nms^{-1}. This again implied that hydrodynamic force has no significant impact on the system being studied. Hence, the speed of 250 nms^{-1} corresponding to the scan rate of 0.5 Hz was used in all the figures below to study the interaction of MF microparticles and cotton films in various liquid medias.

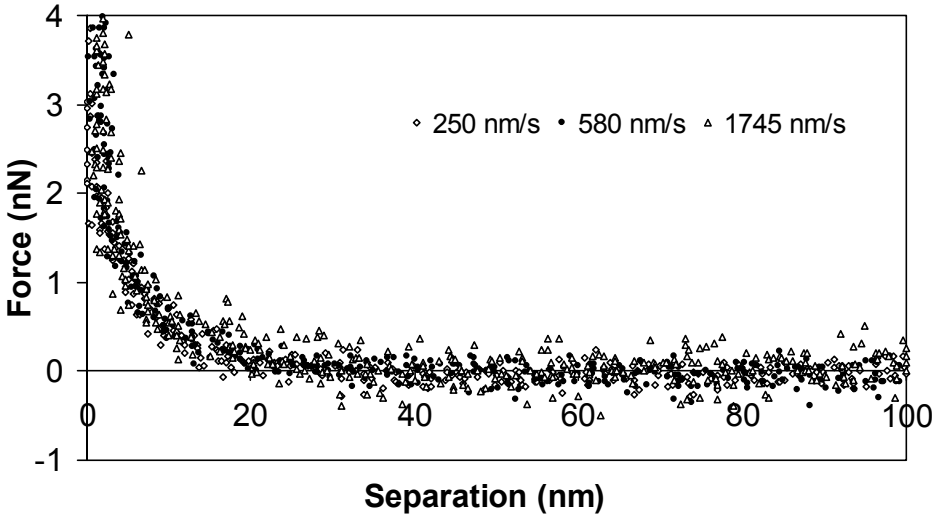

Figure 7.19 The interaction between a MF microparticle (diameter=9.2 μm) and a cotton film immersed in 0.15wt.% detergent solution (pH=8), measured at 3 different piezo approaching speeds.

The interaction between a MF microparticle (diameter=9.2 μm) and a cotton film as a function of the concentration of detergent solution is shown in Figure 7.20. The sinusoidal baseline disappeared, as the backside of the new cantilever was coated with a layer of gold material, which can minimize the passing of stray light as discussed in Chapter 7.4.1. Moreover, the influence of the concentration of detergent solution on the interaction between the MF microparticle and cotton film is obvious due to the use of softer and more sensitive cantilever (spring constant=0.13 Nm^{-1}). At 0.0001wt.% concentration, the repulsion started when the two surfaces were approximately 60 nm apart; the magnitude of maximum repulsive force was around 5 nN. At 10wt.% concentration, the repulsion commences when two surfaces were at a much closer distance of approximately 5 nm away from each other; the magnitude of maximum repulsive force drop to around 1 nN. The force resolution for the data shown in Figure 7.20 is 0.4 nN. It is evident that the repulsion becomes less pronounced with increasing concentration of detergent solution. As reviewed in Chapter 2.5.3.8, it was probably because

the increase of medium concentration generates a poor solvent condition for the polymer chains, and hence the steric repulsion is reduced (Lea *et al.*, 1994).

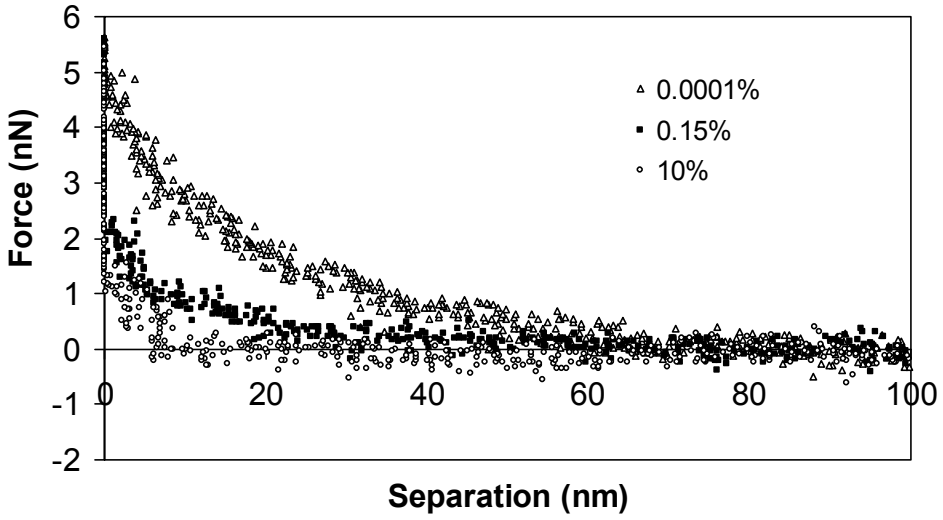

Figure 7.20 The interaction between a MF microparticle (diameter=9.2 μm) and a cotton film immersed in various concentrations (wt.%) of detergent solution at pH 8.

In addition, when a polymer exhibits the shape of a random coil in the solvent, its root mean square radius can be defined as radius of gyration, R_g, and shown in Equation 7.1 (Israelachvili, 1985):

$$R_g = \frac{\sqrt{n_s}\,l}{\sqrt{6}} = \frac{l\sqrt{M/M_0}}{\sqrt{6}} \qquad (7.1)$$

where n_s is the number of segments, and l denotes the effective segment length; M is the molecular weight of the polymer and M_0 is the segment molecular weight. As reviewed in Chapter 2.5.3.8, the interaction leads to repulsive forces when two polymer-covered surfaces approach each other. It was suggested by Israelachvili (1985) that repulsion appears once the separation is below a few R_g. As the effective segment length l of cotton is not available, R_g is taken from literature data of 57 nm for the molecularly dispersed cellulose chain (Chen *et al.*, 2007). The repulsive force commences on separation distance of 60 nm in Figure 7.20, which

is below a few R_g and in agreement with the findings of Israelachvili (1985). The slight fluctuation in the baseline of the force curves is due to thermal fluctuation of the liquid media, as liquid temperature was not perfectly constant (Owen, 2002). Such trend of repulsion reduced with the increase of solution concentration also matched the characteristics of electrostatic repulsion (Cappella & Dietler, 1999). Hence, zeta potential measurement of particles of interest in the surfactant solutions was performed in order to validate this mechanism and the results are presented in Chapter 7.4.2.2. By calculation, the typical concentration of detergent solution in a normal household washing machine is 0.15wt.%, hence, the results in Figure 7.20 suggest that there are no significant adhesion between MF microcapsules and cotton fibres immersed in a typical water environment in washing machine.

The repulsion was observed between the MF microparticle (diameter=9.2 μm) and the cotton film in the detergent solutions in Figure 7.20. However, there were multiple adhesions occasionally detected during retraction using the same cantilever (spring constant=0.13 Nm^{-1}), as illustrated in Figure 7.21. The approach curve shows repulsion as before; however, two adhesive forces were detected during retraction whilst the surface of MF microparticle was 18 nm and 25 nm away from the cotton film without actually touching it. The adhesion might be due to the lifting and stretching of the fibres on cotton film, which is illustrated in Figure 7.22. As a result, the adhesion was observed when the fibres "snapped-off" from the microparticle, whilst they were lifted to 18 nm and 25 nm away from the surface of cotton film. The explanation is further supported by the AFM images of cotton film displayed in Figure 7.4 that depicts the cotton fibres on the surface of the cotton film.

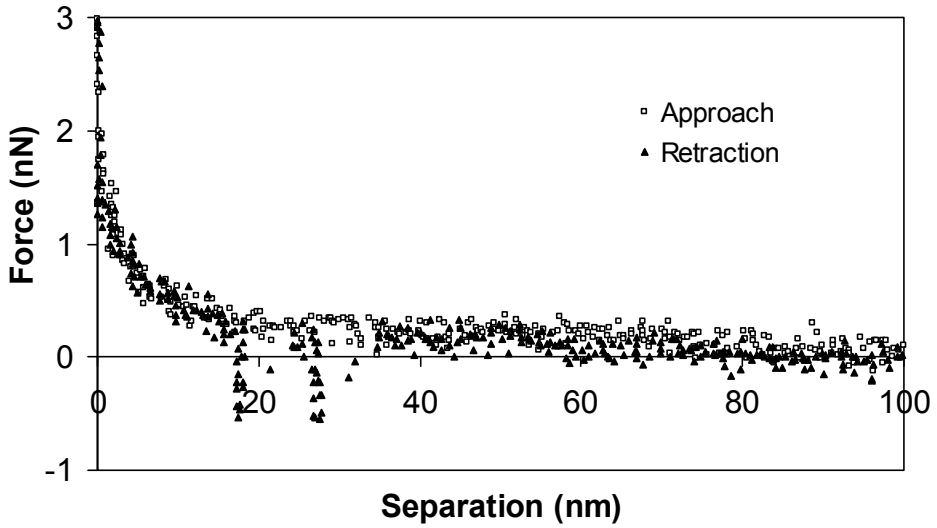

Figure 7.21 The interaction between a MF microparticle (diameter=9.2 μm) and a cotton film immersed in 0.01wt.% detergent solution (pH=8).

The adhesive force due to fibre/polymer chain stretching is also called "bridging force". The forces appeared occasionally, and for example in this study, bridging force was only detected from 2 out of 17 locations on the cotton films (40 force measurements per location). Furthermore, the force was detected intermittently at each of 2 locations with the mean value of 0.75±0.11 nN, based on 60 detected forces out of total 80 force measurements at these 2 locations. The force resolution in Figure 7.21 is 0.17 nN, which is well below the mean detected adhesive force of 0.75 nN. In addition, judging by the shape of force curve and the consecutive detection of adhesive forces within a curve, the detected force is confirmed as bridging force instead of noise.

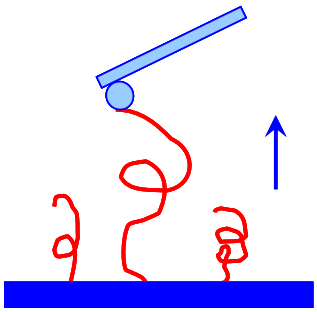

Figure 7.22 A schematic diagram to illustrate the lifting of a cotton fibre on the cotton film by a colloidal probe, causing the formation of bridging forces.

The results are consistent with the findings of Lea *et al.* (1993); bridging forces were occasionally detected for the interaction of polyethylene oxide adsorbed on the silicon nitride surface. This phenomenon is either due to the bridging of long polymer chains or the entanglement of polymer chains between surfaces (Lea *et al.*, 1993; Biggs, 1996). Bridging forces were also observed elsewhere due to the presence of cells with string like "arms" (Dammer *et al.*, 1995) and other long-chain polymers (Rief *et al.*, 1997; Aime *et al.*, 1994). The results obtained here are also in agreement with the findings of Weisenhorn *et al.* (1989) that the adhesive forces in liquid is much smaller compared with that in air due to the absence of capillary forces.

The interaction between a MF microparticle (diameter=9.2 μm) and a cotton film in 0.15wt.% detergent solution as a function of its pH is shown in Figure 7.23. The spring constant of the cantilever used was 0.13 Nm^{-1} and the force resolution in Figure 7.23 is 0.4 nN. At pH 12, repulsion occurred when the MF microparticle was 90 nm away from the cotton film. At lower pH, the repulsion began whilst two surfaces were 20 nm away. The results indicate that the repulsion increases with the increase of pH. This is probably because that the charges of polymers become higher at high pH values (Camesano & Logan, 2000). However, it was

noticed that repulsions at pH 3 and pH 8 were not significantly different. This may be due to the complex components that the detergent is composed of, which prevent a clear trend to be observed in this range of pH values. Hence, the interaction between the microparticle and cotton films was also studied in the solution of surfactant (a major component of the detergent) as a function of pH and presented in the following sections.

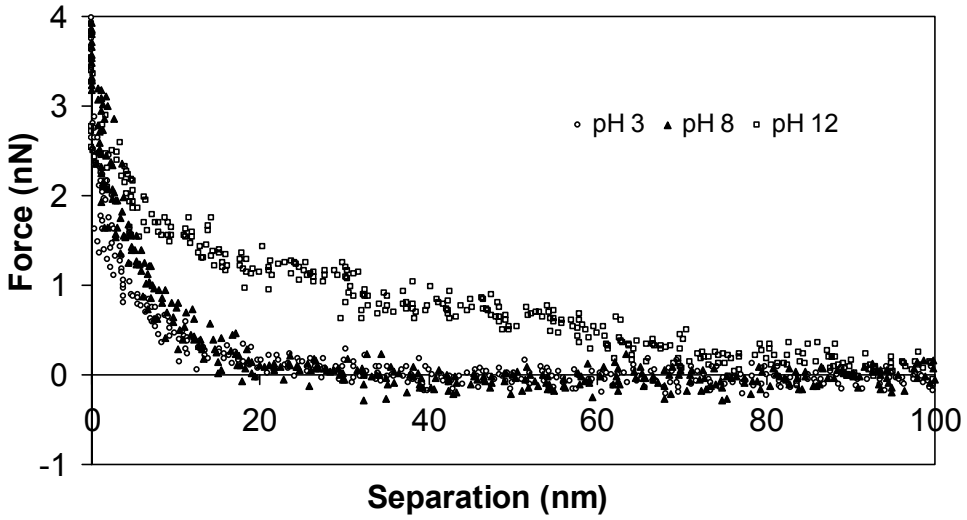

Figure 7.23 The interaction between a MF microparticle (diameter=9.2 μm) and a cotton film immersed in 0.15wt.% detergent solution at varying pH.

7.4.2.2 In SDBS Surfactant Solution

According to the working principle of AFM, the deflection of cantilever is sensed by the means of reflecting laser beam on the top of cantilever, which is immersed in the fluid, to the position sensitive photodiode. The noise that is present in raw data is therefore suppressed if laser beam is reflected in a clear fluid instead of more complex liquid medium. As a result, the detergent liquid medium was replaced with a dodecylbenzenesulfonate (SDBS) surfactant solution, in which the interaction between a MF microparticle (diameter=9.2 μm) and cotton

film was studied, and the spring constant of the cantilever was 0.13 Nm^{-1}. SDBS surfactant itself is one of the main components in the detergent solutions employed above. The concentrations of SDBS solutions used in the experiments were 0.2 mM, 1.4 mM and 14.4 mM, in which the amount of SDBS was equivalent to those in 0.15wt.%, 1.0wt.% and 10wt.% detergent solution, respectively. The data are plotted in Figure 7.24, where the repulsion is reduced with increasing SDBS concentration. The figure displays the similar trend to the interaction in the detergent solutions at increasing concentration, but the force curves are much smoother compared with Figure 7.20 due to a clearer liquid media. The less thermal fluctuation in the baseline of force curve was also observed, which is reflected by the force resolution of 0.02 nN in SDBS solution (Figure 7.24) than 0.4 nN in detergent solutions (Figure 7.20). The results in Figure 7.24 agree with the finding from Figure 7.20 that there is no significant adhesion between MF microparticle and cotton film in the detergent solutions.

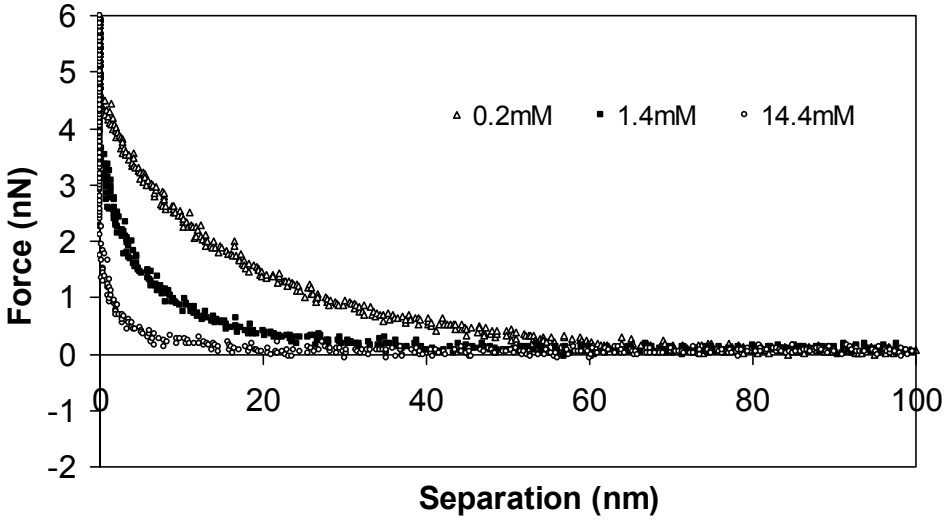

Figure 7.24 The interaction between a MF microparticle (diameter=9.2 μm) and a cotton film immersed in various concentrations of SDBS surfactant solutions at pH 7.

Figure 7.25 shows the interaction between a MF microparticle (diameter=9.2 μm) and a cotton film in 0.2 mM SDBS surfactant solution at varying pH. The spring constant of the cantilever used was 0.09 Nm^{-1}. The amount of SDBS in 0.2 mM surfactant solution is equivalent to that in 0.15wt.% detergent solution. The results in Figure 7.25 show that the interaction becomes more repulsive with increasing pH and the force resolution of the curves is 0.2 nN. There is an explicit indication that the interaction at pH 6 is more repulsive than that at pH 3. Unlike the results in Figure 7.23, the repulsive trend was not very clear in detergent solution between pH 3 and pH 8, which may be due to the interference of other components in the detergent solution.

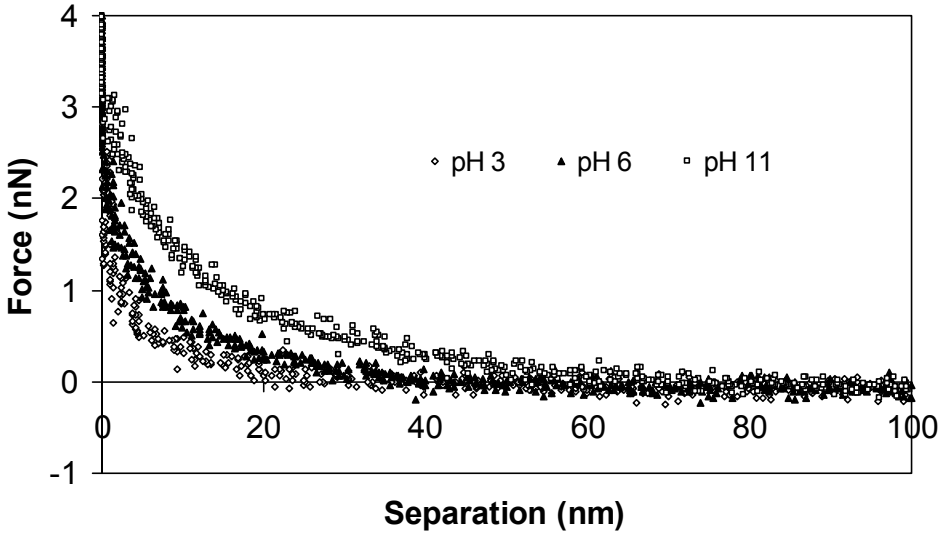

Figure 7.25 The interaction between a MF microparticle (diameter=9.2 μm) and a cotton film immersed in 0.2 mM SDBS surfactant solution at varying pH.

In order to interpret Figure 7.25, zeta potentials of MF microcapsules with a mean diameter of 37.2 μm and cotton powder with a particle size of 20 μm were measured separately in 0.2 mM SDBS surfactant solution at varying pH. The MF microcapsules were used to replace MF microparticles for zeta potential measurements due to the insufficient amount of MF

microparticles being available. The mean value of 10 measurements at each pH is presented in Figure 7.26. Overall, the zeta potentials of MF microcapsules and cotton powder became more negative as pH increased. The AFM measurement results in Figure 7.25 also indicate that repulsion between the MF microparticle and cotton film increases with increasing pH. Qualitatively, the AFM results are consistent with zeta potential measurements. In addition, it was revealed that the zeta potential of MF microcapsules and cotton powder were both negative in the range of pH 7-8. This suggests electrostatic repulsion could be one of mechanisms for the interaction of MF microparticle and cotton films in the detergent/surfactant solutions.

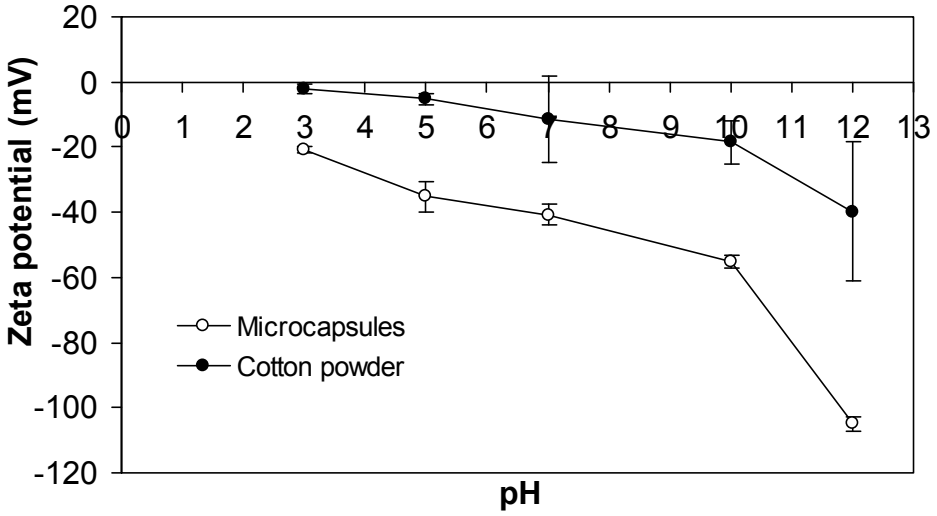

Figure 7.26 Zeta potentials of MF microcapsules (mean diameter=37.2 μm) and cotton powder (particle size=20 μm) in 0.2 mM SDBS surfactant solution at varying pH.

Woven cotton fabric bundles were immersed in 1.6wt.% MF microcapsule suspension in water for 1 hr, and then quickly removed out and shaken vigorously for 1 minute, before being observed under an optical microscope, as shown in Figure 7.27. It was shown that there were microcapsules attached to the fabric bundle; even though the AFM results revealed that there

is very little adhesion between MF microparticle and cotton films in liquids. This implies that the physical structure of woven cotton bundles could in fact entrap the microcapsules to promote the retention of microcapsules on cotton fibres. Therefore, the main mechanism of microcapsule attachment to fibre surface is probably through physical entrapment rather than adhesion.

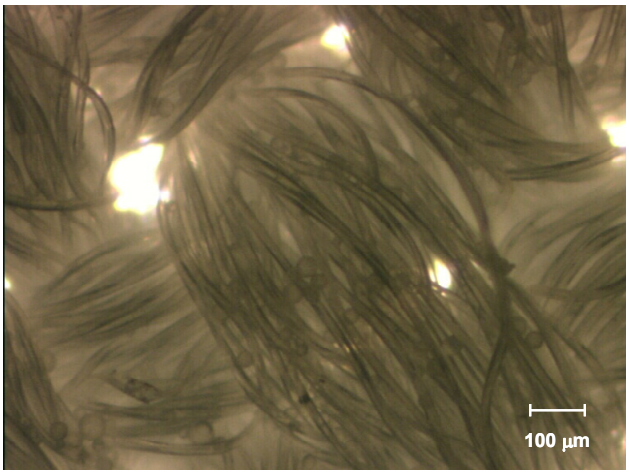

Figure 7.27 A woven cotton fabric bundle after being immersed in 1.6wt.% MF microcapsule suspension in water (mean diameter=37.2 μm).

7.5 Conclusions

It was demonstrated in this work that the novel method proposed by Gunnars *et al.* (2002) can be successfully adapted to generate cotton films using cotton powder/fibres as raw material instead of wood pulps. As a result, adhesion measurement could be performed on the cotton films to overcome the inconsistent topography of fibre bundles. The cotton films were characterised using techniques including AFM, ellipsometry, contact angle measurement and XPS and it was concluded that such films were thin and possessed a relatively smooth surface. In addition, the cotton films were of hydrophilic nature and free of all the dissolving solvents.

The obtained adhesive forces between MF microcapsules/microparticles and cotton films under ambient condition (air RH above 40%) were suggested to be mainly capillary forces, which play an important role between hydrophilic surfaces at high air RH. It was demonstrated that the measured adhesive forces agree well with the capillary force theory, taking the roughness, contact angle and meniscus radius into consideration. The adhesive force between MF microparticle and cotton film is significantly greater than that between MF microcapsule and cotton film. This may be partly due to the presence of perfume oil on the surface of microcapsule; such agent is of hydrophobic nature and could in turn suppress the formation of capillary force. The other reason could be attributed to the composition of microparticle surface that the carbonyl group (C=O) of copolymer acrylamide in the MF microcapsule wall is delta negative and could form a repulsive effect with O bond in the cotton in comparison to MF microparticle which is composed of MF only.

It was found that the piezo approaching speed had no significant influence on the interaction between MF microparticle and cotton films under ambient condition or in the liquid medias. It was revealed that there was little adhesion between MF microparticle and cotton films in the detergent solution with a given force resolution of 0.4 nN. It was also found that there was mainly repulsion between MF microparticle and cotton films in the detergent solution, and the repulsion tended to reduce with the increase in the concentration of detergent solution from 0.0001wt.% to 10wt.%. It was suggested that this is due to the steric interaction which arises when two polymer-covered surfaces are approached together as well as electrostatic repulsion. It was demonstrated that repulsion between MF microparticle and cotton films reduced with the decrease in pH of detergent solution. When liquid media was changed from detergent

solution to the solution of SDBS surfactant which is one of main components of detergent, similar repulsion trends were observed, but the force curves were with less noise without the interference of other complex components in the detergent. It was demonstrated in the zeta potential measurement that zeta potentials of cotton powder and MF microcapsules were both negative and reduced with decreasing pH of SDBS solution, which supported the AFM finding that the repulsion reduced with decreasing pH in both detergent and SDBS solutions. The obtained results in SDBS solution further confirm the finding that no significant adhesion is between MF microparticle and cotton films in the detergent solution. It was suggested that the main reason of microcapsule retention on the woven cotton fabric is due to entrapment.

It is recommended that the attachment of a single MF microcapsule to a tipless cantilever can be improved by equipping the AFM equipment with an inverted microscope (Lulevich *et al.*, 2003) to monitor the bottom view of the microcapsule to prevent rupture of such microcapsule during attachment. Future work can also involve modifying the surface of MF microparticles by coating an appropriate layer of chemicals to render their surfaces bearing opposite charges to their current ones. Moreover, a certain “arms” can be grafted to the microcapsule surface to promote their entrapment into woven fabrics if such “arms” could adhere to fabrics, in order to enhance the adhesion between MF microcapsules and cotton fibres to ensure an efficient deposit of microcapsules containing perfume oils onto target sites in a typical water environment in washing machine.

8. OVERALL CONCLUSIONS AND FUTURE WORK

8.1 Overall Conclusions

Melamine Formaldehyde (MF) microcapsules that may be incorporated into commercial detergent products for the delivery of desirable core contents, such as perfume oil, were investigated in terms of their mechanical properties including rupture strength and adhesion. With the use of ESEM, MF microcapsules produced by an in-situ polymerisation technique were found to be spherical and have a relatively smooth surface. Basic structure and mechanical properties of MF microcapsules, such as wall thickness and elastic properties, were also investigated. It was demonstrated by TEM results that the MF microcapsules of interest had a mean wall thickness 175±11 nm. MF microcapsules in a sample were first compressed to a mean deformation of 7±1%, no visco-elastic behaviour was observed. When they were further compressed to a mean deformation of 12±2%, MF microcapsules were found to exhibit weakly visco-elastic behaviours. The elastic limit was found to be 15±1% for a MF microcapsule sample which had a mean rupture deformation of 24±3%. The applicability and limitation of mechanical strength parameters that had not been addressed properly were discussed in detail. It is concluded that rupture force or nominal rupture stress can be applied to compare the mechanical strength of microcapsules which are similar in size and have comparable deformation at rupture, but the latter is more relevant to end-use applications. Whilst microcapsules of different sizes in a sample or between samples of different mean sizes are compared, a mechanical property parameter of nominal wall tension, which is independent of size, can be applied.

It was found that the rupture force of MF microcapsules within a sample increases with an increase in diameter. The deformation at rupture, which indicates the brittleness of microcapsules, does not seem to change significantly. The nominal rupture stress of microcapsules decreases with an increase in diameter. Such trends were also applicable to microcapsules prepared using the same formulations but with different mean sizes between samples. The factors that have influence on the mechanical strength of microcapsules are identified. The reduction in mean size increased the mean nominal rupture stress of microcapsules. The increase in core/capsule ratio in weight percentage reduced the nominal wall tension of microcapsules.

The mechanical strength of microcapsules composed of various formulations was also studied. It was found that the use of additional coating such as silicate coating can make microcapsules more brittle. The mechanical strength of microcapsules can also be controlled with the use of additives. It was demonstrated that microcapsules with silicate coating had significantly higher nominal wall tension than those without coating. Microcapsules in slurry, which was added with β-keto Butyramide (BKB) in order to reduce the amount of free formaldehyde, were found to have lower nominal wall tension. It was suggested that the lower concentration of free formaldehyde favours the reverse reaction and caused the reduction of crosslinking of MF polymer, resulting in weaker microcapsule walls. The addition of a combination of thickeners of xanthan gum, $MgCl_2$ and biocide of MBS was found to have the same effect of lowering nominal wall tension. The results were subjected to further validation, since the majority of microcapsules were aggregated and the single microcapsules selected for test might not fully represent the whole sample. Microcapsules with core contents of 10% elvax polymer and 90%

perfume oil were found to have no significant difference in their nominal wall tension in comparison to microcapsules containing perfume oil only. In addition, the results also suggested that the nominal wall tension of microcapsules did not differ significantly when the pH of their suspending liquid ranged from 2 to 11 for a duration of 25 hours. The findings are very useful to understand the mechanical strength of microcapsules which are required to possess the desired mechanical strength in the application of detergent products.

The mechanical strength of microcapsules prepared and processed under various conditions has also been studied. The results reveal that, at a constant temperature of 65 ºC, the nominal wall tension of microcapsules had no significant difference when they were made with a polymerisation time of 2 or 4 hours, but was significantly increased when a polymerisation time of 6 hours was used. Furthermore, microcapsules made using 8 hours at 65 ºC and a further 16 hours at 85 ºC possessed significantly higher nominal wall tension than those prepared using 2 hours at 65 ºC. It was suggested that this is because the prolonged polymerisation time alone or combined with the elevated temperature increased the degree of crosslinking of MF wall and in turn strengthened the microcapsules. It is demonstrated that microcapsules produced from pilot plant and full scales had significantly larger size and lower nominal wall tension than those produced in lab scale. The results have highlighted the importance of scaling up process properly as well as the necessity of testing microcapsule strength after their production. Microcapsules underwent a heat treatment by being heated to 120ºC, which is above the glass transition temperature T_g of MF shell material (97 ºC), and then cooled down to room temperature. It was revealed that the heat treated microcapsules had significantly lower mean nominal rupture stress than their original form. It was suggested that

the degree of crosslinking of MF wall was reduced at the rubbery state above T_g and could not resume to the original form even the temperature was reduced to room temperature.

The mechanical strength of microcapsules treated with different drying methods was also studied. Oven dried microcapsules tended to aggregate whilst microcapsules treated by other drying methods exhibited a powder form. It was found that oven drying, fluidized bed drying and freeze drying did not significantly change the nominal wall tension of microcapsules. In contrast, microcapsules after spray drying possessed significantly higher nominal wall tension. This was probably attributed to the breakage of weak microcapsules (in general large) which resulted from the microcapsules hitting the drying chamber during the process of feeding from the top of spray drier. This interpretation is also supported by the size measurement results which show that the volume weighted mean diameter of spray dried microcapsules was approximately 3 μm smaller than those before drying.

The mean Young's modulus of MF microcapsules, E_c, which was predicted from the Hertz model and represents the modulus of single whole microcapsule, was found to be 32±4 MPa. In addition, the Young's modulus of MF microcapsule wall material, E_w, was found to be 8±1 GPa by applying finite element modelling with a linear elastic model; this is in the same order of magnitude as that suggested in the literature using an analytical approach (Keller & Sottos, 2006). Such modelling approach can therefore be applied to other microcapsules in order to determine the Young's modulus of microcapsule wall material. A correlation describing the relationship between E_c and E_w has been developed based on the modelled results, wall thickness and diameter of microcapsules.

The contact stress of a single MF microcapsule during compression, which was determined based on the compressive force and the corresponding contact diameters measured in an environmental scanning electron microscope (Stenson *et al.*, 2008), was demonstrated to be in good agreement with the assumption of Johnson's plastic model that the contact stress in plastic deformation remains constant. Hertz model combined with Johnson's plastic models were therefore further applied to determine the rupture stress of single MF microcapsules which take their rupture deformation into consideration. It was demonstrated that the use of rupture stress is so effective that it can compare the mechanical strength of microcapsules with and without starch coating, whilst it was difficult to identify their difference based on the nominal rupture strength data since they have relatively large standard errors. Furthermore, it was also revealed that the finding from the determination of rupture stress by modelling on the microcapsules with and without silicate coating is in good agreement with the conclusion drawn previously based on the use of nominal rupture stress. The modelled rupture stress has proven to be of good use especially to compare the mechanical strength of microcapsules with significantly different rupture deformations. This is very beneficial to different industrial sectors which have used or intend to use microcapsules in a wide range of products including detergents.

For the studies of adhesion between MF microcapsule and cotton fibres under ambient condition and in the liquid, cotton films were successfully generated by dissolving cotton powder/fibres to overcome the inconsistent topography of fibre bundles, and so to permit the measurement of adhesion. The characterisation results using ellipsometry, AFM, contact angle

measurement and XPS show that the cotton films had a mean thickness of 13.1±2.5 nm, a mean roughness of 5.1±0.2 nm, a hydrophilic nature and free of dissolving solvents on the surface respectively. It was proved that the adhesive forces between MF microcapsules/MF microparticles and cotton films under ambient condition (air RH above 40%) were mainly capillary forces. However, the adhesive force between MF microparticle and cotton film was found to be much higher than that between MF microcapsule and cotton film. It was suggested that this was due to the different compositions of microparticle surface. In addition, there may be presence of perfume oil with hydrophobic nature on the surface of microcapsule that minimized the effect of capillary force.

It was found that there was little adhesion between MF microparticles and cotton films in detergent solution with a force resolution of 0.4 nN. The obtained force curves showed that there was mainly repulsion between the MF microparticle and cotton films in the detergent solution, and the repulsion tended to reduce with the increase in the concentration of detergent solution from 0.0001wt.% to 10wt.%. The repulsion is suggested to be contributed from two mechanisms; first being steric interaction which normally arises when two surfaces covered with polymer molecules are approached together. Secondly, it could be attributed to the electrostatic repulsion since the zeta potentials of cotton powder and MF microcapsules in the surfactant solution were measured to be both negative. Zeta potentials are the potentials of a shear plane at some distance from the particle in the bulk solution and are the resultants of the particles and liquid medium as a joint system. Reduction in repulsion was also observed from the decrease in pH of detergent solution, which is consistent with the measured result that zeta potentials of cotton powder or MF microcapsules decreased with the decrease in pH of

surfactant solution. Similar trends were observed for the interaction between MF microparticle and cotton film in the solution of SDBS surfactant that is one of main components of detergent. The obtained results further concluded that there is little adhesion between the MF microparticle and cotton film in the detergent solution; the main reason for the retention of some MF microcapsules in the woven fabrics was due to physical entrapment. The findings of this work have provided an insight into the interaction between MF microparticles and cotton films in the detergent solution, which is of great use for the further research to enhance adhesion of microcapsules on fabric surface.

8.2 Future Work

It was suggested that MF microcapsules in the slurry containing BKB had significantly lower nominal wall tension, which was due to the triggering of reverse reaction to weaken the MF wall. This may be validated by conducting further TEM measurements to examine the wall of microcapsules. It was also found that microcapsules in a suspending liquid with pH from 2 to 11 for a duration of 25 hours had no significant change in their nominal wall tension. It is of great interest to study whether the mechanical strength of MF microcapsules can remain the same at such range of pH for a longer period of time in order to include them in the liquid detergent products effectively.

The assumption of Johnson's plastic model that the contact stress in the plastic deformation remains constant has been validated using the experimentally measured compressive force and contact diameters of a single MF microcapsule during compression; this approach requires further validation using more experimental data such as compressive force and corresponding

contact diameters. It is always important to validate the models directly using the experimental data including the data of force-displacement, contact diameters and lateral extension during compression. The latter two are very scarce in the literatures; it is recommended that nanomanipulation (Stenson *et al.*, 2008) can be employed for microcapsules with diameters around 10 μm. A sensitive microscope visualisation instrument (Liu *et al.*, 2002) can be applied to microcapsules with diameters ranging from 60 μm to 120 μm. In addition, modelling methods such as finite element modelling (Nguyen *et al.*, 2009) coupled with other plastic models can be further applied to model contact diameters of microcapsules and then validated using the experimental data.

The rate of successful attachment of MF microcapsules to the tipless cantilever was found to be less than 50%. It is recommended that the attachment process can be improved by equipping the AFM equipment with an inverted microscope (Lulevich *et al.*, 2003) to monitor the bottom view of single microcapsule to be attached to prevent rupture of such microcapsule during attachment. In this study, MF microcapsules were replaced with MF microparticles as the particle of interest due to the difficult attachment of soft microcapsules using the available equipment. As a result, the interaction between MF microparticles and cotton films in the detergent/surfactant solutions has been realized in this work. Future work should focus on improving the adhesion between MF microcapsules/microparticles and fabric surfaces. For the MF microparticles used in this work, which was obtained from Microparticles Gmbh Germany, their surface carried positive charges (Dong *et al.*, 2005). The adhesion in the detergent/surfactant solution could be improved by modifying the surface of MF microparticle to an opposite charge such as negative charge. Zeta potential measurement could be performed

to study the zeta potential of modified MF microparticles in the detergent solution. Furthermore, AFM force measurement can then be conducted using the modified MF microparticles. Moreover, the areas to enhance the physical entrapment of microcapsules can also be explored by grafting certain "arms" to their surface. If such "arms" could adhere to fabrics, the retention of microcapsules in the woven fabrics may in turn be promoted in a typical water environment in the washing machine.

Appendix A Calibration of Cantilever

After a single microcapsule was attached to the rectangular shape tipless cantilever (NSC12), the spring constant of this cantilever was calibrated using a reference cantilever method (Tortonese and Kirk, 1997), which was proven to be straightforward on Veeco AFM systems (Ohler, 2007). The cantilever under test was measured against a hard surface (Si wafer) and the end of a reference cantilever (CLFC-NOBO, Veeco, France) which had been accurately calibrated by manufacturer. Figure A1 shows the top view of contact area between the reference cantilever and the cantilever under test for its spring constant calibration. The slopes of the contact region of two separate extending force curves obtained shown as curve C in Figure 2.5, were sometimes called deflection sensitivity. The equation to calculate the spring constant of the cantilever under test k_{test} is shown in Equation A1:

$$k_{test} = k_{ref} \frac{m_{tot} - m_{test}}{m_{test} \cos\theta_t} \qquad \text{(A1)}$$

where, k_{ref} refers to the spring constant of the reference cantilever. m_{tot} is the slope of the "force versus piezo-sample distance" curve when the cantilever under test is in contact with a hard surface and m_{test} is the slope of the "force versus piezo-sample distance" curve when cantilever under test is in contact with the free end of the reference cantilever. θ_t is the angle between the cantilever under test and the reference cantilever, which is normally 11º. Using the reference cantilever calibration method, the calibrated spring constants of NSC12 silicon cantilevers attached with a MF microcapsule or a MF microparticle were averaged from three calibration results and are presented in Chapter 7 in detail.

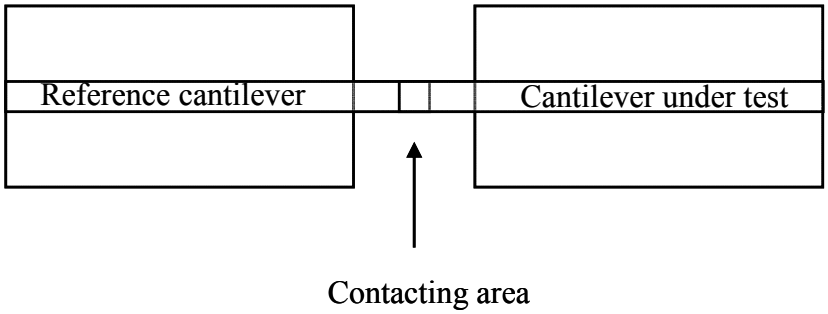

Figure A1 Illustration of contact area (top view) between the reference cantilever and the cantilever under test during spring constant calibration using the reference cantilever method.

The reference cantilever method was not suitable for calibration of soft cantilevers. When the deflection sensitivity is measured against a hard surface, force curve cannot be acquired if the adhesive force is beyond the force value the soft cantilever can measure. As a result, the deflection sensitivity cannot be obtained. Hence, in this case, a thermal noise method (Hutter, 1993) can be used to calibrate the spring constant of a soft cantilever. Thermal noise method is probably the most popular and widely available method to calibrate cantilever (Ohler, 2007). In this method, the thermal motion of the cantilever's fundamental oscillation mode was related to its thermal energy via Equation A2:

$$k_t = \frac{k_B T}{P} \qquad \text{(A2)}$$

where k_t (Nm^{-1}) is the spring constant of the cantilever to be calibrated, k_B (NmK^{-1}) is Boltzmann's constant with a value of 1.38×10^{-23}, and T (K) is the absolute temperature. P (m^2) refers to area of the power spectrum of the thermal fluctuations of the cantilever and can be obtained from AFM software. By using the thermal noise method, the calibrated spring constants of the MLCT cantilevers attached with single MF microparticles were also obtained by averaging three calibration results and are presented in Chapter 7.

Appendix B Data Analysis Using Statistical Tests

Confidence Interval on the Mean of a Normal Distribution with Unknown Variance

Statistical tests were applied to analyse the micromanipulation data so as to compare the mechanical strength of microcapsules between samples. An independent population with a normal distribution has an unknown mean μ and unknown variance σ^2; σ is standard deviation of the population. A random sample of size n is taken from this population. This random sample refers to the microcapsules in a given sample which were tested using micromanipulation. The mean $\overline{X}$ and variance S^2 of this random sample are therefore known; S is standard deviation of the random sample. A 100(1-α)% confidence interval on μ is given in Equation B1 (Montgomery *et al.*, 2001):

$$\overline{X} - t_{\alpha/2,n-1} S/\sqrt{n} \le \mu \le \overline{X} + t_{\alpha/2,n-1} S/\sqrt{n} \qquad \text{(B1)}$$

where α is defined as significance level, $t_{\alpha/2,n-1}$ is the t statistic value with n-1 degrees of freedom, given in the table of Montgomery *et al.* (2001) titled "Percentage points of the t distribution". If α is equal to 0.05, the confidence interval is 95%. $\overline{X} - t_{\alpha/2,n-1} S/\sqrt{n}$ and $\overline{X} + t_{\alpha/2,n-1} S/\sqrt{n}$ are the lower and upper confidence limits. The sample size, n, of micromanipulation data is generally between 30 and 60, therefore, the value of $t_{\alpha/2,n-1}$ in the table is approximately equal to 2. Hence, Equation B1 can be represented by Equation B2:

$$\overline{X} - 2S/\sqrt{n} \le \mu \le \overline{X} + 2S/\sqrt{n} \qquad \text{(B2)}$$

Consequently, by applying twice standard errors ($S/\sqrt{n}$ denotes one standard error), the results suggest the population mean falls between $\overline{X} - 2S/\sqrt{n}$ and $\overline{X} + 2S/\sqrt{n}$ with 95% confidence. Taking a mechanical strength parameter of nominal rupture stress as an example, the mean of two nominal rupture stress population is represented by μ_A and μ_B, which is for microcapsule sample A & B and their standard errors are shown in Equation B3 & B4 respectively:

$$\overline{X}_A - 2S_A/\sqrt{n_A} \le \mu_A \le \overline{X}_A + 2S_A/\sqrt{n_A} \quad \text{(B3)}$$

$$\overline{X}_B - 2S_B/\sqrt{n_B} \le \mu_B \le \overline{X}_B + 2S_B/\sqrt{n_B} \quad \text{(B4)}$$

For the analysis of micromanipulation data, if the lower confidence limit of sample B $\overline{X}_B - 2S_B/\sqrt{n_B}$ is clearly greater than the upper confidence limit of sample A $\overline{X}_A + 2S_A/\sqrt{n_A}$, this suggests $\mu_B > \mu_A$ with 95% confidence. In other words, μ_B is significantly greater than μ_A. However, if there is any overlapping between the ranges of upper and lower confidence limits of sample A and B, a *t*-test is used and described in detail below.

_t_ Test to Test the Means of Two Normal Distribution with Unknown Variance

A two-sample *t* test is applied to test the hypotheses on the means of two normal distributions with unknown variance (Hines & Montgomery, 1990; Montgomery *et al.*, 2001). X_1 and X_2 are two independent normal populations with unknown means μ_1 and μ_2. It is supposed that X_{11}, X_{12}, …, X_{1n1} is a random sample of n_1 observations from X_1; X_{21}, X_{22}, …, X_{2n2} is a random sample of n_2 observations from X_2. $\overline{X}_1$ and $\overline{X}_2$ are the mean of each sample; S_1^2 and S_2^2 are

the variance of each sample. If variance of each population is unknown and unequal, that is to say, $\sigma_1^2 \neq \sigma_2^2$.

At the beginning of *t* test, null hypothesis H_0 is given below in Equation B5 as:

$$H_0 : \mu_1 = \mu_2 \tag{B5}$$

The null hypothesis, H_0, is then tested using the calculated test statistic, t_0^*, which is defined in Equation B6 as follows:

$$t_0^* = \frac{\overline{X}_1 - \overline{X}_2}{\sqrt{\frac{S_1^2}{n_1} + \frac{S_2^2}{n_2}}} \tag{B6}$$

H_0 is true if the calculated test statistic, t_0^*, is distributed as $t_{\alpha/2,\nu}$ as illustrated in the table of Montgomery *et al.* (2001) titled "Percentage points of the *t* distribution". When α is equal to 0.05, the confidence interval is 95%. Degree of freedom, ν, is given in Equation B7:

$$\nu = \frac{\left(\frac{S_1^2}{n_1} + \frac{S_2^2}{n_2}\right)^2}{\frac{\left(S_1^2/n_1\right)^2}{n_1+1} + \frac{\left(S_2^2/n_2\right)^2}{n_2+1}} - 2 \tag{B7}$$

If $t_0^* > t_{\alpha/2,\nu}$ or $t_0^* < -t_{\alpha/2,\nu}$, the null hypothesis H_0 is rejected. As such, the alternative hypothesis H_1 is true ($H_1 : \mu_1 \neq \mu_2$). The detailed rejection criterion for null hypothesis H_0 is shown in Table A.1. $H_1 : \mu_1 > \mu_2$ is true, if $t_0^* > t_{\alpha,\nu}$. Alternatively, $H_1 : \mu_1 < \mu_2$ is true, if

$t_0^* < -t_{\alpha,\nu}$. If H_0 cannot be rejected, that suggests no significant difference is between $\overline{X}_1$ and $\overline{X}_2$ with 95% confidence interval (α=0.05).

Table B.1 List of rejection criterion on the null hypothesis.

Alternative Hypothesis	Rejection Criterion
$H_1 : \mu_1 \neq \mu_2$	$t_0^* > t_{\alpha/2,\nu}$ or $t_0^* < -t_{\alpha/2,\nu}$
$H_1 : \mu_1 > \mu_2$	$t_0^* > t_{\alpha,\nu}$
$H_1 : \mu_1 < \mu_2$	$t_0^* < -t_{\alpha,\nu}$

Since $\overline{X}_1$, $\overline{X}_2$, S_1^2, S_2^2, n_1 and n_2 are known through the micromanipulation results, *t*-test can therefore be performed on the mechanical property parameters of microcapsules, e.g. nominal rupture stress, to compare the mechanical strength of microcapsules between samples.

References

Abu-Lail, N. I. & Camesano, T. A. 2003, "Role of ionic strength on the relationship of biopolymer conformation, DLVO contributions, and steric interactions to bioadhesion of Pseudomonas putida KT2442", *Biomacromolecules*, vol. 4, no. 4, pp. 1000-1012.

Adams, M. J., Lawrence, C. J., Urso, M. E. D., & Rance, J. 2004, "Modelling collisions of soft agglomerates at the continuum length scale", *Powder Technology*, vol. 140, no. 3, pp. 268-279.

Aime, J. P., Elkaakour, Z., Odin, C., Bouhacina, T., Michel, D., Curely, J., & Dautant, A. 1994, "Comments on the Use of the Force Mode in Atomic-Force Microscopy for Polymer-Films", *Journal of Applied Physics*, vol. 76, no. 2, pp. 754-762.

Arshady, R. 1999, "Manufacturing Methodology of Microcapsules," in *Microspheres Microcapsules & Liposomes Volume 1: Preparation & Chemical Applications*, R. Arshady, ed., Citus Books, London, UK.

Ashby, M. F. & Jones, D. R. H. 2005, *Engineering Materials 1 - An Introduction to Properties, Applications and Design*, 3rd edn, Elsevier Butterworth-Heinemann, Oxford.

Attard, G. & Barnes, C. 1998, *Surfaces* Oxford University Press Inc., New York.

Aulin, C., Shchukarev, A., Lindqvist, J., Malmstrom, E., Wagberg, L., & Lindstrom, T. 2008, "Wetting kinetics of oil mixtures on fluorinated model cellulose surfaces", *Journal of Colloid and Interface Science*, vol. 317, no. 2, pp. 556-567.

Bauer, D. R. 1986, "Melamine Formaldehyde Cross-Linker - Characterization, Network Formation and Cross-Link Degradation", *Progress in Organic Coatings*, vol. 14, no. 3, pp. 193-218.

Bhargava, G., Gouzman, I., Chun, C. M., Ramanarayanan, T. A., & Bernasek, S. L. 2007, "Characterization of the "native" surface thin film on pure polycrystalline iron: A high resolution XPS and TEM study", *Applied Surface Science*, vol. 253, no. 9, pp. 4322-4329.

Biggs, S. 1996, "Non-equilibrium interaction forces between adsorbed polymer layers", *Journal of the Chemical Society-Faraday Transactions*, vol. 92, no. 15, pp. 2783-2789.

Binnig, G., Rohrer, H., Gerber, C., & Weibel, E. 1982, "Tunneling Through A Controllable Vacuum Gap", *Applied Physics Letters*, vol. 40, no. 2, pp. 178-180.

Binnig, G., Quate, C. F., & Gerber, C. 1986, "Atomic Force Microscope", *Physical Review Letters*, vol. 56, no. 9, pp. 930-933.

Blythe, D., Churchill, D., Glanz, K., & Stutz, J. 1999, "Microcapsules for Carbonless Copy Paper," in *Microspheres Microcapsules & Liposomes*, A. Reza, ed., Citus Books, London, U.K..

Bowen, J., Manickam, M., Evans, S. D., Critchley, K., Kendall, K., & Preece, J. A. 2008, "The pH-dependent adhesion of nanoparticles to self-assembled monolayers on gold", *Thin Solid Films*, vol. 516, no. 10, pp. 2987-2999.

Bowen, W. R., Hilal, N., Lovitt, R. W., & Wright, C. J. 1999, "Characterisation of membrane surfaces: direct measurement of biological adhesion using an atomic force microscope", *Journal of Membrane Science*, vol. 154, no. 2, pp. 205-212.

Bowen, W. R., Lovitt, R. W., & Wright, C. J. 2001a, "Atomic force microscopy study of the adhesion of Saccharomyces cerevisiae", *Journal of Colloid and Interface Science*, vol. 237, no. 1, pp. 54-61.

Bowen, W. R., Lovitt, R. W., & Wright, C. J. 2001b, "Atomic force microscope studies of stainless steel: Surface morphology and colloidal particle adhesion", *Journal of Materials Science*, vol. 36, no. 3, pp. 623-629.

Briggs, D. & Seah, M. P. 1996, *Practical Surface Analysis Volume 1: Auger and X-ray Photoelectron Spectroscopy*, 2nd edn, John Wiley and Sons (Chichester).

Brown, H. G. & Hoh, J. H. 1997, "Entropic exclusion by neurofilament sidearms: A mechanism for maintaining interfilament spacing", *Biochemistry*, vol. 36, no. 49, pp. 15035-15040.

Brown, R. W. & Bowman, R. P. 1985, *Capsule manufacture*, US 4552811 (patent).

Brydson, J. A. 1999, *Plastics Materials*, 7th edn, Butterworth-Heinemann.

Burdis, J., Procter & Gamble Technical Centre, Newcastle, UK Glass transition temperature of melamine formaldehyde. 16-9-2009.
Ref Type: Personal Communication

Burnett, D. S. 1987, *Finite Element Analysis* Addison-Wesley Publishing Company, US.

Butt, H. J., Siedle, P., Seifert, K., Fendler, K., Seeger, T., Bamberg, E., Weisenhorn, A. L., Goldie, K., & Engel, A. 1993, "Scan Speed Limit in Atomic Force Microscopy", *Journal of Microscopy-Oxford*, vol. 169, pp. 75-84.

Butt, H. J., Jaschke, M., & Ducker, W. 1995, "Measuring Surface Forces in Aqueous-Electrolyte Solution with the Atomic-Force Microscope", *Bioelectrochemistry and Bioenergetics*, vol. 38, no. 1, pp. 191-201.

Butt, H. J., Cappella, B., & Kappl, M. 2005, "Force measurements with the atomic force microscope: Technique, interpretation and applications", *Surface Science Reports*, vol. 59, no. 1-6, pp. 1-152.

Cahn, A. 1997, "Liquid Detergents: An Overview," in *Liquid Detergents*, K. Lai, ed., Marcel Dekker, Inc. New York.

Camesano, T. A. & Logan, B. E. 2000, "Probing bacterial electrosteric interactions using atomic force microscopy", *Environmental Science & Technology*, vol. 34, no. 16, pp. 3354-3362.

Cappella, B. & Dietler, G. 1999, "Force-distance curves by atomic force microscopy", *Surface Science Reports*, vol. 34, no. 1-3, p. 1-104.

Chamberlain, P. & Symes, K. C. 1993, "Polymeric Formulations of Pest Control Agents," in *Encapsulation and Controlled Release*, D. R. Karsa & R. A. Stephenson, eds., The Royal Society of Chemistry, Cambridge.

Charcosset, C., Limayem, I., & Fessi, H. 2004, "The membrane emulsification process - a review", *Journal of Chemical Technology and Biotechnology*, vol. 79, no. 3, pp. 209-218.

Chen, X. M., Burger, C., Wan, F., Zhang, J., Rong, L. X., Hsiao, B. S., Chu, B., Cai, J., & Zhang, L. 2007, "Structure study of cellulose fibers wet-spun from environmentally friendly NaOH/urea aqueous solutions", *Biomacromolecules*, vol. 8, no. 6, pp. 1918-1926.

Cheng, L. Y. 1987, "Deformation Analyses in Cell and Developmental Biology .1. Formal Methodology", *Journal of Biomechanical Engineering-Transactions of the Asme*, vol. 109, no. 1, pp. 10-17.

Cheong, Y. S., Adams, M. J., Hounslow, M. J., & Salman, A. D. 2009, "Microscopic interpretation of granule strength in liquid media", *Powder Technology*, vol. 189, no. 2, pp. 365-375.

Chung, J. T., Vlugt-Wensink, K. D. F., Hennink, W. E., & Zhang, Z. 2005, "Effect of polymerization conditions on the network properties of dex-HEMA microspheres and macro-hydrogels", *International Journal of Pharmaceutics*, vol. 288, no. 1, pp. 51-61.

Cleveland, J. P., Manne, S., Bocek, D., & Hansma, P. K. 1993, "A Nondestructive Method for Determining the Spring Constant of Cantilevers for Scanning Force Microscopy", *Review of Scientific Instruments*, vol. 64, no. 2, pp. 403-405.

Clifford, C. A. & Seah, M. P. 2005, "The determination of atomic force microscope cantilever spring constants via dimensional methods for nanomechanical analysis", *Nanotechnology*, vol. 16, no. 9, pp. 1666-1680.

Cohen, S. R. 1992, "An Evaluation of the Use of the Atomic Force Microscope for Studies in Nanomechanics", *Ultramicroscopy*, vol. 42, pp. 66-72.

Dammer, U., Popescu, O., Wagner, P., Anselmetti, D., Guentherodt, H. J., & Misevic, G. N. 1995, "Binding Strength Between Cell Adhesion Proteoglycans Measured by Atomic Force Microscopy", *Science (Washington D C)*, vol. 267, no. 5201, pp. 1173-1175.

Dihora, J., Procter & Gamble, US, Density of MF microcapsule wall and core. 2006. Ref Type: Personal Communication

Ding, P., Norton, I. T., Zhang, Z., & Pacek, A. W. 2008, "Mechanical properties of gelatin-rich micro-particles", *Journal of Food Engineering*, vol. 86, no. 3, pp. 307-314.

Dong, W. F., Ferri, J. K., Adalsteinsson, T., Schonhoff, M., Sukhorukov, G. B., & Mohwald, H. 2005, "Influence of shell structure on stability, integrity, and mesh size of polyelectrolyte capsules: Mechanism and strategy for improved preparation", *Chemistry of Materials*, vol. 17, no. 10, pp. 2603-2611.

Dubreuil, F., Elsner, N., & Fery, A. 2003, "Elastic properties of polyelectrolyte capsules studied by atomic-force microscopy and RICM", *European Physical Journal e*, vol. 12, no. 2, pp. 215-221.

Dubreuil, F., Shchukin, D. G., Sukhorukov, G. B., & Fery, A. 2004, "Polyelectrolyte capsules modified with YF3 nanoparticles: An AFM study", *Macromolecular Rapid Communications*, vol. 25, no. 11, pp. 1078-1081.

Ducker, W. A., Senden, T. J., & Pashley, R. M. 1991, "Direct Measurement of Colloidal Forces Using An Atomic Force Microscope", *Nature*, vol. 353, no. 6341, pp. 239-241.

Ducker, W. A., Senden, T. J., & Pashley, R. M. 1992, "Measurement of Forces in Liquids Using A Force Microscope", *Langmuir*, vol. 8, no. 7, pp. 1831-1836.

Edwards-Levy, F. & Levy, M. C. 1999, "Serum albumin-alginate coated beads: mechanical properties and stability", *Biomaterials*, vol. 20, no. 21, pp. 2069-2084.

Eriksson, J., Malmsten, M., Tiberg, F., Callisen, T. H., Damhus, T., & Johansen, K. S. 2005, "Enzymatic degradation of model cellulose films", *Journal of Colloid and Interface Science*, vol. 284, no. 1, pp. 99-106.

Evans, E. A. & Skalak, R. 1980, *Mechanics and Thermodynamics of Biomembranes* CRC Press, Boca Raton, FL.

Falt, S., Wagberg, L., Vesterlind, E. L., & Larsson, P. T. 2004, "Model films of cellulose II - improved preparation method and characterization of the cellulose film", *Cellulose*, vol. 11, no. 2, pp. 151-162.

Feng, W. W. & Yang, W. H. 1973, "Contact Problem of An Inflated Spherical Nonlinear Membrane", *Journal of Applied Mechanics-Transactions of the Asme*, vol. 40, no. 1, pp. 209-214.

Fery, A. & Weinkamer, R. 2007, "Mechanical properties of micro- and nanocapsules: Single-capsule measurements", *Polymer*, vol. 48, no. 25, pp. 7221-7235.

Fiddes, L. K., Chan, H. K. C., Wyss, K., Simmons, C. A., Kumacheva, E., & Wheeler, A. R. 2009, "Augmenting microgel flow via receptor-ligand binding in the constrained geometries of microchannels", *Lab on A Chip*, vol. 9, no. 2, pp. 286-290.

Fiedler, H. 2008, *Synthesis and Properties of Monodisperse Melamine Resin Particles*, Microparticles GmbH, Germany.

Finch, C. A. 1993, "Industrial Microencapsulation: Polymers for Microcapsule Walls," in *Encapsulation and Controlled Release* , D. R. Karsa & R. A. Stephenson, eds., The Royal Society of Chemistry, Cambridge.

Finch, C. A. & Bodmeier, R. 2002, "Microencapsulation," in *Ullmann's Encyclopedia of Industrial Chemistry*, John Wiley & Sons, Inc..

Fossum, R. D., Bodet, J., Dihora, J. O., Jordan, G. T., Kirksey, S. T., & Waits, L. D. 2008, *Fabric care compositions comprising formaldehyde scavengers* , EP1991648 (patent).

Fritz, J., Anselmetti, D., Jarchow, J., & FernandezBusquets, X. 1997, "Probing single biomolecules with atomic force microscopy", *Journal of Structural Biology*, vol. 119, no. 2, pp. 165-171.

Fuji, M., Machida, K., Takei, T., Watanabe, T., & Chikazawa, M. 1999, "Effect of wettability on adhesion force between silica particles evaluated by atomic force microscopy measurement as a function of relative humidity", *Langmuir*, vol. 15, no. 13, pp. 4584-4589.

Fujiwara, H. 2007, *Spectroscopic Ellipsometry - Principles and Applications* John Wiley & Sons, West Sussex, England.

Gao, C. Y., Moya, S., Lichtenfeld, H., Casoli, A., Fiedler, H., Donath, E., & Mohwald, H. 2001, "The decomposition process of melamine formaldehyde cores: The key step in the fabrication of ultrathin polyelectrolyte multilayer capsules", *Macromolecular Materials and Engineering*, vol. 286, no. 6, pp. 355-361.

Garoff, N. & Zauscher, S. 2002, "The influence of fatty acids and humidity on friction and adhesion of hydrophilic polymer surfaces", *Langmuir*, vol. 18, no. 18, pp. 6921-6927.

Gaserod, O., Sannes, A., & Skjak-Braek, G. 1999, "Microcapsules of alginate-chitosan. II. A study of capsule stability and permeability", *Biomaterials*, vol. 20, no. 8, pp. 773-783.

Genta, I., Perugini, P., Pavanetto, F., Maculotti, K., Modena, T., Casado, B., Lupi, A., Iadarola, P., & Conti, B. 2001, "Enzyme loaded biodegradable microspheres in vitro ex vivo evaluation", *Journal of Controlled Release*, vol. 77, no. 3, pp. 287-295.

Gerlock, J. L., Dean, M. J., Korniski, T. J., & Bauer, D. R. 1986, "Formaldehyde Release from Acrylic Melamine Coatings During Photolysis and the Mechanism of Photoenhanced Cross-Link Hydrolysis", *Industrial & Engineering Chemistry Product Research and Development*, vol. 25, no. 3, pp. 449-453.

Gewirth, A. A. & LaGraff, J. R. 1995, "Atomic Force Microscopy," in *The Handbook of Surface Imaging and Visualization*, A. T. Hubbard, ed., CRC Press, Inc..

Giesbers, M., Kleijn, J. M., & Stuart, M. A. C. 2002, "The electrical double layer on gold probed by electrokinetic and surface force measurements", *Journal of Colloid and Interface Science*, vol. 248, no. 1, pp. 88-95.

Greenblatt, H. C., Dombroski, M., Klishevich, W., Kirkpatrick, J., Bajwa, I., Garrison, W., & Redding, B. K. 1993, "Encapsulation and Controlled Release of Flavours and Fragrances," in *Encapsulation and Controlled Release*, D. R. Karsa & R. A. Stephenson, eds., The Royal Society of Chemistry, Cambridge.

Gunnars, S., Wagberg, L., & Stuart, M. A. C. 2002, "Model films of cellulose: I. Method development and initial results", *Cellulose*, vol. 9, no. 3-4, pp. 239-249.

Hillier, A. C., Kim, S., & Bard, A. J. 1996, "Measurement of double-layer forces at the electrode/electrolyte interface using the atomic force microscope: Potential and anion dependent interactions", *Journal of Physical Chemistry*, vol. 100, no. 48, pp. 18808-18817.

Hines, W. W. & Montgomery, D. C. 1990, *Probability and Statistics in Engineering and Management Science*, 3rd edn, John Wiley & Sons, Inc..

Ho, L. T. T. 2000, *Formulating Detergents and Personal Care Products* AOCS Press, Champaign, Illinois.

Hochmuth, R. M. 2000, "Micropipette aspiration of living cells", *Journal of Biomechanics*, vol. 33, no. 1, pp. 15-22.

Hodges, C. S., Cleaver, J. A. S., Ghadiri, M., Jones, R., & Pollock, H. M. 2002, "Forces between polystyrene particles in water using the AFM: Pull-off force vs particle size", *Langmuir*, vol. 18, no. 15, p. DOI.

Hodges, C. S., Looi, L., Cleaver, J. A. S., & Ghadiri, M. 2004, "Use of the JKR model for calculating adhesion between rough surfaces", *Langmuir*, vol. 20, no. 22, pp. 9571-9576.

Hoh, J. H., Cleveland, J. P., Prater, C. B., Revel, J. P., & Hansma, P. K. 1992, "Quantized Adhesion Detected with the Atomic Force Microscope", *Journal of the American Chemical Society*, vol. 114, no. 12, pp. 4917-4918.

Hong, K. & Park, S. 1999, "Melamine resin microcapsules containing fragrant oil: synthesis and characterization", *Materials Chemistry and Physics*, vol. 58, no. 2, pp. 128-131.

Huang, Q. X., Fei, Y. T., Gonda, S., Misumi, I., Sato, O., Keem, T., & Kurosawa, T. 2006, "The interference effect in an optical beam deflection detection system of a dynamic mode AFM", *Measurement Science & Technology*, vol. 17, no. 6, pp. 1417-1423.

Hutter, J. L. & Bechhoefer, J. 1993, "Calibration of Atomic-Force Microscope Tips", *Review of Scientific Instruments*, vol. 64, no. 7, pp. 1868-1873.

Hwang, J. S., Kim, J. N., Wee, Y. J., Jang, H. G., Kim, S. H., & Ryu, H. W. 2006, "Factors affecting the characteristics of melamine resin microcapsules containing fragrant oils", *Biotechnology and Bioprocess Engineering*, vol. 11, no. 5, pp. 391-395.

Iqbal, P., Critchley, K., Attwood, D., Tunnicliffe, D., Evans, S. D., & Preece, J. A. 2008, "Chemical Manipulation by X-rays of Functionalized Thiolate Self-Assembled Monolayers on Au", *Langmuir*, vol. 24, no. 24, pp. 13969-13976.

Israelachvili, J. N. 1985, *Intermolecular and Surface Forces with Applications to Colloidal and Biological Systems* Academic Press Inc. (London) Ltd..

Janssen, R. Q. F., Derks, G. J. W., Van Herk, A. M., & German, A. L. 1993, "On-line Monitoring and Control of the (Co-) Polymer Encapsulation of TiO_2 in Aqueous Emulsion

Systems," in *Encapsulation and Controlled Release*, D. R. Karsa & R. A. Stephenson, eds., The Royal Society of Chemistry, Cambridge.

Jay, A. W. L. & Edwards, M. A. 1968, "Mechanical Properties of Semipermeable Microcapsules", *Canadian Journal of Physiology and Pharmacology*, vol. 46, no. 5, p. 731-&.

Jellinek, J. S. 1975, *The Use of Fragrance in Consumer Products* John Wiley & Sons, Inc. Canada.

Johnson, K. L. 1985, *Contact Mechanics* Cambridge University Press.

Jones, R., Pollock, H. M., Cleaver, J. A. S., & Hodges, C. S. 2002, "Adhesion forces between glass and silicon surfaces in air studied by AFM: Effects of relative humidity, particle size, roughness, and surface treatment", *Langmuir*, vol. 18, no. 21, pp. 8045-8055.

Ju, B. F., Ju, Y., & Saka, M. 2005, "A methodology for damage strength evaluation of a single biomimetic microcapsule", *Advances in Fracture and Strength, Pts 1- 4*, vol. 297-300, pp. 1730-1735.

Kaupp, G. 2006, *Atomic Force Microscopy, Scanning Nearfield Optical Microscopy and Nanoscratching* Springer-Verlag Berlin Heidelberg.

Keller, M. W. & Sottos, N. R. 2006, "Mechanical properties of microcapsules used in a self-healing polymer", *Experimental Mechanics*, vol. 46, no. 6, pp. 725-733.

Kendall K. 2001, *Molecular Adhesion and Its Applications* Kluwer Academic/Plenum Publishers, New York.

Kinloch, A.J. & Taylor, A.C. 2006, "The mechanical properties and fracture behaviour of epoxy-inorganic micro- and nano-composites", *Journal of Materials Science*, vol. 41, no. 11, pp. 3271-3297.

Kontturi, E., Thune, P. C., & Niemantsverdriet, J. W. 2003, "Novel method for preparing cellulose model surfaces by spin coating", *Polymer*, vol. 44, no. 13, pp. 3621-3625.

Lardner, T. J. & Pujara, P. 1980, "Compression of spherical cells", *Mechanics Today*, vol. 5, pp. 161-176.

Lea, A. S., Andrade, J. D., & Hlady, V. 1993, "Measurement of Steric Exclusion Forces with the Atomic-Force Microscope", *Colloid-Polymer Interactions*, vol. 532, pp. 266-279.

Lea, A. S., Andrade, J. D., & Hlady, V. 1994, "Compression of Polyethylene-Glycol Chains Grafted Onto Silicon-Nitride Surface As Measured by Scanning Force Microscopy", *Colloids and Surfaces A-Physicochemical and Engineering Aspects*, vol. 93, pp. 349-357.

Leblond, F. A., Tessier, J., & Halle, J. P. 1996, "Quantitative method for the evaluation of biomicrocapsule resistance to mechanical stress", *Biomaterials*, vol. 17, no. 21, pp. 2097-2102.

Leite, F. L. & Herrmann, P. S. P. 2005, "Application of atomic force spectroscopy (AFS) to studies of adhesion phenomena: a review," in *Atomic force microscopy in adhesion studies*, J. Drelich & K. L. Mittal, eds., Koninklijke Brill NV, Leiden, The Netherlands.

Leporatti, S., Gerth, A., Kohler, G., Kohlstrunk, B., Hauschildt, S., & Donath, E. 2006, "Elasticity and adhesion of resting and lipopolysaccharide-stimulated macrophages", *Febs Letters*, vol. 580, no. 2, pp. 450-454.

Li, X. & Logan, B. E. 2004, "Analysis of bacterial adhesion using a gradient force analysis method and colloid probe atomic force microscopy", *Langmuir*, vol. 20, no. 20, pp. 8817-8822.

Lim, C. T., Zhou, E. H., Li, A., Vedula, S. R. K., & Fu, H. X. 2006, "Experimental techniques for single cell and single molecule biomechanics", *Materials Science & Engineering C-Biomimetic and Supramolecular Systems*, vol. 26, no. 8, pp. 1278-1288.

Liu, K. K., Williams, D. R., & Briscoe, B. J. 1996, "Compressive deformation of a single microcapsule", *Physical Review e*, vol. 54, no. 6, pp. 6673-6680.

Liu, K. K., Williams, D. R., & Briscoe, B. J. 1998, "The large deformation of a single micro-elastomeric sphere", *Journal of Physics D-Applied Physics*, vol. 31, no. 3, pp. 294-303.

Liu, K. K., Wang, H. G., Wan, K. T., Liu, T., & Zhang, Z. 2002, "Characterizing capsule-substrate adhesion in presence of osmosis", *Colloids and Surfaces B-Biointerfaces*, vol. 25, no. 4, pp. 293-298.

Liu, T. & Zhang, Z. 2004, "Mechanical properties of desiccated ragweed pollen grains determined by micromanipulation and theoretical modelling", *Biotechnology and Bioengineering*, vol. 85, no. 7, pp. 770-775.

Liu, T., Donald, A. M., & Zhang, Z. 2005, "Novel manipulation in environmental scanning electron microscope for measuring mechanical properties of single nanoparticles", *Materials Science and Technology*, vol. 21, no. 3, pp. 289-294.

Loxley, A. & Vincent, B. 1998, "Preparation of poly(methylmethacrylate) microcapsules with liquid cores", *Journal of Colloid and Interface Science*, vol. 208, no. 1, pp. 49-62.

Luckham, P. F. 2004, "Manipulating forces between surfaces: applications in colloid science and biophysics", *Advances in Colloid and Interface Science*, vol. 111, no. 1-2, pp. 29-47.

Lulevich, V. V., Radtchenko, I. L., Sukhorukov, G. B., & Vinogradova, O. I. 2003, "Mechanical properties of polyelectrolyte microcapsules filled with a neutral polymer", *Macromolecules*, vol. 36, no. 8, pp. 2832-2837.

Lulevich, V. V., Andrienko, D., & Vinogradova, O. I. 2004a, "Elasticity of polyelectrolyte multilayer microcapsules", *Journal of Chemical Physics*, vol. 120, no. 8, pp. 3822-3826.

Lulevich, V. V. & Vinogradova, O. I. 2004b, "Effect of pH and salt on the stiffness of polyelectrolyte multilayer microcapsules", *Langmuir*, vol. 20, no. 7, pp. 2874-2878.

Luo, W. J., Yang, W., Jiang, S., Feng, J. M., & Yang, M. B. 2007, "Microencapsulation of decabromodiphenyl ether by in situ polymerization: Preparation and characterization", *Polymer Degradation and Stability*, vol. 92, no. 7, pp. 1359-1364.

Magonov, S. N. & Whangbo, M. 1996, *Surface Analysis with STM and AFM* VCH Verlagsgesellschaft mbH, Weinheim, Germany.

Malvern 1996, *Zetasizer Manual* Malvern Instruments Ltd..

Malvern 2007, *Mastersizer 2000 user manual* Malvern Instruments Ltd..

Malvern 2009, *Zetasizer Nano series technical note* Malvern Instruments Ltd..

Marten, J., Erbe, A., Critchley, K., Brarnble, J. P., Weber, E., & Evans, S. D. 2008, "Self-assembled layers based on isomerizable stilbene and diketoarylhydrazoitie moieties", *Langmuir*, vol. 24, no. 6, pp. 2479-2486.

Matei, G. A., Thoreson, E. J., Pratt, J. R., Newell, D. B., & Burnham, N. A. 2006, "Precision and accuracy of thermal calibration of atomic force microscopy cantilevers", *Review of Scientific Instruments*, vol. 77.

Mclean, S. C., Lioe, H., Meagher, L., Craig, V. S. J., & Gee, M. L. 2005, "Atomic force microscopy study of the interaction between adsorbed poly(ethylene oxide) layers: Effects of surface modification and approach velocity", *Langmuir*, vol. 21, pp. 2199-2208.

Meyer, E., Heinzelmann, H., Grutter, P., Jung, T., Hidber, H. R., Rudin, H., & Guntherodt, H. J. 1989, "Atomic Force Microscopy for the Study of Tribology and Adhesion", *Thin Solid Films*, vol. 181, pp. 527-544.

Montgomery, D. C., Runger, G. C., & Hubele, N. F. 2001, *Engineering Statistics*, 2nd Edition edn, John Wiley & Sons, Inc..

Muller, E., Chung, J. T., Zhang, Z., & Sprauer, A. 2005, "Characterization of the mechanical properties of polymeric chromatographic particles by micromanipulation", *Journal of Chromatography A*, vol. 1097, no. 1-2, pp. 116-123.

Nefedov, V. I. 1988, *X-ray Photoelectron Spectroscopy of Solid Surfaces* VSP BV, The Netherlands.

Neumeister, J. M. & Ducker, W. A. 1994, "Lateral, Normal, and Longitudinal Spring Constants of Atomic-Force Microscopy Cantilevers", *Review of Scientific Instruments*, vol. 65, no. 8, pp. 2527-2531.

Nguyen, V. B., Wang, C. X., Thomas, C. R., & Zhang, Z. 2009a, "Mechanical properties of single alginate microspheres determined by microcompression and finite element modelling", *Chemical Engineering Science*, vol. 64, no. 5, pp. 821-829.

Nguyen, V. B., Post-doctorate researcher, The University of Birmingham, Wall thickness to diameter ratio limit to exclude the bending effect using FEA. 2009b. 14-11-2009. Ref Type: Personal Communication

Nonhebel, G. & Moss, A. A. H. 1971, *Drying of Solids in the Chemical Industry* Butterworth & Co. Ltd..

Notley, S. M., Eriksson, M., Wagberg, L., Beck, S., & Gray, D. G. 2006, "Surface forces measurements of spin-coated cellulose thin films with different crystallinity", *Langmuir*, vol. 22, no. 7, pp. 3154-3160.

Ohler, B. 2007, *Practical Advice on the Determination of Cantilever Spring Constants*, Veeco Instruments Inc..

Ohtsubo, T., Tsuda, S., & Tsuji, K. 1991, "A Study of the Physical Strength of Fenitrothion Microcapsules", *Polymer*, vol. 32, no. 13, pp. 2395-2399.

Ortmanis, A., Neufeld, R. J., & Chang, T. M. S. 1984, "Study of Microencapsulated Urease in A Continuous Feed, Stirred Tank Reactor", *Enzyme and Microbial Technology*, vol. 6, no. 3, pp. 135-139.

Owen, R. 2002, *A Practical Guide to AFM Force Microscopy and Data Analysis*, JPK Instruments AG, Germany.

Partanen, R., Hakala, M., Sjovall, O., Kallio, H., & Forssell, P. 2005, "Effect of relative humidity on the oxidative stability of microencapsulated sea buckthorn seed oil", *Journal of Food Science*, vol. 70, no. 1, p. E37-E43.

Pernot, J., ., Pouyet, B., Brun, H., & Briancon, S. 1999, "Microendapsulation in Adhesive Technology," in *Microspheres Microcapsules & Liposomes*, A. Reza, ed., Citus Books, London, U.K..

Poncelet, D. & Neufeld, R. J. 1989, "Shear Breakage of Nylon Membrane Microcapsules in A Turbine Reactor", *Biotechnology and Bioengineering*, vol. 33, no. 1, pp. 95-103.

Popplewell, L. M., Brain, J., Pluyter, J. G. L., Zhen, Y., & Lee, K. D. 2009, *Encapsulated materials*, US7491687, International Flavors & Fragrances Inc., New York, (patent).

Prater, C. B., Maivald, P. G., Kjoller, K. J., & Heaton, M. G. 1995, *Probing Nano-Scale Forces with the Atomic Force Microscope*, DI Digital Instruments, Veeco Metrology Group, Santa Barbara, California, U.S..

Quon, R. A., Ulman, A., & Vanderlick, T. K. 2000, "Impact of humidity on adhesion between rough surfaces", *Langmuir*, vol. 16, no. 23, pp. 8912-8916.

Rabinovich, Y. I., Adler, J. J., Ata, A., Singh, R. K., & Moudgil, B. M. 2000a, "Adhesion between nanoscale rough surfaces - II. Measurement and comparison with theory", *Journal of Colloid and Interface Science*, vol. 232, no. 1, pp. 17-24.

Rabinovich, Y. I., Adler, J. J., Ata, A., Singh, R. K., & Moudgil, B. M. 2000b, "Adhesion between nanoscale rough surfaces - I. Role of asperity geometry", *Journal of Colloid and Interface Science*, vol. 232, no. 1, pp. 10-16.

Rabinovich, Y. I., Adler, J. J., Esayanur, M. S., Ata, A., Singh, R. K., & Moudgil, B. M. 2002, "Capillary forces between surfaces with nanoscale roughness", *Advances in Colloid and Interface Science*, vol. 96, no. 1-3, p. II.

Rabinovich, Y. I., Esayanur, M. S., & Moudgil, B. M. 2005, "Capillary forces between two spheres with a fixed volume liquid bridge: Theory and experiment", *Langmuir*, vol. 21, no. 24, pp. 10992-10997.

Rachik, M., Barthes-Biesel, D., Carin, M., & Edwards-Levy, F. 2006, "Identification of the elastic properties of an artificial capsule membrane with the compression test: Effect of thickness", *Journal of Colloid and Interface Science*, vol. 301, no. 1, pp. 217-226.

Rehor, A., Canaple, L., Zhang, Z. B., & Hunkeler, D. 2001, "The compressive deformation of multicomponent microcapsules: Influence of size, membrane thickness, and compression speed", *Journal of Biomaterials Science-Polymer Edition*, vol. 12, no. 2, pp. 157-170.

Reimer, L. & Kohl, H. 2008, *Transmission Electron Microscopy - Physics of Image Formation*, 5th edn, Springer, New York.

Ren, Y. L., Donald, A. M., & Zhang, Z. B. 2007, "Investigation of radiation damage to microcapsules in environmental SEM", *Materials Science and Technology*, vol. 23, no. 7, pp. 857-864.

Ren, Y. L., Donald, A. M., & Zhang, Z. B. 2008, "Investigation of the Morphology, Viability and Mechanical Properties of Yeast Cells in Environmental SEM", *Scanning*, vol. 30, no. 6, pp. 435-442.

Rief, M., Oesterhelt, F., Heymann, B., & Gaub, H. E. 1997, "Single molecule force spectroscopy on polysaccharides by atomic force microscopy", *Science*, vol. 275, no. 5304, pp. 1295-1297.

Roesler, J., Harders, H. and Baeker, M. 2007, *Mechanical Behaviour of Engineering Materials - Metals, Ceramics, Polymers, and Composites*, Springer Berlin Heidelberg.

Roos, Y. & Karel, M. 1991, "Applying state diagrams to food processing and development" *Food Technology*, vol. 5, no. 12, pp. 66-71.

Roos, Y. & Karel, M. 1993, "Effects of glass transitions on dynamic phenomena in sugar containing food systems", *Glassy State in Foods*, pp. 207-222.

Rosenau, T., Potthast, A., Sixta, H., & Kosma, P. 2001, "The chemistry of side reactions and byproduct formation in the system NMMO/cellulose (Lyocell process)", *Progress in Polymer Science*, vol. 26, no. 9, pp. 1763-1837.

Rosinski, S., Grigorescu, G., Lewinska, D., Ritzen, L. G., Viernstein, H., Teunou, E., Poncelet, D., Zhang, Z., Fan, X., Serpy, D., Marisony, I., & Hunkeler, D. 2002,

"Characterization of microcapsules: recommended methods based on round-robin testing", *Journal of Microencapsulation*, vol. 19, no. 5, pp. 641-659.

Sachdev, A. & Krishnan, S. 1997, "Heavy-Duty Liquid Detergents," in *Liquid Detergents*, K. Lai, ed., Marcel Dekker, Inc. New York.

Schaefer, D. M., Carpenter, M., Reifenberger, R., Demejo, L. P., & Rimai, D. S. 1994, "Surface Force Interactions Between Micrometer-Size Polystyrene Spheres and Silicon Substrates Using Atomic-Force Techniques", *Journal of Adhesion Science and Technology*, vol. 8, no. 3, pp. 197-210.

Schuldt, U. & Hunkeler, D. 2000, "Characterization methods for microcapsules", *Minerva Biotecnologica*, vol. 12, no. 4, pp. 249-264.

Sgraja, M., Blomer, J., Bertling, J., & Jansens, P. J. 2008, "In Situ Encapsulation of Tetradecane Droplets in Oil-in-Water Emulsions Using Amino Resins", *Journal of Applied Polymer Science*, vol. 110, no. 4, pp. 2366-2373.

Skalak, R., Tozeren, A., Zarda, R. P., & Chien, S. 1973, "Strain Energy Function of Red Blood-Cell Membranes", *Biophysical Journal*, vol. 13, no. 3, pp. 245-280.

Smith, A. E., Moxham, K. E., & Middelberg, A. P. J. 1998, "On uniquely determining cell-wall material properties with the compression experiment", *Chemical Engineering Science*, vol. 53, no. 23, pp. 3913-3922.

Smith, A. E., Zhang, Z., & Thomas, C. R. 2000a, "Wall material properties of yeast cells: Part 1. Cell measurements and compression experiments", *Chemical Engineering Science*, vol. 55, no. 11, pp. 2031-2041.

Smith, A. E., Moxham, K. E., & Middelberg, A. P. J. 2000b, "Wall material properties of yeast cells. Part II. Analysis", *Chemical Engineering Science*, vol. 55, no. 11, pp. 2043-2053.

Stenson, J. D., Ren, Y., Donald, A. M., & Zhang, Z. 2008, "Compression testing by nanomanipulation in environmental scanning electron microscope (ESEM)", *Experimental Techniques* (in press).

Stenson, J. D., Thomas, C. R., & Hartley, P. 2009, "Modelling the mechanical properties of yeast cells", *Chemical Engineering Science*, vol. 64, no. 8, pp. 1892-1903.

Sugawara, Y. 2007, "Atomic Force Microscopy," in *Roadmap of Scanning Probe Microscopy*, S. Morita, ed., Springer-Verlag Berlin Heidelberg.

Sun, G. & Zhang, Z. 2001, "Mechanical properties of melamine-formaldehyde microcapsules", *Journal of Microencapsulation*, vol. 18, no. 5, pp. 593-602.

Sun, G. & Zhang, Z. 2002, "Mechanical strength of microcapsules made of different wall materials", *International Journal of Pharmaceutics*, vol. 242, no. 1-2, pp. 307-311.

Taft, E. A. 1988, "Growth of Native Oxide on Silicon", *Journal of the Electrochemical Society*, vol. 135, no. 4, pp. 1022-1023.

Tatara, Y. 1991, "On Compression of Rubber Elastic Sphere Over A Large Range of Displacements .1. Theoretical-Study", *Journal of Engineering Materials and Technology-Transactions of the Asme*, vol. 113, no. 3, pp. 285-291.

Tatara, Y., Shima, S., & Lucero, J. C. 1991, "On Compression of Rubber Elastic Sphere Over A Large Range of Displacements .2. Comparison of Theory and Experiment", *Journal of Engineering Materials and Technology-Transactions of the Asme*, vol. 113, no. 3, pp. 292-295.

Thu, B., Bruheim, P., Espevik, T., Smidsrod, O., SoonShiong, P., & SkjakBraek, G. 1996, "Alginate polycation microcapsules .1. Interaction between alginate and polycation", *Biomaterials*, vol. 17, no. 10, pp. 1031-1040.

Torras, C., Pitol, L., & Garcia-Valls, R. 2007, "Two methods for morphological characterization of internal microcapsule structures", *Journal of Membrane Science*, vol. 305, pp. 1-4.

Tortonese, M. & Kirk, M. 1997, "Characterization of application specific probes for SPMs", *Micromachining and Imaging*, vol. 3009, pp. 53-60.

Turner, B. & Levey, L. 1993, "Small Packages That Deliver Big Ideas: An Inside Look into Microcapsule Technology," in *Encapsulation and Controlled Release*, D. R. Karsa & R. A. Stephenson, eds., The Royal Society of Chemistry, Cambridge.

Usami, T., Sano, S., & Yoshida, S. 1999, "Microencapsulation in Printing and Recording," in *Microspheres Microcapsules & Liposomes*, vol. 1 A. Reza, ed., Citus Books, London, U.K..

Van Raamsdonk, J. M. & Chang, P. L. 2001, "Osmotic pressure test: A simple, quantitative method to assess the mechanical stability of alginate microcapsules", *Journal of Biomedical Materials Research*, vol. 54, no. 2, pp. 264-271.

Veeco 2000, *Scanning Probe Microscopy (SPM) training note book*, Version 3.0 edn, Digital Instruments Veeco Metrology Group.

Vinogradova, O. I., Butt, H. J., Yakubov, G. E., & Feuillebois, F. 2001, "Dynamic effects on force measurements. I. Viscous drag on the atomic force microscope cantilever", *Review of Scientific Instruments*, vol. 72, no. 5, pp. 2330-2339.

Visser, J. 1995, "Particle adhesion and removal: A review", *Particulate Science and Technology*, vol. 13, no. 3-4, pp. 169-196.

Wakelyn, P. J., Bertoniere, N. R., French, A. D., Thibodeaux, D. P., Triplett, B. A., Rousselle, M., Goynes, W. R., Edwards, J. V., Hunter, L., McAlister, D. D., & Gamble, G. R. 2006, *Cotton Fiber Chemistry and Technology* CRC Press.

Wang, C., Cowen, C., Zhang, Z., & Thomas, C. R. 2005, "High-speed compression of single alginate microspheres", *Chemical Engineering Science*, vol. 60, no. 23, pp. 6649-6657.

Wang, C. X., Wang, L., & Thomas, C. R. 2004, "Modelling the mechanical properties of single suspension-cultured tomato cells", *Annals of Botany*, vol. 93, no. 4, pp. 443-453.

Ward I.M. & Hadley, D. W. 1993, *An Introduction to the Mechanical Properties of Solid Polymers* John Wiley & Sons Chichester.

Watts, J. F. & Wolstenholme, J. 2003, *An Introduction to Surface Analysis by XPS and AES* John Wiley & Sons, West Sussex, England.

Weidenhammer, P. & Jacobasch, H. J. 1996, "Investigation of Adhesion Properties of Polymer Materials by Atomic Force Microscopy and Zeta Potential Measurements", *Journal of Colloid and Interface Science*, vol. 180, no. 1, pp. 232-236.

Weisenhorn, A. L., Hansma, P. K., Albrecht, T. R., & Quate, C. F. 1989, "Forces in Atomic Force Microscopy in Air and Water", *Applied Physics Letters*, vol. 54, no. 26, pp. 2651-2653.

Woollatt, E. 1985, *The Manufacture of Soaps, Other Detergents and Glycerine* Ellis Horwood Limited, West Sussex, England.

Xue, J. & Zhang, Z. B. 2009, "Physical, Structural, and Mechanical Characterization of Calcium-Shellac Microspheres as a Carrier of Carbamide Peroxide", *Journal of Applied Polymer Science*, vol. 113, no. 3, pp. 1619-1625.

Yan, Y., Zhang, Z. B., Stokes, J. R., Zhou, Q. Z., Ma, G. H., & Adams, M. J. 2009, "Mechanical characterization of agarose micro-particles with a narrow size distribution", *Powder Technology*, vol. 192, no. 1, pp. 122-130.

Yang, S. Y., Hirasaki, G. J., Basu, S., & Vaidya, R. 1999, "Mechanisms for contact angle hysteresis and advancing contact angles", *Journal of Petroleum Science and Engineering*, vol. 24, no. 2-4, pp. 63-73.

Yap, S. F., Adams, M. J., Seville, J. P. K., & Zhang, Z. B. 2008, "Single and bulk compression of pharmaceutical excipients: Evaluation of mechanical properties", *Powder Technology*, vol. 185, no. 1, pp. 1-10.

Yeoh, O. H. 1993, "Some Forms of the Strain-Energy Function for Rubber", *Rubber Chemistry and Technology*, vol. 66, no. 5, pp. 754-771.

Youan, B. B. C., Jackson, T. L., Dickens, L., Hernandez, C., & Owusu-Ababio, G. 2001, "Protein release profiles and morphology of biodegradable microcapsules containing an oily core", *Journal of Controlled Release*, vol. 76, no. 3, pp. 313-326.

Young, P. M., Price, R., Tobyn, M. J., Buttrum, M., & Dey, F. 2003, "Investigation into the effect of humidity on drug-drug interactions using the atomic force microscope", *Journal of Pharmaceutical Sciences*, vol. 92, no. 4, pp. 815-822.

Yuan, L., Liang, G., Xie, J., Li, L., & Guo, J. 2006, "Preparation and characterization of poly(urea-formaldehyde) microcapsules filled with epoxy resins", *Polymer*, vol. 47, no. 15, pp. 5338-5349.

Zhang, H. Z. & Wang, X. D. 2009, "Fabrication and performances of microencapsulated phase change materials based on n-octadecane core and resorcinol-modified melamine-formaldehyde shell", *Colloids and Surfaces A-Physicochemical and Engineering Aspects*, vol. 332, no. 2-3, pp. 129-138.

Zhang, Z., Saunders, R., & Thomas, C. R. 1999, "Mechanical strength of single microcapsules determined by a novel micromanipulation technique", *Journal of Microencapsulation*, vol. 16, no. 1, pp. 117-124.

Zhang, Z., Stenson, J. D., & Thomas, C. R. 2009, "Chapter 2 Micromanipulation in Mechanical Characterisation of Single Particles," in *Advances in Chemical Engineering Characterization of Flow, Particles and Interfaces*, Volume 37 edn, L. Jinghai, ed., Academic Press, pp. 29-85.

Zhao, L. & Zhang, Z. B. 2004, "Mechanical characterization of biocompatible microspheres and microcapsules by direct compression", *Artificial Cells Blood Substitutes and Immobilization Biotechnology*, vol. 32, no. 1, pp. 25-40.

Zhong, Q., Inniss, D., Kjoller, K., & Elings, V. B. 1993, "Fractured Polymer Silica Fiber Surface Studied by Tapping Mode Atomic-Force Microscopy", *Surface Science*, vol. 290, no. 1-2, p. L688-L692.